UNIVERSIDAD AUTÓNOMA DE NUEVO LEÓN

FACULTAD DE CIENCIAS QUÍMICAS

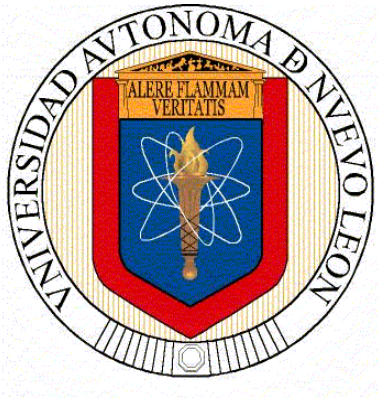

TESIS

"INVESTIGATION OF THE NIOBIUM-BASED MXENES AND HYBRID NANOSTRUCTURES FOR ELECTROCHEMICAL BIOSENSING APPLICATIONS"

QUE PRESENTA

KARAN KISHOR SINGH

COMO REQUISITO PARA OBTENER EL GRADO DE

DOCTORADO EN CIENCIAS

CON ORIENTACIÓN EN PROCESOS SUSTENTABLES

OCTUBRE 2022

UNIVERSIDAD AUTÓNOMA DE NUEVO LEÓN

FACULTAD DE CIENCIAS QUÍMICAS

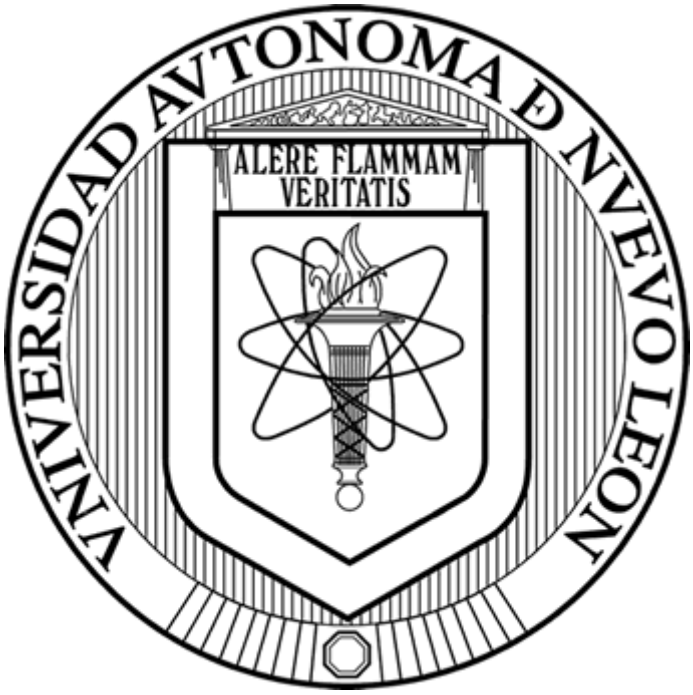

"INVESTIGATION OF THE NIOBIUM-BASED MXENES AND HYBRID NANOSTRUCTURES FOR ELECTROCHEMICAL BIOSENSING APPLICATIONS"

by

KARAN KISHOR SINGH

The thesis submitted in partial fulfilment of the requirements for the **DEGREE OF DOCTOR OF PHILOSOPHY IN SCIENCE** with orientation in sustainable processes.

Signature of the Advisor: _____

DR. SANAL KOZHIPARAMBIL CHANDRAN

OCTOBER 2022

“INVESTIGATION OF THE NIOBIUM-BASED MXENES AND HYBRID NANOSTRUCTURES FOR ELECTROCHEMICAL BIOSENSING APPLICATIONS”

THESIS AUTHORIZATION

_____

DR. SANAL KOZHIPARAMBIL CHANDRAN

PRESIDENT

_____

DR.

SECRETARY

_____

DR.

FIRST VOCAL

_____

DR.

SECOND VOCAL

_____

DR.

THIRD VOCAL

_____

DRA. MARIA ELENA CANTU

SUBDIRECTOR OF STUDIES OF POSTGRADUATE

"INVESTIGATION OF THE NIOBIUM-BASED MXENES AND HYBRID NANOSTRUCTURES FOR ELECTROCHEMICAL BIOSENSING APPLICATIONS"

_____

DR. SANAL KOZHIPARAMBIL CHANDRAN

THESIS DIRECTOR

_____

DR.

CO-DIRECTOR

_____

DRA. SHADAI LUGO LOREDO

REVIEWER

_____

DR. IVAN ALONSO SANTOS LOPEZ

REVIEWER

_____

DRA. ANABEL ALVAREZ MENDEZ

REVIEWER

_____

DRA.

REVIEWER

DEDICATIONS

To Lord Shiva,

my loving parents Shri Stayendra Singh and Smt. Baby Devi who have been giving me a different meaning of life, an endless source of support, and the most precious love,

My elder brothers Sunny Singh and Sonu Singh,

and Moni.

ACKNOWLEDGMENT

I express my deepest gratitude to the Almighty for providing me with guidance and the quick thinking required to complete my thesis within the allotted time. I extend my sincere appreciation to CONACYT and PAICYT for their unwavering financial support throughout my three-year Ph.D. journey. Their assistance has been invaluable. I am indebted to the EGAII FCQ, CIIDIT, CIIA, and FIME at the Universidad Autonoma de Nuevo Leon for generously providing the research facilities that were essential for the synthesis and characterization phases of my work. My heartfelt thanks go to Dr. Sanal Kozhiparambil Chandran for his unwavering guidance, support, and mentorship throughout my research and my stay in Monterrey. His expertise has been instrumental in shaping my work. For the past three years, he has always been inspiring, patient, and responsive with sharp insight on my work and research .I would like to express my profound gratitude to my doctoral committee members, Dr. Ivan Lopez, Dra. Anabel Mendez, and Dra. Shadai Loredo, for their continuous support and guidance over the past couple of years. Thank you for taking time from their busy schedules to review and evaluate this work, providing valuable feedback and guidance.. I am grateful to Dr. Javier Rivera for his official support and guidance during the seminar. His assistance was instrumental in shaping my research. A significant portion of my thesis was completed at the University of Ioannina, Greece. I wish to thank Prof. Mamas Podrimidis for graciously accepting me as a visiting student in his lab and providing me with a valuable learning opportunity. A special mention goes to Alexandros and Maria for their warm welcome, affection, and care during my stay in Ioannina, Greece. During my stay in Greece, I would like to thank two friends, Jon Ander and Vitek, for the wonderful times we had outside the laboratory. We explored the campus and ventured to many places in Greece together, creating cherished memories beyond our research. I extend my gratitude to Dra. Soorya Pushpan for her valuable assistance during the experimental characterization process. I would like to express my heartfelt thanks to Sr. Daniel and Sra. Sandra for their exceptional hospitality, treating me like family and introducing me to the wonderful places in Mexico. My academic journey was made smoother by the unwavering support of my friends from Posgrado, especially Oswaldo and Carlos. I am also thankful for the enriching experiences shared with my friends and flatmates from Pakistan, Atiqa and Ramsha, as we explored life in Monterrey beyond academia. Special appreciation goes to Moni, who provided emotional support and motivation throughout my journey, despite being miles away in India.

ABSTRACT

Karan Kishor Singh, October, 2022

Universidad Autonoma de Nuevo Leon,

Facultad de Ciencias Quimicas.

Title of the thesis: INVESTIGATION OF THE NIOBIUM-BASED MXENES AND HYBRID NANOSTRUCTURES FOR ELECTROCHEMICAL BIOSENSING APPLICATIONS

Number of Pages: 235

The thesis is submitted for partially fulfils the requirements for the **DEGREE OF DOCTOR OF PHILOSOPHY IN SCIENCE** with an orientation in sustainable processes.

Area of study: Sustainable Processes

Purpose and method of the study: This study undertakes an exploratory investigation into MXene materials, focusing on the synthesis of high-quality Nb-based MXenes, such as Nb_2SnC, Nb_2AlC, and $Nb_4C_3T_x$, utilizing environmentally sustainable chemical techniques. The comprehensive scientific approach incorporates solid-state processes for the synthesis of MAX phases and a regulated etching procedure that emphasizes safety and environmental conscientiousness. In addition, the utilization of bath sonication serves to enhance the separation of multilayer MXene, hence increasing the material's applicability across several domains. The synthesized MXene materials were thoroughly characterized in this study using a range of techniques, such as X-ray Diffraction (XRD), Scanning Electron Microscopy (SEM), Transmission Electron Microscopy (TEM), X-ray Photoelectron Spectroscopy (XPS), and Energy-Dispersive X-ray Spectroscopy (EDX). These techniques were employed to gain a comprehensive understanding of the structure, morphology, composition, and elemental content of the materials. The results of this study serve as the foundation for the production of MXene-nanomaterial composites, which can be utilized to develop adaptable electrodes for a wide range of applications. Moreover, the objective of this study is to determine the electrochemical durability of MXene materials, which is a crucial factor in facilitating sustained functionality in electrochemical biosensors. This study establishes a foundation for the advancement of electrochemical sensing platforms by expanding the utilization of synthesized MXenes. These platforms have the ability to accommodate a wide range of analytes, encompassing both biological and non-biological substances. This research represents a paradigm of novelty, accuracy, and environmental consciousness, aiming to influence the trajectory of scientific and technological advancements in the foreseeable future.

Contributions and Conclusions: The extensive investigation conducted on MXene materials has yielded significant advancements in the fields of materials science and analytical chemistry. The utilization of environmentally conscious techniques in the production of high-caliber Nb-based MXenes, such as Nb_2SnC, Nb_2AlC, and $Nb_4C_3T_x$, presents novel opportunities for the advancement of sustainable materials engineering. The foundational basis for the fabrication of new MXene-nanomaterial composites and their subsequent applications in many domains is established through the acquisition of insights derived from structural, morphological, and compositional characterizations. The elucidation of the electrochemical stability of MXene structures is a crucial aspect in ensuring the sustained operation of electrochemical biosensors over an extended period. Through the expansion of the utilization of these artificially produced MXenes, this research establishes a foundation for the development of sophisticated electrochemical sensing systems capable of detecting a diverse array of analytes. This advancement holds substantial potential for making substantial contributions to both the biological and non-biological domains. In summary, this study exemplifies a dedication to novelty, accuracy, and ecological consciousness, and it has the potential to influence the trajectory of scientific and technological advancements by expanding the limits of what may be accomplished using MXenes.

Signature of advisor

_____

DR. SANAL KOZHIPARAMBIL CHANDRAN

Table of Contents

LIST OF FIGURES

LIST OF TABLES

CHAPTER 1: INTRODUCTION

This chapter presents a comprehensive examination of the key issues and concepts investigated in this thesis. The text provides an overview of the wider domain of nanomaterials, followed by an in-depth exploration of 2-dimensional nanomaterials, with specific emphasis on their synthesis methodologies and practical applications. The subsequent chapter delimits the focus to MXenes, which are 2-dimensional transition metal carbides, nitrides, and carbonitrides. The essay examines the importance of electrochemical sensors and delves into their significance within this particular environment. Furthermore, the chapter explores additional uses of MXenes, with a specific focus on their utilisation in the field of energy storage. The present study provides a concise overview of the anticipated scientific results, the formulated hypothesis, and the specific aims and goals. This comprehensive framework serves as a coherent guide for the reader, facilitating a clear understanding of the study's trajectory.

1.1 Introduction to Nanomaterials

In the past century, the field of nanotechnology has experienced significant growth and development. Currently, a wide range of research endeavours are either directly or indirectly linked to the field of nanotechnology. Nanotechnology encompasses the processes of generating, synthesising, characterising, and using materials and technologies through the manipulation of their size and shape at the nanoscale. The user's text is not provided. Please provide the text that needs to be rewritten in the prefix "nano" is consistently utilised as a term across various domains, including product promotion. The term "nano" is etymologically derived from the Greek word "nanos" or the Latin word "nanus," both of which translate to "dwarf." The amalgamation of physics, chemistry, material science, solid state, and biosciences is observed. A comprehensive understanding of multiple disciplines, including physics, chemistry, material science, solid state, and biosciences, is necessary, as expertise in a single field is insufficient. The utilisation of Nanotechnology is becoming increasingly prevalent across various disciplines within the realms of science and technology. The distinction between nanoscience and nanotechnology lies in their respective focuses. Nanoscience pertains to the

understanding of atomic arrangements and fundamental properties at the nanoscale. In contrast, nanotechnology involves the application of technology to manipulate matter at the atomic level, enabling the synthesis of novel nanomaterials with distinct characteristics[1]. Nanotechnology has garnered significant interest across various engineering disciplines. However, the general public remains mostly unaware of its presence in everyday life. Nevertheless, its extensive applications in fields such as medical, engineering, environment, electronics, defence, and security continue to expand[2]. Despite the extensive utilisation of this technology, there remains ample room for the advancement of unique nanomaterials across diverse domains to further the growth of humanity. The researchers are deeply intrigued and diligently engaged in advancing the frontiers of knowledge with regards to the dimensions, capabilities, and financial outlay associated with their work. The current emphasis on the miniaturisation of devices with cost-effectiveness primarily centres around the domains of medicine and electronics. In the foreseeable future, nanotechnology is anticipated to exert significant influence over various aspects of human existence, including living arrangements, occupational pursuits, and modes of communication. This engenders interest in the field, prompting a subsequent exploration of the fundamental and principal themes within nanotechnology. The fundamental and essential components of nanotechnology are referred to as "nanomaterials." Nanomaterials are defined as materials that possess dimensions of less than 100 nm in at least one of their dimensions. This implies that they possess significantly smaller dimensions compared to those of the microscale. Nanomaterials often exhibit dimensions on the order of 10^{-9} m, corresponding to one billionth of a metre. Nanomaterials exhibit distinct physicochemical characteristics compared to their bulk counterparts, a phenomenon that is intrinsically influenced by their size and shape. Remarkably, nanoparticles exhibit distinct properties and functionalities through the manipulation of their shape and size at the nanoscale. Nanomaterials exhibit various morphologies, such as nanorods, nanoparticles, and nanosheets, which can be classified according to their dimensional attributes. Nanomaterials can be classified into three categories based on their dimensional characteristics. Zero-dimensional nanomaterials refer to nanoparticles, while one-dimensional nanomaterials encompass nanorods or nanotubes. Two-dimensional nanomaterials typically manifest as films or layers. These categories primarily pertain to individual, isolated nanoparticles. The physical properties of particles can be altered

through their interaction with one another. The term "bulk" or "three-dimensional nanomaterials" refers to particles composed of various elements.

Nanoscale entities, with dimensions less than 100 nm, are categorised according to specific classifications.

- Zero-dimensional nanomaterials, often known as 0-D nanomaterials, are a class of materials that possess unique properties at the nanoscale. In this context, the dimensions of the nanomaterials are confined to the nanoscale range across all three axes. Nanoparticles can be categorised within this categorization.
- One-dimensional nanomaterials (1-D) refer to materials that exhibit nanoscale dimensions in one dimension, while the remaining two dimensions fall beyond the nanoscale range. Nanorods, nanotubes, and nanowires are pertinent to this particular academic discipline.
- Two-dimensional nanomaterials, sometimes known as 2-D materials, refer to materials where two dimensions are within the nanoscale range, while the remaining dimension is outside of this range. The aforementioned entities encompass nanofilms, nanolayers, and nanocoatings.
- Three-dimensional or bulk nanomaterials refer to materials that do not fall within the nanoscale range in any dimension. In three dimensions of arbitrary nature, the objects in question exhibit a scale greater than 100 nm. The aforementioned categories encompass nanocomposites, core-shell structures, multi-nanolayers, bundles of nanowires, and bundles of nanotubes[1].

Nanomaterials exhibit a diverse range of characteristics, which can be attributed to variations in their form, size, qualities, and constituent composition. The materials encompass carbon-based nanomaterials, metal nanoparticles, semiconductor nanomaterials, polymeric nanomaterials, and lipid-based nanomaterials.

- **Nanomaterials Composed of Carbon**

The primary component of this particular class of nanomaterials is carbon. Carbon nanotubes and fullerenes are closely associated with this particular category. The carbon nanotubes (CNTs) are encapsulated by graphene sheets that have been formed into a tubular structure. These materials possess significantly greater strength than steel and have the potential to be advantageous in enhancing structural integrity. Carbon nanotubes (CNTs) exist in two primary forms: single-walled and multi-walled. Fullerenes are a class of carbon-based nanoparticles

characterised by their distinctive hollow cage structure, often composed of sixty or more carbon atoms. The following are many forms of carbon allotropes. The structure of this object has resemblance to that of a hollow football, featuring pentagonal and hexagonal carbon units arranged in a regular pattern. The materials exhibit favourable electrical conductivity, electron affinity, and notable strength[3], [4].

- **Nanomaterials with a metal composition**

The initial constituents of the metal nanoparticles consist of divalent and trivalent metal ions. Various techniques exist for the synthesis of metal nanoparticles, including chemical and photochemical processes. The metal ions undergo reduction to become metal nanoparticles by the utilisation of reducing agents. These materials possess a significant surface area and exhibit a strong capacity for adsorbing tiny molecules. They are extensively utilised in several scientific domains, including environmental and bioimaging investigations[5]. Size control can be done not only with a single nanoparticle, but also by the mixing of two or more nanoparticles. The introduction of several metals, including rare earth metals, by doping can induce alterations in the fundamental features of the primary element. The properties of different constitutions vary when different elements are doped into them[6].

- **Nanomaterials in the field of semiconductors**

Semiconductor nanoparticles exhibit both metallic and non-metallic characteristics. The modification of broad band gaps results in the manifestation of distinct features. Photocatalysis and electrical gadgets frequently employ these materials in a widespread manner. Examples of group II-VI semiconductor materials include ZnS, ZnO, CdS, CdSe, and CdTe [7]. Gallium Nitride (GaN), Gallium Phosphide (GaP), Indium Phosphide (InP), and Indium Arsenide (InAs) belong to the group III-V compound semiconductors. In recent years, there has been a growing interest among researchers in semiconductor graphene nanocomposites. Graphene has the potential to enhance both the physical and chemical characteristics of semiconductors. Graphene composite materials can be employed for enhancing the gas sensing sensitivity through their piezoelectric capabilities[8][9].

- **Nanocomposites: A Review of Current Research and Applications**

The nanocomposite is a solid material consisting of many phases, wherein at least one phase possesses one, two, or three dimensions that are smaller than 100 nm. Nanocomposites exhibit a significantly elevated surface-to-volume ratio in comparison to conventional composites. The

physicochemical qualities may vary depending on the size and shape of the object. The topic under consideration is the concept of size. The activity being discussed has a size of less than 5 nm. The catalytic activity of particles with a size less than 20 nm. The objective is to convert the hard magnetic material into a soft magnetic material with a size below 50 nm. In order to modify the refractive index, it is necessary to manipulate the material at a scale smaller than 100 nm[10]. In order to attain super-paramagnetism various categories of nanocomposites exist, including those composed of nanoparticles. There exist various categories of nanocomposites, including Ceramic Matrix Nanocomposites (CMNC), Metal Matrix Nanocomposites (MMNC), and Polymer Matrix Nanocomposites (PMNC).

The development of polymer composites based on graphene has experienced significant growth in recent times. Graphene is comprised of carbon atoms. The carbon atoms are organised in a hexagonal matrix, forming a single layer. The material under consideration possesses a band structure characterised by a vanishing band gap, and its electrons exhibit properties akin to those of nearly massless particles. These electrons serve as effective charge carriers within a two-dimensional system, rendering the material a favourable electrical medium. Graphene oxide (GO) serves as the precursor of graphene, exhibiting significantly lower electrical conductivity. The process of converting graphene oxide (GO) to reduced graphene oxide (rGO) has been found to yield improved outcomes in terms of enhanced conductivity[11]. Various techniques, such as the Chemical Vapour Deposition (CVD) method[12], Exfoliation method[13], chemical reduction[14], thermal reduction[15], and multistep reduction method[16], can be employed to transform Graphene Oxide (GO) into Reduced Graphene Oxide (rGO). There exist various categories of semiconductor graphene family nanocomposites, namely metal oxide/graphene nanocomposites and metal chalcogenide/graphene nanocomposites. Metal oxides have a diverse range of applications. Zinc oxide (ZnO)[17], manganese dioxide (MnO_2)[18], titanium dioxide (TiO_2)[19], and iron(III) oxide (Fe_2O_3)[18] have been found to exhibit various activities such as photovoltaics, battery applications[20], photocatalysis, drug delivery[21] and gas sensing[22]. The fundamental primary function of these applications involves the interaction between matter and its surrounding environment.

- **Distinctive characteristics of nanomaterials**

Nanomaterials possessing dimensions below the crucial threshold of 100 nm exhibit distinctive and captivating features, hence generating significant interest in their study. The characteristics

exhibited by nanoparticles differ from those of their bulk counterparts. The macro-structured characteristics exhibit similarity to their bulk counterparts. Decreasing the particle size leads to an increase in the number of particles present on the surface. The coordination number of surface atoms is lower compared to that of inner atoms, resulting in enhanced mobility for the former. Nanomaterials find applications in diverse disciplines such as catalysis, functional coatings, adsorbents, nanoelectronics, and sensors, owing to their surface properties[1]. The features of excitation, emission, chemical reactivity, and stability also exhibit size-dependence when considering the nano-regime. The property of nanomaterials was not solely determined by their size, but also influenced by their shape. Quantum size effects are observed in nanoparticles when their size approaches the de Broglie wavelength limit, and their diameter is smaller than the quasiparticle interaction. The manipulation and control of nanomaterial qualities can be achieved through the deliberate regulation of their size throughout the synthesis process, employing various methodologies. The increased surface area enables their utilisation as catalysts. Metal nanoparticles are commonly employed as effective catalysts. The application of nanomaterials can be extended to various fields through the utilisation of surface phenomena[23]. The electronic properties of metals are determined by their electronic band structure. The band structure is contingent upon the size of the particles. The presence of delocalized bands can be observed within the molecular states. The band structure of nanocrystals lies intermediate to the discrete states exhibited by atoms and molecules, as well as the continuous bands observed in crystals. The energy separation between neighbouring lines is contingent upon the particle's size. When the size is decreased, the separation of energy levels rises. The metallic character exhibits a steady reduction, transitioning towards a semiconductor nature. Various types of magnetic materials exist, including diamagnetic, paramagnetic, ferromagnetic, antiferromagnetic, and ferrimagnetic materials. Soft and hard magnetic materials are distinct categories of magnetic materials that can be differentiated by their coercivity. Soft materials exhibit a low coercivity and possess a limited hysteresis area, rendering them susceptible to magnetization by a low-intensity magnetic field. The hard magnets are juxtaposed with this. The coercivity of a material is influenced by the size of its particles. In general, it has been observed that an increase in surface area and a decrease in grain size lead to an increase in coercivity and saturation magnetization. The nanoparticles exhibit a larger surface area-to-volume ratio due to their reduced grain size, resulting in enhanced magnetic strength. In the event that the particle size is reduced, the ferromagnetic particles undergo a transition to paramagnetic materials as a consequence of their increased instability. Paramagnetic materials exhibit distinct behaviour compared to their bulk

counterparts, leading to their classification as superparamagnetic. Magnetic materials find utility in a wide range of applications, including but not limited to data storage capacity, electronic circuits, actuators, transformers, and power generators, among others[3].The nanomaterials have unique optical characteristics. The phenomenon of light interacting with a material is commonly referred to as its optical property. This property is influenced by various factors, including the material's size, shape, doping, surface properties, and the nature of its surrounding environment. The observed feature is attributed to the presence of surface plasmons and the quantum confinement of electrons. The surface plasmon resonance energy is determined by the free electron density and the dielectric medium of the nanomaterial. The gold particle demonstrates the occurrence of the surface plasmon resonance band at a wavelength of 520 nm, while for silver, this phenomenon is observed at a wavelength of 410 nm. The phenomenon of size-dependence The optical qualities of a material are contingent upon its size. As an example, it can be observed that CdSe nanoparticles with a diameter of 2.3 nm exhibit blue light emission, while CdSe nanoparticles with a diameter of 5.5 nm exhibit red light emission. Nanomaterials possess optical properties that can be utilised in polymers to enhance their refractive index. LCDs and LEDs have the capability to produce higher quality images. Optoelectronic materials can be potentially utilised in several applications. The properties of nanomaterials are primarily contingent upon their size and form. The manipulation and control of nanomaterial qualities can be achieved through the regulation of their size throughout the synthesis process, employing various methodologies.

The synthesis of nanoparticles can be achieved by three distinct methodologies. The items listed are as follows. The three primary categories of procedures utilised in scientific research include biological methods, physical methods, and chemical approaches[23].

- **Synthesis of nanomaterials using microorganisms**

The biological methodology is characterised by its simplicity, ease of implementation, typically involving a single procedural step, and its environmentally beneficial nature. In the present context, microbes and various plant components can be employed for the synthesis of nanomaterials[24]. Various types of microorganisms, such as bacteria, fungi, and algae, have the potential to be utilised in the synthesis of diverse nanomaterials derived from aqueous solutions containing metal salts. Through the process of biomineralization, living organisms

engage in the synthesis of nanoparticles by employing a protein. In anaerobic environments, magnetotactic bacteria utilise magnetosomes, protein-coated structures, to synthesise nanosized magnetic iron oxide crystals[25]. These crystals serve as a compass, enabling the bacteria to orient themselves towards their preferred habitat located at the bottom of the sea. Under laboratory circumstances, it is possible to generate particles that are homogeneous with a core diameter ranging from 20 to 45 nm. Despite these factors, magnetosomes demonstrate favourable magnetic characteristics in medicinal applications, potentially serving as a means of hyperthermia treatment. The utilisation of photosynthetic bacteria, such as Rhodopseudomonas capsulata, In their study, He et al. successfully synthesised gold nanoparticles with a size range of 10-20 nm by an extracellular method. The enzymatic reduction of gold ions to gold nanoparticles is predominantly facilitated by the bacterial enzyme Nicotinamide Adenine Dinucleotide Hydride (NADH)-dependent reductase[26]. The researchers made an observation that the pH of the growing media has an influence on the structure and morphology of the nanoparticles. Schluter et al. reported on the extracellular synthesis of palladium nanoparticles through the utilisation of Pseudomonas bacteria derived from the alpine site[27]. The utilisation of the Fusarium oxysporum fungus was employed in the production of extracellular silver nanoparticles. The nanoparticles exhibit long-term stability owing to the enzymatic activity of NADH-reductase. Fungal cells exhibit a greater degree of protein production compared to bacterial cells[28]. Currently, T. reesei is extensively utilised in several industries such as food, animal feed, medications, paper, and textile. Singaravelu and colleagues (year) presented a method for the synthesis of extracellular gold nanoparticles using Sargassum wightii algae. A production rate of 95% was attained within a 12-hour incubation period. Insufficient attention has been given to the investigation of nanoparticle synthesis by the utilisation of algae. One of the drawbacks associated with this particular method is the presence of dangerous bacteria, fungi, and algae, necessitating the implementation of safety measures. The production of nanomaterials within an organism can be performed through the use of biological processes. Biological templates serve as the primary instruments for attaining this objective. Unique and sophisticated nanostructures are generated by the use of biological templates such as DNA and proteins. Biosensors[29], bio NEMS, and bioelectronics systems can be constructed utilising nanoparticles[30]. Proteins serve as the primary constituent elements in the composition of nanocomposite materials. In both prokaryotes and eukaryotes, the protein responsible for intracellular iron storage is known as Ferritin. The substance is stored in the chemical composition of iron oxide and subsequently released in a regulated manner. In the context of human physiology, it serves as a regulatory

mechanism, maintaining homeostasis in relation to both iron deficiency and iron overload states. The structure consists of a protein shell that encapsulates an iron oxide core. To acquire apoferritin, the iron oxide core can be selectively dissolved without causing harm to the encompassing protein structure. Iron oxide or other desirable nanoparticles can be placed within the vacant core of Apoferritin. The protein-inorganic nanocomposite has been successfully synthesised. The gold nanoparticles were synthesised by Fan et al. in horse spleen ferritin[31]. Wu et al. synthesised yttrium phosphate radionuclide nanoparticles within the apoferritin protein cage and subsequently conjugated them with biotin[32]. Gold nanoparticles of various shapes are synthesised using the biomass derived from the plants Medicago sativa (commonly known as lucerne) and Pelargonium graveolens (also known as Geranium). Bimetallic gold (Au), silver (Ag), and bimetallic Au core-Ag shell nanoparticles are fabricated using Azadirachta indica (neem) leaves as a precursor[33]. The sugars and/or terpenoids present in this plant function as effective reducing agents. Gold nanotriangles are synthesised using an extract derived from the leaves of Aloe vera. Silver, nickel, cobalt, zinc, and copper nanoparticles can be synthesised by the utilisation of several plant species such as Brassica juncea (commonly known as Indian mustard)[34] and Helianthus annuus (often referred to as sunflower)[35].

- **Physical route of synthesis of nanomaterials**

The physical methods can be classified into two main categories, namely the "top-down" and "bottom-up" approaches. The "top-down" strategy involves the utilisation of mechanical milling process to reduce big materials into smaller particles. One primary drawback associated with this approach pertains to the challenge of achieving the correct particle size and form. The magnetic characteristics of the prepared samples, obtained through the milling process, exhibit a variation when compared to regular particles of equivalent size[36]. This deviation can be attributed to the flaws in the lattice parameters that arise as a result of the milling process. The "bottom-up" approach involves the condensation of nanoparticles in either a liquid or gaseous phase, resulting in the formation of larger materials through the chemical combination of smaller ions. Laser evaporation is a highly promising bottom-up technique utilised in the creation of magnetic nano powders. The laser has been employed for the purpose of vaporising the initial metal oxide compounds that serve as the precursor materials in the synthesis process. Therefore, the formation of nanoparticles occurs beyond the evaporation zone by rapid

condensation and nucleation resulting from the significant temperature difference. The manipulation of laser intensity and atmospheric composition within the evaporation chamber allows for the alteration of particle size and magnetic phase[37]. Another physical technique that can be employed is the RF Plasma approach, which necessitates the application of elevated temperatures. The metal within the evacuated system is heated to a temperature beyond its evaporation point through the utilisation of high voltage RF coils that are enveloping the system[23]. Subsequently, helium gas is introduced into the system, causing the coils within the designated area to attain elevated temperatures. Metal vapour nucleation happens on helium gas atoms. The process of diffusion facilitates the entry of the substance into the collecting rod, which is at a lower temperature, leading to the formation of nanoparticles. The thermal breakdown is a result of the application of heat. The reaction under consideration is classified as an endothermic process. The application of heat induces the disruption of chemical bonds within the complex, leading to its fragmentation into smaller constituent entities. Hyeon et al conducted the synthesis of iron oxide nanoparticles using the thermal decomposition method[38]. In the field of biomedicine, monodispersed nanoparticles have emerged as a favourable option for the treatment of cancer. Kelly et al. suggested that the utilisation of coordination compounds and metallocenes as precursors is most suitable for the synthesis of monodispersed nanoparticles through thermal breakdown[39]. Prior to performing the thermal breakdown, it is necessary to submit the coordination compounds to stabilising agents and capping agents. The alteration of size and morphology can be achieved by modifying stabilising agents and capping agents, adjusting the concentration of precursors or solvents, or manipulating the reaction time. In certain instances, the stabilising agent may also serve as a capping agent. For example, the production of tiny lithium particles can be achieved through the use of lithium azide, denoted as LiN_3. The material is introduced into a quartz tube that has been evacuated, and subsequently heated to a temperature of 400 °C. The compound LiN_3 undergoes thermal decomposition at around 370 °C, resulting in the liberation of nitrogen gas (N_2). Following a brief period, the entirety of the N_2 gas is eliminated, resulting in a subsequent decrease in pressure. The unreacted lithium atoms undergo a process of combination, resulting in the formation of colloidal particles composed of the metal. This approach enables the production of nanoparticles with a minimum size of less than 5 nm[40].

- **Chemical route of synthesis of nanomaterials**

The chemical method offers a diverse range of bottom-up synthesis strategies for the creation of nanoparticles. This approach is mostly applicable to both gas and liquid phases. The

utilisation of this approach facilitates the attainment of particle size that is both pure and controlled. The bottom-up technique encompasses many methodologies employed in the synthesis of nanoparticles. The optimal method for preparation of nanocomposites is determined by factors such as the size and type of nanomaterial, the ease of the method, and the qualities of the resulting nanocomposite. The many processes employed for synthesis include sol-gel method, intercalation, ion-exchange , vapour deposition, hydrothermal technique co-precipitation, sonochemical, , solvothermal, microemulsion and microwave aided[41]. The method described is a commonly employed and straightforward approach for the synthesis of diverse nanoparticles. The utilisation of an aqueous medium is necessary for the process of precipitation in this approach. The co-precipitation method is a process that entails the combination of two or more water-soluble salts containing divalent and trivalent metal ions. The soluble salts primarily consist of trivalent metal ions. The water-soluble salts undergo a chemical reaction and are ultimately reduced to generate at least one salt that is insoluble in water, resulting in precipitation. The solution must be continually stirred, potentially in accordance with the heat conditions dictated by the reaction parameters and the specific reducing agent employed. Typically, the utilisation of this approach results in a reduction of the crystalline characteristics exhibited by the particles. The application of heat energy can be utilised to increase the level of crystallinity inside the particles[42]. The entire process is sustained inside an alkaline environment with the addition of typical reducing agents such as ammonia solution, sodium hydroxide, and other substances, in order to maintain the necessary pH level[43]. The size of nanoparticles is influenced by various parameters, including the ratio of the chosen salt, the pH of the solution, the temperature of the reaction medium, and the type of base employed. The solvent can be effectively isolated and subsequently purified and dehydrated using the processes of filtration or centrifugation. Doped ferrites can be created by introducing several rare earth metals into the ferrite material. The utilisation of nanoparticles of extremely small dimensions is necessary in biomedical applications[44]. By employing this approach, it is possible to synthesise biocompatible nanoparticles as well. The primary stages involved in this process are nucleation and growth. Nucleation refers to the phenomenon wherein the smallest elementary particles of a new thermodynamic phase come into existence. The degree of supersaturation is the primary determinant of the nucleation process. In a state of supersaturation, the concentration of dissolved elements in a solution exceeds the maximum solubility of the solvent. The concentration of the solute surpasses the solubility at equilibrium. During the growth process, larger particles undergo a reduction in surface energy by assimilating smaller particles. The

phenomenon being referred to is commonly referred to as coarsening or Ostwald ripening. Agglomeration may also occur as a means to reduce surface energy. If the coarsening and agglomeration processes are not effectively controlled, there is a risk that the particles may undergo further growth beyond the nanoscale range. Certain capping or stabilising compounds have been found to be beneficial in inhibiting the growth of nanomaterials. The capping agents form a binding interaction with the surface of the nanoparticle through chemisorption of charged species, resulting in the generation of electrostatic (van der Waals) repulsion on the nanoparticle's surface[40]. The formation of stable nanoparticles is contingent upon the presence of strong repulsive forces, as their absence may lead to the occurrence of coagulation. Initially, the sol-gel technique was devised to fabricate glass and ceramic materials under low-temperature conditions. In this approach, the metal alkoxide solution is subjected to hydrolysis with water or alcohols in the presence of an acid or base, which is subsequently followed by polycondensation. The transition from the liquid phase to the gel phase was facilitated by polycondensation, which involved the loss of water molecules from the solution and resulted in an increase in solution viscosity. Once all the water molecules have undergone condensation, the gel phase undergoes a transition into the powder phase. The attainment of a fine crystalline structure in the powder necessitates the application of more heat. The technique proved to be advantageous in the synthesis of various oxides, composites, and hybrids comprising both organic and inorganic components. The sol-gel method is founded upon the principles of inorganic polymerization processes. The primary benefit of this approach lies in its straightforward methodology[45]. However, the method's purity is diminished as a result of the creation of composites inside it. Post-treatment of the sample is necessary for its purification. The hydrothermal process involves subjecting the solutions to elevated pressure and temperature conditions. One notable benefit of employing this particular approach lies in its ability to facilitate the production of high-quality crystals while simultaneously allowing for precise control over their composition[46]. The divalent and trivalent transition metal salts are combined in a 1:2 molar ratio. In order to obtain the homogenous solution, it is necessary to combine the organic solvent with continuous stirring to the aforementioned solution. Subsequently, the solutions are introduced into the hermetically sealed container, generally referred to as an autoclave or bomb. The application of heat induces an autogenous rise in pressure, resulting in the direct elevation of the solvents beyond their respective boiling points. The temperature adjustment and duration of synthesis are contingent upon the specific characteristics of the nanoparticle under consideration. This technology demonstrates efficacy in producing nanoparticles of minimal size suitable for utilisation in the realm of biology.

Copper ferrites, a commonly employed type of magnetic nanoparticle, were synthesised utilising the hydrothermal method, and afterwards, their cytotoxic properties were evaluated through the MTT test[47]. The biological reaction of MCF-7 human breast cancer cells was detected[48]. The production of nanoparticles with regulated and desired size, shape, and surface chemistry can be achieved through the careful selection of appropriate solvents and the manipulation of many parameters such as temperature, pressure, pH, ageing time, reactant concentration, and reaction duration. This technology enables the production of nanoparticles with a high degree of homogeneity. The approach described does not allow for the creation of nanoparticles of the smallest size in the desired crystalline phase at relatively lower temperatures, unless post-annealing treatments are employed. The utilisation of this approach garnered a greater level of interest from researchers in comparison to conventional procedures. This process is employed to synthesise several materials, including single crystals, zeolites, oxides, doped metals, selenides, and sulphides. The sonochemical approach is considered to be both safe and efficient in terms of speed. The cavities (bubbles) are generated with the application of ultrasonic irradiation within a liquid medium using this particular technique. The ultrasonic energy disperses inside the medium, resulting in an elevation of the internal energy of the bubble. This energy rise is accompanied by a high temperature of around 5000 K and a pressure of 20 MPa. Consequently, the bubbles undergo autogenous collapse, leading to the chemical stimulation of the matter both within the bubbles and in their vicinity. This methodology demonstrates utility in the production of metallic compounds such as cobalt disulfide (CoS2), alloys, oxides, and selenides including cadmium selenide (CdSe) and zinc selenide (ZnSe)[49]. The utilisation of the microwave assisted approach originated in the 1950s, however, its widespread acceptance has primarily been achieved within the past two decades. Microwave radiation is employed to induce thermal energy transfer to materials by the excitation of mobile electric charges via electromagnetic radiation. In this process, electromagnetic energy undergoes conversion into thermal energy. The frequency spectrum utilised falls within the region of 1 to 2.5 GHz, resulting in the generation of temperatures ranging from 100 to 200 °C[50]. A reduced response time is necessary in order to expedite the completion of time-consuming reactions within a few minutes. This process enables the preparation of small size particles with a limited size distribution. This process is utilised for the preparation of colloidal metals, ferrites, oxides, and selenides[51]. The microwave polyol technique, which was invented by Fievet et al., is an enhanced method of microwave synthesis. When exposed to polyalcohols, the metal precursors undergo microwave irradiation. Subsequently, the metals are generated in the form of colloids.

- **Application of Nanomaterials**

The following are notable applications of nanoparticles.

- **The Field of Cosmetics and Sunscreens**

The typical sunscreen designed to provide protection against ultraviolet (UV) radiation exhibits limited durability over extended periods of use. The utilisation of nanoparticles, such as titanium dioxide, in sunscreen offers a multitude of benefits. The utilisation of titanium oxide and zinc oxide nanoparticles in certain sunscreens has been attributed to their UV protection capabilities, which arise from their transparency to visible light and their ability to absorb and reflect UV radiation. Certain lipsticks incorporate iron oxide nanoparticles as a form of pigment[18].

- **The Field of Electronics**

The increasing need for larger and brighter screens in computer monitors and televisions has prompted the exploration of nanoparticle utilisation in display technologies[52]. Nanocrystalline lead telluride, cadmium sulphide, zinc selenide, and sulphide are commonly employed in the light emitting diodes (LEDs) found in contemporary display technologies[53]. The proliferation of portable consumer devices, including as mobile phones and laptop computers, has resulted in a significant surge in the need for batteries that are compact, lightweight, and possess high capacity. Nanoparticles represent a highly favourable option for the implementation of separator plates inside battery systems. The foam-like (aerogel) structure of these batteries enables a significantly higher energy storage capacity in comparison to conventional batteries. Batteries composed of nanocrystalline nickel and metal hydrides exhibit enhanced performance characteristics, such as reduced recharging requirements and extended lifespan, owing to their substantial surface area. The utilisation of nanoparticles' enhanced electrical conductivity has been employed for the purpose of gas detection, specifically for gases such as NO_2 and NH_3[54]. The observed phenomenon can be attributed to the augmentation of nanoparticle porosity resulting from the transfer of charge from nanoparticles to NO_2, which facilitates the binding of gas molecules and enhances their efficacy as gas sensors.

- **Catalysis**

Catalysis, in the context of chemical reactions, refers to the process by which a catalyst facilitates the conversion of reactants into nanoparticles possess a significant surface area,

which results in enhanced catalytic activity. The nanoparticles exhibit high catalytic efficiency in chemical synthesis owing to their significantly increased surface-to-volume ratio. One prominent use pertains to the utilisation of platinum nanoparticles in automotive catalytic converters. This application is noteworthy as it allows for a reduction in the needed amount of platinum, owing to the nanoparticles' exceptionally large surface area[55]–[57]

. Consequently, this reduction in platinum quantity leads to a substantial decrease in cost and an enhancement in performance. Nanoparticles are utilised in various chemical reactions, such as the reduction of nickel oxide to produce metallic nickel (Ni)[58].

- **In the field of Medicine**

Medicine refers to the field of study and practise that encompasses the diagnosis, The application of nanoparticles in medication delivery has significantly enhanced the medical domain, thanks to the advancements in nanotechnology[59]. Nanoparticles can serve as a means of targeted medicine delivery to certain cells. The administration of drugs in the appropriate anatomical site and prescribed dosage leads to a notable reduction in overall drug consumption and associated adverse effects. This approach effectively mitigates both the financial burden and adverse effects. Tissue engineering, which involves the replication and restoration of damaged tissue, can be facilitated through the utilisation of nanotechnology[60]. Tissue engineering has the potential to supplant conventional therapeutic approaches, such as artificial implants and organ transplants. An illustrative instance is to the proliferation of bone carbon nanotube scaffolds. The utilisation of gold in the field of medicine has a longstanding history. Gold is utilised in several practises within Ayurveda, an ancient Indian medical system. An often prescribed intervention is the utilisation of gold as a means to increase memory function. To improve the cognitive well-being of an infant, gold is incorporated into specific pharmaceutical formulations[61], [62].

- **Food Technology**

Food Nanotechnology is utilised to enhance the manufacturing, processing, preservation, and packaging of food[63]. An illustration of the application of nanocomposite coatings in the food packaging industry is the direct incorporation of antimicrobial agents onto the surface of the coated sheet. An illustrative instance pertains to the canola oil production sector, whereby nanodrops, an additive specifically formulated to facilitate the transfer of vitamins and minerals within food, are employed[64], [65].

- **Construction**

The utilisation of nanotechnology has resulted in enhanced construction processes, characterised by increased efficiency, reduced costs, and improved safety measures. An instance of enhanced mechanical qualities and durability in concrete can be observed when nanosilica (SiO_2) is incorporated into the mixture[66]. The incorporation of haematite (Fe_2O_3) nanoparticles enhances the mechanical properties of the concrete. Steel is the predominant and extensively utilised material within the building sector due to its widespread availability[67]. The application of nanotechnology in steel has been found to enhance its qualities, as exemplified by its implementation in bridge construction. Specifically, the utilisation of nano-sized steel has been observed to yield stronger steel cables. Another significant construction material is glass. Considerable research is currently being conducted to explore the potential applications of nanotechnology in the field of construction glass. Titanium dioxide (TiO_2) nanoparticles are utilised for glazing coating due to their sterilising and anti-fouling qualities, as well as their ability to catalyse potent chemical reactions that degrade volatile organic compounds (VOCs) and organic contaminants[68]. The utilisation of nanotechnology offers enhanced light and heat obstruction capabilities for windows. The incorporation of nanoparticles into paint formulations enables the development of paints that possess self-healing capabilities, corrosion resistance, and enhanced insulating properties. The hydrophobic nature of these paints provides water repellency, making them suitable for the use of coating metal pipes to provide defence against corrosion caused by saltwater exposure. The incorporation of nanoparticles into paint formulations has been found to enhance their performance characteristics, resulting in lighter weight paints with improved properties. This has potential benefits in various applications, such as the use of nanoparticle-infused paints on aircraft, where it could potentially reduce the overall weight of the aircraft and the quantity of paint needed. These outcomes are advantageous not only from an environmental standpoint but also for companies seeking to achieve cost savings.

- **The Utilisation of Renewable Energy Sources for Environmental Remediation**

The distinctive physical and chemical characteristics exhibited by nanoparticles have rendered them a very suitable option for utilisation in contemporary environmental cleanup efforts, as well as for augmenting the efficacy of renewable energy systems. Naturally occurring nanoparticles have been observed to possess environmental remediation properties. Nanoparticles, also known as nanoremediation, have been effectively employed for more than

ten years in the field of environmental remediation to clean and decontaminate air, water, and soil[69]. Nanoremediation is considered an efficacious approach because to its ability to provide in situ treatment, hence obviating the requirement for groundwater extraction and excavation to access the intended site. The nanoparticles are introduced via injection into the targeted site, where they are subsequently transported by the subsurface flow of groundwater. Through their immobilisation properties, these nanoparticles effectively mitigate the presence of contaminants, resulting in water decontamination. Redox reactions are the fundamental mechanism involved in the process of decontamination. Nanoparticles are employed for the purpose of surface water treatment through processes such as disinfection, filtration, and desalination. It is quite probable that certain contaminants present in the environment consist predominantly of heavy metals, microorganisms, and organic contaminants[70]. It has been demonstrated to be effective in reducing reliance on chemical substances that can occasionally generate secondary reaction byproducts. The global issue of oil spills is a significant concern due to their potential to disperse over extensive geographical areas. The task of cleaning them using traditional methods poses challenges in terms of difficulty and time consumption, exacerbating the situation by perhaps facilitating further spread. Nanoparticles are employed for the purpose of oil spill remediation and have been demonstrated to be an efficacious approach. Nanoparticles are primarily employed for the purpose of treating both municipal and industrial wastewater, in addition to the sludge generated during the treatment process. The substitution of nanoparticles in place of traditional chemicals is attributed to reduced costs, enhanced efficacy, and decreased treatment quantities. Nanofiltration is a relatively new membrane filtration technique that has gained significant popularity in the field of water purification, particularly within the food and dairy sectors. The issue of soil contamination is also becoming a growing concern. The remediation of contaminated soil involves the utilisation of nanoparticles, which are introduced into designated areas with high concentrations of heavy metals, hazardous industrial waste, and similar contaminants. The increased surface area shown by specific nanoparticles has been effectively utilised as a nanocatalyst in gaseous processes. One of the most commonly employed applications of this technology is in industrial stacks, where it is utilised to mitigate the concentration of contaminants to meet predetermined thresholds or to eliminate them entirely, hence mitigating air pollution. Considerable investigation is currently being conducted in the realm of nanoparticle utilisation for the purpose of renewable energy[71]. The efficiency of solar cells has been significantly enhanced with the implementation of coatings that exhibit heightened light and UV absorption capabilities, along with less reflection. The self-cleaning functionality of solar cells has been

achieved through the use of hydrophobic nanoparticles. The application of nanoparticles with high thermal conductivity and heat absorption capacity has been employed to enhance the thermal efficiency of boilers and solar concentrators through their coating.

- **Role of nanomaterials in Electrochemical sensing**

The incorporation of nanomaterials into the domain of electrochemical sensors has initiated a significant transformation within the discipline of analytical chemistry. Nanomaterials, including substances like graphene, carbon nanotubes (CNTs), metal nanoparticles, and others, possess remarkable properties that revolutionise the boundaries of detection, sensitivity, and selectivity within sensor technology. The exceptional surface-to-volume ratio is considered to be one of the defining properties of nanomaterials. The distinctive characteristic, which is particularly prominent in two-dimensional materials such as graphene and carbon nanotubes (CNTs), facilitates a significant augmentation in the accessible surface area for electrochemical processes[72]. Consequently, electrodes that have been changed with nanomaterials demonstrate a notable increase in sensitivity when compared to electrodes without such modifications. The extensive surface area offers numerous locations for the adsorption of the target analyte and catalytic reactions, hence enhancing the electrochemical signal produced during their interaction. An illustration of the notable sensitivity exhibited by electrodes modified with graphene is their ability to detect neurotransmitters such as dopamine, even at concentrations as low as picomolar levels[73]. This characteristic is of utmost importance in the realm of neurological illness research, as it aids in the comprehension of these conditions. Nanomaterials function as highly adaptable electrode materials that can be customised to meet the requirements of various sensing applications. Graphene's remarkable electron mobility and electrical conductivity render it a very suitable contender for electrochemical transduction[74]. The shape of a single atom layer enables efficient electron transport between the electrode and analyte, leading to fast response times and high sensitivity in detecting analytes. In a similar vein, the utilisation of carbon nanotubes in sensor design has been widespread due to their exceptional mechanical and electrical characteristics. The tubular construction of the object facilitates a channel for conduction and can be modified to improve the selectivity of the analyte. Carbon nanotube-based sensors have been utilised in the identification of diverse gases, such as NO_2 and NH_3, for the purpose of environmental monitoring[75]. Nanomaterials possess a significant advantage in terms of their inherent flexibility. The surfaces of these materials can be carefully modified to produce a high degree of selectivity towards specific analytes. The significance of this characteristic is especially vital when dealing with intricate

sample matrices, such as biological fluids or environmental samples, as the presence of other species might complicate the precision of measurements. By carefully selecting appropriate functional groups or nanoparticles, it is possible to design nanomaterial-based sensors that specifically detect and react to the desired analyte. An example of a potential application involves the functionalization of gold nanoparticles through the attachment of certain ligands[76]. This process can result in the development of sensors that exhibit great selectivity towards heavy metal ions present in water samples, hence minimising the potential interference from other ions. Metal nanoparticles, such as gold and platinum, exhibit remarkable electrocatalytic properties and find extensive utility in various electrochemical sensing applications[77]. The utilisation of nanoparticles can expedite electrochemical reactions that would otherwise occur at a slow rate, hence improving the efficiency of analyte detection. Gold nanoparticles have been widely recognised for their remarkable catalytic properties in facilitating the oxidation of diverse analytes, such as glucose and hydrogen peroxide. The catalytic activity of this process significantly decreases the necessary operating potential, resulting in decreased interference and enhanced sensor performance. The integration of nanomaterials and electrochemistry has spurred progress in various disciplines. Nanomaterial-based sensors have significantly transformed point-of-care testing in clinical diagnostics by facilitating the rapid and accurate identification of biomarkers associated with diseases such as diabetes, cancer, and infectious pathogens[78]. Within the field of environmental monitoring, sensors have been utilised to detect several types of pollutants, including heavy metals and microbiological contaminants. Nanomaterials are of significant importance in the energy sector as they contribute significantly to the advancement of sophisticated energy storage devices, such supercapacitors and lithium-ion batteries. Although the potential of nanomaterials in electrochemical sensors is undoubtedly exciting, there are still some obstacles that need to be addressed. These encompass concerns pertaining to the reproducibility, scalability, and long-term stability of the subject matter. Moreover, it is imperative to thoroughly evaluate the possible toxicity of specific nanomaterials, especially when applied in biosensing contexts. In summary, the incorporation of nanomaterials into electrochemical sensors has initiated a novel phase in the field of analytical chemistry. These materials provide sensors with exceptional levels of sensitivity, selectivity, and adaptability. Through continuous research and development, the use of nanomaterial-based sensors holds the potential to bring about a significant transformation in various domains, including healthcare and environmental monitoring. These sensors provide enhanced capabilities in terms of sensitivity, specificity, and

speed, so presenting promising prospects for the advancement of analytical instruments in the times to come[73], [79], [80].

1.2 2-Dimensional Nanomaterials (Synthesis and Application)

The scientific community has shown significant interest in two-dimensional (2D) nanostructures since the discovery of graphene in 2004. This attention is mostly due to the unique physicochemical features exhibited by these nanostructures, which can be linked to factors such as the quantum size effect, peculiar surface shape, and high aspect ratio. Additionally, these materials possess a significant surface area, exhibit great stability, can be synthesised in a cost-effective manner, demonstrate remarkable physiochemical and mechanical capabilities, exhibit intercalated morphological features, and possess piezoelectric coupling properties. Due to their exceptional characteristics, two-dimensional (2D) materials have opened up several potential applications in various fields including photocatalysis, electrocatalysis, energy production, bioimaging, biomedicine, environmental applications, fuel cells, solar cells, batteries, and sensing[81].

Graphene, the prevailing two-dimensional (2D) nanomaterial, consists of a solitary layer of carbon atoms that are organised in a hexagonal arrangement within a two-dimensional plane. The emergence of graphene, characterised by its unique optoelectronic capabilities, large surface area, exceptional thermal conductivity, impressive tensile strength, and high Young's modulus, has generated significant interest among researchers and enterprises involved in nanotechnology. Graphene has been employed in diverse applications, including but not limited to energy storage devices, biological sensing, and high-speed electrical and optical systems[82]. Consequently, subsequent to the discovery of graphene, researchers have exhibited significant enthusiasm in the exploration of two-dimensional (2D) nanomaterials. This pursuit encompasses a diverse range of materials, spanning from metals to insulators, semiconductors, and even superconductors. These 2D nanomaterials exhibit distinct properties in comparison to their bulk counterparts. Following extensive research conducted in the field of 2D nanomaterials, a number of novel 2D nanomaterials have been successfully synthesised. These materials exhibit exceptional characteristics and occasionally surpass the performance of graphene. The electron confinement phenomenon in single-layered 2D nanomaterials results in exceptional electrical characteristics. Nanomaterials possess a notable surface area due to

the presence of exposed edge sites, as well as atomic-level flexibility. These characteristics render them well-suited for applications in optoelectronics and transparent electrical devices. Based on existing scholarly sources, it has been observed that the reactivity of nanomaterials' edge sites surpasses that of their basal planes. This heightened reactivity can be attributed to the abundance of active sites located on the edges, facilitating the intercalation process with ions and electrolytes. In addition to graphene, there are several prominent 2D nanostructures that are now seeing a surge in popularity. These nanostructures can be categorised into various sorts or classifications. Several popular materials including graphitic carbon nitride (g-C_3N_4), 2D layered metal hydroxide, germanene, transition metal dichalcogenides (TMDs), silicene, 2D metal oxides (Fe_3O_4, NiO, Co_3O_4), phosphorene, 2D metal nanoparticles, 2D polymers, and 2D crystals such as metal-organic framework (MOF)[83]–[87].

- **Synthesis of 2D nanomaterials**

The inherent characteristics of 2D nanomaterials, such as their crystal structure, crystal size, chemical and physical properties, render them highly suitable for the production of advanced materials in the new-generation. Within the existing body of literature, a multitude of techniques have been documented for the production of two-dimensional nanomaterials. These synthesis methods can be roughly classified into two distinct approaches: the top-down and bottom-up methodologies. The top-down approach is a method characterised by its destructive nature, involving the formation of nanoparticles through the removal of the components from the base material or the cutting and scaling of atomic crystal surfaces[88]. On the other hand, the bottom-up strategy, also known as the gathering up method, involves the synthesis of nanoparticles through the assembly of simpler units or atoms[89]. In this procedure, atoms are added to the substrate in order to build the nanomaterial. The top-down approach is classified into many categories, as seen in ***Figure 1***. In comparison, the bottom-up strategy is a somewhat simpler method for synthesising 2D nanomaterials. This methodology holds greater significance for researchers due to its lower energy consumption and the reduced occurrence of flaws in the nanostructure. The prevalent procedure of synthesis employed in bottom-up approaches is depicted in **Figure *1***. Indeed, it is accurate to assert that these two methodologies are widely recognised as the predominant approaches for the synthesis of two-dimensional nanomaterials. Nonetheless, it is a verifiable fact that scientists have devoted significant efforts

over the course of several decades to explore novel approaches aimed at facilitating the synthesis process and enhancing the output of nanomaterials by utilising minimal precursor quantities. In the subsequent sections, a comprehensive analysis of the both top-down and bottom-up procedures has been presented.

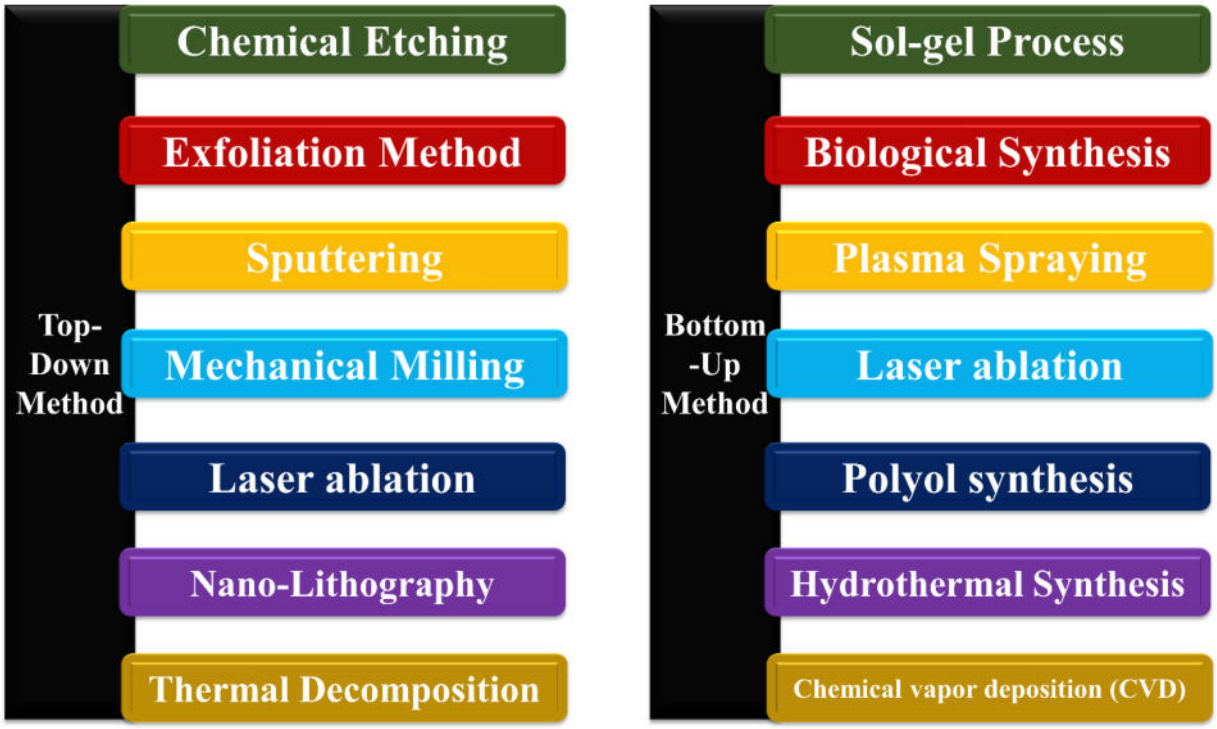

Figure 1: Top-Down and Bottom-Up approach for the synthesis of Nanomaterials

- **Bottom-Up Approach**

Various methodologies have been employed and documented in the scientific literature in order to attain the intended chemical composition, dimensions, morphology, stacking configuration, crystal lattice, and surface or edge irregularities. The subsequent sections will examine many of these approaches, first with the bottom-up methodology employed in the synthesis of two-dimensional nanomaterials. The hydrothermal synthesis approach has gained significant recognition among researchers as a highly esteemed method for synthesising 2D nanomaterials. The semantic content of the term "hydrothermal" can be deduced from its constituent parts: "hydro" refers to water, while "thermal" pertains to heat. Consequently, hydrothermal processes include the application of elevated temperature and pressure in a moist environment[90]. The precursor ingredients are combined and confined within a singular reaction vessel, typically

referred to as a hydrothermal vessel, for the course of this procedure. The hydrothermal vessel operates at high-pressure conditions. In this procedure, the solvent functions as a catalyst in facilitating the formation of nanoparticles. The approach has numerous benefits, including cost-effective instrumentation, high product yield, environmentally sustainable procedures, and the ability to synthesise various morphological variants of nanomaterials with precise size control. The procedure does not necessitate the use of costly catalysts or detrimental surfactants, hence yielding crystals of superior quality. This process has the potential for modification by the integration of additional processes, techniques, or devices, such as ultrasound, microwave, electrochemistry, and hot pressing. The synthesis of Bi-TiO_2 nanotube/graphene composites was conducted by Alam et al. using a straightforward hydrothermal synthesis method[91]. Chemical vapour deposition (CVD) is a widely employed gas phase technique utilised for the production of thin films or crystals by the deposition of solid materials[92]. Chemical vapour deposition (CVD) involves the introduction of volatile precursors in their gaseous state into a chamber, where they undergo a reaction at room temperature. Thin films of the desired product are present on the surface of the substrate, and the method does not include a specific chemical reaction. Thin film materials with variable sizes ranging from nanometers to millimetres, exhibiting diverse chemical and physical properties, can be generated by manipulating the substrate, temperature, pressure, and gas mixture concentration. CVD offers several advantages, including the ability to produce films that exhibit uniformity, low porosity, high purity, and stability. Nevertheless, this technique does have certain drawbacks. Firstly, it necessitates the use of costly equipment. Organic ligand-assisted synthesis represents a bottom-up synthesis methodology employed in the fabrication of two-dimensional nanomaterials[93]. During this particular procedure, the initial step involves the formation of crystal sheets composed of metallates under high temperature conditions. Subsequently, the nucleation of nanosheets occurs by the introduction of voluminous intercalating ions. The intercalating ions referred to in this context are characterised by their long-chain structure and bulky carbon-containing nature. These ions have the ability to create metal-ligand complexes through a wet colloidal synthesis process. The primary objective of this procedure involves the production of a complex, namely a metal-ligand complex. This complex formation serves to decrease the overall energy of the reaction and offers steric stabilisation to large ligands. The ligands employed in this particular method can be categorised into four distinct types: cationic, anionic, nonionic, and polymeric. Ionic organic liquids are composed of hydrophobic carbon chains that are prolonged in nature, along with hydrophilic cationic heads. The organic ligands under

consideration possess characteristics of being nonvolatile, exhibiting high viscosity, and displaying solubility in a range of organic solvents[58], [94].

- **Top-Down Synthesis Method**

The process of chemical exfoliation involves two sequential processes. The initial step entails the enlargement of the interlayer spacing by reducing the strength of the van der Waals forces. Subsequently, the layers are exfoliated with the application of either sonication or rapid heating techniques[95]. One effective method for mitigating the effects of van der Waals forces involves the dissolution of the bulk material within a liquid medium. Solvents with a surface tension of approximately 40 mN m^{-1} are primarily employed for the process of exfoliation. Laser ablation is a methodology that involves the use of laser technology to remove a solid substance, typically a precursor of metal, through the process of vaporisation. This removal takes place inside an environment that is both gaseous and wet in nature. The ablation threshold of the material surface is significantly lower than that of the laser beam incident onto it. The laser ablation approach possesses several notable advantages, including its rapidity, independence from elevated temperatures, and straightforward synthesis procedure. The process of laser ablation can be shown by considering the study conducted by Phuoc et al. In their research, they present a straightforward approach for producing electrically conductive graphene using a laser-assisted synthesis methodology[96].

- **Classification of 2D nanomaterials**

Graphene is an innovative two-dimensional nanomaterial composed of a single layer of carbon atoms that are arranged in a hexagonal lattice resembling a honeycomb structure. This lattice consists of an endless number of interconnected benzene rings. The layered form of the material was initially synthesised in 2004 by Geim et al. using the "scotch tape" mechanical approach, an achievement that was recognised with the Nobel Prize[97]n. Graphene exhibits distinctive electrical characteristics, including elevated thermal conductivity, substantial specific surface area, optical transparency, and exceptional catalytic capabilities[98]. The material finds utility

in diverse applications, including but not limited to electronic storage devices, photodetectors, biosensors, light-emitting diodes, drug delivery systems, and supercapacitors. Graphite serves as the primary precursor for the synthesis of graphene, a material that can be produced using a range of top-down and bottom-up methodologies. Chemical vapour deposition (CVD) is known for its ability to generate graphene with exceptional reactivity and quality. Additionally, several additional well-established methods, namely the Brodie technique, Staudenmaier method, Hummer's method, modified Hummers method, and improved Hummers method, are extensively employed in the production of graphene. The enhanced Hummers method is a chemical exfoliation technique that is non-toxic in nature. This process yields graphene with reduced flaws and exhibits nanosized two-dimensional morphological structures. Numerous scholarly articles have been published regarding the production of graphene utilising different top-down and bottom-up approaches[12]. For instance, Guan et al. conducted a study on the synthesis of graphene with extensive surface area and exceptional quality on nickel foil through the utilisation of laser-assisted chemical vapour deposition (LCVD)[99]. The atomic arrangement of thin-film transistors (TMDs) influences their chemical, physical, optical, and catalytic capabilities. Monolayer transition metal dichalcogenides (TMDs) have garnered significant attention in the realm of sustainable energy applications owing to their possession of a direct bandgap and the ability to redistribute charge carriers[100]. Additionally, these materials exhibit the advantageous capability of accommodating intercalation of ions, small molecules, and chemical functionalization. This property proves to be particularly valuable in facilitating reversible oxidation reduction processes within the domain of electrocatalysis. Nevertheless, the process of intercalation with ease leads to a reduction in the overall quantity of active sites. Transition metal dichalcogenides (TMDs) are composed of transition metals belonging to groups IV and VI, which are covalently bonded to chalcogens like sulphur, selenium, and tellurium[101]. This bonding arrangement gives rise to many stacked morphological patterns and kinds. The three most significant polytypes or known phase transitions are 1T, 2H, and 3R. The polytypes under consideration correspond to unit cells with tetragonal (T), hexagonal (H), and rhombohedral (R) symmetries, respectively. The polytype that has been subject to the most comprehensive investigation is the 2H phase. This particular phase can be adjusted to various morphological configurations based on its effectiveness for diverse purposes. Hydrothermal and solvothermal synthesis processes are being employed by researchers with growing frequency for the synthesis of transition metal dichalcogenides (TMDs) owing to their expeditious, scalable, cost-effective, and extensive synthesis capabilities. The techniques employed in this study entail the utilisation of a transition metal

precursor in conjunction with chalcogenide sources, including sulphur powder, thiourea, thioacetamide, and L-cysteine. Numerous methodologies have been devised by researchers to achieve the economical, expeditious, and extensive production of transition metal dichalcogenides (TMDs), due to their wide-ranging and adaptable utility as two-dimensional nanomaterials. The primary method employed for the production of TMDs on a large scale is chemical vapour deposition (CVD). This technique enables the controlled manufacturing of TMDs with high-quality layers, adjustable thickness, scalable dimensions, and superior electrical characteristics, hence facilitating the manufacture of TMDs on wafer scales. Several improvements have been implemented to further the development of novel and extensive synthesis methods for Transition Metal Dichalcogenides (TMDs). In a study conducted by Lin et al., a novel technique was developed for the synthesis of $MoSe_2$ films on SiO_2/Si substrates at a large scale[102]. The utilisation of sonication-assisted exfoliation has emerged as a novel approach in the synthesis of thin-metal (TMD) materials, employing a diverse range of solvents. The synthesis of layered MoS2 nanosheets has been achieved by researchers employing liquid exfoliation methods. Additionally, few-layered MoS_2 nanosheets have been successfully synthesised utilising shear-exfoliating devices[103]. Furthermore, the production of MoS_2 quantum dots has been accomplished through microfluidic processes. Additional approaches that can be employed include mechanical exfoliation, polymer-assisted deposition, solution-phase exfoliation, chemical exfoliation, and laser ablation procedures[104]. The process of liquid-phase exfoliation has been found to result in significant catalytic activity for oxygen evolution processes. On the other hand, laser ablation has demonstrated the capability to rapidly generate both two-dimensional (2D) and three-dimensional (3D) colloidal nanostructures of MoS_2 within nanosecond time scales. The utilisation of laser ablation has also been employed in the synthesis of quasi-amorphous thin films composed of MoS_x, with the purpose of facilitating hydrogen evolution reactions. Various synthesis approaches involving organic ligands have been investigated in the field. For instance, ultrathin MoS_2 nanosheets have been synthesised by incorporating oxygen with the aid of PEG400, which serves as a nonionic organic ligand[105]. Additionally, MoS_2 microspheres have been synthesised using 1-ethyl-3-methylimidazolium bromide as an organic cationic ligand. Another approach involves surfactant-assisted hydrothermal synthesis, where CTAB is employed as a surfactant[106]. Similarly, Xu et al. achieved the synthesis of sulfur-doped $MoSe_2$ composites incorporating nitrogenated graphene, employing triethylenetetramine as a cationic ligand in their experimental procedure[107]. In contrast, Chen and colleagues conducted a synthesis of edge terminated MoS2, achieving a significant interlayer spacing through the utilisation of

graphene and CTAB. This synthesised material was afterwards utilised for supercapacitor applications. The nanomaterials that have been synthesised exhibit a significant quantity of electroactive sites and possess a greater specific capacitance. Hexagonal boron nitride (h-BN) is a compound characterised by a hexagonal Bernal lattice structure, consisting of an equal number of boron (B) and nitrogen (N) atoms, which bears resemblance to the structure of graphene[108], [109]. The compound exhibits a relatively low degree of ionic character and demonstrates promising prospects for utilisation in many domains, including but not limited to wastewater treatment, photocatalysis, and electronic devices. Boron nitride (BN) was initially developed by Balmain in the year 1842. It exists in four distinct crystalline structures, namely h-BN, rhombohedral boron nitride (r-BN), cubic boron nitride (c-BN), and wurtzite boron nitride (w-BN). Graphitic carbon nitride (g-C_3N_4) exhibits structural resemblances to graphite, although possesses distinctive physiochemical characteristics as a result of the inclusion of s-triazine units. The material exhibits a notable surface area, commendable stability, excellent thermal conductivity, a substantial bandgap, satisfactory mechanical stability, and favourable carrier mobility. Graphitic carbon nitride (g-C_3N_4) has been identified as the most thermodynamically stable allotrope of carbon nitride[110]. It exhibits excellent catalytic properties for various important reactions, including hydrogen evolution, oxygen evolution, CO_2 activation, and photodegradation of dyes[111]. Layered oxides and hydroxides can be synthesised by both top-down and bottom-up methodologies. The top-down strategy is widely recognised as the most effective way for synthesising them, with the option of conducting the synthesis in either the gas phase or liquid phase. The chemical exfoliation technique is well recognised as a prominent approach for the synthesis of two-dimensional transition metal oxides (2D TMOs). In this procedure, organic cations are employed to facilitate the formation of polycationic or anionic nanosheets composed of 2D oxides. Additional wet chemical synthesis methods encompass solvothermal, hydrothermal, and microwave-assisted synthesis techniques.

Phosphorene (Pn), alternatively referred to as black phosphorus, is a recently discovered addition to the group V elements within the graphene family[112]. The material has a two-dimensional structure consisting of either a single layer or a double layer. The interlayer interaction between the stacked layers is characterised by weak van der Waals forces[113]. Thin-layered black phosphorus can be synthesised using many methods, including chemical vapour deposition (CVD), liquid exfoliation, lithiation, plasma-assisted synthesis, and solvothermal synthesis[114]. The conversion of thin-layered phosphorene to single-layered

phosphorene can be achieved using the mechanical exfoliation method. Additionally, the synthesis of atom-thick flakes of phosphorene can be accomplished using the plasma-assisted synthesis process involving Arþ gun plasma[115]. Two-dimensional metal-organic frameworks (2D MOFs) are highly appealing crystalline porous materials composed of metal bridging nodes and multipodal organic ligands that are interconnected by fundamental coordination chemistry principles. Nanomaterials possess desirable characteristics, including a significant surface area, notable photonic, electrical, and chemical capabilities, a multitude of active sites, and commendable chemical resilience.

- **Application of 2D Nanomaterials**

Two-dimensional (2D) materials exhibit distinct physical, electrical, and chemical characteristics that render them highly favourable for utilisation in electrochemistry applications[116]. The substantial specific surface areas of these catalysts offer a plethora of active sites, rendering them very suitable as model catalysts for investigating the relationship between structure and performance. In addition to precious metal catalysts, there exist non-precious metal and metal-free catalysts, including transition metal dichalcogenides (TMDs), derivatives of graphene, and porous carbon nanosheets (PCNs)[30], [100], [117]. The utilisation of atomic engineering techniques in the manipulation of two-dimensional (2D) materials is a very effective approach for attaining enhanced performance. This is primarily due to the inherent ease with which the surface and interfacial electronic structure may be controlled and regulated. The manipulation of surface strain and phase can potentially enhance the electron transfer capacity. The growing apprehension surrounding environmental issues and the depletion of fossil fuel resources has underscored the significance of establishing sustainable and energy-efficient electrochemical conversion methods for the production of fuels and chemicals. The utilisation of two-dimensional (2D) materials in electrocatalysis has demonstrated remarkable efficacy owing to their exceptionally large specific surface area and unique pore structure. Economically viable alternatives to costly precious-metal catalysts, such as MoS_2 for the hydrogen reversible process (HER)[118] and graphene for the carbon dioxide reduction reaction (CO_2RR)[119], are being actively investigated. Furthermore, 2D materials have demonstrated significant potential for the development of efficient energy storage devices, including lithium-ion batteries (LIBs) and supercapacitors[120]. This is attributed to their notable attributes, such as high surface-to-volume ratios, excellent conductivity, and thermal

stability even in demanding operational conditions. The electrochemical performance of lithium-ion batteries (LIBs) and supercapacitors has been investigated by researchers through the utilisation of 2D nanomaterials such as graphene, MXenes, and TMDs. Rechargeable lithium-ion batteries (LIBs) are extensively employed as energy storage devices owing to their superior energy density, reduced ecological footprint, and extended operational lifespan in comparison to alternative battery technologies[100], [121], [122]. Two-dimensional (2D) materials have enhanced lithium-storage capacity in both cathodes and anodes of lithium-ion batteries (LIBs) owing to their increased specific surface area. Supercapacitors are energy storage devices that possess notable attributes such as high-power density, rapid charging and discharging capabilities, exceptional cycling longevity, and a secure operational environment. There are two main categories of energy storage devices: electrochemical double-layer capacitors (EDLCs) and pseudo-capacitors[123], [124]. These devices store energy through the process of reversible ion adsorption and desorption. Graphene, MXenes, and TMDs exhibit favourable potential as potential candidates for supercapacitors owing to their notable resistance to oxidation. Several tactics have been implemented in order to enhance the efficiency of materials, such as defect engineering, heteroatom doping, control of thickness/size, and building of 2D heterostructures. Over the course of recent decades, one-dimensional (1D) nanomaterials have exhibited significant potential for utilisation in electrical and optoelectronic devices. This is primarily attributed to their notable mechanical flexibility, ability to adjust electronic characteristics, and exceptional optical transparency. The presence of unpaired electrons, known as dangling bonds, on the surfaces of two-dimensional nanomaterials has the potential to mitigate the adverse effects of surface scattering. Two-dimensional (2D) semiconducting nanomaterials, such as transition metal dichalcogenides (TMDs), hexagonal boron nitride (h-BN), and black phosphorus (BP), exhibit exceptional device performance owing to their comparatively high carrier mobility and the ability to tune their band structures[83], [89], [109], [115]. Two-dimensional transition metal dichalcogenides (2D TMDs) are highly regarded as potential materials for the advancement of electronics and optoelectronic devices in the future. This is primarily attributed to their significant bandgap and exceptional ability to withstand the short-channel effect. MoS_2 is considered a prototypical example of semiconducting transition metal dichalcogenides (TMDs)[103]. The relationship between mobility and temperature exhibits conspicuous indications of the significant reduction in charged-impurity dispersion in dual-gate devices using a top-gate dielectric. Black phosphorus (BP) is classified as a p-type semiconductor and serves as a valuable foundational component for two-dimensional (2D) electronics. In 2014, Zhang et al. successfully

demonstrated the initial BP transistor, while Miao et al. reported the achievement of high-performance top-gated BP field-effect transistors featuring channel lengths as small as 20 nm[125]. The 2D hexagonal boron nitride (h-BN) nanosheet possesses desirable properties for electronic and optoelectronic applications. It exhibits a bandgap of 5.9 electron volts (eV) and finds utility in various devices such as tunnelling junctions, gate dielectrics, and electrical packaging. Heterostructures have been employed to enhance the carrier mobility of 2D semiconducting materials or semimetals, such as graphene, MoS_2, and BP[126]. The implementation of heterostructures has the potential to mitigate rippling effects and minimise scattering originating from the substrate in the context of layered two-dimensional (2D) semiconductors or semimetals. The utilisation of graphene-based photodetectors exhibits significant promise as light harvesting photocatalysts owing to its augmented photoluminescence (PL). Nevertheless, the current body of research concerning the direct utilisation of transition metal dichalcogenides (TMDs) as photocatalysts for visible light is constrained by the restricted thickness of single-layer structures. The utilisation of 2D heterostructures, comprising graphene and other 2D crystals, has emerged as a significant approach in the development of innovative photodetectors[127]. Metal oxide semiconductors has advantageous characteristics for incorporation into photoelectric devices, owing to their nanostructures with low dimensions, appropriate bandgap, distinctive conduction properties, and restricted paths for carrier conduction[86]. Sensors have garnered significant interest as a result of their extensive utilisation in the realms of process control, environmental monitoring, and medical diagnostics. The integration of molecular identification approaches has been explored in the development of low-power-consumption sensors based on the unique localised surface plasmon resonance (LSPR) features shown by 2D materials. Electrochemical sensors operate by facilitating electron transport between active materials and target analytes within a working system consisting of three electrodes. The investigation of 2D nanomaterials as active materials has been undertaken because to their inherent benefits, including improved mass transport, increased surface area, and greater signal-to-noise ratio. Various materials such as graphene, metal dichalcogenides, black phosphorus (BP), h-BN, and g-C_3N_4 have been extensively investigated for their potential applications in sensing[78], [128]. In a study conducted in 2017, Lee et al. successfully synthesised two-dimensional (2D) $Ti_3C_2T_x$ sheets, also known as MXene, for the purpose of gas sensing at room temperature. The researchers were able to detect several gases such as ethanol, methanol, acetone, and ammonia at ambient conditions[129]. The utilisation of fluorescent probe nanomaterials has garnered significant attention in the field of cancer imaging and therapy, owing to their exceptional

performance[130]. The use of inorganic quantum dots (QDs) and heavy metals in bioimaging is advantageous owing to their ability to emit strong fluorescence signals. This is attributed to their capacity for wavelength customization, exceptional resistance to photobleaching, and elevated quantum efficiency[131]. The utilisation of 2D nanomaterials as agents for the purpose of labelling specific tissues or cells has the potential to enhance imaging sensitivity and diagnostic capabilities. The biocompatibility of MoS_2 has been demonstrated to be favourable, exhibiting great stability in physiological fluids and possessing desirable features for both single- and two-photon fluorescence imaging[132]. Graphene and similar two-dimensional nanoparticles have demonstrated considerable potential as metal-free luminous nanomaterials. Solar energy is a highly effective means of converting solar radiation into electrical energy. However, its extensive adoption has been hindered by the considerable expenses involved as well as concerns regarding the presence of hazardous substances.The utilisation of graphene and transition metal dichalcogenides (TMDs) has been extensively investigated in the context of functional photovoltaic systems, owing to their remarkable characteristics of elevated optical transparency and electrical conductivity[3], [111], [133]. The emergence of dye-sensitized solar cells (DSCs) presents a formidable alternative to traditional solid-state photovoltaic technologies, wherein graphene films are employed as transparent window electrodes for DSSCs.

1.3 2-Dimensional transition Metal carbides, Nitrides and Carbonitrides (MXenes)

In the ever-emerging landscape of materials science and nanotechnology, the two-dimensional (2D) nanomaterials have been surfaced as a captivating pathway for transformation in modern science. These family of materials holds unique and often remarkable properties due to their limited dimensionality which holds immense promise for a wide territory of applications. The discovery of graphene, a single layer of carbon atoms organized in a hexagonal lattice, emphasized the development of the 2D materials creation[134].There is a great deal of interest in other 2D materials as a result of graphene's several ground-breaking features, which include its exceptional electrical conductivity, mechanical strength, and thermal conductivity.[98]. Transition metal dichalcogenides (TMDs)[135], for instance, such as molybdenum disulfide (MoS_2)[136] along with tungsten di-selenide (WSe_2)[137], exhibited fascinating optical and electronic characteristics due to their semiconducting nature. The family of 2D materials

extends rapidly to incorporate black phosphorus (phosphorene)[125], hexagonal boron nitride (h-BN)[108], and beyond, each of them offering a unique suite of properties that sparked exploration for various applications. Recently, in 2011, a novel family of transition metal carbides, nitrides, and carbonitrides known as MXenes was introduced[138][139]. Since that time, MXenes have grown enormously and quickly as a family of 2D materials.

$M_{n+1}X_nT_x$ is the formula for the MXene family, where M belongs to the family of transition metal (Ti, Hf, Y, Zr, Sc, V, Ta, Nb, Mo, Cr, or W), and X is either carbon or nitrogen where n = 1, 2, and 3[140], [141] as it appears in Fig. 1's periodic table.

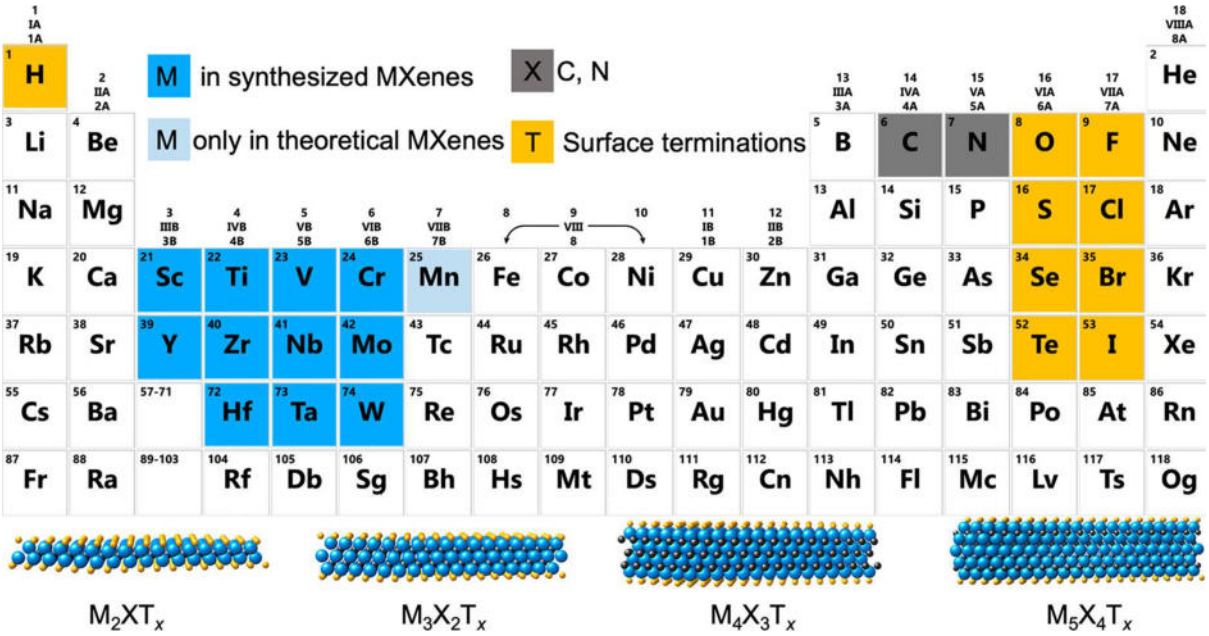

Figure 2:Periodic table showing the composition of MXenes. Transition metal family (M) are shown in blue boxes, Elements in yellow boxes represents surface terminations group and elements in grey box marked as Carbon and Nitrogen[142].

In above **Figure *2*** it has shown different types of groups of MXenes which changes with the value of n in given formula $M_{n+1}X_{n+1}T_x$ which has been categorised as M_2XT_X, $M_3X_2T_X$, $M_4X_3T_X$ and $M_5X_4T_X$. The -O, -F, and -OH terminal groups are the most popular. Typically, the "A" atom is carefully etched from the precursor MAX phase to create MXene. The $M_{n+1}X_n$ layers of layered ternary nitrides and carbides known as MAX phases are joined by the "A" element[143][144]. The $M_{n+1}X_n$ etching of the A layers is kept feasible by the bonds which are

metallic between the M-A layers in MAX phases, which was first described during 1960s and subsequently bounced back in the late 1990s. Because this bonding is frequently fragile as compare to the M-X bonds, the MAX phases are chosen[145]. The MAX phases' incredible properties are due to their layered structure, coupled metallic-covalent nature, and the toughness of their M-X and M-A bonds. Due to their remarkable mix of properties, the MAX phases are being investigated for a variety of applications, including microelectromechanical systems, protective coatings, electrical connections, high temperature structural applications, sensors, and more. Some of China's high-speed trains' pantographs are currently constructed using a MAX phase. MAX phases are a distinctive category of materials characterised by their layered crystal structures. These materials are produced by the solid-state reaction process. The experimental procedure involves the combination of preparation materials that consist of transition metals, 'A' group elements, and carbon and/or nitrogen. These materials are then exposed to elevated temperatures up to 1600 ^{o}C[146]. The solid-state reaction takes place in carefully regulated environments, leading to the synthesis of the MAX phase molecule. The thermal-induced reactions result in the dispersion of constituent atoms, finally resulting in the formation of the intended stratified configuration. This method has been utilised to synthesise several MAX phases, such as Titanium Aluminium Carbide (Ti_3AlC_2)[147], Niobium Aluminium Carbide (Nb_2AlC)[148], Vanadium Aluminium Carbide (V_2AlC)[149], and Molybdenum Gallium Carbide (Mo_2GaC)[150]. These MAX phases are significant as they act as precursors for the synthesis of MXenes, and their applications span across diverse scientific disciplines. The aforementioned instances exemplify the adaptability and importance of the solid-state reaction technique in generating MAX phases, which function as precursors for the fabrication of MXenes and possess utility in diverse scientific fields[144].

Scholars have conducted investigations into alternative methodologies for the synthesis of MXenes, wherein non-MAX phase chemicals are employed as precursor materials. These chemical compounds, frequently consisting of components that are similar in nature, expand the spectrum of MXene compositions and attributes. This enables the customization of qualities that go beyond what can be achieved only through MAX phases. When exposed to selective etching techniques like to those employed for MAX phases, these precursor materials exhibit distinct characteristics, hence enhancing the adaptability of an intriguing category of two-dimensional (2D) materials. Two instances of Non-MAX phases that are commonly employed in the fabrication of MXene materials are titanium silicon carbide (Ti_3SiC_2)[151] and vanadium nitride carbide (VN_xC_y)[152]. The investigation of non-MAX phase precursors serves as a

valuable addition to the recognised MAX phase pathway and contributes to the developing field of MXene research, presenting new prospects for materials advancement and a wide range of applications.

The year 2011 marked a significant advancement in the field of materials science with the introduction of MXene, a two-dimensional material that emerged from the process of selectively etching A layers from MAX phases. This breakthrough resulted in the creation of MXene, which exhibits exceptional composition changes and possesses the ability to tune its properties[138].

Various metals such as titanium (Ti), niobium (Nb), vanadium (V), molybdenum (Mo), tantalum (Ta), chromium (Cr), hafnium (Hf), zinc (Zn), scandium (Sc), and others, are denoted by the symbol X. A class of materials known as MXenes can be defined by the generic formula $M_{n+1}X_n$, where M indicates element from early transition metal, N is the element X, and n is a number between 1 and 3. These values of n correspond to the three common structures observed in MXenes, namely M_2X, M_3X_2, and M_4X_3. In recent times, there has been an expansion in the family of structures by intentional design. The synthesized MXenes that have been described so far have surface terminations that include oxygen (O), hydroxyl (OH), and fluorine (F). These terminations produce hydrophilic surfaces that make it easier to process solutions in organic, free-standing films, deposit thin, aqueous systems, and collect intense powders or slurries. Following the initial successful selective separation of aluminium from titanium aluminium carbide (Ti_3AlC_2) to obtain titanium carbide (Ti_3C_2), top-down synthesis techniques have emerged as the predominant approach for MXene production. The term "top-down method" pertains to a procedure in which a large quantity of powder or material is subjected to reduction or removal of bulk structure, resulting in the formation of particles at the micro- to nanoscale. The processes of wet chemical etching, lithography, and polishing are a few examples of top-down fabrication methods.

MXenes have gained significant popularity as a class of materials in recent times. There are numerous factors contributing to the significant level of interest that MXenes have garnered within the scientific community. One of the primary advantages is in the inherent simplicity with which substantial quantities can be produced. Two pieces of equipment are necessary for admission: an etching-specific high-temperature furnace with a controlled atmosphere and fume hood. It is crucial to acknowledge at this juncture that the production of high quality MXene powders, films, and colloidal suspensions can be achieved even when commencing

with highly impure materials, as long as the latter cannot undergo delamination. The utilisation of this particular attribute was leveraged in the production of affordable MXenes, commencing with rutile, aluminium, and carbon[153]. During this particular procedure, low-cost rutile has a reaction with aluminium (Al) and carbon (C) to produce either titanium aluminium carbide (Ti_3AlC_2) or titanium aluminium carbide (Ti_2AlC) together with alumina. The alumina flakes are then treated to centrifugation after being exposed to the etching and delamination processes. Consequently, the colloidal suspension obtained consists of highly pure MXene.

The process of top-down synthesis of MXene entails the targeted removal of specific layers from the original layered precursor material, which could be a precursor in the MAX phase or a non-MAX phase. The initial MXene compound, namely titanium carbide (Ti_3C_2), was synthesised by means of a process including the targeted removal of aluminium (Al) from the titanium aluminium carbide (Ti_3AlC_2) compound, also known as MAX, with hydrofluoric acid (HF)[138]. Subsequently, the utilisation of top-down synthesis methods including hydrofluoric acid (HF) or the generation of HF in situ through the use of fluoride solutions has played a crucial role in the production of several MXenes derived from layered precursors[154]. Presently, the majority of top-down synthesis techniques employed for MXene continue to depend on fluoride-based etchants owing to their preferential ability to etch out the A element. However, there are recorded examples of using alkaline solutions, molten salts along with hydrothermal treatments as alternative synthesis procedures, increasing the spectrum of potential synthesis routes and ultimately impacting the final properties. The material's surface exhibits imperfections and is frequently adorned with diverse distributions of surface functions, including oxygen(O), hydroxyl (OH) and fluorine (F) [155]. The dependence of the concentration of each component has been demonstrated to be influenced by the process of synthesis. In comparison to regions or areas with monodisperse terminations, nuclear magnetic resonance (NMR) data show that random dispersion of surface terminations are more realistic[156]. Surfaces produced by the selective etching of A elements are thought to have a major impact on a number of material characteristics, such as electrical band gaps, optical absorbance, and surface chemistry.[157]–[161].

- **Highlights of Nb based MXenes**

Currently, over 30 MXenes have been investigated as potential candidates for various applications including adsorbents, energy storage, membrane materials, solid-state laser

absorbers, near-infrared-1 (NIR-I) along with second NIR (NIR-II) photothermal tumour, antibacterial agents for water treatment, and biomedical application. Niobium-carbide MXene is classified as a member of the MXene family, specifically as a second representative. The Nb_2CT_x MXene was initially identified in 2013[162]. It demonstrates favourable characteristics in terms of its capacity to withstand high cycling rates, rendering it a potentially valuable material for energy storage applications. The niobium MXenes that are frequently employed include Nb_2CT_x and $Nb_4C_3T_x$, which are synthesised through the process of acid etching of their corresponding MAX phases, namely Nb_2AlC and Nb_4AlC_3. Nb_2CT_x exhibits high electrical conductivity, characterised by a band gap that approaches zero or even smaller values[163]. This material possesses metallic properties due to its versatile arrangement of functional groups, thereby demonstrating significant promise for various applications including its use as an electrode material in lithium-ion batteries, supercapacitors, and as a photocatalyst for hydrogen evolution. The study conducted by Nb_2CT_x also exhibited favourable ion intake capacity, so establishing its potential as a viable electrode material for metal-ion batteries. Niobium MXenes shown comparable efficacy to closely related 2D materials, namely 2D graphene oxide (GO) and titanium carbide MXene, in the context of biotechnology applications, namely in terms of their antibacterial and antifouling properties. The Nb_2CT_x MXene material exhibited exceptional photothermal conversion efficiency in both the near-infrared region I (NIR-I) and near-infrared region II (NIR-II) light windows, achieving conversion efficiencies of 35.4% and 46.65% respectively[164]. Additionally, this material demonstrated notable biocompatibility and photothermal stability. The composite of Nb_2CT_x-polyethyleneglycol exhibited no cytotoxicity when exposed to cancer cells for a duration of 24 hours, even at concentrations above 300 μg/mL[165]. In addition, composites based on Nb_2CT_x shown a notable capacity for drug encapsulation, achieving a loading efficiency of 32.77%. Moreover, these composites exhibited significant effectiveness in inducing photothermal hyperthermia in cancer cells resulting in an impressive inhibitory efficiency of 92.57%[165]. The volumetric capacitance of a free-standing film composed of $Nb_4C_3T_x$ MXene, characterised by a significant interlayer spacing, was seen to be 511, 691, and 1085 F cm^{-3} in 1 M $MgSO_4$, KOH, and H_2SO_4 electrolytes, respectively[166]. These measurements were obtained at a scan rate of 5 mV s^{-1}. The volumetric capacitance values exhibited by these electrodes are comparatively higher than those observed in the bulk of other supercapacitor electrodes. The utilisation of Niobium MXene has demonstrated a notably rapid relaxation time of 38.13 fs, as well as a comparatively slower relaxation time of 0.5813 ps[167]. Furthermore, it exhibits enhanced non-linear optical characteristics, hence rendering it a promising candidate

for incorporation into ultrafast photonic and optoelectronic devices. The Nb_2CT_x MXene material demonstrated electron-phonon scattering phenomena with intensities in proximity to 300 Kelvin. This phenomenon can be attributed to the interaction between phonons, known as phonon-phonon scattering, which is markedly different from the typical scenario. The pronounced electron-phonon scattering observed in this case can lead to a substantial decrease in the thermal conductivity of the lattice. The significant investigation of niobium MXene nanosheets in the realm of photocatalytic applications is attributed to their distinctive atomic configuration and their capacity to function as co-catalysts for the process of photocatalytic hydrogen production. In their study, Wang et al. observed that the photocatalytic activity of TiO_2/Nb_2CT_x, where Nb_2CT_x was used as a co-catalyst, exhibited a greater efficiency of 0.41% in comparison to $TiO_2/Ti_3C_2T_x$ (0.29%) and TiO_2-Ti_2CT_x (0.17%)[168]. The remarkable attributes of niobium MXene highlight its significant potential for practical implementation in several fields including as electronics, biotechnology, photocatalysis, water disinfection, and sensors. In the past ten years, extensive research has been conducted on the application of MXenes as a sophisticated nanostructured material in several fields such as biomedical, energy, electromagnetic, microwave shielding applications and lasers, among others[169]–[171].

The synthesis of Niobium MXenes typically involves the selective etching of the aluminium (Al) element from their MAX phase precursors. The MAX phase precursors, namely Nb_2AlC and Nb_4AlC_3, are employed in the synthesis of Nb_2CT_x and $Nb4C_3T_x$ MXenes, respectively. The predominant method employed for targeted removal of aluminium (Al) layers from Nb_2AlC and Nb_4AlC_3 MAX phases involves the direct application of hydrogen fluoride (HF) solution. To achieve efficient etching of the aluminium (Al) layer, the Nb_2AlC powder was submerged in a solution consisting of 50% hydrofluoric acid (HF) and agitated at ambient temperature for a duration of 90 hours[169]. The full removal of the aluminium layer from Nb_2AlC was seen when it was immersed in a 55°C aqueous solution containing 50% hydrofluoric acid (HF) and stirred for a duration of 40-48 hours. In their study, Zhao et al. fabricated multilayered Nb_2CT_x (referred to as m-Nb_2CT_x) and few-layered Nb_2CT_x (referred to as f-Nb_2CT_x) MXenes through the process of etching Nb_2AlC using a 40% aqueous solution of hydrofluoric acid (HF) at a temperature of 60°C for durations of 70 and 90 hours, respectively[172]. In their study, Halim et al. employed a selective etching technique to remove aluminium (Al) and scandium (Sc) atoms from a novel quaternary MAX phase compound, specifically $(Nb_2/3Sc_{2/3})_2AlC$[173]. The etching process was carried out at room temperature for a duration of either 96 hours or 140 hours, as documented in previous studies. The synthesis

of Nb_2CT_x was achieved through the utilisation of an in-situ HF etching technique. This involved subjecting Nb_2AlC to a mixed solution consisting of hydrochloric acid (37%) and lithium fluoride (LiF) at a temperature of 60°C for a duration of 90 hours[174]. During the etching process, there was a pre-intercalation of Li^+ ions seen. This phenomenon can be represented as Li-Nb_2CT_x, where the interlayer spacing is increased and characterised by a higher proportion of –O groups and a lower proportion of –F groups. This discovery presents novel opportunities for utilising this material in various energy-related applications. In all instances, namely direct HF and in situ HF etching, the resulting Nb_2CT_x and $Nb_4C_3T_x$ MXenes displayed surface termination (T_x) groups, including –F, –OH, –O–, and physiosorbed H_2O[175].

The influence of the transition metal M and the number of X layers on the structural characteristics of MXene materials has been widely acknowledged. MXene demonstrates promising potential as a viable contender for utilisation in Li-ion batteries due to its enhanced electrical conductivity and equivalent Li storage capacity when compared to graphite electrodes. The Li-ion-specific capacity of M_2X structures is found to be larger than that of M_3X_2 and M_4X_3 counterparts, based on the analysis of the number of atomic layers per MXene sheet. Additionally, it has been observed that the lithium-ion-specific capacity of DL MXene surpasses that of multilayered MXene, hence endowing DL MXene with a greater charge storage capability compared to multilayer MXenes. In addition, the exfoliation process of MXenes results in the detachment of metallic M-Al bonds, which subsequently leads to an elevated resistivity when compared to that of their corresponding MAX phases[176]–[178]. The resistivity of multilayered $Nb_4C_3T_x$ MXene was found to be lower compared to Nb_2CT_x MXene. This difference can be explained by two factors: the larger value of n (number of NbC layers) in $Nb_4C_3T_x$ and the existence of extra NbC layers, resulting in a greater abundance of MAX (M: transition metal, A: A-group element, X: carbon/nitrogen) character in $Nb_4C_3T_x$. The experimental results indicate that $Nb_4C_3T_x$ exhibits an electrical conductivity that is over 110 times greater than that of Nb_2CT_x. In the instance of $Nb_4C_3T_x$, a singular monolayer of $Nb_4C_3T_x$ exhibits an electrical conductivity of 1,026 ± 155 S cm^{-1}, surpassing that of bulk $Nb_4C_3T_x$ assemblies by a factor of two[162]. The researchers observed that the electrical conductivity of Ti_3C_2Tx MXene was measured to be 750 S cm^{-1}. Following calcination at 600°C, the conductivity of the MXene increased by a factor of three, reaching a value of 2,510 S cm^{-1}, surpassing the conductivity of the untreated MXene. The electrical conductivity of $Ti_3C_2T_x$ was seen to increase by around 70% following calcination at a temperature of 450°C, in comparison

to a sample that did not undergo calcination[179]. In a similar vein, the electrical conductivity of $Nb_4C_3T_x$ can be chemically augmented. Additionally, there have been reports indicating that $Nb_4C_3T_x$ demonstrates a significantly elevated breakdown current density of around 1.1 $nA.cm^{-2}$, a value that is equivalent to that of $Ti_3C_2T_x$ and graphene[179]. The high breakdown current densities exhibited by $Nb_4C_3T_x$ suggest that additional members of the niobium MXene family are also likely to possess high breakdown current densities, making them suitable for applications involving high current-carrying capacities. The limited oxidative stability exhibited by MXenes has a notable impact on their overall durability and hinders their potential for extensive utilisation. According to predictions, Niobium MXenes exhibit greater stability in comparison to Ti MXenes. Previous studies have demonstrated that the process of oxidation takes place gradually in Nb_2CT_z, as evidenced by the observed reduction in the Nb/O ratio of Nb_2CT_z MXenes over a period of time. The investigation of the oxidative stability of MXenes in aqueous dispersions revealed a positive correlation between the value of "n" and the level of oxidative stability exhibited by the MXenes. The observed stability of $Nb_4C_3T_z$ can be attributed to the presence of shielded inner layers of Nb, which distinguishes it from Nb_2CT_z. Furthermore, it was discovered that the incorporation of an antioxidant, such as ascorbic acid, and the implementation of low-temperature storage conditions resulted in an enhancement of the oxidative stability of $Nb_{n+1}C_nT_z$ MXenes. Under standard circumstances at ambient temperature, the oxidizable percentage of $Nb_4C_3T_x$ and Nb_2CT_z was determined to be 0.52 and 0.61, respectively, in the absence of any antioxidant[180]. These oxidizable fractions were decreased to 0.15 and 0.44 for $Nb_4C_3T_z$ and Nb_2CT_z, respectively, even while held at ambient temperature. Likewise, the portion of the substance that is susceptible to oxidation exhibited a minor decrease when subjected to lower temperatures. The mechanical properties of monolayer $Nb_4C_3T_x$ membranes were examined by Lipatov et al. using atomic force microscopy (AFM) nanoindentation[179]. The effective Young's modulus of the $Nb_4C_3T_x$ monolayer was determined to be 387 ± 14 GPa, whereas the breaking strength was measured to be 25.1 ± 1.7 GPa. The Young's modulus value of the $Nb_4C_3T_x$ monolayer is the highest among other 2D materials, including GO, reduced GO (rGO), and $Ti_3C_2T_x$ MXene, as determined through nanoindentation tests. This observation highlights the potential utility of $Nb_4C_3T_x$ in various applications such as structural composites, membranes, textiles, protective coatings, and others. Further exploration of the magnetic characteristics of MXenes is necessary in order to advance research in this field. The superconductivity of niobium carbide MXenes is governed by the presence of surface groups, as evidenced by recent findings. Babar et al.[181] reported the observation of an anomalous magnetic Meissner effect in a two-dimensional (2D) Nb_2CT_x

MXene material. This phenomenon is indicative of the material's superconducting behaviour, with an initial transition temperature measured at 12.8 K. The magnetic properties of Nb_2CT_x were further assessed using density functional theory (DFT) calculations. The findings of this analysis revealed a negative magnetic moment in Nb_2CT_x, thus providing confirmation of the existence of diamagnetism and superconducting characteristics[181].

1.4 Electrochemical Sensors

A sensor is characterized as a device that reacts to a physical stimulus, such as sound, light, heat, movement, magnetic, or pressure. This response is then converted into an electrical impulse, which serves as a method for quantifying the alteration of any inherent characteristic of the material composing the sensor. The etymology of the term "sensor" can be traced back to its Latin root "sentire," which denotes the act of perceiving or experiencing through the senses[182]. Sensors have the intrinsic ability to perceive and interpret their immediate environment to establish a relationship or engage in interaction. Electrochemical sensors, which use an electrode as the transducer element when exposed to an analyte, are under the category of chemical sensors. A vast range of characteristics including chemical, physical, biological and chemical aspects of our daily life are detected by modern electrochemical sensors using a variety of features. Examples of sensors include those used in instruments, machines, and vehicles including airplanes, digital media and mobile phones as well as those intended to monitor the environment, human health, and other factors. In recent decades, advancements in microelectronic and microengineering have significantly contributed to the enhancement of modern sensing systems[183]. These developments mainly concern the manufacturing of smaller sensors with improved parameters like selectivity and sensitivity with reduced maintenance costs and production.

In this particular framework, the integration of approaches and principles related to nanotechnology and nanoscience has a significant role on the quick development of nano-sensors. This is primarily attributable to the surface-to-volume ratio, a very consequential attribute inherent to the nanoscale regime. Nevertheless, the current situation falls short of satisfying the increasing consumer expectations of societies characterised by social disparities. As a result, the matter of democratising knowledge and the utilisation of emerging technologies, such as nanotechnology and nanoscience (N&N), pose significant challenges for scientific endeavours in the 21st century[184]. As a result, the social and political facets of

science are becoming increasingly important. The current paradigms in electrochemical sensor research and development enable the investigation of novel materials, assessment of various sample types, investigation of novel production procedures, and formulation of strategies to enhance lower detection limits and selectivity. These paradigms, which are connected to N&N, include interdisciplinary contacts and place a focus on the role that scientists played in the recent scientific revolution. Electrochemical sensors were first used in the 1950s, largely to measure the oxygen levels in industrial settings[185]. The health and safety regulations pertaining to employees necessitated the monitoring of poisonous gases and fuels in enclosed areas, thereby stimulating a surge of scholarly investigation into electrochemical sensors capable of demonstrating high selectivity for the identification of various gases. The concept of oxygen sensor was initially introduced by C. Clark, who proposed a design including the utilisation of two electrodes within a cell. An oxygen-permeable membrane separates these electrodes and serves as a partition between the electrolyte solution and electrodes. Oxygen was reduced at the indicator electrode as a result of the membrane's process of diffusion. As a result, an electrical current was generated, and its magnitude exactly correlated with the sample's oxygen content[186]. Numerous industries, including medical, environmental monitoring, and industrial applications, have made substantial use of the Clark oxygen sensor. In order to monitor water quality across the former Soviet Union Socialist Republics, a unique sensor for oxygen was developed and put into use in 1963, during the Cold War. The signal of electric current derived by Clark oxygen sensors was shown to be unstable, despite the sensors' great commercial appeal. Due to the regular pre-calibration required by the oxygen analyzers using these sensors, their practical application was limited[186].

The invention of the scanning tunnelling microscope and the atomic force microscope by the teams led by Binnig and Rohrer in 1981 and 1986, respectively, can be credited as the key catalyst for the modern improvement of electrochemical sensors[187], [188]. Because they can see material structures at the nanoscale, which is typically on the order of 1.0 109 m, advances in scientific instrumentation have allowed the development of novel goods and processes (1 nm). The disciplines of nanoscience and nanotechnology have emerged as a result of this. With a vast spectrum of materials, including semiconductors, metals, polymers, ceramics, biomaterials nanoscience and composites has quickly developed into a very broad and inter-disciplinary field of study. Nanoscale structures like nanoparticles, nanotubes, nanofibers, and nanospheres are produced by purposefully structuring these materials at the manometer scale.

1.5 MXenes for Electrochemical Sensors

Two-dimensional (2D) materials have drawn a lot of attention from researchers because of their unique electrical, chemical and physical. Due to these qualities, they can be used in electrical, catalytic, and energy storage applications. Professor Gogotsi and colleagues introduced the class of 2-dimensional transition metal carbides, nitrides, or carbo-nitrides known as MXenes into the category of 2D nanomaterials in 2011.[189]. By removing layer, A from the precursor MAX phases during a procedure called as selective etching, MXenes are created. In this context, M designates an early transition metal, A identifies an element from group A, and X designates either carbon (C) or nitrogen (N), which have been extensively explored in earlier sections. The M and A layers alternate in the MAX phase's densely packed multilayer structure. Both the metallic-covalent bond between M and X as well as the M-A bond are stronger. It is significant to remember that MAX phases have excellent electrical and thermal conductivity qualities, are immune to chemical corrosion, and have a low coefficient of thermal expansion.

Since the initial identification of MXenes, they have garnered considerable interest within the broader scientific community and various sectors owing to their distinctive layered structure, exceptional electrical conductivity, substantial surface area, impressive hydrophilic properties, commendable thermal stability, and environmentally sustainable attributes. The distinctive attributes of MXenes render them a highly attractive contender for various applications such as sensing, catalysis, energy storage, electronics and environmental remediation. MXenes exhibit comparable structural and electrical characteristics to other two-dimensional (2D) materials, including metal oxides and graphene. As a result, they have become a promising replacement for many 2D materials in applications like electromagnetic interference shielding, nanomedicine ,energy storage, sensing, electromagnetic interference shielding, and other cutting-edge ones. Ti, C, or N are among the plentiful and non-toxic components that make up MXenes. In addition, the byproducts of their breakdown, CO_2 and N_2, are also non-toxic. MXenes have consequently been the focus of extensive research in the area of environmental remediation applications.

A very promising method for enhancing the performance characteristics of electrochemical sensing systems is the optimization of electrode parameters. This entails improving dynamic ranges, detection limits, analyte adhesion, sensitivity, and selectivity. The use of electrochemical (bio) sensors based on nanomaterials has increased interest in the detection of diverse analytes in recent years. Utilizing 2D nanomaterials, such graphene and MoS_2, both individually and as parts of nanocomposites, has been the focus of extensive study for the creation of extremely responsive sensing devices. Nevertheless, 2D nanomaterials exhibit certain limitations, such as inadequate electrical conductivity in the case of MoS_2, elevated hydrophobicity in both MoS_2 and graphene, as well as challenges in surface functionalization. Functionalization of graphene primarily occurs at surface flaws and edges, whereas the process of functionalizing MoS_2 is notably more challenging. Furthermore, the process of producing these materials on a big scale is arduous and time-consuming, so imposing further constraints on the advancement of research and innovation in this particular domain. In contrast, MXene exhibits exceptional electrical conductivities, notable hydrophilicity resulting from surface termination groups such as -F, =O, and –OH, convenient functionalization, favourable ion intercalation behaviour and dependable large-scale production. Due to these characteristics, MXene is the best material to use when creating high-performance electrochemical (bio) sensors.

Thus far, two comprehensive evaluations have been published regarding MXenes, highlighting their efficacy in the development of sensor technologies. Zhu et al.[190] conducted a comprehensive analysis that specifically examines the various applications of MXenes in the fields of catalysis, sensing, and adsorption. Nevertheless, the portion pertaining to the sensor is quite concise and lacks extensive illustrative instances. Sinha et al. [170] describe the wide range of applications for MXenes in several types of sensors, including electrochemical, solid state gas adsorptive, piezoresistive wearable sensors, and photoluminescent sensors. The most recent developments in the field of electrochemical (bio) sensors based on MXene materials are thoroughly reviewed in this chapter. These sensors have demonstrated a promising ability to identify disease biomarkers, pharmaceutical drugs, and environmental contaminants.

MXene nanostructures have recently seen an increase in usage in the realm of sensor creation. These nanostructures have been used to make a variety of detecting devices, including optical sensors, electrochemical (bio) sensors, piezoresistive wearable, and gas adsorptive sensor.[170]. MXenes can incorporate different elements like enzymes, metal nanoparticles, metal oxides and conducting polymers, much like graphene and other two-dimensional

materials can do. Enhanced structural and electrical qualities are the outcome of this integration.[190]. An experiment was conducted to demonstrate the one-step hybridization of Pd, Ag, and Au nanoparticles onto the $Ti_3C_2T_x$ MXene surface from their aqueous solutions. This hybridization process did not require the usage of external reducing agents. The resulting hybrid material was then utilised as a substrate for surface-enhanced Raman spectroscopy (SERS)[191]. In a similar manner, the synthesis of a $Ti_3C_2T_x$–Pt-NP composite was achieved using the in-situ oxidation of a Pt precursor on the surface of MXene, both with and without the usage of external reducing agents. This composite material was then utilised for the purpose of electrochemical sensing, as reported in reference [192]. The MXene–Pt-NP nanocomposite exhibited enhanced electrochemical performance in comparison to MXene in isolation, owing to the Pt-NP's elevated conductivity, higher catalytic activity, and increased surface area. The synthesis of nitrogen decorated MXene quantum dots with improved redox characteristics for application in photoluminescent was described by Xu et al. [193]. Ethylamine was utilised as the nitrogen source in this study. A composite material made of glucose oxidase (GOx) restrained on MXene/AuNP was created by Rakhi and her coworkers. According to a prior study, this composite was used to amperometrically detect glucose using an enzyme.[194]. Electron transport between the glucose oxidase (GOx) redox active canters and the electrode has been significantly improved by the use of gold nanoparticles (AuNPs). In their research, Kumar et al. described a brand-new technique for aminosilane-based functionalization of MXene. By creating a covalent bond between the aminosilane and the bio-receptor (anti-CEA), CEA can be measured electrochemically using this method.[195]. The process of surface modification of MXene has been conducted through two main methods: physical absorption and electrostatic attraction. As an illustration, a positively charged redox molecule, especially methylene blue (MB), was used to modify the negatively charged MXene-$Ti_3C_2T_x$ through electrostatic attraction. With the addition of the urease enzyme, this was further modified to enable the electrochemical detection of urea and uric acid in whole blood.[196]. The authors Zheng et al. [197] documented the utilisation of graphene oxide (GO) for the purpose of enhancing stability and electrochemical performance through the alteration of Ti_3C_2. The Ti_3C_2–GO composite was synthesised using an Ink printing method, and subsequently modified with haemoglobin (Hb) for the purpose of electrochemical sensing. A separate investigation involved the creation of a TiO_2 nanoparticle-modified Ti_3C_2 nanocomposite by an in-situ hydrolysis procedure followed by a hydrothermal process. Subsequently, haemoglobin was immobilised onto the Ti_3C_2-TiO_2 composite [198]. Zheng et al. [199] presented a noteworthy methodology for enhancing the electrocatalytic activity of Ti_3C_2 through the incorporation of

DNA and Pd/Pt nanoparticles. DNA helps to promote the homogeneous development of Pd/Pt nanoparticles while When Pd/Pt nanoparticles are loaded into this composite material, MXene serves as a conducting matrix. The synthesis of sulphonic groups functionalized MXene (Ti_3C_3–SO_3H) was successfully achieved by Lei et al. [200] by the use of an effective approach including aromatic coupling–diazotization. The synthesised MXene was then applied for the purpose of removing MB, demonstrating its efficacy in this application.

The electron transfer pathway connecting the electrode surface and biomaker is theoretically restricted since the protein shell encloses the redox active centre. In order to encourage the direct transfer of electrons and maintain the bioactivity of enzymes, it is crucial to use nanomaterials.[201]. Due to its extraordinary powers in oxidation and reduction processes, hydrogen peroxide (H_2O_2) has a wide range of applications in the chemical, clinical, and medical fields. Furthermore, hydrogen peroxide (H_2O_2) serves as a crucial substrate in various oxidase reactions and holds considerable significance in the context of oxidation mechanisms. Hence, the accurate detection of hydrogen peroxide (H_2O_2) holds significant importance. In their study, Wang et al.[202] documented the use of haemoglobin (Hb) as a representative protein for the electrochemical detection of H_2O_2. The researchers achieved this by immobilising Hb onto a graphene-like MXene material, thereby creating an electrochemical sensor. With a limit of detection (LOD) of 20 nM and a low detection range of 0.1 to 20 M, the electrochemical(bio) sensor showed a linear connection in its response to H_2O_2. Because of their unique 2-dimensional structure and remarkable electrical properties, MXene nanoparticles may be used to enhance the electrochemical capabilities of the sensor. MXene increases the possibility of immobilizing the enzyme in addition to providing an environment that is conducive to the enzyme maintaining its activity.

The bromate ion (BrO^{3-}) is a significant pollutant that is commonly found in drinking water [203]. Nevertheless, traditional detection methods typically depend on intricate instrumentation and laborious separation procedures of BrO^{3-}. In a separate study, electrochemical techniques have been employed to detect BrO^{3-} owing to its inherent attributes of simplicity and prompt responsiveness. In a study conducted by Rasheed et al. [204], it was shown that electrochemical methods can reliably detect bromate ions. These methods were found to be cost-effective and easy to operate [205]. The electrochemical sensor exhibited excellent selectivity and sensitivity in the detection of BrO^{3-}. This was accomplished by using lamellar $Ti_3C_2T_x$ as a signal-enhancing matrix and a sensing platform. Its success in this application was largely due to $Ti_3C_2T_x$'s remarkable qualities, which included its layered

structure, hydrophilic surface, and excellent electrical characteristics. Excellent selectivity and stability were found in the artificially made MXene-Ti_3C_2 sensor. The limit of detection for BrO^{3-} was determined to be 41 nM, and the bromate ion concentration range was linear from 20 nM to 5 M. Using differential pulse voltammetry (DPV) and 0.5 M H_2SO_4 as the electrolyte, the examination of the detection limit was carried out. As the concentration of BrO^{3-} changed from 50 nM to 5 M, the peak current showed a noticeable increase. Comparing the electrochemical sensor to previously known sensors for detecting BrO^{3-}, it showed the lowest detection limit.

The monitoring of hepatotoxic medicines holds significant importance in both clinical diagnosis and safety control [206]. Furthermore, the concurrent ingestion of acetaminophen (ACOP) and isoniazid (INZ) has been associated with an elevated susceptibility to liver injury. In their study, Zhang et al.[207] a screen-printed electrode (SPE) with $Ti_3C_2T_x$ for the purpose of point-of-care testing of ACOP and INZ has been integrated into a new electrochemical sensing platform. The acetaldehyde (ACOP) and indazole oxidation by the MXene-modified Screen-Printed Electrode (SPE) demonstrated remarkable electrocatalytic efficacy, selectivity, and stability (INZ). Additionally, the electrochemical sensor that was proposed proved exceptional effectiveness and usefulness for the simultaneous determination of ACOP and INZ in human serum samples as well as in particular pharmaceutical formulations. MXene, a substance with a layered structure and remarkable electrical conductivity, was used in the sensor's manufacturing process as a medium to boost the signal.

In a separate investigation, Peng and colleagues [208] devised a very responsive fluorescent DNA detection system utilising ultrathin Ti_3C_2. This platform was used to detect PCR-amplified HPV-18 DNA by integrating DNA hybridization with exonuclease III and enhancing the sensitivity of the sensor. Contrary to standard methods, the use of fluorescent probes results in a highly sensitive, straightforward, and consistent mix-and-detect assay for HPV analysis. With the aim of enhancing signals, a newly developed fluorescent electrochemical sensor has demonstrated good specificity and sensitivity in the detection of HPV-18. The limit of detection (LOD) achieved by this sensor was 100 pM. The investigations demonstrate that the utilisation of MXene in electrochemical sensors has resulted in notable electrochemical reactivity and specificity in detecting biomarkers.

Despite having remarkable qualities, MXenes have trouble achieving the exacting standards of electrochemical sensors because of their propensity for aggregation and restacking. Enhancing the electrochemical properties of MXene materials and enabling the incorporation of additional functions requires the use of surface modification techniques, including as electrostatic attraction, physical adsorption, non-covalent interactions and covalent strategies, [209]. To make it easier to find different biomarkers, a lot of electrochemical sensors, including MXene materials, have been produced. The electrochemical characteristics of these sensors have significantly improved, showing a low limit of detection (LOD) and a broad detection range. Due of MXene's propensity to aggregate in the atmosphere, it is unknown exactly what characteristics these MXene sensors possess. The incorporation of high-performance conductive materials, such as metal oxide, graphene oxide and carbon nanotubes, has been used to lessen the clustering of MXene in order to enhance the properties of electrochemical sensors and encourage the interaction between biomarkers and the active material[210]. The terminal groups of MXene exhibit the capability to directly enable ion exchange processes, in addition to showing promise as a dependable reducing agent for specific metallic ions. The impressive capacity of MXene to undergo self-reduction showcases its potential for application in the realm of electrochemical sensing. The decreased interlayer attraction and increased interlayer separation of MXene have led to the recognition of MNPs/MXene composites as electrodes with exceptional efficacy. An new electrochemical biosensor that uses an MXene-Au nanocomposite for the determination of glucose has been developed, according to Rakhi et al[211]. The in-situ reduction approach was employed to immobilise Au nanoparticles onto the interface of MXene nanosheets. Enzyme biological functionality was successfully preserved by the method, and the electrode's surface electron transfer efficiency was also increased. The catalytic activity of the MXene-Au-Nafion-GO_x-GCE along with MXene-Nafion-GO_x-GCE configurations demonstrated a higher level of electrochemical response in comparison to the MXene/Nafion/GO_x/GCE configuration. MXene and CPs/MXene nanocomposites' interlayer spacing has been improved by the use of polymers, producing notable electrical and mechanical properties. The propensity of nanosheets to aggregate and suffer oxidation upon exposure to ambient conditions, however, means that the issue with MXene-based electrochemical sensors still exists. Yang et al. [212]introduced a novel methodology in their research to develop a volatile organic compounds (VOCs) sensor that exhibits improved sensitivity. The outcomes were attained through the utilisation of MXene/PVA/PEI nanocomposites, which demonstrated significant attributes including a wide detection range, a low limit of detection (LOD), and swift reaction and recovery durations.

The application of graphene and carbon nanotubes as interlayer spacers was utilised to augment the stability of the layer structure of MXene. The utilisation of a 2D substrate consisting of water-soluble MXene nanosheets demonstrated a notable ability to inhibit the occurrence of restacking among MXene nanosheets. Consequently, an augmented interlayer gap between the various Ti_3C_2 layers ensued, thereby enhancing conductivity, capacity, and structural stability. The generated MIP layer demonstrates the ability to concurrently identify and quantify biomarkers, while also exhibiting a notable level of specificity for the fisetin sensor[213]. Zheng et al.[213] effectively synthesised nanocomposites of MXene-Ti_3C_2/graphene oxide (Ti_3C_2/GO) in their research endeavour. Limits of detection (LOD) of 1.5 M and a linear concentration range of 2 M to 1 mM for hydrogen peroxide detection are examples of the nanocomposites' outstanding specificity and sensitivity (H_2O_2). The visual legibility of the printed patterns was enhanced through the augmentation of both the quantity of layers and lines. Additionally, it was observed that the printed path of Ti_3C_2–GO displayed a narrower breadth in comparison to Ti_3C_2, indicating a decrease in the rate of diffusion. The utilisation of specific two-dimensional nanomaterials as interlayer spacers possesses the capability to hinder the aggregation of MXene nanosheets and promote the creation of a robust porous structure. The artificially created sensors exhibited the ability to facilitate electron transfer, improve conductivity, and enhance electrochemical reactivity. Nevertheless, the composites of MXene/2D nanomaterials that have been described thus far have predominantly been achieved using electrostatic adsorption and physical accumulation methods. However, these approaches exhibit limitations in terms of durability and necessitate further advancements.

1.6 Other Applications of MXenes (Energy Storage)

Several studies conducted in recent years have extensively documented the development of MXene-based materials for the purpose of energy storage applications. These studies have consistently highlighted the significance and potential of MXene-based materials in the field of electrochemical energy storage devices[214]. Rechargeable batteries and supercapacitors are significant within the realm of electrochemical energy storage devices due to their considerable potential for making substantial contributions towards the realisation of sustainable energy solutions. MXenes are regarded as promising materials for electrode applications in batteries and supercapacitors due to their 2D layered structures, high electrical conductivity, surface functionality, and environmentally friendly characteristics. Nevertheless, the issues of restacking and self-oxidation of MXene NSs have posed significant challenges in the context

of electrode fabrication. Hence, the utilisation of MXene Nanosheets (NSs) in electrochemical energy storage applications has led to the development of effective strategies to enhance their performance. One such strategy involves the fabrication of MXene Nanosheet Composite Particles (NCPs) by introducing heteroatoms or molecules to increase the interlayer spacing, or by creating heterostructures through combination with other electroactive nanostructured materials. These approaches effectively mitigate the issues of restacking and self-oxidation of MXene NSs, resulting in improved charge storage capacity and enhanced stability.

Supercapacitors are highly significant electrochemical energy storage devices that have garnered considerable interest due to their exceptional power density, rapid charging and discharging capabilities, and extended lifespan. Like other types of rechargeable batteries, supercapacitors are composed of two electrodes, namely the positive and negative electrodes. These electrodes are accompanied by electrolytes and separators, which play crucial roles in the functioning of the supercapacitor. The charge storage mechanisms of supercapacitors rely on the surface reactions of electrode materials. These reactions involve the adsorption-desorption of electrolyte ions at the electrode/electrolyte interface, known as the electric double-layer capacitor, as well as surface faradaic redox reactions, referred to as pseudocapacitors. Consequently, the selection of electrode materials in supercapacitors is of utmost importance as it significantly impacts the electrochemical performance of the supercapacitor device. In recent times, there has been a growing interest in the utilisation of 2D MXene-based electrode materials for supercapacitor applications. This is primarily due to their exceptional properties such as metallic conductivity, notable hydrophilicity, significant pseudocapacitive behaviour, and the convenience of fabricating freestanding flexible electrode films. Nevertheless, the reconfiguration of MXene nanosheets (NSs) and their oxidation during the fabrication of electrode films have posed significant obstacles in fully harnessing the capabilities of MXene-based materials in the realm of supercapacitors. Hence, the integration of MXenes with various materials, including conducting polymers, pseudocapacitive metal oxides, and carbon nanomaterials, has been documented as a viable approach to mitigate self-oxidation and restacking issues, while enhancing pseudocapacitive characteristics. These factors collectively contribute to the enhancement of electrochemical performance in MXene-based materials. The electrochemical performance of MXene has been enhanced by combining it with conducting polymers that exhibit notable pseudocapacitive properties, including PPy, PEDOT, and PANI[215]. This has resulted in the fabrication of MXene-conducting polymer NCPs. The enhanced electrochemical performance observed in this study can be attributed to

the combined effects of intercalation and the formation of a conductive aligned pathway for charge percolation. These effects are facilitated by the presence of conducting pyrrole on the $Ti_3C_2T_x$ MXene material. Nevertheless, the specific capacitance experienced a significant decrease when the pyrrole concentration in the NCPs was elevated to a 1:1 ratio of PPy to $Ti_3C_2T_x$. This decline can be attributed to the existence of electrochemically inert, non-doped PPy in conjunction with MXene. It is worth noting that an increased proportion of PPy (1:1) resulted in the development of a substantial polymer layer, leading to its detachment from the MXene network[205]. The robust connection established between the polymer backbone and MXene surfaces not only guarantees favourable electrical conductivity but also facilitates an appropriate route for the transportation of charges. Furthermore, the incorporation of MXene-polymer NCPs resulted in an enhancement of structural stability. Additional studies have documented the utilisation of MXene-polymer nanocomposites (NCPs) with enhanced performance as electrode materials for supercapacitors. Notably, MXene/PEDOT:PSS and MXene/PANI have been investigated for their potential in this application. The MXene/PEDOT:PSS nanocomposites (NCPs) were designed such that the conductive PEDOT component served as a structural support, connecting the MXene nanosheets (NSs) and facilitating the exposure of a greater number of electroactive surfaces[216]. Additionally, the formation of a conductive bridge served to reduce ion diffusion pathways, thereby facilitating electron transport channels and enhancing the electrochemical reaction process. Hence, the aforementioned non-conductive polymer (NCP) film demonstrated a significant volumetric capacitance of 1065 F cm−3 when tested at a scan rate of 2 mV s−1, displaying excellent performance in terms of rate capability in an acidic electrolyte consisting of 1 M H_2SO_4. In a recent study, researchers reported the synthesis of MXene/PANI NCPs using an oxidant-free in-situ polymerization method. Similar to conducting polymers, transition metal oxides (TMOs) and hydroxide nanostructures are recognised for their pseudocapacitive characteristics. Numerous pseudocapacitive transition metal oxides (TMOs) and hydroxides, including molybdenum trioxide (MoO_3), manganese oxides (MnO_2), tungsten oxides (WO_3), and layered double hydroxides, have been integrated with MXenes. These composites have been employed as electrode materials in the development of supercapacitors. The study documented the application of hydrothermal methods to deposit MoO_3 nanoparticles onto 2D MXene ($Ti_3C_2T_x$)[217], [218]. This deposition process was found to enhance the contact area between the electrode and electrolyte, resulting in a reduction in the distance travelled by ions during migration and intercalation. The two-dimensional MXene material provided support for the MoO_3 nanoparticles, effectively preventing their self-agglomeration. This support enabled

efficient charge transport, thanks to the high conductivity of the MXene material. The electrochemical characterizations revealed that the MoO_3/MXene nanocomposite material demonstrated a significantly higher specific capacitance of 151 F g^{-1} when tested at a scan rate of 2 mV s^{-1}. In comparison, the pure MXene material exhibited a specific capacitance of 103 F g^{-1} under the same experimental conditions. Furthermore, the NCP exhibited remarkable cyclic stability, as evidenced by a retention rate of 93.7% for the specific capacitance after subjecting it to 8000 consecutive galvanostatic charge-discharge (GCD) cycles at a current density of 1 A g^{-1}.[123] Manganese dioxide (MnO_2) is a frequently investigated pseudocapacitive material within the realm of transition metal oxides (TMOs). This material is particularly noteworthy due to its affordability, lack of toxicity, impressive specific capacitance, and its capacity to be adjusted to various morphologies. Tang et al. reported the synthesis of a novel nanocomposite material consisting of MnO_2 nanoparticles decorated on MXene nanosheets[219]. The MnO_2 nanoparticles, with a size range of 20-40 nm, were uniformly incorporated into the MXene matrix as intercalating agents. In a similar vein, the integration of various morphologies of MnO_2 with MXene has resulted in the formation of MnO2-MXene NCPs, which exhibit enhanced electrochemical properties suitable for applications as supercapacitor electrodes. This improvement can be attributed to the synergistic effect arising from the combination of MnO_2's high specific capacitance and MXene's high electrical conductivity. Additional non-carbonaceous composites of MXene-metal oxides have been documented in the literature for utilisation in supercapacitor systems. Notably, the MXene/WO_3 and MXene-NiO composites have exhibited remarkable electrochemical properties, showcasing elevated specific capacitance values and superior durability in comparison to pristine MXene materials. In addition to metal oxides, metal-layered double hydroxides (LDHs) have also been employed for the creation of heterostructures with MXene materials, with the aim of enhancing their performance as supercapacitor electrodes. Zhao et al. reported the synthesis of a heterostructure at the molecular level, composed of MXene and Ni-Co-Al-LDH. The MXene/metal-LDH NCPs exhibited a distinctive layered heterostructure, characterised by the sequential arrangement of molecular-level NSs. The electrochemical performance of the heterostructures consisting of MXene-metal LDH at the molecular level was significantly improved due to their combined conductive and pseudocapacitive properties. In the MXene/Ni-Co-Al-LDH NCPs under consideration, the MXene layers were observed to allow for electron penetration, while the 2D galleries facilitated rapid diffusion of electrolyte ions. Consequently, this arrangement facilitated the shortest diffusion pathway and resulted in the highest charge transfer efficiency. The MXene/Ni-Co-Al-LD composite material exhibited

a specific capacitance of 748.2 F g^{-1} when subjected to a current density of 1 A g^{-1}. Additionally, it demonstrated an improved rate capacity, indicating that the combination of MXene and metal LDH at the molecular level holds great potential for utilisation as an electrode material in high-energy supercapacitors[124], [155], [220], [221]. The enhanced electrochemical performance of the MXene/metal oxide NCPs can be attributed to the synergistic effects resulting from the combination of MXene's electrical conductivity and the redox charge storage behaviour exhibited by the nanostructured metal oxide materials. Furthermore, a considerable assortment of electrode materials for supercapacitors has been produced by integrating MXenes with diverse carbon materials such as carbon nanotubes (CNTs), carbon nanofibers (CNFs), graphene (Gr), and activated carbon (AC)[123]. This amalgamation aims to enhance the electrochemical efficacy of supercapacitor devices. The inclusion of carbon materials between the $Ti_3C_2T_x$ NSs in the majority of reports has been observed to effectively hinder the restacking of MXene NSs. This intercalation process leads to an increase in interlayer spacing and a subsequent enhancement in electrical conductivity. Consequently, these modifications contribute to an improved surface area that is accessible to electrolyte ions and facilitates more efficient charge transfer processes. It is noteworthy to mention that the electrochemical performance of the MXene/SWCNT and MXene/MWCNT NCPs. As previously documented, sandwich-like architectures comprising one-dimensional (1D) and two-dimensional (2D) nanomaterials have exhibited exceptional electrochemical properties, notably in terms of cycling stability. In recent studies, carbon materials have been employed as conductive bridges to establish connectivity between $Ti_3C_2T_x$ MXene flakesIn addition, the reduced graphene oxide nanosheets (rGO NSs) served a dual role by offering structural support during electrode preparation and functioning as a nanoscale current collector. The utilisation of electrospun MXene/CNF composites has been documented in the literature as a promising approach for the development of supercapacitor electrodes. One notable benefit of electrospun MXene/ CNF NCPs is their formation as a mat structure, wherein the CNFs are incorporated with delaminated MXene sheets. This characteristic allows for the direct utilisation of MXene/CNF mats as electrodes, eliminating the need for binders or additives. Consequently, the ion transport process is enhanced due to the reduced path length for both ions and electrons, resulting in accelerated transport kinetics. The results obtained from the electrochemical impedance spectroscopy (EIS) measurements indicated that the MXene/holey Gr NCPs demonstrated a reduction in interfacial charge-transfer resistance compared to the pure MXene film. This observation suggests an enhancement in the ionic conductivity of the MXene/holey Gr NCPs. The development of high-performance asymmetric supercapacitors is

a significant approach in achieving increased energy density while maintaining the power density of supercapacitor devices. MXene nanosheets have been employed in the production of asymmetric and hybrid supercapacitors to achieve superior energy and power density[222]. The electrolyte employed in this study was a 1.0 M solution of potassium hydroxide (KOH), while cellulose papers were utilised as the separator material. The device exhibited a significant potential range of 1.6 V, and subsequent increments in the operational voltage to 1.8 V resulted in the decomposition of the electrolyte. The triangular GCD curves, characterised by minimal charge and discharge platforms, indicate the combined influence of the positive and negative electrodes on the specific capacity. In recent times, the advancement in the field of miniaturised electronics has necessitated the exploration and creation of miniaturised energy storage devices to cater to the requirements of wearable gadgets and wireless sensor networks. Micro-supercapacitors are regarded as highly promising energy storage components in miniature form due to their rapid charge-discharge kinetics. In this context, the utilisation of MXene-polymer and MXene-Gr nanocomposite particles (NCPs) has demonstrated significant promise in the development of micro-supercapacitors. A micro-supercapacitor with electrochromic properties was successfully produced by employing MXene-conducting polymer NCP electrodes. The micro-supercapacitor, which exhibits asymmetry, demonstrated a notable maximum areal capacitance of 69.5 mF cm^{-2} and an exceptionally high energy density of 250.1 mWh cm^{-3} at 1.6 V[129]. Furthermore, it exhibited excellent cyclic stability. In a separate investigation, Liu and colleagues conducted an experiment to showcase the remarkable self-healing capabilities of a three-dimensional micro-supercapacitor. This device utilised MXene-Gr NCP aerogel and exhibited a substantial areal capacitance of 34.6 mF cm^{-2} when subjected to a scan rate of 1 mV s^{-1}. Additionally, the micro-supercapacitor demonstrated an exceptional cycling performance, with a capacitance retention rate of 91% after undergoing 15,000 cycles. These findings further underscore the potential of MXene-polymer and MXene-Gr NCPs in the advancement of diverse miniaturised energy storage devices. In brief, the enhancement of electrochemical performance in supercapacitor applications was achieved through the synthesis of MXene NCPs in conjunction with various materials such as conducting polymers, metal oxides, and carbon materials. The observed improvements in the electrochemical performances of the MXene NCPs can be primarily attributed to one of the three factors mentioned, or a synergistic combination thereof. One contributing factor was the observed augmentation in the interlayer spacing among the discrete MXene flakes, which effectively hindered the phenomenon of self-restacking. Consequently, this led to an improvement in electrical conductivity, as well as an increase in the surface area available for interaction with

electrolyte ions and facilitating the charge transfer process. The second factor that contributed to the phenomenon was the synergistic amalgamation of the pseudocapacitive-conducting polymer or metal oxides' high specific capacitance and the MXenes' high electrical conductivity. The third factor involved the establishment of a highly interconnected network of nanopores. This network facilitated the rapid movement of ions by reducing the distance they needed to travel, as well as enhancing the transport of electrons. Consequently, the interfacial charge-transfer resistance of the nanoporous carbon particles (NCPs) was reduced.

Rechargeable electrochemical batteries are widely acknowledged and commonly utilised as the predominant means of energy storage. Due to their extended lifespan and substantial energy density, they are extensively employed as energy sources for diverse electronic devices and electric automobiles. There exists a diverse range of rechargeable electrochemical batteries, encompassing various types such as lithium-ion batteries (LIBs), lithium-sulfur batteries (LSBs), sodium-ion batteries (NIBs), and potassium-ion batteries (KIBs). The development of high-performance rechargeable batteries with improved charge storage capacities, energy density, power density, and cyclic stability requires new advanced nanostructured electrode materials. Hence, the development of electrode materials for high-performance batteries represents a captivating field of study. MXene nanosheet-based composite particles (NCPs) have garnered significant attention for their potential in electrode applications. Notably, a range of MXene NCPs, including MXene-carbon and MXene-metal oxides, have been investigated as promising electrode materials for diverse battery systems. Lithium-ion batteries (LIBs) are presently regarded as the most versatile electrochemical energy storage devices. A conventional lithium-ion battery (LIB) comprises a pair of electrodes, namely an anode and a cathode, along with an electrolyte, a separator, and two current collectors, one positive and one negative. The charge storage mechanism of lithium-ion batteries (LIBs) relies on the intercalation and deintercalation processes to store Li-ions in the anode and cathode. The primary focus of research in the field of lithium-ion batteries (LIBs) has been directed towards the advancement of electrode materials that possess enhanced capacity for Li-ion storage.[223]–[229]

1.7 Scientific Outcome

The goal of this project is to develop a simple, low-cost, and environmentally friendly technique for synthesizing Nb-based MXene. To increase the electrochemical performance of Nb-based MXene by combining other nanomaterials with it, and to broaden the applicability of Nb-based Nanosheets for electrochemical sensing.

1.8 Hypothesis

MXene materials have demonstrated considerable promise in the field of electrochemical sensing. Nb-based MXenes and their nanocomposite-modified electrodes exhibit considerable potential as a multifaceted electrochemical sensing platform that may be effectively employed for a wide array of analytes, spanning both biological and non-biological entities.

1.9 Objective and Goals

1.9.1 General Objective

The objective of this study is to employ ecologically sustainable chemical techniques in the production of high-quality Nb-based MXenes and their composites. The synthesised materials will be utilised to explore their distinctive characteristics for the advancement of electrochemical biosensing applications.

1.9.2 Specific Objective

- The objective of this study is to perform solid-state reactions to synthesise MAX phase compounds, with a specific focus on Nb_2SnC and $Nb_4C_3T_x$. Subsequently, a safe and controlled etching technique will be employed to create high-quality Nb_2CT_x and $Nb_4C_3T_x$ MXenes. Throughout the experimental procedure, utmost consideration will be given to minimising any potential environmental impact.
- In order to improve the quality of MXene, the utilisation of bath sonication is employed, which facilitates efficient separation of many layers and enhances its applicability across various domains.
- In order to perform a thorough characterization of the synthesised MXene materials, various analytical techniques were employed. These techniques encompassed a detailed structural analysis using X-ray Diffraction (XRD), an examination of the morphology through Scanning Electron Microscopy (SEM), an assessment of the composition using Transmission Electron Microscopy (TEM) and X-ray Photoelectron Spectroscopy (XPS), as well as an analysis of the elemental composition using Energy-Dispersive X-ray.

- In order to utilise the acquired MXene in the production of a wide range of electrode materials, it is important to integrate different types of nanomaterials. The aforementioned procedure establishes the foundation for the creation of adaptable electrochemical sensing platforms that can be utilised across several scientific disciplines.
- In order to evaluate and ascertain the electrochemical durability of the MXene framework, thereby confirming its appropriateness for extended use in electrochemical biosensors and its resilient functionality even in demanding circumstances.
- In order to broaden the scope of utilisation for synthesised MXene materials, this study aims to serve as a catalyst for the advancement of sophisticated electrochemical biosensors. The utilisation of MXenes' distinctive features can greatly boost the performance and reliability of sensors, enabling them to detect a broad range of analytes, including both biological and non-biological substances.

The objective of this research endeavour is to foster innovation and promote sustainable practises, in line with the worldwide initiative towards environmentally conscious science, precise analytical techniques, and a wide range of potential future applications. The act of exploration has a fundamental role in laying the groundwork for future research and progress within this dynamic and groundbreaking discipline. The forthcoming era is abundant with captivating prospects, and this study signifies a hopeful advancement in the exploration of MXenes, which will undoubtedly have a profound impact on the domains of science and technology in the foreseeable future. With a commitment to intellectual curiosity, groundbreaking ideas, and ethical scientific practises, the culmination of this endeavour symbolises the commencement of the subsequent phase, whereby the mantle of scientific inquiry is entrusted to enterprising individuals who are enthusiastic about advancing it.

1.10 Scientific Goals

- Study the effect of various synthesis parameters of the properties of Nb based MXenes Nanostructures.
- To compare all synthesis methods and will apply the method which is more economic and ease.

- Extending the application of prepared Nb based MXenes Nanosheets for Electrochemical biosensing.

1.11 Academic Goals

- To earn a Doctorate in Science degree with specialization in sustainable processes.
- To present my work in international and national workshops and conferences.
- To investigate in depth the performance of the synthesized materials and working of the asymmetric supercapacitors.
- To publish this work in the proposed 3 year of duration in reputed high impact factor journals.

CHAPTER 2: EXPERIMENTAL TECHNIQUES AND THEORETICAL ASCPECTS

The present chapter functions as a comprehensive and scholarly manual, providing both practical and theoretical guidance for the research endeavours conducted within the context of this thesis. This work encompasses the synthesis of MXenes and the manufacture of electrochemical biosensors, which are crucial components for achieving the research aims. The segment pertaining to characterizations presents a range of key techniques employed in material analysis, including X-ray Diffraction, Energy-dispersive X-ray Spectroscopy, Scanning Electron Microscopy, X-ray Photoelectron Spectroscopy, and Transmission Electron Microscopy. These techniques serve as the foundation for the examination and evaluation of materials. The chapter finishes by examining fundamental electrochemical techniques, such as potentiometry, chronoamperometry, and voltammetric procedures, which are crucial for assessing the electrochemical characteristics of the materials being studied. The establishment of a comprehensive foundation is of utmost importance in order to provide a thorough comprehension and ensure the subsequent success of the research endeavour.

2.1 Synthesis of MXenes

MXenes are a noteworthy group of two-dimensional (2D) transition metal carbides, nitrides, and carbonitrides that have garnered significant attention due to their diverse range of characteristics and wide array of potential uses. The materials, which were initially synthesised in 2011, have subsequently attracted significant interest across multiple disciplines, encompassing energy storage, electrocatalysis, environmental remediation, and sensor technologies. The synthesis of MXenes plays a vital role in determining their structural features, surface chemistry, and subsequent applicability for certain purposes. The process of synthesising MXenes predominantly entails the targeted extraction of the 'A' component from the stratified precursor materials known as MAX phases. In this context, 'M' means an early transition metal, 'A' represents elements from group A, and 'X' signifies carbon and/or nitrogen. Multiple techniques exist for the synthesis of MXene, each contributing unique characteristics

to the resultant MXene material, hence allowing for customization to suit specific applications. In this chapter, two main methodologies for MXene production are examined: the conventional acid etching technique and the molten salt etching method. The conventional method of acid etching, which can be traced back to the initial exploration of MXenes, entails the separation and removal of layers from precursor materials of MAX phases through the utilisation of powerful acids. In contrast, molten salt etching presents an alternate pathway that allows for enhanced control and scalability in the production process. Both methodologies present their own distinct advantages, problems, and opportunities for MXene design. This chapter provides a comprehensive exploration of the synthesis techniques, focusing on the underlying principles, experimental methodologies, and influential factors that impact the final results. Furthermore, we will examine the most recent progress and alterations made to these techniques, providing insight into developing patterns in the synthesis of MXene materials. Upon completion of this chapter, readers will possess a thorough comprehension of the synthesis processes employed in the production of MXenes. This knowledge will enable them to make well-informed decisions when customising MXenes for particular applications within the domain of advanced materials and technologies.

- **HF etching**

MXenes have gained significant popularity as a class of materials in recent times. There are numerous factors contributing to the significant level of interest that MXenes have garnered within the scientific community. One of the primary advantages is in the inherent simplicity with which substantial quantities can be produced. Two pieces of equipment are necessary for admission: an etching-specific high-temperature furnace with a controlled atmosphere and fume hood. It is crucial to acknowledge at this juncture that the production of high quality MXene powders, films, and colloidal suspensions can be achieved even when commencing with highly impure materials, as long as the latter cannot undergo delamination. The utilisation of this particular attribute was leveraged in the production of affordable MXenes, commencing with rutile, aluminium, and carbon[153]. During this particular procedure, low-cost rutile has a reaction with aluminium (Al) and carbon (C) to produce either titanium aluminium carbide (Ti_3AlC_2) or titanium aluminium carbide (Ti_2AlC) together with alumina. The alumina flakes are then treated to centrifugation after

being exposed to the etching and delamination processes. Consequently, the colloidal suspension obtained consists of highly pure MXene. The process of top-down synthesis of MXene entails the targeted removal of specific layers from the original layered precursor material, which could be a precursor in the MAX phase or a non-MAX phase. The initial MXene compound, namely titanium carbide (Ti_3C_2), was synthesised by means of a process including the targeted removal of aluminium (Al) from the titanium aluminium carbide (Ti_3AlC_2) compound, also known as MAX, with hydrofluoric acid (HF)[138]. Subsequently, the utilisation of top-down synthesis methods including hydrofluoric acid (HF) or the generation of HF in situ through the use of fluoride solutions has played a crucial role in the production of several MXenes derived from layered precursors[154]. Presently, the majority of top-down synthesis techniques employed for MXene continue to depend on fluoride-based etchants owing to their preferential ability to etch out the A element. However, there are recorded examples of using alkaline solutions, molten salts along with hydrothermal treatments as alternative synthesis procedures, increasing the spectrum of potential synthesis routes and ultimately impacting the final properties. The material's surface exhibits imperfections and is frequently adorned with diverse distributions of surface functions, including oxygen(O), hydroxyl (OH) and fluorine (F) [155]. The dependence of the concentration of each component has been demonstrated to be influenced by the process of synthesis. In comparison to regions or areas with monodisperse terminations, nuclear magnetic resonance (NMR) data show that random dispersion of surface terminations are more realistic[156]. Surfaces produced by the selective etching of A elements are thought to have a major impact on a number of material characteristics, such as electrical band gaps, optical absorbance, and surface chemistry.[157]–[161]. As of the present time, approximately 22 distinct MXenes have been successfully synthesised, with numerous others being projected[159], thus establishing it as one of the most swiftly progressing families of two-dimensional materials[154], [159], [230], [231]. The present methodologies employed for the synthesis of MXenes from layered precursors including aluminium can be classified into five distinct categories: (i) employment of hydrofluoric acid (HF), (ii) utilisation of HF-forming agents, (iii) application of etchants containing HF (sometimes referred to as mixed acid etchants), (iv) using molten-salt etching techniques, and (v) using alkaline and/or hydrothermal treatments, which were covered in **Table *1***.

Table 1: Various techniques for the synthesis of different MXenes

MXene	AI-Containing Precursers	Etchant	Time(h)	Temp (^oC)	References
Ti_2C	Ti_2AlC	10 wt% HF	10	RT	[139]
		13.5 M LiF in 6M	15	40	[232]
		1.6 M FeF_3 6M HCL	50	50	[233]
		21.5 M NH_4F in 12 M HCL	24	30	[234]
V_2C	V_2AlC	50 wt% HF	90	RT	[162]
Nb_2C	Nb_2AlC	50 wt% HF	90	RT	[162]
$(Ti,V)_2AlC$	$(Ti,V)_2AlC$	50 wt% HF	19	RT	[139]
$(Ti,Nb)_2C$	$(Ti,Nb)_2AlC$	50 wt% HF	28	RT	[139]
Ti_3C2	Ti_3AlC_2	50% wt HF	22	RT	[235]
		5 M LiF in 6M HCL	45	40	[236]
		30 M LiF in 6 MCL	15	40	[237]
		31 M KF in 12 M HCL	24	30	[238]
		5M LiCl in 6 M HF			[239]
		1M Na_4HF_2	12	60	[142]
Ti_3CN	Ti_3AlCN	30 wt% HF	18	RT	[142]
Zr_3C_2	$Zr_3Al_3C_5$	1 M $NaHF_2$	12	RT	[240]
Mo_2TiC_2	Mo_2TiAlC_2	10 wt% HF + 10 wt% HCL	40	40	[241]
Hf_3C_2	$Hf_3(AlSi)_4C_6$	35 wt% HF	48	55	[242]
Nb_4C_3	Nb_4AlC_3	50 wt% HF	96	RT	[163]
Ta_4C_3	Ta_4AlC_3	50 wt% HF	72	RT	[139]
Ti_4N_3	Ti_4AlN_3	Molten salts (NaF, KF and LiF)	0.5	550	[243]

One of the initial methods employed to diminish the strength of M-A metallic bonds while preserving the integrity of M-X bonds involved subjecting Ti_3AlC_2 to HF as an example:

$$Ti_3AlC_2 + 3HF = AlF_3 + 1.5H_2 + Ti_3C_2 \quad (1)$$

In the course of this process as depicted in **Figure 3**, the intercalated aluminium layers undergo removal from the interstitial spaces between individual Ti_3C_2 layers, hence leading to the dissipation of the metallic connection that exists between titanium (Ti) and aluminium

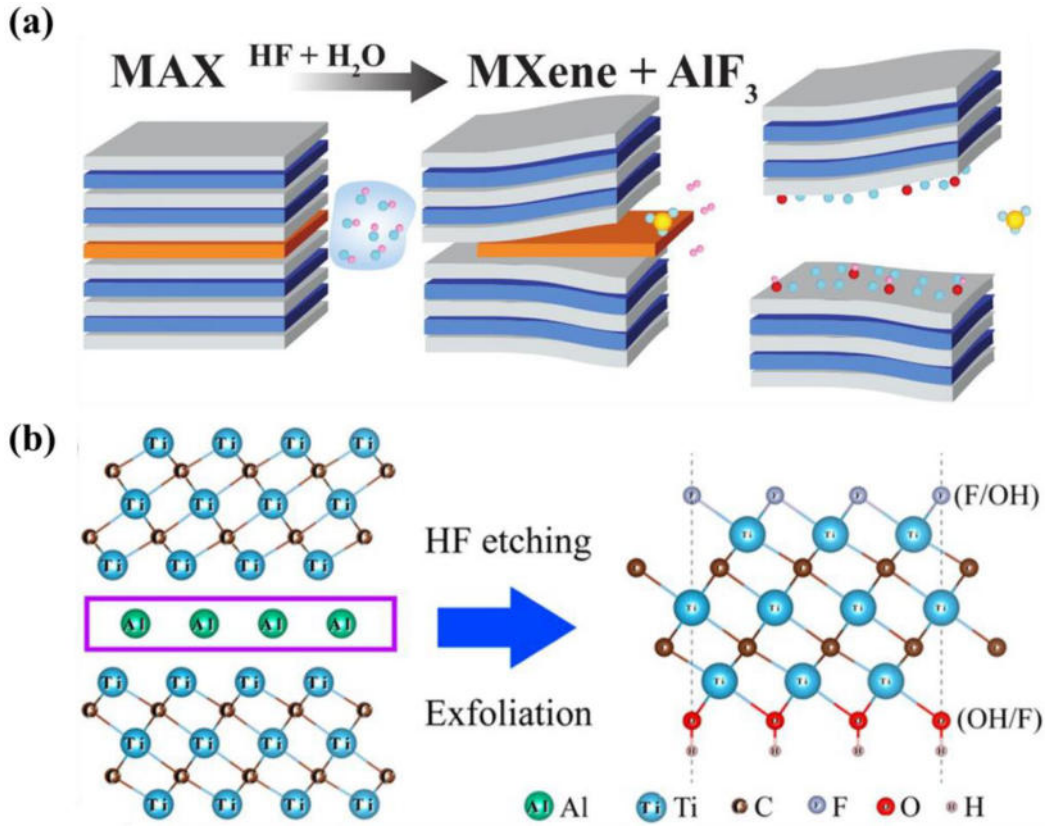

Figure 3:Schmetic Diagram of MXene synthesis by HF acid

(Al)[244].

From a few hours to many days, various exposure periods to hydrofluoric acid (HF) have been documented in the literature. The etching temperature has also been shown to range from ambient temperature (about 22 °C) to high temperatures, like 50 °C[154]. The alteration in HF concentration, specifically from a low concentration of around 3 wt% HF to a higher concentration of 7 wt% HF, has been observed to result in variations in the defect concentration of the generated materials. It has been noted that an increase in the HF content within the etchant solution leads to an augmented presence of defects. In response to the high level of risk and potential harm associated with hydrofluoric acid (HF), researchers have identified alternate approaches aimed at reducing the amount of HF employed and enhancing the safety of the reaction. Both methods have been employed for the development of in situ HF etchants in order

to achieve selective etching of MAX phase precursors. Recently, there have been successful syntheses of new MXene members, namely Hf_3C_2 and $Mo_{1.33}C$, in addition to the existing MXenes. These new MXenes were synthesised using HF from $Hf_3(AlSi)_4C_6$ and $(Mo_{0.67}Sc_{0.33})_2AlC$ [245], [246]. MXenes synthesised through the process of selective etching using hydrofluoric acid (HF) demonstrate a higher prevalence of surface terminations consisting of fluorine (-F) and hydroxyl (-OH) groups, as opposed to oxygen (-O) groups[247]. Etchants comprising acid mixes with a reduced proportion of hydrofluoric acid (5-10 wt%) have the potential to be employed in the synthesis of diverse metal oxides, specifically MXenes. Etching solutions utilising hydrofluoric acid (HF) and hydrochloric acid (HCl) have been employed in the synthesis of Mo_2TiC_2 and $Mo_2Ti_2C_3$ compounds, derived from the Mo_2TiAlC_2 and $Mo_2Ti_2AlC_3$ MAX phases, respectively[248]. The synthesis approach involving a combination of HF and HCl exhibits greater control over the selection of etchant components and the quantity of HF employed, hence conferring a notable advantage over the exclusive use of HF for etching purposes. The utilisation of aqueous acidic solutions for etching nitride-based MAX phases has yielded unsatisfactory results due to the lower predicted cohesion energies seen for nitride MXenes compared to carbides. By employing molten salts such as sodium fluoride (NaF), lithium fluoride (LiF), and potassium fluoride (KF), it has been possible to synthesize nitride MXenes, particularly Ti_4N_3[249]. In order to facilitate the etching process, the molten salt and Ti_4AlC_3 mixture underwent heating to a temperature of 550 ◦C in an argon environment for a duration of 30 minutes. This heating procedure aimed to potentially augment the reaction by providing additional energy, hence enabling the overcoming of bonding disparities between metals in a MAX phases which contains nitrite(N)[250]. The strong binding ability of alkalis with aluminium makes alkaline etchants potentially beneficial for etching Ti_3AlC_2 or other layered precursors. Nevertheless, in order to eliminate aluminium (Al) in an alkaline setting, it is imperative to employ elevated temperatures and pressures, which are commonly achieved through hydrothermal treatment. The synthesis of Ti_3C_2 involved the initial pretreatment of Ti_3AlC_2 powders in a low-concentration solution of hydrofluoric acid (HF) for a duration of 30 minutes, followed by immersion in a solution of tetramethylammonium hydroxide (TMAOH)[251]. Nevertheless, this methodology continues to depend on the exposure of hydrofluoric acid (HF), and it has not been demonstrated that tetramethylammonium hydroxide (TMAOH) may directly and selectively etch aluminium (Al) from titanium aluminium carbide (Ti_3AlC_2). Furthermore, it has been shown that Ti_3AlC_2 is hydrothermally treated with an alkali to produce Ti_3C_2, which produces a material without fluorine terminations[252]. The procedure, commonly referred to

as the Bayer process, entails the oxidation of aluminium to form aluminium oxide/hydroxides. Subsequently, the aluminium compounds are dissolved in an alkali solution, resulting in the production of a Ti_3C_2 MXene that is terminated exclusively with -OH and -O groups. Al-containing MAX or non-MAX phases have been etched to produce MXenes, which are synthesized top-down from layered precursors. The observed phenomena can be attributed to aluminum (Al) having a comparatively lower reduction potential than other elements in group A. Additionally, the etchants containing hydrofluoric acid (HF) have the capability to weaken the bonds between aluminium (M) and other elements (A), unlike the connections involving other elements in group A. The preferred precursor for the synthesis of Ti_3C_2 is Ti_3AlC_2, as opposed to Ti_3SiC_2 or Ti_3GeC_2 for example as mentioned in Table 1. The processing parameters utilised in the synthesis of MXene exhibit variability contingent upon factors such as the chosen method, flake size, shape, medium or solvent, desired qualities, and intended application. The process of delamination of multilayered powders is commonly employed to produce 2-dimensional MXene sheets. These sheets can then be used in a variety of fabrication processes to produce thin films, including spin coating, dip coating, vacuum filtration, and spray coating. Additionally, they can be added to conductive ink formulations, polymer, metal, or ceramic composites, drop cast for measurements involving single flakes, or be included in those materials. Intercalation, a procedure that involves the insertion of big organic bases, organic molecules or cations is widely used to cause delamination. The delaminated components are then separated from the residual multilayered powders using a series of procedures that include washing, optional sonication, and centrifugation. The morphological characteristics of layered precursors, such as Ti_3C_2 derived from the Ti_3AlC_2 MAX phase, undergo expansion, resulting in hydrophilic surfaces upon contact to hydrofluoric acid (HF). However, pre-intercalation with huge organic molecules, like dimethyl sulfoxide (DMSO), which serves to reduce interlayer connections and ease the separation of flakes, has been the only method of exfoliation of MXene in liquid phase into individual flakes that has been effectively done[235]. The inclusion of intercalation stages plays a vital role in the production of aqueous colloidal solutions of MXenes, enabling subsequent processing and fabrication of MXene films that are capable of standing independently[235], [253]. The achievement of dispersing MXene in both aqueous and organic solutions is possible following the process of delamination[254]. The investigation of the surface charge of Ti_3CN, V_2C, and Ti_3C_2 has revealed the presence of negative zeta potentials across a broad spectrum of pH values[255], [256]. This finding suggests that neutral liquids can easily scatter these MXenes. Using simple techniques like mixing, solvent exchange, or self-assembly, MXene can be formed with other nanomaterials or polymers

thanks to its high degree of dispersibility. The deterioration of MXenes in aquatic environments has been observed, wherein Ti_3C_2 MXene undergoes degradation resulting in the formation of a turbid transparent solution composed of tetragonal titanium dioxide (TiO_2)[257]. The assessment of degradation plays a remarkable role in ascertaining the lifespan and resultant characteristics of a material, necessitating the implementation of measures to regulate, mitigate, or halt the process of oxidation. The storage environment significantly influences the shelf life of a solution, as higher-concentration solutions tend to degrade at a slower rate compared to solutions with lower concentrations. In order to achieve industry-scale development and deployment, it is imperative to prioritise scalability and mass production efficiency. Graphene, an analogous two-dimensional substance, may be manufactured on a large scale by either growth or exfoliation methods. However, in the case of liquid exfoliation procedures, the attainment of high concentrations necessitates the utilisation of organic solvent dispersions, surfactants, or stabilisers such as polymers or proteins. MXene biomedicine, wireless communication, electromagnetic shielding, electronics and huge-scale production capabilities are just a few of the disciplines that could benefit from the scalability of MXene synthesis. The possibilities in these areas would be substantially increased by using MXene films produced on a massive scale[258]–[261].

- **Molten Salt Etching**

The schematic representation of the synthesis process for MXenes, which includes the etching of the "A" layer, exfoliation, intercalation, and delamination, is illustrated in **Figure 3**. As previously mentioned, the initial synthesis of MXene involved the utilisation of aqueous HF at ambient temperature. This method has since been widely employed for the production of other MXenes, such as Nb_2AlC, V_2AlC, Ti_2AlC, Ta_4AlC_3, $(Ti_{0.5}V_{0.5})_2AlC$, among others. The process of etching can effectively eliminate the "A" element from MAX phases. However, the resulting MXenes necessitate a further intercalation procedure involving organic base intercalants including tetrabutylammonium hydroxide (TBAOH), choline hydroxide, and n-butylamine. It is important to mention that the research on aluminum-containing MAX phases has predominantly utilised typical HF-based etching techniques. Furthermore, the surface of MXenes also exhibits functional groups such as -O, -OH, and -F. In 2014, Ghidiu et al. utilised an in-situ HF (a mixture of HCl and LiF) technique to synthesise MXenes, thereby mitigating

the need for meticulous handling of HF acid[262]. Furthermore, this approach also obviated the need for an additional intercalation step, as Lithium would fulfil the job of the intercalant. In the identical year, the utilisation of ammonium bifluoride (NH_4HF_2) was also observed for the purpose of etching the aluminium from titanium aluminium carbide (Ti_3AlC_2). Furthermore, the field of chemical vapour deposition (CVD) technology became involved in this competition in the year 2015, when researchers successfully acquired high-quality crystals of molybdenum carbide. In the subsequent year, the process of utilising molten fluoride salt to remove aluminium (Al) from the precursor compound Ti_4AlN_3 was conducted at a temperature of 650 ◦C. The utilisation of electrochemical etching was initially documented in the year 2017. In this experimental procedure, hydrochloric acid (HCl) solutions were employed to partially etch the aluminium (Al) layer. It is worth noting that the MAX precursor utilised in this study was a porous titanium aluminium carbide (Ti_2AlC) electrode. However, it is worth noting that a relatively elevated etching temperature of 270 ◦C was employed in their experimental procedure. Despite the effectiveness of these approaches in addressing numerous complex issues, it is important to note that these methods present challenges when it comes to scaling up and require a significant time investment ranging from hours to days in order to get MXenes[139].

In recent times, the Lewis-acidic molten salt approach has garnered significant interest among researchers, leading to the emergence of several adaptations and implementations of this technique. This approach offers the opportunity to employ MXenes that are free of hydrofluoric acid (HF) and environmentally safe. Additionally, it introduces new MAX phases that can be selectively etched using this method, allowing for the control of surface functional groups. The initial achievement occurred in the year 2019, when researchers successfully synthesised Zn-based MAX phases including Ti_3ZnC_2, Ti_2ZnC, Ti_2ZnN, and V_2ZnC, as well as their related MXenes[263]. During the process of MS etching, the Zn element first replaces the Al element in the MAX phase at a temperature of 650 ◦C. However, the excessive presence of $ZnCl_2$ is responsible for the removal of this Zn-based layer. Consequently, $Ti_3C_2T_x$ MXenes were synthesised, exhibiting functional groups ended with -Cl and -O. The etching mechanism in this study was not explicitly elucidated, as the removal of the Zn-based A-site element by the Zn-containing salt was not explained in detail. The elucidation of this mechanism occurred in the year 2020, wherein the process involved the etching of Ti_3SiC_2 through treatment with molten salt $CuCl_2$ at a temperature of 750 ◦C. The Lewis acid, specifically the $Cu2^+$ ion, facilitates the oxidation of Si to $Si4^+$ within the MAX phase. Following the procedure,

ammonium persulfate (APS) is employed to eliminate copper (Cu) particles from the $Ti_3C_2Cl_2$ MXenes, thereby introducing oxygen functional groups onto the surface of the MXenes. This article presents a study in which several novel MAX phases were anticipated from an analysis of the redox potential of molten salt etchant and the A-site element. The procedure entails extracting the A-site elements with lower electrochemical redox potential by combining them with molten halides possessing greater electrochemical redox potentials. The pathway that had been recently created underwent further expansion in late 2020 with the addition of new halogen groups, including –Cl, –Br, –I, –BrI, and –ClBrI, onto the surface of Ti_3C_2 MXenes. In this study, a series of compounds including $CuCl_2$, $CuBr_2$, $CuCl_2/CuBr_2$, $CuCl_2/CuI$, $CuBr_2/CuI$, and $CuCl_2/CuBr_2/CuI$ were employed in conjunction with Ti_3AlC_2 to synthesise $Ti_3C_2T_x$ MXenes[264]. These resulting MXenes were subsequently utilised as cathode materials in zinc ion batteries. The $Ti_3C_2Br_2$ and $Ti_3C_2I_2$ MXenes shown notable capacities in comparison to typical MXenes, which will be further elaborated upon in subsequent sections. Subsequently, a study emerged detailing the open air synthesis of MAX, wherein the researchers employed titanium, aluminium, and graphite powders, which were combined with inorganic salts (NaCl and KCl) to produce a pellet. The pellet was then immersed in a solution containing a mixture of NaCl, KCl, and $CuCl_2$, and subjected to a temperature of 1300 ◦C. This process resulted in the formation of an in-situ MAX phase, which was later subjected to in-situ Lewis's salt etching. The etching process was initiated by introducing $CuCl_2$ at a temperature of 700 ◦C, resulting in the etching of the aluminium layer in a time span of 10-40 minutes. The $NaCl/KCl/CuCl_2$ mixture was employed as a surface coating that undergoes melting at a temperature of 300 ◦C. This coating serves as a protective shield for the pellet, safeguarding it from the surrounding environment. Another investigation involved the synthesis of a film by intercalating TBAOH into MS-$Ti_3C_2T_x$ with -Cl terminations, followed by subsequent processing. The MS-$Ti_3C_2T_x$ material was employed as an anode for a lithium-ion battery, demonstrating a notable specific capacity of 225 mAh g^{-1} when charged and discharged at a rate of 1 C. Furthermore, the study also introduced Nb_2CT_x based MXenes that had functional groups primarily composed of oxygen. These MXenes exhibited a notably high specific capacity of 330 mAh g^{-1}. The growing need for research on MXenes has prompted the exploration of a more environmentally friendly approach to producing MXenes. The utilisation of the molten salt Lewis acidic etching method has emerged as a prominent approach in this endeavour, as it enables the customization of surface chemistry and the incorporation of numerous desirable functionalities that are readily available. The utilisation of this approach has demonstrated significant electrochemical efficacy by means of adjusting the surface

moieties.Huang et al. conducted an extensive investigation on the synthesis of MXenes by employing a diverse set of MAX precursors (including Al, Zn, Si, and Ga-containing MAX) in combination with different Lewis acids (such as $NiCl_2$, $CuCl_2$, AgCl, and $CoCl_2$). The synthesis pathway was devised through meticulous anticipation of the redox coupling of both reagents. The MAX phase was selectively oxidised at the "A" site element by the Lewis acid, which exhibited a greater redox potential. The predictability of the reaction between the "A" element of MAX and the Lewis acid chloride melt was assessed using Gibbs free energy mapping[264]. In their study, Gu et al. employed the molten salt Lewis acidic etching technique to synthesise Zinc immobilised on MXene sheets, resulting in the formation of Zn-MXene. Furthermore, they successfully developed dendrite-free lithium metal anodes using this material. A homogeneous mixture was prepared by combining 0.2 g of Ti_3AlC_2 and 0.8 g of $ZnCl_2$, which were subjected to ball milling for a duration of 6 hours within an environment insulated by argon gas. The mixture was subjected to a heating process, reaching a temperature of 550 ◦C with a heating rate of 5 ◦C per minute. Subsequently, it was allowed to remain in an atmosphere of argon for a duration of 10 hours. In order to prevent oxidation of the Zn-MXene, the resultant material underwent a series of washes in water saturated with argon. This process was employed to effectively eliminate any remaining traces of acid and salts[265]. Li et al. conducted a comprehensive investigation on MXenes, with a focus on enhancing the surface functions of these materials. The Lewis acids employed in this study included $CuCl_2$, $CuBr_2$, CuI, or a mixture thereof. These Lewis acids were utilised to synthesise $Ti_3C_2T_x$ MXenes, resulting in the formation of mono (–Cl, –Br, and –I), bi (–ClBr, –ClI, and –BrI), and tri (–ClBrI) halogenated surface terminals. Additionally, the researchers successfully produced a highly effective microwave absorber aerogel composed of MXene-based materials associated with graphene oxide, employing a dopamine crosslinker. This resulting material was denoted as Ti_3CNCl_2/RGO. Recent literature has presented findings on the favourable impact of MXene quantum dots on the efficacy of perovskite solar cells (PSCs). Nevertheless, conventionally synthesised $Ti_3C_2T_x$ exhibits a significant presence of hydroxyl (-OH) groups, which adversely affects the stability of perovskite solar cells (PSCs).

Other Synthesis Methods (Alkaline and/or Hydrothermal Treatment Alkaline)

The strong binding capacity of alkalis with aluminium may render alkaline etchants potentially effective for etching Ti_3AlC_2 or other layered precursors. In certain instances, the application of elevated temperatures or pressures becomes imperative for the extraction of aluminium in an alkaline setting and is employed in conjunction with hydrothermal treatment. The Ti_3AlC_2

powders were subjected to pretreatment in a low-concentration (10-20 wt%) HF solution for a duration of 30 minutes. Subsequently, the powders were immersed in a solution of tetramethylammonium hydroxide (TMAOH), resulting in the formation of Ti_3C_2. However, it is important to note that this technique still depends on the utilisation of HF for etching, and the direct selective etching of Al from Ti_3AlC_2 using TMAOH has not been demonstrated. It is important to acknowledge that in the event of successful alkaline treatments for the selective etching of aluminium (Al) from titanium aluminium carbide (Ti_3AlC_2), the outcome would involve the creation of aluminium oxide/hydroxide layers on the surface. This would occur instead of the exclusive production of Ti_3C_2. Consequently, an additional step would be necessary to cleanse the surface and eliminate these compounds. One of the initial instances of hydrothermal synthesis was documented, when a combination of Ti_3AlC_2 and ammonium fluoride (NH_4F) was subjected to a sealed Teflon-lined autoclave, and subsequently heated at a temperature of 150 ◦C for a duration of 24 hours. Fluoride-free etchants have been suggested as a viable alternative for surface treatment by employing a mix of alkali and hydrothermal processes. One such approach involves the utilisation of sodium hydroxide (NaOH) as the initial treatment, followed by a subsequent hydrothermal treatment with H_2SO_4. In this particular instance, the aluminium (Al) layers were exclusively eliminated from the external surface of titanium aluminium carbide (Ti_3AlC_2), leading to an incomplete etching process. In a more recent study, the synthesis of Ti_3C_2 was achieved by subjecting Ti_3AlC_2 to alkali-assisted hydrothermal treatment in concentrated NaOH. The treatment employed in this study, commonly referred to as the Bayer process, involved the utilisation of concentrated sodium hydroxide (NaOH) solutions at elevated temperatures and pressures. This process effectively initiated the oxidation of aluminium (Al) layers within Ti_3AlC_2, resulting in the formation of aluminium oxide/hydroxides. Subsequently, the aluminium compounds were dissolved into the alkali solution, leaving behind a Ti_3C_2 MXene with terminal functional groups consisting solely of hydroxyl (-OH) and oxide (-O)[169], [178], [180], [266]–[268].

2.2 Fabrication of Electrochemical biosensors

The development of quick in situ analysis poses hurdles for analytical chemists, primarily stemming from the intricate nature and high expenses associated with commercial laboratory testing. SPEs have become a prominent area of focus in electrochemical research due to their ability to facilitate rapid, selective, portable, sensitive, low-cost, and exact tests. Screen printing

is a cost-effective alternative to conventional manufacturing techniques, rendering it a very suitable option for large-scale manufacture of replicable, inexpensive, dependable, disposable sensors intended for on-site monitoring purposes[269]. SPEs enable the production of a significant quantity of carbon electrodes in a consistent, cost-effective, and disposable manner by including functionalized chemicals. These devices find application in several electrochemical domains, encompassing the quantification of chemical and biochemical substances, microelectronics, as well as energy conversion and storage[270]. SPEs are also utilised in the field of flexible electronics, facilitating the deposition of diverse carbon forms such as graphite, activated carbon, and carbon black. SPEs provide convenient manipulation of electrode thickness, surface characteristics, and composition. Moreover, they can be easily deposited onto flexible plastic substrates such as polycarbonate, polyamide, and polyetheretherketone[271]. Additionally, they facilitate the experimental statistical confirmation of findings without the need for duplicate electrodes. Nevertheless, these vehicles are restricted to flatbed configurations and exhibit a range of diverse shapes and structures. SPEs can be produced as needed for analytical purposes and are available in several configurations, including discs, rings, or bands. These tools facilitate the calibration and concurrent, immediate analysis of unfamiliar samples. Nevertheless, their compatibility with nonplanar substrates is limited, hence restricting their potential for use in various fabrication methods. Hence, it is imperative to pursue additional advancements in the field of SPEs. This study examines the utilisation and efficacy of SPEs as electrochemical biosensors between the years 2015 and 2022[272]–[275]. The analysis specifically focuses on the application of SPEs in several types of biosensors, including DNA sensors, aptasensors, immunosensors, and enzyme biosensors[276], [277]. Electrochemical biosensors have the potential to supplant analytical techniques in the realm of in-field screening and monitoring solutions. These biosensors find utility across a range of domains, including but not limited to the food industry, environmental applications, forensics, and the detection of cancer biomarkers. This study provides a comprehensive overview of the most recent improvements in biosensors based on SPE, accompanied by an analysis of potential future advancements in the field. Screen-printing is a commonly employed technique in the fabrication of electroanalytical devices, which have extensive utility in several domains such as biomedical research, food analysis, and environmental monitoring for the detection of pollutants. SPE devices, initially established during the 1990s, are versatile instruments capable of accommodating many configurations and can be adjusted using various biological components, including synthetic diagnostic elements, DNA, enzymes, and antibodies. Disposable tools are intentionally designed to be

discarded after use, mostly because of their affordable cost, ability to be replicated, dependable performance, and capability for large-scale production. SPEs are composed of three distinct electrodes, namely the pseudo reference electrode (RE), counter electrode (CE), and working electrode (WE), which are all printed on a solid substrate. These devices possess advantageous characteristics such as simplicity, affordability, adaptable selectivity, little consumption of sample volume, and minimal generation of trash. These substances exhibit compatibility with a wide range of analytical techniques and can be effectively utilised for the identification and quantification of analytes in diverse domains such as clinical, pharmaceutical, environmental, and microbiology areas. Additionally, they demonstrate efficacy in the analysis of heavy metal ions and liquid biofuel samples. Nevertheless, it is important to acknowledge that SPEs do possess certain limits. These limitations encompass a repeatability rate that is approximately 5% or more, elevated costs arising from the need for specialised substances for SPE production or the analysis of many samples, as well as unproductive analysis following automated or mechanised methods. The construction of most SPEs typically involves the use of materials sourced from reputable manufacturers such as Metrohm DropSens or Gamry Instruments. However, it is worth noting that certain manufacturers in China and Europe have established expertise in the development and design of electrochemistry assessment tools. The construction method of SPEs exhibits a high degree of expediency, enabling the fabrication of single-use electrodes characterised by compact dimensions and cost-effectiveness. The compression of carbon and metallic inks, which are frequently employed in writing instruments (WEs), is achieved through the utilisation of a mesh screen on the substrate. The formulation of paste in commercial settings presents a complex challenge, primarily due to the intricate analytical processes involved and the significant economic value associated with manufacturing sensors. Various types of inks commonly employed in writing instruments (WEs) encompass carbon-based substances such as graphite, fullerene, graphene (Gr), carbon nanotubes (CNTs), as well as conductive metallic inks. Aurum ink is frequently employed owing to its structural similarity to thiol functional groups and its capacity for facile protein surface modification. However, the utilisation of such inks is seldom and restricted to certain applications. Silver or silver/silver chloride inks are frequently utilised in the field of resistive electrode (RE) construction, which is classified as quasi or pseudo RE due to its inherent instability in potential. The chemical composition of ink, particularly in relation to its electrochemical applications, holds considerable importance. The formulation and structural details of SPEs used in ink are protected by patents held by various firms, thereby preventing their disclosure to end-users. Controlling the potential in solid-state electrochemical evaluations might provide challenges,

although the utilisation of detecting methods is rather straightforward. SPEs exhibit a high degree of versatility owing to their wide range of ink configurations, which play a crucial role in determining the electrochemical parameters of the electrode. The alterations are implemented with the aim of improving the electroanalytical characteristics and immobilisation capabilities of recognition elements, which may encompass both biological and synthetic components. In order to enhance the conductivity of SPEs, it is common practise to subject ink slurries to pulverisation in ball mills. This process results in the formation of minuscule conductive carbon particles, referred to as fines, which possess sizes ranging from 1 to 100 nm. Poly (vinylidene fluoride) is a commonly utilised thermoplastic and thermosetting polymer binder, representing one of the two prevalent kinds. The predominant technique employed by electrochemists involves the dissolution of a thermoplastic polymer in a solvent with a high boiling point. Various adhesives, including ethylene glycol, cellulose acetate, resin, and cyclohexanone, are incorporated to affix the paste onto the substrate. Additionally, blended additives may be employed to augment sensitivity, specificity, and signal-to-noise ratio (S/N). The process of SPE construction encompasses multiple stages, including the design of mesh or screen, selection and provision of conductive inks and substrate materials, thin film fabrication through layer-by-layer deposition, drying using hot air and infrared radiation, and curing to achieve ink solidification. The execution of analytical evaluations can be achieved through the use of an insulating substance to envelop the electrical circuits. The pretreatment of SPEs plays a critical role in addressing the limitations imposed by reduced electron transport kinetics at the interface with the electrolyte. Electrochemical techniques are commonly employed to activate edge planes of SPE materials. The research conducted by Sundaresan's group involved the implementation of ten cycles of cyclic voltammetry in a phosphate buffer solution. In contrast, Pan's group employed a different approach by subjecting an electrode to a constant potential for a duration of twenty seconds, while also introducing a drop of NaOH. SPEs have garnered significant interest within the biological and clinical domains owing to their capacity for customization and miniaturisation. Commercially available products have been utilised in a range of applications across the therapeutic, environmental, and food sectors. In order to enhance their analytical characteristics, many modifications have been implemented utilising diverse nanomaterials and synthetic differentiation agents. Various carbonaceous substances, including carbon black (CB), carbon nanotubes (CNTs), graphene (Gr), metallic nanoparticles (Au and Ag), magnetic beads (MBs), and mediator nanoparticles (cobalt phthalocyanine and Prussian blue), have been employed for the purpose of modifying SPE. Nanosubstances have the ability to exhibit similar dimensions as biological diagnostic elements such as proteins and

DNA. The composition of these nanosubstances can lead to synergistic effects, resulting in unexpected benefits. The advancements in nanotechnology have had a significant impact on research in the field of enzyme biosensors. The utilisation of nanomaterials in biosensor development is advantageous due to their capacity to enhance electrocatalytic activities and mitigate electrode surface deposition. The electrochemical performance of sensors modified with nanomaterials was assessed through the application of cyclic voltammetry (CV), electrochemical impedance spectroscopy (EIS), and amperometry. These techniques were employed to effectively convey the electrochemical behaviour of the sensor in relation to the characteristics of the nanomaterials, as well as to ascertain the influence of the nanomaterials on the analytical properties of the sensor. The most straightforward approach for changing screen printed micro electrodes (SPME) fibres involves depositing the modifying agent onto the working electrode (WE). This can be achieved using an automated dispenser during mass production processes. The alteration of the electrode surface of these tools is commonly carried out using three established procedures: ink mixing with a modifier agent, progressive electrochemical deposition of a metallic substance, or drop casting of nanomaterials. Drop casting methods offer a suitable approach for the modification of SPE due to the ability to prepare the ink prior to doing the adjustments. Potentiostatic methods are commonly employed for the manipulation of SPEs, while galvanostatic methods are found to be more efficacious in the context of SPEs. The inclusion of the mediator on the electrode surface and the formation of surface oxygen functions are regarded as supplementary fundamental attributes in comprehending the reactivity of solid polymer electrolytes. The utilisation of graphene (Gr) and carbon nanotubes (CNTs), which are well recognised carbon-based materials, has significantly transformed the field of electroanalysis. The application of carbon nanomaterials has been demonstrated as a viable approach, from both analytical and economic perspectives, for producing modified SPE devices. Electrochemical biosensors based on screen-printed (SP) technology have garnered significant interest as analytical tools in several fields such as agriculture, pharmacy, medicine, and food analysis. This can be attributed to their cost-effectiveness, user-friendly nature, small sample volumes required, and portability. Nevertheless, it should be noted that a SPE, while commonly employed as an electrode, does not possess the same level of robustness as a solid electrode with a highly polished surface like a mirror. The cost-effectiveness and compactness of SPEs have contributed to their increased use as transducers in biosensing applications in recent times.Sensitive and selective sensors have been widely employed in the clinical and pharmacy domains for the fabrication of SPE devices. These SPEs have found significant application in the detection and analysis of diverse

analytes. The utilisation of SPEs in conjunction with paper-based microfluidics offers distinct advantages in the acquisition of electrochemical biosensors, as compared to conventional analytical instruments fabricated using alternative substrates such as polymers, silicon, or glass. The cellulose papers provide a notable surface area, which renders them suitable substrates in conjunction with SPE for the development of novel point-of-care detection instruments, including microfluidic systems, inside clinical environments. One domain in which self-propelled entities SPEs have demonstrated notable proficiency is in the realm of environmental detection. A range of paper samples, which have been appropriately treated with metal nanoparticles or carbon nanostructures, have been utilised for the purpose of detecting contaminants, such as heavy metals and anions.

2.3 Characterizations used for the synthesized Materials.

2.3.1 X-ray Diffraction

Within the field of materials research, scientists often encounter several analytical inquiries pertaining to the chemical composition and crystalline structure of various materials. X-ray diffraction (XRD) is a laboratory technique that allows for the non-destructive and precise acquisition of various types of information, including crystal structure, preferred orientation, chemical composition, lattice strain, crystallite size and layer thickness. Hence, researchers in the field of materials science employ X-ray diffraction (XRD) as a technique for the analysis of diverse materials, encompassing powders, solids, thin films, and nanomaterials[278]. X-ray diffraction (XRD) is a highly adaptable non-destructive analytical method employed for the examination of many physical properties, including phase composition, crystal structure, and orientation of samples in powder, solid, and liquid forms. Numerous materials consist of tiny crystallites. The designation of the chemical composition and structural arrangement of these crystals is commonly referred to as their 'phase'. Materials can exist in either a single phase or a multiphase state and can consist of both crystalline and non-crystalline constituents. The X-ray diffractometer is capable of producing distinct diffraction patterns for various crystalline phases. The process of phase identification entails the comparison of X-ray diffraction patterns acquired from unidentified materials with patterns contained inside reference databases. The aforementioned procedure bears resemblance to the act of comparing fingerprints in the context of a criminal investigation[279]. The International Centre of Diffraction Data (ICDD) is

responsible for maintaining the most extensive chemical database available. One can alternatively construct a reference database by utilising pure-phase diffraction patterns obtained by measurement, patterns documented in scientific literature, or patterns acquired through personal experimentation. The comprehensive composition of a sample is determined by assessing the relative intensities of the patterns derived from various phases within a multiphase mixture. X-Ray Diffraction is the result of constructive interference between X-rays and a crystalline material. The X-rays employed possess a wavelength that is comparable to the interatomic spacing within a crystalline lattice. The phenomenon leads to the formation of a diffraction pattern, which can be subjected to several analytical methods. Among these methods, the widely utilised approach involves the application of Bragg's Law (as depicted in **Figure *4***) ($n\lambda=2d \sin \theta$), a renowned equation employed in the examination of crystals and their respective phases.

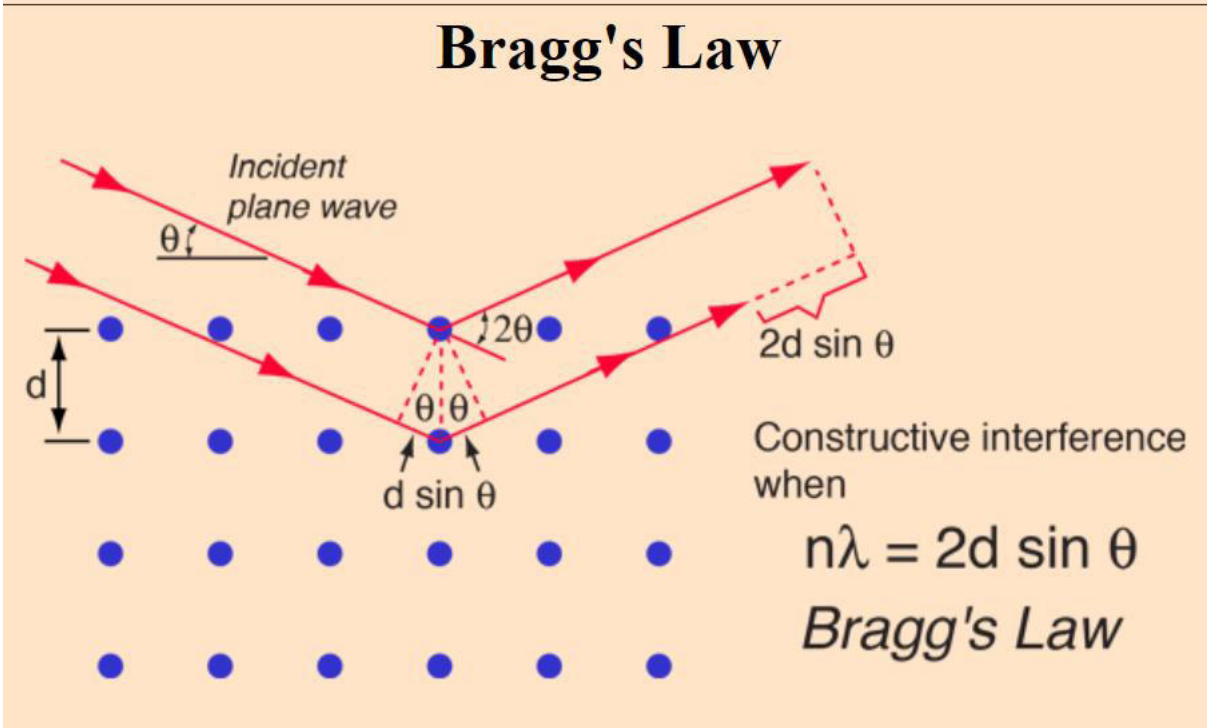

Figure 4: Bragg's Law and scattering of crystal lattice.

The X-ray instrument comprises three primary components, namely an X-ray source, a sample holder, and an X-ray diffraction (XRD) detector as depicted in **Figure *5***. The sample is illuminated by the X-rays generated by the source. thereby, the incident beam undergoes diffraction upon interaction with the sample phase, thereby penetrating the detector. The intensity is assessed, and diffraction data are collected by altering the diffraction angle (2θ), which involves relocating the tube or sample and detector to modify the angle between the

incident and diffracted beams. The angle between the incident beam and the sample can be either constant or variable, depending on the diffractometer's geometry and the type of sample. This angle is typically associated with the angle of the diffracted beam[280].

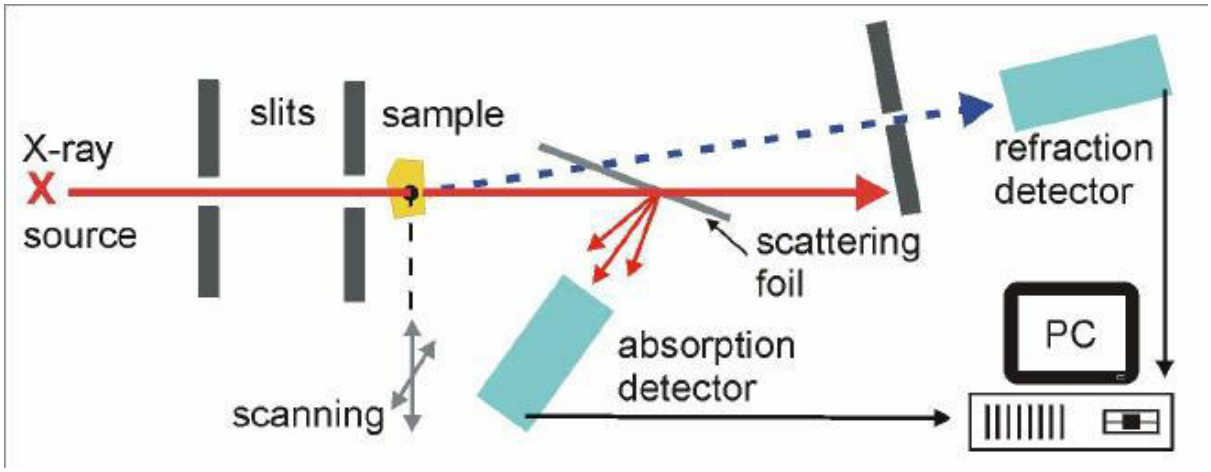

Figure 5: Instrumentation of XRD for the sample detection

X-ray diffraction (XRD) is widely utilised by researchers in both industrial and scientific institutions for the purpose of developing novel materials and enhancing production efficiency. The advancements in X-ray diffraction techniques are closely aligned with the ongoing research in various fields, including semiconductor technologies and medicinal investigations, which focus on the development of novel materials. Industrial research is focused on enhancing the velocity and effectiveness of manufacturing operations. The implementation of fully automated X-ray diffraction examinations at mining and building materials manufacturing sites has been found to yield more economically efficient methods for production control. X-ray powder diffraction (XRPD) is widely recognised as the prevailing technique for phase analysis. These investigations extend beyond typical ambient conditions, allowing for a comprehensive understanding of phase transitions in diverse environments. The examination of physical characteristics, including the diameter of crystallites, the orientation of crystals, and the presence of residual stress, collectively referred to as the "microstructure" of polycrystalline materials, is subject to analysis[281].

Additionally, X-ray diffraction (XRD) is a powerful tool that enables researchers to obtain comprehensive knowledge regarding the structural properties and crystalline structure of MXenes[282]. The relevance of this technique resides in its capacity to clarify the organisation of atoms within the crystal lattice, which is a critical factor in investigating the distinctive layered architectures of MXenes. The crystallography and polymorphism of MXenes are frequently characterised by intricate features, and X-ray diffraction (XRD) provides a robust

method for unravelling these intricacies. X-ray diffraction (XRD) is a valuable technique employed by researchers to accurately ascertain crystal phases, quantify crystallinity, and ascertain lattice parameters[283]. These characteristics are crucial in the customization of MXene features to suit applications such as catalysis, energy storage, and electrochemical sensing. Additionally, X-ray diffraction (XRD) is an essential instrument for verifying the efficacy of synthesis operations, guaranteeing the lack of contaminants, and monitoring structural changes during etching or modification protocols. This study serves as a fundamental basis in the field of MXene research, facilitating a thorough comprehension of the underlying structural factors that dictate their diverse properties and functionalities. In essence, X-ray diffraction (XRD) analysis serves as more than just a tool; rather, it acts to access significant structural understandings that are crucial for effectively utilising the whole capabilities of MXenes within the advancing field of materials science and nanotechnology. X-ray diffraction (XRD) has become an essential method in the investigation of material structures, with special relevance in the examination of MXenes. Within this particular context, X-ray diffraction (XRD) plays a pivotal role in accessing crucial data pertaining to crystallography, crystallinity, and the identification of different phases[284].

2.3.2 Energy-dispersive X-ray Spectroscopy (EDS)

EDS approach utilises X-rays to analyse the elemental composition of materials, serving as a non-destructive testing tool for the investigation of material composition. The field frequently exhibits interconnections with several other disciplines within the realm of materials science, including physics, biology, geology, and mineralogy. The utilisation of EDS analytical techniques has significant importance across diverse domains such as chemical industries, fertiliser manufacturing, production of alkalis, acids, salts, dyes, polymers, medicines, soaps, detergents, metals, alloys, and other inorganic and organic compounds, including emerging nanomaterials. Energy-dispersive X-ray spectroscopy (EDS), often known as EDX, is well recognised as a valuable technique for the determination of elemental composition and X-ray mapping. The electrical configuration of each atom serves as its defining characteristic. When subjecting a sample to the bombardment of high-energy electrons, the displacement of electrons from their inner shell results in the creation of a void or vacancy in said inner shell(**Figure 6**). Subsequently, the electron's higher energy state is transitioned to a lower energy state, thereby emitting energy in the form of X-rays. The EDS is capable of detecting distinctive X-rays. The estimation of the elemental composition of a sample can be achieved

by measuring the energy and intensity of distinctive X-rays emitted by each element. In the EDS spectrum, most peaks are formed by the X-rays, which are produced by distinctive fluorescence radiation. The utilisation of this characterization approach holds significance in relation to the underlying principle of the periodic table, as every element within the periodic table possesses a distinct atomic configuration that results in a certain arrangement of peaks on an X-ray radiation spectrum. When a high-energy beam composed of energetic particles, such as electrons, protons, or X-rays, interacts with the sample, the sample releases X-ray radiation that possesses distinct characteristics. The magnitude of each radiation is contingent upon the abundance of each constituent element within the specimen. Every atom possesses distinct and discrete energy levels and is capable of emitting radiation in the form of fluorescence. Numerous endeavours have been undertaken to elucidate X-ray microanalysis from the perspective of chemical analysis; nonetheless, it has been ascertained that each microanalytical approach possesses distinct merits and limitations[285]. X-ray microanalysis is a technique employed for the detection of X-rays released from materials through the application of high-energy beams onto the surface of the sample. The electron microscope was initially developed with the purpose of stimulating particular specimens and afterwards quantifying the X-rays emitted as a result. The static-beam electron microscope was invented by Raymond Castaing, who also provided the fundamental concepts for X-ray microanalysis. Additionally, Fitzgerald et al. were responsible for the development of the initial lithium-drifted silicon (Si(Li)) detector, which enabled the measurement of X-ray photons with varying energy levels[286].

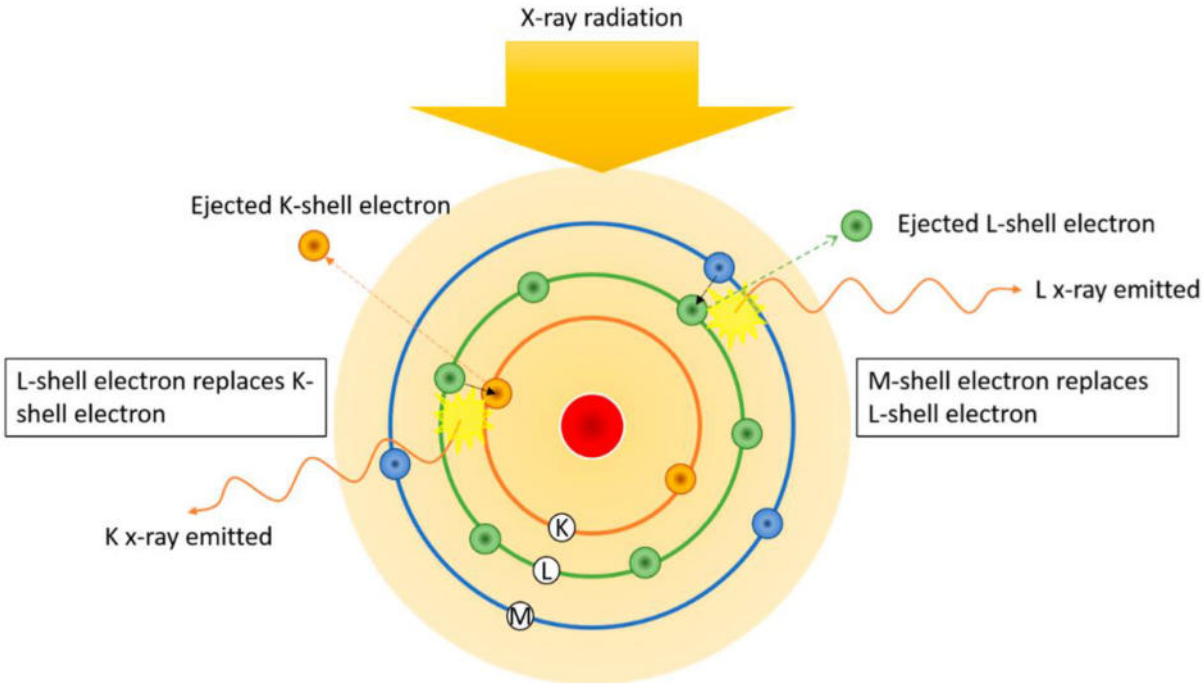

***Figure 6: Working Principle of EDS* [287]**

Silicon lithium (Si(Li)) detectors possess an appealing characteristic whereby they may effectively mitigate the presence of impurities or flaws inside the silicon crystal. This methodology has been employed to bridge the technological disparity between nondispersive analysis and energy-dispersive X-ray spectroscopy or spectrometry. Si(Li) detectors have demonstrated their significant utility and adaptability as detectors for microanalysis through empirical investigations. Every energy-dispersive spectrometer is equipped with a solid-state detector, specifically a monocrystalline silicon material. The covalent bonding of silicon atoms results in the formation of a periodic structure characterised by the sharing of valence electrons. When an X-ray penetrates the crystal, it induces the emission of a high-energy photoelectron, which subsequently interacts with the electrons of the silicon atoms. The energy of the ejected photoelectron is dissipated when it transitions into a conduction band, resulting in the creation of a vacancy within the valence band. The energy of X-ray radiation spans from 100 electron volts (eV) to 100 kilo-electron volts (keV). The electrical conductivity of a crystal is contingent upon the quantity of liberated charge carriers resulting from the absorption of X-rays, hence engendering the flow of electric current. The energy of absorbed X-rays can be determined by integrating the current with respect to time. The background or leakage current, on the other hand, is produced by the extrinsic charge carriers within the crystalline structure. Energy-dispersive X-ray (EDX) is a non-destructive analytical technique employed for characterising

the elemental composition of materials. It facilitates the determination of the spatial distribution of components by means of mapping. The examination of physical and chemical properties as well as the composition of micro to nanomaterials holds significant utility within the field of material science and technology. In the field of nanomaterial synthesis, where achieving precise control over composition is of utmost importance, the use of Energy Dispersive Spectroscopy (EDS) emerges as a valuable technique for confirming the effective conversion of precursor materials into the necessary nanomaterial structures[288]. The major significance of EDS resides in its capacity to detect subtle variations in elemental ratios, which is a critical factor in the analysis of nanoscale materials. The technique offers a quantitative evaluation of the elemental composition, hence providing insights into the origin and level of impurities in nanomaterials. The level of specificity mentioned holds great significance in the context of MXenes, as even little differences in composition can have a substantial influence on their properties and performance[289]. In addition, Energy-Dispersive X-ray Spectroscopy (EDS) plays a crucial role in the detection and characterization of any potential contaminants or unintentional consequences, hence safeguarding the authenticity and quality of the synthesised nanomaterial. The ability of the detection system to identify even minute quantities of components is crucial in verifying the absence of impurities that may potentially undermine the performance of the material. In conclusion, the analysis of energy-dispersive X-ray spectroscopy (EDS) plays a crucial role in the characterization of nanomaterials, such as MXenes[290]. This technique serves the dual purpose of confirming the successful synthesis of these materials and offering a comprehensive assessment of their elemental composition and purity. Consequently, EDS analysis serves as a foundation for further investigations and potential applications in this field.

2.3.3 Scanning Electron Microscopy (SEM)

The utilisation of scanning electron microscopy is a multifaceted method employed to get high-resolution visual representations and comprehensive surface data of various specimens. Scanning electron microscopy (SEM) is a technique employed in the field of electron microscopy, wherein a concentrated electron beam is utilised to examine the surface of a specimen, hence producing images with significantly enhanced resolution in comparison to

optical microscopy. The resolution of scanning electron microscopy (SEM) instruments can vary from less than one nanometer to several nanometers. The scanning electron microscope (SEM) utilises electron beams to project and scan a concentrated stream of electrons across the surface of a specimen, while employing specialised detectors to gather and analyse the resulting signals as shown in **Figure** *7*. The interaction between the electrons in the beam and the atoms present in the sample results in the generation of diverse signals, which can be utilised for acquiring insights into the surface's topography and composition[291]. The captured electron intensities are correlated with the beam's position using software, allowing real-time viewing of images on an external monitor. In scanning electron microscopy (SEM), the two predominant detectors employed for high-resolution imaging are the secondary electron detector (SED) and the backscattered electron detector (BSD). The investigation of surface composition can be conducted by the utilisation of energy dispersive X-ray spectroscopy (EDS) detectors. The resolution and possible imaging modes of the scanning electron microscope (SEM) are ultimately determined by its distinct configuration. SEM is capable of directly analysing a diverse array of solid materials. Specialised imaging techniques, such as low-vacuum or low-kV imaging, are frequently employed for the examination of biological materials and insulating samples. These techniques are utilised to mitigate surface charge and minimise beam damage. To mitigate the effects of charging, it is common practise to apply a small layer of gold or platinum via sputter coating onto insulating samples. Under optimal lighting conditions, the human eye has the ability to discern two distinct locations in space that are separated by a distance of 0.2 mm, without the need of supplementary lenses. The term used to describe this distance is known as the resolving power or resolution of the human eye. A lens or a collection of lenses, commonly known as a microscope, can be utilised to increase the magnification of this distance, allowing the human eye to perceive points that are significantly closer than 0.2 mm[292]. The largest magnification achievable by a contemporary light microscope is approximately 1000 times. The limitations of the microscope's resolving power are influenced not only by the quantity and calibre of lenses employed, but also by the wavelength of the light utilised for illumination. The range of accelerating voltages for scanning electron microscopy (SEM) spans from values below 5 kiloelectron volts (keV) to as high as 30 keV. The transmission electron microscope (TEM) and scanning transmission electron microscope (STEM) are capable of achieving electron beam energies of 300 keV or above, rendering them the most formidable electron microscopy instruments. The substantial disparity in wavelength between accelerated electrons and visible light is the key factor that endows electron microscopes with the capability to see materials at atomic and nanoscale

scales. In practical applications, the attainment of diffraction-limited resolution is hindered by the presence of defective electromagnetic lenses. However, it is important to note that electron microscopes, such as scanning electron microscopes (SEMs), provide significant enhancements in resolution compared to light microscopes[293].

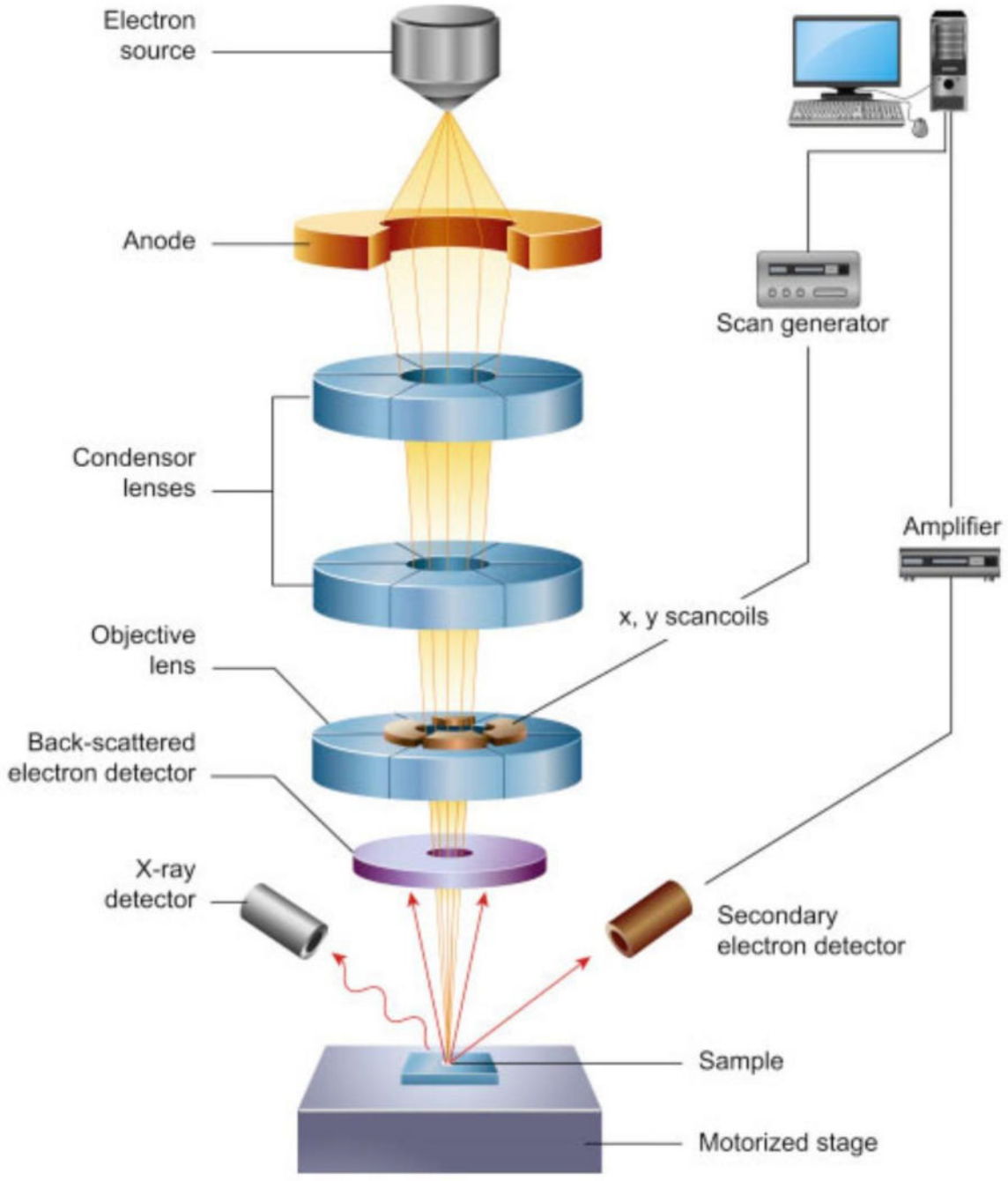

Figure 7:Schematic description of SEM

Electrons are generated at the uppermost section of the electron gun and subsequently propelled through the column by means of a predetermined accelerating voltage range, typically spanning

from 1 kV to 30 kV. Condenser lenses and apertures function to decrease the diameter of the beam. The ultimate lens within the column is the objective lens, responsible for concentrating the beam onto the surface of the sample. The diameter of the beam in a scanning electron microscope (SEM) can vary between less than 1 nm and up to 20 nm, contingent upon the specific electron gun, accelerating voltage, and lens arrangement employed. The specimen is affixed to a platform within the chamber region, while both the column and the chamber are upheld in a vacuum state by the utilisation of pumps. The magnitude of the vacuum will be contingent upon the specific configuration of the microscope. Certain types of microscopes include the capability of adjustable pumping, which enables the sample chamber to maintain a lower level of vacuum compared to the rest of the column. This feature facilitates the acquisition of low-vacuum images. The localization of the electron beam on the sample is regulated by scan coils positioned above the objective lens. The utilisation of these coils facilitates the scanning of the beam across the sample's surface inside the X-Y plane. The incident beam interacts with the sample, resulting in the production of diverse signals such as secondary electrons, backscattered electrons, and distinctive X-rays. Subsequently, these signals are detected by suitable detectors. The scan generator, in conjunction with an external computer equipped with specialised software, facilitates the synchronisation of data between the scan generator (which records the X and Y coordinates of the beam at each time interval) and the intensity data captured by the detector. This synchronisation enables the real-time display and examination of a grayscale image, with each pixel being processed individually. The modulation of signal-to-noise can be achieved by varying the dwell period of the electron beam at different X and Y positions. The phenomenon of magnification arises from variations in the size of the scanned region, with higher magnifications corresponding to increasingly smaller scanned areas. The pixel count can be modified within a designated scanning region, hence influencing the perceived resolution[294].

The utilisation of Scanning Electron Microscopy (SEM) is considered essential in the field of nanomaterial investigation due to its ability to provide vital information regarding the surface morphology and structural properties of materials[295]. Within the realm of MXene research, scanning electron microscopy (SEM) assumes a crucial role in the visualisation of the microstructure and the verification of the intended nanosheet development. The utilisation of scanning electron microscopy (SEM) enables researchers to meticulously examine the layer-by-layer organisation, distribution of particle sizes, and surface characteristics of MXenes through the production of high-resolution pictures. Moreover, scanning electron microscopy

(SEM) enables a comprehensive analysis of the impact of etching techniques on the structural characteristics of materials, particularly in the context of MXene production[296]. These observations play a crucial role in customising MXenes for diverse applications, namely in the fields of electrochemical sensing and energy storage. In the domain of sophisticated materials such as MXenes, the significance of Scanning Electron Microscopy (SEM) is of utmost relevance. The scanning electron microscope (SEM) plays a crucial role in providing a detailed examination of MXene structures and morphologies at the nanoscale, making it an essential tool in understanding this complex field. The significance of MXenes extends beyond their visual characteristics, as they serve as a gateway to comprehending and utilising the diverse qualities exhibited by MXenes. The role of scanning electron microscopy (SEM) is diverse and essential in the toolkit for analysing MXene materials. The technique demonstrates exceptional proficiency in elucidating the topographical characteristics, dimensions of particles, and intricate structural features of MXenes. These traits play a crucial role in customising these materials for particular purposes. In a global context where MXenes commonly demonstrate intricate and layered structures, scanning electron microscopy (SEM) offers a valuable approach to visually see and decipher their internal mechanisms. Nevertheless, it is important to note that scanning electron microscopy (SEM) goes beyond the mere acquisition of still pictures. Its true value lies in the ability to analyse and interpret the dynamic changes that MXenes experience throughout processes like as synthesis, etching, or modification. Through the act of visualising these processes, researchers are able to make well-informed decisions, thereby guaranteeing the materials' appropriateness for a wide range of applications[297]. In conclusion, it can be stated that scanning electron microscopy (SEM) serves as more than just a tool, but rather as a gateway to explore the intriguing realm of MXenes[220]. This technology enables individuals to explore beyond superficial aspects, comprehend the underlying structures and forms, and effectively utilise their capabilities in several domains, ranging from energy storage to catalytic processes, and beyond. The investigation of MXene materials is a scholarly endeavour, whereby scanning electron microscopy (SEM) serves as an invaluable tool for providing crucial insights and guidance throughout the research process.

2.3.4 X-ray Photoelectron spectroscopy (XPS)

X-ray photoelectron spectroscopy (XPS) is an analytical technique with surface sensitivity, wherein X-rays are employed to irradiate the surface of a material, enabling the measurement of the kinetic energy of the released electrons. This methodology has been employed to investigate the surface properties of a wide range of materials, encompassing plastics, textiles, dirt, and semiconductors. The investigation and comprehension of surfaces have significant importance because to their influence on corrosion, surface wettability, charge transfer, adhesion and catalysis. These properties are primarily governed by the characteristics of surfaces and the presence of surface contaminants[298]. X-ray photoelectron spectroscopy (XPS) is grounded on the fundamental principle of the photoelectric effect, initially observed by Heinrich Hertz in the year 1887. The concept was subsequently elucidated by Albert Einstein in 1905, leading to his recognition and subsequent receipt of the Nobel Prize in Physics in 1921. The initial utilisation of photoemission as an analytical technique was introduced by Steinhardt and Serfass in 1951. The technique of X-ray Photoelectron Spectroscopy (XPS) as we currently understand it was invented by Kai Siegbahn at the University of Uppsala in Sweden. This approach involves the use of an x-ray source, sample stage, extraction lenses, analyzer, and detector, all of which are housed within an atmosphere of ultra-high vacuum. X-ray sources employ a heated filament made of tungsten or LaB6 to generate a stream of electrons, which are subsequently accelerated towards a high-voltage anode. The selection of the anode material is contingent upon various elements, encompassing energy, linewidth, analysis depth, and ionisation cross-section. X-ray photoelectron spectroscopy (XPS) systems were initially outfitted with aluminium (Al) and/or magnesium (Mg) sources, frequently in the configuration of a dual anode source[299]. A monochromator is commonly integrated into various instruments, often utilised with an aluminium source. Monochromatic sources offer numerous advantages, one of which is the elimination of excitation caused by x-ray lines that are not the most intense primary line. A monochromatic source provides the advantage of decreased x-ray linewidth, hence enhancing the spectral resolution of X-ray photoelectron spectroscopy (XPS). Nevertheless, it is worth noting that certain samples have the potential to sustain damage when exposed to high levels of x-ray intensity. Observable signs of sample damage may encompass alterations in sample colour and spectral changes, such as the broadening of peaks, which may occur gradually over time. Certain materials exhibit a higher susceptibility to x-ray damage, including oxides, polymers, and thin coatings. Extraction lenses in electron optics establish the acceptance angle for the retrieval of electrons released from the sample, hence enhancing the efficiency of electron collection. Additionally, the ability to manipulate the region of the specimen from which electrons are gathered allows for precise

study of small areas. The energy resolution in X-ray photoelectron spectroscopy (XPS) is constrained by the energy of the electrons under detection. Enhanced energy resolution is attainable at lower electron energies. The electrons' energy, as they travel towards the analyzer, is often diminished or constrained by the extraction lenses to a predetermined energy level known as the pass energy, prior to entering the analyzer. X-ray photoelectron spectroscopy (XPS) systems have been created using two primary types of analyzers (as shown in **Figure *8***): cylindrical mirror analyzers and concentric hemispherical analyzers. The design of the concentric hemispherical analyzer has demonstrated superior performance in terms of energy resolution and, ultimately, throughput. The application of voltages to the hemispheres involves establishing a potential difference, where the outer hemisphere is maintained at a comparatively lower electrical potential than the inner hemisphere. The passage of electrons into the analyzer occurs via a narrow aperture, whereby alone electrons possessing a predetermined energy level are capable of traversing the analyzer. The energy resolution of the analyzer is determined by the radius of the analyzer, thus analyzers with bigger radii yield superior resolution. Contemporary instrumentation is capable of attaining an energy resolution that is lower than 0.5 electron volts full width at half maximum (FWHM) while analysing the Ag 3d5/2 peak. All detectors employed in X-ray photoelectron spectroscopy (XPS) equipment are categorised as electron multipliers. To enhance the electron collection, numerous detectors are strategically positioned along the exit slit of the analyzer. X-ray photoelectron spectroscopy (XPS) systems are frequently equipped with a sputtering gun, typically using Ar^+ ion sources in older systems. However, it is worth noting that the usage of Ar+ ion sources in these older systems sometimes resulted in sample damage. Recent advancements in technology have led to the development of more refined sputter sources, such as C60 or gas cluster ion sources (GCISs), typically utilising argon clusters[300]. In addition, XPS imaging and tiny spot spectroscopy can be considered as alternative techniques. The proper handling of samples is crucial when working with conducting or semiconducting materials. It is recommended to use gloves and utilise metal tweezers to manipulate the sample, ensuring that direct contact with the region to be analysed is avoided. It is imperative to ensure that samples are stored and transported in a manner that minimises the risk of surface contamination. ASTM International and the International Standards Organisation have issued guidelines pertaining to sample handling, encompassing techniques for mitigating sample oxidation and contamination. Fracture systems, when utilised, have the advantage of exposing samples to pristine surfaces without any contact with atmospheric air. On the other hand, the more recent systems equipped with argon cluster ion guns have demonstrated greater efficacy in cleansing polymer surfaces without causing any

damage to the samples. Every individual element possesses a distinct X-ray photoelectron spectroscopy (XPS) spectrum, which is determined by the energy levels specific to that element. In the XPS spectrum, any transition with a binding energy lower than the energy of the x-ray source should be detectable. Software analysis tools commonly contain libraries of peak positions. However, it is worth noting that these libraries sometimes lack information regarding chemical shifts, relative peak intensities, and peak shapes. Novice users of X-ray photoelectron spectroscopy (XPS) may encounter many sorts of peaks that might potentially cause confusion. These include satellite peaks, shakeup peaks, shakeoff peaks, and multiplet splitting. Satellite peaks manifest when a specimen is stimulated by x-rays possessing several energy levels, hence leading to supplementary peaks in X-ray photoelectron spectroscopy (XPS) at reduced binding energies. Shakeup peaks arise as a consequence of a de-excitation mechanism, wherein the departing core electron engages in an interaction with a valence electron, thereby inducing its excitation to a more elevated energy state. Shakeoff peaks exhibit similarities to shakeup peaks, albeit with a distinct mechanism. While shakeup peaks involve the excitation of an electron to a higher energy state within an atom, shakeoff peaks entail the ejection of the electron from the atom altogether. The occurrence of multiple splitting of core level peaks is observed when there are unpaired electrons present in the valence levels. This phenomenon typically leads to the unexpected splitting of peaks. The X-ray Photoelectron Spectroscopy (XPS) method is widely utilised for surface investigation due to its notable attributes, namely its high surface sensitivity of approximately 10 nm and its capability to discern variations in chemical surroundings. The detection capabilities of this method encompass all elements, excluding hydrogen and helium, with detection limits ranging from roughly 0.1% to 1%. Moreover, it possesses the ability to provide quantitative results without the need for standards, and it is characterised by its comparatively non-destructive nature. Nevertheless, it is imperative to exercise caution in order to prevent any potential surface contamination, given the high sensitivity of the subject matter. In summary, it is important to exercise caution and possess a thorough understanding of XPS in order to prevent any potential misinterpretation or distortion of data, despite its continued use as a surface analysis technique. It is advisable to seek consultation with experienced XPS analysts and to refer to other resources within this series in order to assure the attainment of precise outcomes.

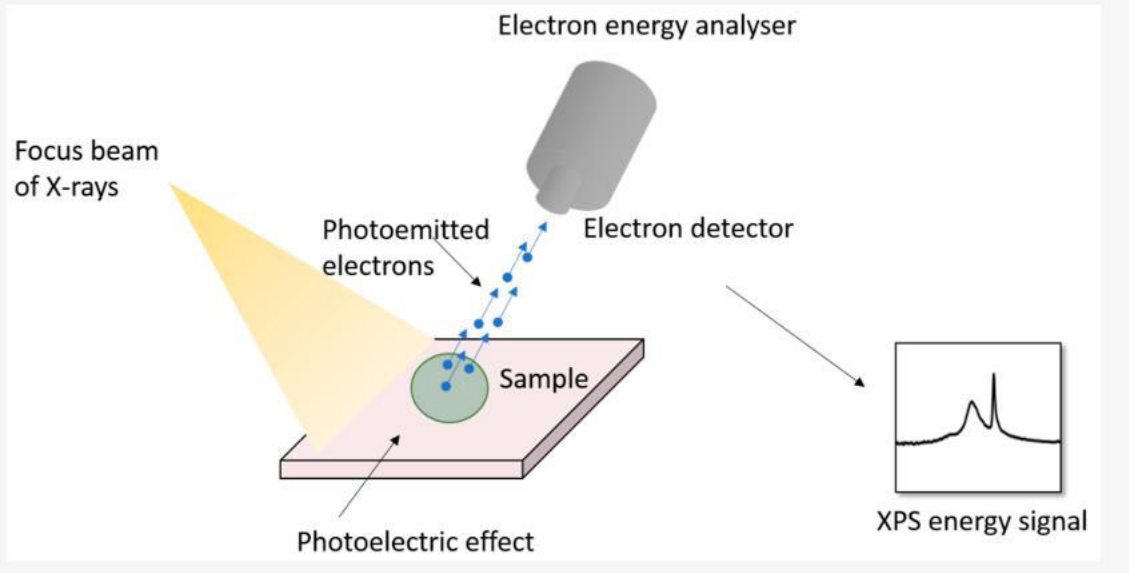

Figure 8: Working principle of XPS [287]

X-ray Photoelectron Spectroscopy, or XPS, stands as a powerful analytical technique in the realm of material science. Its ability to provide critical insights into the surface composition and chemical states of elements within a material makes it an essential tool for characterizing nanomaterials like MXenes. XPS employs X-ray irradiation to induce the emission of photoelectrons from the sample's surface, and by analyzing the kinetic energies of these emitted electrons, it reveals the elemental composition, chemical bonding, and oxidation states of the elements present[301]. In the study of MXenes, XPS plays a pivotal role in confirming the formation of the desired MXene structure, identifying surface functional groups, and assessing the purity of the material. The utilisation of this adaptable analytical technique is crucial in comprehending the intricate surface chemistry of these nanomaterials with unmatched accuracy. Through the utilisation of X-ray photoelectron spectroscopy (XPS), valuable insights regarding the elemental composition and chemical states existing on the surface of MXene samples can be obtained by researchers. The significance of X-ray photoelectron spectroscopy (XPS) within the field of MXenes is of utmost relevance and should not be underestimated. The utilisation of this instrument is highly effective in verifying the successful synthesis of MXenes, distinguishing between various chemical states of elements, and clarifying the existence of functional groups and surface terminations[302]. Acquiring such understanding is of utmost importance in order to customise MXenes for particular applications, such as energy storage, sensing, or catalysis[303]. In addition, X-ray photoelectron spectroscopy (XPS) allows researchers to evaluate the extent of surface oxidation or contamination, which are important variables that can have a substantial impact on the characteristics and functionality of the

material. The capacity to accurately identify the chemical signatures of MXenes provides scientists with the means to refine their synthesis techniques and post-processing procedures, hence improving the materials appropriateness for many advanced applications. In conclusion, X-ray photoelectron spectroscopy (XPS) proves to be a highly helpful instrument, enabling the examination of the underlying chemistry of Nb_2SnC MAX phase and Nb_2CT_x MXene materials. This technique enables the identification of both the elemental composition and the subtle chemical states, thereby enhancing our comprehension of the properties and prospective applications of these materials.

2.3.5 (Transmission Electron Microscopy) TEM

Transmission electron microscopy (TEM) is a powerful imaging technology that enables the capture of precise and unique information pertaining to a given sample or research project. The tool, artefact, or instrument in question has been specifically constructed for the purpose of analysing and visualising samples that fall within a range of dimensions spanning from the microscale, denoted as $1*10^{-6}$ (1 mm), to the nanoscale, denoted as $1*10^{-9}$ (1 nm). Transmission electron microscopy (TEM) possesses the capacity to unveil intricate levels of detail that are beyond the reach of conventional light microscopes[304]. An instance illustrating the substitution of light optical microscopes by transmission electron microscopes (TEM) is the examination of the morphology of bacterial cells and exceptionally big viruses. The size of bacteria varies, with smaller samples typically ranging between 100 and 200 nm, while larger samples can reach up to 7 µm in size. In order to elucidate the subcellular architecture of bacteria, the utilisation of transmission electron microscopy (TEM) is imperative, as it offers the capability to visualise entities with dimensions less than 0.2µm. Replacing the light beam with the electron beam, which possesses a wavelength of around 0.005nm, yields a superior resolution. The transmission electron microscope (TEM) is comprised of an electron source, sometimes referred to as a gun or electron cannon(**Figure 9**)[305]. This source typically consists of a V-shaped filament constructed from materials such as lanthanum hexaboride or tungsten. A positive electric potential is provided to the anode, resulting in the warming of the filament (cathode) until it generates an electron current characterised by a wavelength as determined by the De Broglie equation. Subsequently, the electron beam interacts with the

sample, undergoing various processes wherein the electrons that interact with the sample undergo dispersion to prevent energy loss (elastic scattering). Additionally, there are other processes in which electrons transfer a portion of their energy to internal electrons within the sample (inelastic scattering). The objective lens is responsible for concentrating the dispersed beams in order to generate the initial image, facilitated by the diffraction process executed by the projection lens. This process involves enlarging the electron beam and reflecting it onto the phosphor screen. The primary consideration in sample preparation is to ensure that the chosen technique does not introduce any alterations or biases to the sample under observation. In transmission electron microscopy (TEM) situations, many methodologies for sample preparation are employed, contingent upon the nature of the material under investigation and the desired information to be extracted. The transmission electron microscope (TEM) is a versatile instrument utilised for the examination of the structural, compositional, and property characteristics of samples across various domains of study, including materials science, geology, environmental science, medicine, electronics, and biology[293]. The technique encompasses several key functions, such as conducting morphological analysis on small organism samples, incorporating samples for future collection and the creation of three-dimensional images, manipulating samples while observing, generating X-rays for microanalysis, and analysing the composition of the sample or the atomic bonding states through electron energy loss spectroscopy[306].

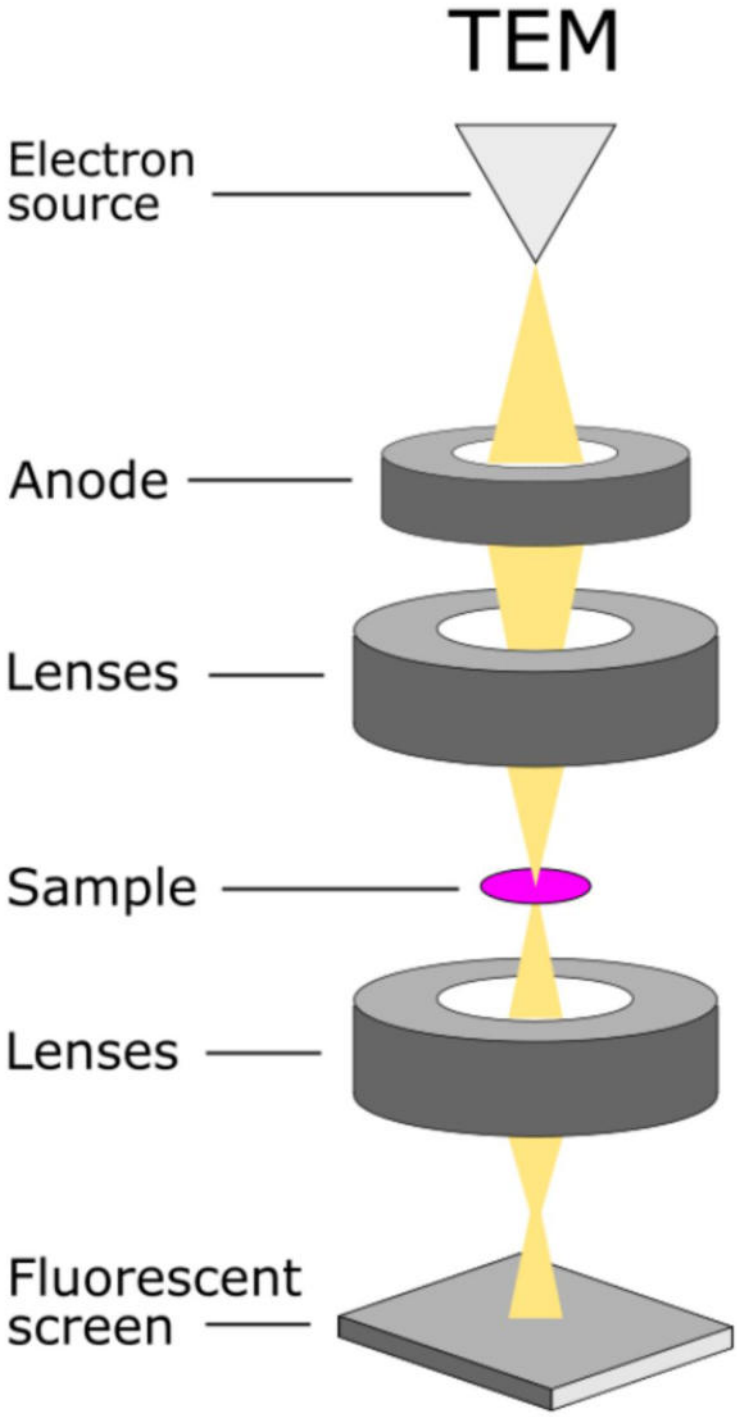

Figure 9:TEM Instrumentation and working principle.

The utilisation of a focussed electron beam in this robust imaging approach allows for the transmission through samples that are extremely thin, thereby unveiling subtle characteristics pertaining to their shape, crystal structure, and even elemental makeup[307]. TEM investigation is crucial for MXenes due to its ability to offer direct visual observations of their

two-dimensional layered structures and the atomic arrangement within them. The utilisation of transmission electron microscopy (TEM) enables researchers to authenticate the creation of MXenes, examine their sheet-like architectures, and quantify significant features, such as interlayer spacing. This chapter utilises transmission electron microscopy (TEM) to investigate the detailed structural complexities of Nb_2CT_x MXene and Nb_2SnC MAX phase. This analysis is crucial for understanding their properties and potential applications in advanced technologies. Transmission Electron Microscopy (TEM) is an indispensable analytical technique that has gained significant importance in the investigation of advanced materials, including MAX phases and MXenes. The transmission electron microscope (TEM) possesses a notable capacity to investigate materials at the atomic and nanoscale dimensions. As a result, it offers invaluable observations regarding the shape, crystalline structure, and chemical composition of nanomaterials. In the context of MXenes, transmission electron microscopy (TEM) plays a crucial role in elucidating the detailed characteristics of their two-dimensional layered structures. This technique facilitates the visualisation of the arrangement of individual layers, determination of interlayer spacing, and identification of any flaws or structural alterations by researchers. In addition, transmission electron microscopy (TEM) enables the acquisition of high-resolution images, hence enabling the examination of minute characteristics and nanoscale phenomena present in MXene materials.

The significance of transmission electron microscopy (TEM) investigation in the field of MXene research cannot be overemphasised. The utilisation of this technique not only facilitates the verification of particular structural characteristics but also yields quantitative information, such as d-spacing values, which exhibit a correlation with X-ray diffraction (XRD) results. Moreover, transmission electron microscopy (TEM) plays a crucial role in evaluating the quality and consistency of MXene samples, which is essential for their effective incorporation into diverse applications, ranging from energy storage to sensors and beyond. As scientists delve more into the realm of MXenes and their intricate nanoscale characteristics, transmission electron microscopy (TEM) emerges as an invaluable tool, providing insights into the atomic-level enigmas that underlie the exceptional capabilities and potential uses of MXenes. Transmission Electron Microscopy (TEM) is a crucial technique for elucidating the atomic-level complexities of synthesised materials, which is essential for comprehending their properties and performance. Within the domain of MAX phases and MXenes, transmission electron microscopy (TEM) assumes a prominent role, providing researchers with the means to explore the nanoscale realm[308].

2.4 Electrochemical Techniques

Table 2:Electrochemical methods along with their monitored properties

Electrochemical Methods	**Monitored Electrochemical Properties**	**Units**
Potentiometry	Potential difference (Volts)	V
Conductometry	Resistance (ohms)	Ω
Amperometry and Voltammetry	Currents (amps) as a function of applied potential	I
Coulometry (Q)	Current as a function of time (coulombs)	C = I. s
Capacitance (C)	Potential load (Farads)	$F = C V^{-1}$

Potential opportunities in the development of electrochemical sensors and electroanalytical techniques have emerged as a result of research into the behaviour of materials at the nanometric scale. Typically, an electrochemical sensor will produce an electrical signal in response to the presence of an analyte. A list of well-known electrochemical procedures is provided in **Table *2***, along with the related monitored electrical signals. The information in **Table *2***demonstrates that electrochemical reactions are mostly dependent on variables like voltage, resistance, and electrical current when they are detected using different approaches. For example, in order to calculate their relative responses, coulometry and capacitance techniques depend on the measurement of potential, resistance, and electrical current.[309]. The two main categories of electrochemical techniques, which can be used as analytical instruments, are interfacial methods and non-interfacial methods, which encompass monitoring the entire solution. As a non-interfacial approach, conductometry is categorized[309], as indicated by the instances provided in **Table *2***. This method is based on a cell which contains two electrodes that are equally spaced apart and has specified size. Measurement of a solution's overall electrical conductance, which practically equates to its resistance, is the main goal of conductometry. The phenomenon of electrode polarisation does not take place when an alternating current signal is applied. Instead, the solution's electric resistance—which is influenced by the cell constant—defines the response. The electrode’s surface area, their

spacing, and the volume of the electrochemical cell's solution are some examples of the variables that affect the cell constant. The term "interfacial methods" describes a collection of procedures that show a direct or indirect reaction to the existence of the analyte on the electrode surface, which functions as the sensory unit[309]. An electric signal is perturbed as a result of this response, and the magnitude of the disturbance can then be measured. Dynamic and static methods are the two main groups that make up interfacial approaches. The definition of a static method is one in which there is no interruption, and the electric current is at zero I = 0). The employment of a redox reaction in dynamic techniques, however, involves the transfer of electrons between the analyte and the electrode. Dynamic methods are important because they make use of the current flow, which facilitates reactions involving electron transport and charge transfer. The creation of nanostructured materials as well as analytical determination, such as sensors, find applications for these methods.

2.4.1 Potentiometry

Figure 10: Bench 780 pH meter and glass electrode (Metrohm). Adapted from https://www.metrohm.com/es_mx/products/2/7800/27800010.html

Potentiometry is a commonly employed electrochemical technique in analytical applications, known for its static interfacial nature[309]. The pH meter (**Figure 10**) is a well-known example of potentiometry since it frequently uses membrane made of glass electrodes as indicators of the concentration (or more correctly, the activity) of H^+ ions inside a solution. A pH meter typically works by determining the activity of (Hydrogen) H^+ ions on each side of a glass membrane, with the internal activity (concentration) being predetermined and established and the external activity (analysis solution) being assessed. The measurements are made by calculating the potential difference (V) between the solutions on either side of the membrane. The results are then converted into a pH scale using the Nernst equation (2), which creates a link between potential and concentration.

$$E = E^o + \frac{RT}{nF} ln \frac{[RED]}{OXI}$$

…… .2

where E represents the cell potential, E^0 represents the standard potential of a half-reaction, R represents the universal gas constant, T represents the temperature, and n represents the number of electrons (in units of equivalent moles) engaged in the half-reaction. The symbols used in this context are as follows: F represents the Faraday constant, [RED] denotes the activity of the reduced species, and [OXI] represents the activity of the oxidised species.

An electric inducement with a nonzero current (i≠0) is applied to the surface of the indicator electrode, working electrode, or sensor in techniques known as "dynamic interfacial approaches." It is important to highlight controlled potential procedures like amperometry, voltammetry, and coulometry within this group of methods, together with coulometric titrations that use controlled current. The main electrochemical processes and the subclasses within each are shown in **Figure *11***. The fundamental idea behind electrochemical sensors is the detection of the analyte using the active surface layer of the constituent material (as shown in **Figure *12***), followed by the transformation of this knowledge into a detectable signal that can be transferred to the recording apparatus.

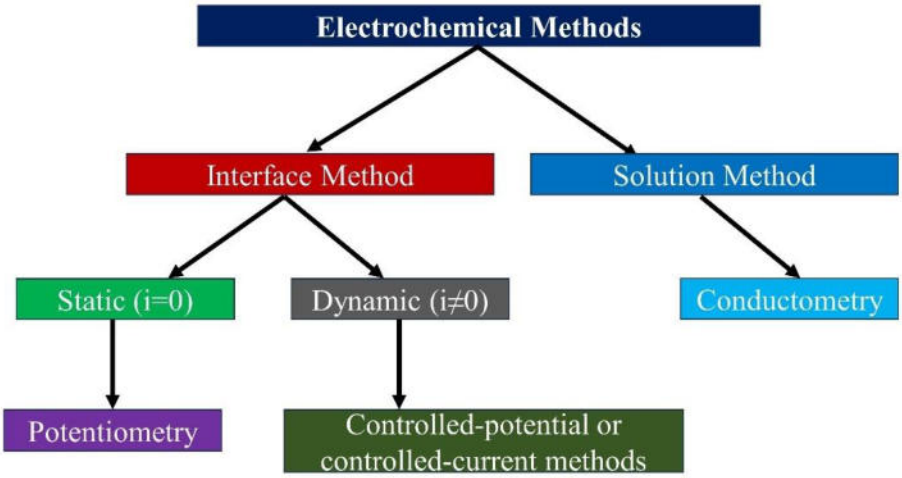

Figure 11: Major electrochemical methods and their sub-partition . Adapted from, Principles of Instrumental Analysis, sixth edition, F.J. Holler, D.A. Skoog, S.R. Crouch Thomson Brooks/Cole, 2007[309]

A conclusion that can be drawn from looking at the electrochemical methods shown in **Figure *11*** is that an electrochemical sensor works by using interface methods. Electrochemical cells that are specifically created with an active surface material on the working electrode make up electrochemical sensors for analytes in solution (also known as the sensory unit). These sensors employ a set of electrodes to detect and quantify the analyte when it is present in a reaction media.

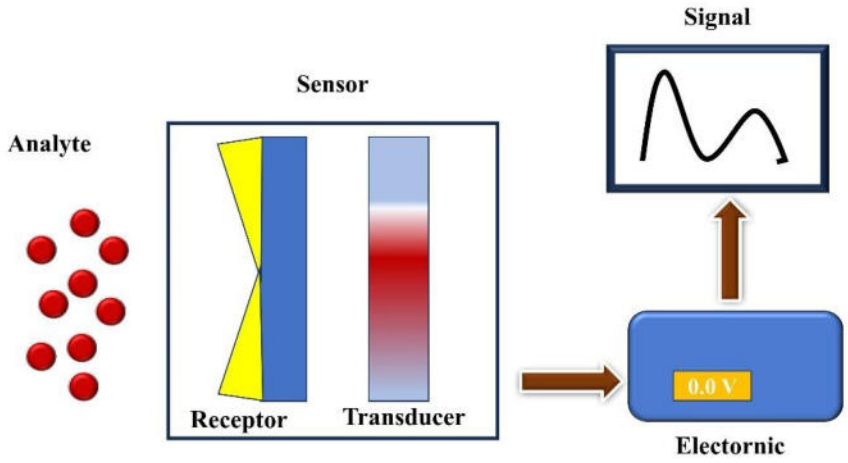

Figure 12: Schematic diagram of Electrochemical sensor

In the interface approaches, an electrochemical reaction is started by polarizing the electrodes, i.e., the cathode and anode, in an electrolyte procedure. Typically, a power supply, a voltmeter, an anode, and a cathode are included in an electrolyte cell with two electrodes (as depicted in **Figure *12***). In light of the advancements in electrochemical analytical techniques, there emerged a necessity for the implementation of potential control.

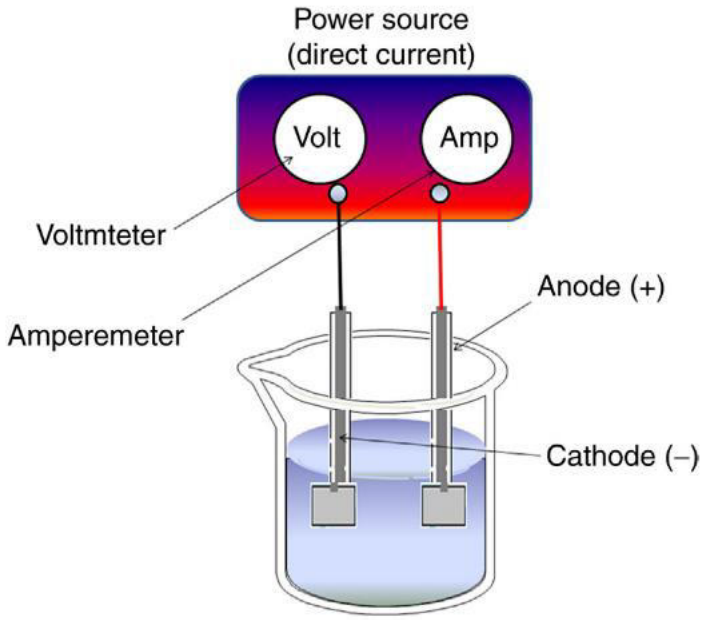

Figure 13: 2 Electrode system electrochemical cell

As was previously mentioned, Equation (2) states that the activity of the analyte determines the potential value of an electrochemical cell (also known as the Nernst equation). As the analyte activity declines as a result of a chemical reaction, the cell potential changes. The issues with the application of overpotential (η) are successfully addressed by the potential control approach. Overpotential, also known as activation energy, is the excess potential necessary to overcome the effects of kinetic and electric resistance. A potentiostat is the device that was created in answer to this demand. Its job is to continuously track the reference electrode's reversible reaction potential in order to control the cell potential. All electrochemical sensors, including voltametric, amperometric and potentiometric, need reference electrodes. A reference electrode is a type of electrode with a fixed potential that does not change over time and is unaffected by the fluid under study's chemical makeup. The reference electrode should be built around a reversible reaction that complies with the rules specified in the Nernst equation. Furthermore, it is preferred that this electrode show little response to temperature variations[309]. Some reference electrodes successfully meet these requirements. The saturated calomel electrode (SCE), the normal hydrogen electrode (NHE or SHE), and the saturated silver/silver chloride electrode (EAg/AgCl) are the electrodes that are frequently used in electrochemical applications. The Normal Hydrogen Electrode, also known as the NHE, is a frequently used and historically significant point of reference in scientific studies. It is easily fabricatable in a lab environment. Due to the preparation required before each use, its applicability is limited to certain circumstances. In order for electrochemical sensors to function and be used, metal electrodes, more specifically ScE and EAg/AgCl, are essential. These electrodes are more durable and may be kept for longer periods of time, which greatly improves the performance and usefulness of such sensors as a whole. Within the electrode structure, a metallic element and a soluble compound of that element make up the electrodes. The reference electrodes are thoroughly described in **Table *3***, specifically at a temperature of 25 °C, along with their relative compositions and potential constants.

Table 3: List of reference electrode and thier reversible reaction

Reference Electrode	Reversible Reaction	Standard Potential at 25 °C
NHE	$2H^+ + 2e^- \leftrightarrow H_2$	E0 = 0.0 V
SCE	$Hg_2Cl_{2(s)} + 2e^- \leftrightarrow Hg_{(l)} + 2Cl^-$	E0 = +0.244 V (vs NHE)

$E_{Ag/AgCl}$	$AgCl_{(s)} + e^- \leftrightarrow Ag_{(s)} + Cl^-$	E^0_{AgCl} = +0.199 (vs NHE)

An essential component of voltammetric and amperometric processes is the use of a reference electrode within the parameters of its configuration to cause polarization of the working electrode (also known as the indicator electrode or sensory unit). Three electrodes are used in these dynamic analysis techniques (**Figure *13***). Two alternative techniques are used to examine the electric current in the electrochemical system: voltammetric techniques and amperometric techniques, where the current is being measured as a function of the altering analysis potential. Each of the three electrodes in a typical electrochemical cell has a specific job to do. The participating species' oxidation and reduction processes are aided by the working electrode. The counter electrode, sometimes referred to as the auxiliary electrode, performs the essential electrical circuit establishment within the electrochemical system. The reference electrode also provides a point of comparison for assessing other measured values (**Figure *14***).

2.4.2 Chronoamperometry

The chronoamperometry approach in potentiostatic mode involves the measurement of current passing through the working electrode over time, while maintaining a constant potential at the working electrode[310]. The Cottrell equation can be used to characterize the link between the amount of reduced or oxidised species present on the working electrode surface and the current flow (3).

$$It = \frac{nFAC_O^0 D_O^{1/2}}{\pi^{1/2} t^{1/2}} = bt^{1/2} i_i \quad \text{.....3}$$

where I_t stands for current at time t, n is the number of electrons (eq. mol^{-1}), F stands for Faraday's constant (96,485 Ceq.$^{-1}$), A is the electrode's geometric area (cm^2), c_0 is the concentration of oxidized species (mol cm^{-3}), and D_o is the diffusion coefficient of oxidized species (cm^2 s^{-1}).

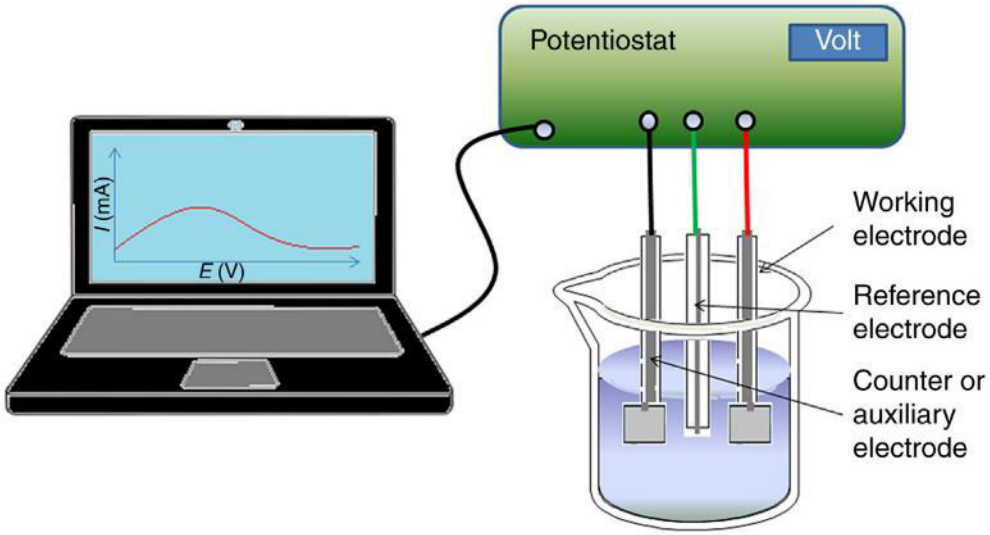

Figure 14: Three Electrode system electrochemical cell

By directly measuring the current as a function of a constant voltage applied to the electrochemical system, chronoamperometry is a technique that makes it possible to investigate processes. In electrochemical experiments, the current is affected by two different processes: charge transfer and mass transfer. Charge transfer involves the transfer of electrons at the surface of the working electrode. Mass transfer involves the movement of species from the solution to the electrode-solution interface. Additionally, these primary processes may be carried out in parallel with other chemical reactions, including as desorption, adsorption polymerization, protonation and crystallization. Understanding these secondary events can help characterize materials and understand how mass transfer and charge work, which involves reduction and oxidation reactions at the surface interface between electrodes and solutions.[310]. Numerous studies to clarify the mechanics underlying the nucleation and development of polymers used the potentiostatic chronoamperometry approach in the 1960s. These research investigated the possibility of controlled crystal nucleation in polymers by treating them as crystalline materials. **Figure *15*** shows the chronoamperometry that was done to concurrently find nitrite and nitrate in an aqueous solution. The composite electrode of the electrochemical sensor used in this analysis is made of graphite-epoxy, zeolite, and silver (Ag) (GE).

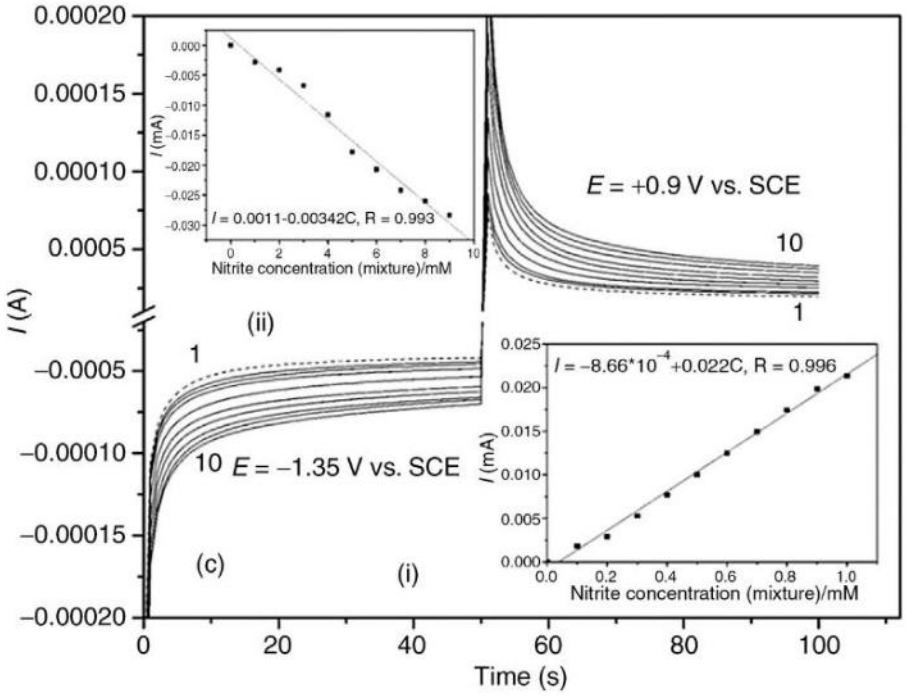

Figure 15:Chronoamperograms of Ag-ZEGE electrode at -1.4 V and 0.90 V versus SCE were recorded in 0.5 M Na_2SO_4 electrolyte with nitrite and nitrate mixture. Calibration plots were used for current readings at 50 s [311].

The concentration ranges of nitrate and nitrite, 1–10 mM for nitrate and 0.1–1 mM for nitrite, were shown to be directly correlated by the researchers.[312]. The historical fluctuations shown in **Figure *15*** have been seen to follow a pattern of early peak values followed by a quick drop. The electrical double layer's charging mechanism is sometimes blamed for these variations, which go through an evolution with a peak value that gradually declines over time. Despite the difficulties encountered in illuminating these phenomena at the surface of the working electrode, Hills, Schiffrin, and Thompson carried out ground-breaking research in 1974 that connected the maximum current value seen in the chronoamperometry to equations related to the nucleation and growth model of metals.[313]. Further investigation by Scharifker revealed evidence that the expansion of the metal core did not conform to the linear ion-diffusion theory, which had been widely accepted, but rather followed the diffusion of spherical nuclei. The previously described description of how single nuclei develop was subsequently confirmed through technical simulation and the observation of metal core formation in micro-electrodes.

2.4.3: Voltammetric Methods

The development of voltammetric methods can be traced back to the invention of polarography in 1922 by Jaroslav Heyrovsky, a chemist from Czech, who was awarded the Nobel Prize in Chemistry in 1959[314]. Polarography is a scientific technique that investigates the behaviour of electrolytic solutions and compounds undergoing reduction or oxidation processes. This is achieved by use a falling mercury electrode in conjunction with a reference electrode. The potential difference across the electrodes is manipulated, and the resultant alterations in the flow of electric current are quantified. The generation of a current against potential polarographic graph (I × E) is achieved by graphing the alterations in current flow in relation to the fluctuations in potential[309]. Plotting the changes in current flow versus the potential variation is what this procedure entails. In the 1960s and 1970s, significant advancements were made in the field of voltammetry, leading to the development of theories, methods, and apparatus. These advancements played a crucial role in enhancing the sensitivity and expanding the range of electroanalytical procedures[315]. All voltammetric procedures share the common feature of applying a potential (E) to an electrode and seeing the consequent current (I) that passes through the electrochemical cell. In numerous instances, the applied potential is subject to variation or the current is regulated over a specific duration (t). Hence, it can be stated that all voltammetric procedures can be characterised by the variables of potential (E), current (I), and time (t). The various voltammetric techniques offer several analytical advantages. These include high sensitivity, allowing for the detection of both organic and inorganic species within a detectable concentration range. Additionally, a wide range of solvents and electrolytes can be utilised, along with the ability to operate at different temperatures. The analysis times are also relatively fast, typically taking only seconds. Furthermore, these techniques enable the simultaneous determination of multiple analytes, as well as the estimation of unknown parameters and the determination of kinetic parameters. The generation of different potential wavelength shapes is also easily achievable. The measurement of tiny currents is also possible using these approaches. The voltammetric methods, also known as potential sweep methods, apply a working electrode continuously to a potential that changes over time[309]. This causes electro-active species in the solution to undergo faradaic reactions, or the redox of electroactive species. Adsorption of particular species at certain potentials, as well as a capacitive current brought on by the electrical double layer, both have an impact on these reactions. As a result, there is a discrepancy between the measured current and the current that exists in an equilibrium state. Numerous approaches, such as cyclic sweep techniques, pulse and linear apart from

cyclic voltammetry (CV), are frequently used to facilitate the investigation of activities occurring in the working electrode (CV). These techniques have mostly been used to diagnose electrochemical reaction mechanisms, identify species in solutions, and perform semiquantitative analyses of reaction rates.

2.4.3.1: Cyclic Voltammetry

Linear sweep voltammetry involves the execution of a unidirectional potential sweep, which concludes at a predetermined value E_f, such as at time $t = t_1$[314]. The sweep direction may exhibit either a positive or negative orientation, while the initial sweep speed is capable of assuming any arbitrary magnitude. In the context of cyclic voltammetry (CV), the direction of the sweep is changed and reversed at $t = t_1$, leading to a change in direction until the minimum potential (Emin) is attained. Subsequently, the direction is reversed again and changed to the maximum potential (E-max), and this process is repeated, resulting in the generation of cycles comprising multiple sweeps. **Figure *16*** illustrates the fundamental diagram depicting the implementation of a potential sweep. The parameters most commonly studied in a cyclic voltammogram are as follows: The characteristics that will be taken into account for this study are the initial sweep direction, the sweeping speed, the maximum potential, $E_{máx}$, the minimum potential, Emin, and the final potential, E_f. As an illustration of the measured current response in relation to the potential for a reversible system, a cyclic voltammogram is presented in **Figure *17***. The potential window appears when the analyte interacts on the electrode surface when measuring the faradaic current (I_f) produced by the electrode reaction[315]. Additionally, there exists a capacitive component (I_c) due to the variation in charge of the electrical double layer (EDL) (C_d) when the potential is swept. The magnitude of its contribution exhibits a positive correlation with the rate of sweeping.

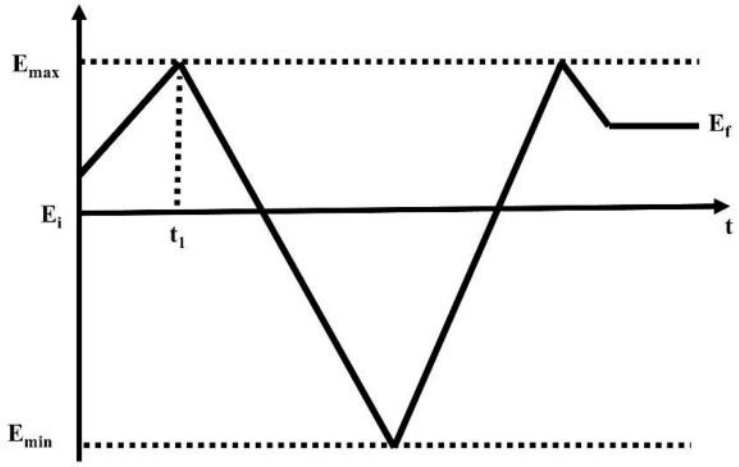

Figure 16: In cyclic voltammetry (CV) (E_{inic}, starting potential; E_f, final potential; $E_{máx}$, maximum potential; E_{min}, minimum potential) applied potential as time function. Sweep speed v = dE/dt [313]

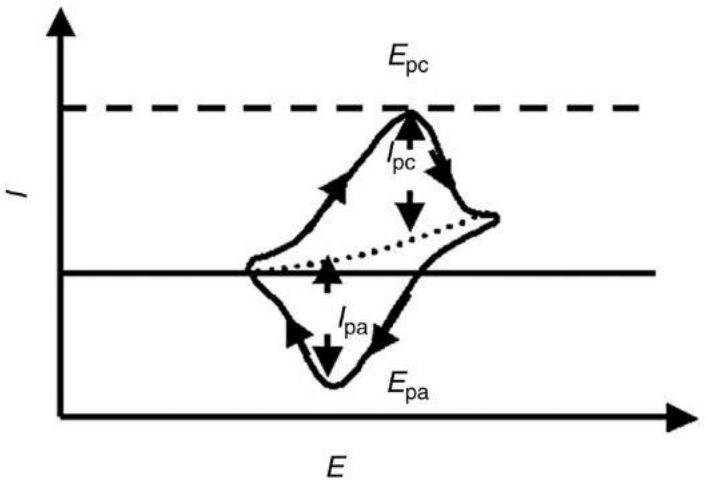

Figure 17: CV for a reversible system

Capacitive and faradaic currents combine to form the total electrical current. A rise in sweeping speed is correlated positively with both currents. This connection limits the sensitivity of the technique since it may have an impact on how sensitive the huge capacitive current is to the faradaic current. The faradaic current is directly proportional to the analyte concentration in the linear region. The Nernst equation (Eq. 2) governs the behaviour of potential and hence serves as a distinguishing feature of a certain oxidation and reduction process or analyte. Consequently, the coefficient of variation (cV) can be employed for quantitative analyses. Nevertheless, due to its inherent limits, it is commonly utilised for exploratory investigations, specifically to ascertain the redox processes of various analytes. In order to mitigate the impact of capacitive current and enhance the performance of voltammetric techniques, researchers have devised potential impulse techniques such as pulse voltammetry and square wave voltammetry (SWV)[312]. These findings provide a fundamental understanding for the application of the amperometric method.

2.4.3.2: Differential Pulse Voltammetry (DPV)

Differential pulse voltammetry is an electrochemical method that employs amplitude potential pulses on a linear ramp potential (DPV). A baseline initial potential value is selected for differential pulse voltammetry (DPV), in which reaction occurs without faradic current, and this value is then implemented to the electrode.[314]. Equal quantities are added to the baseline potential between each pulse. The current is analysed both before and after the pulse is administered, with the difference between the two readings being recorded afterward. The waveform of the pulse in DPV is shown in **Figure *18*** according to the reference. The first derivative of a linear voltammogram and the DPV approach are both differential techniques. It is used to identify the occurrence of a peak linked to a particular redox process. The voltammogram produced by the linear sweep method resembles a wave and has a peak-like look that was caused by the first derivative. By determining the half-wave potential ($E_{1/2}$), linear sweep voltammetry—which functions similarly to polarography with a mercury electrode that drops—offers qualitative insights into an analyte[310].

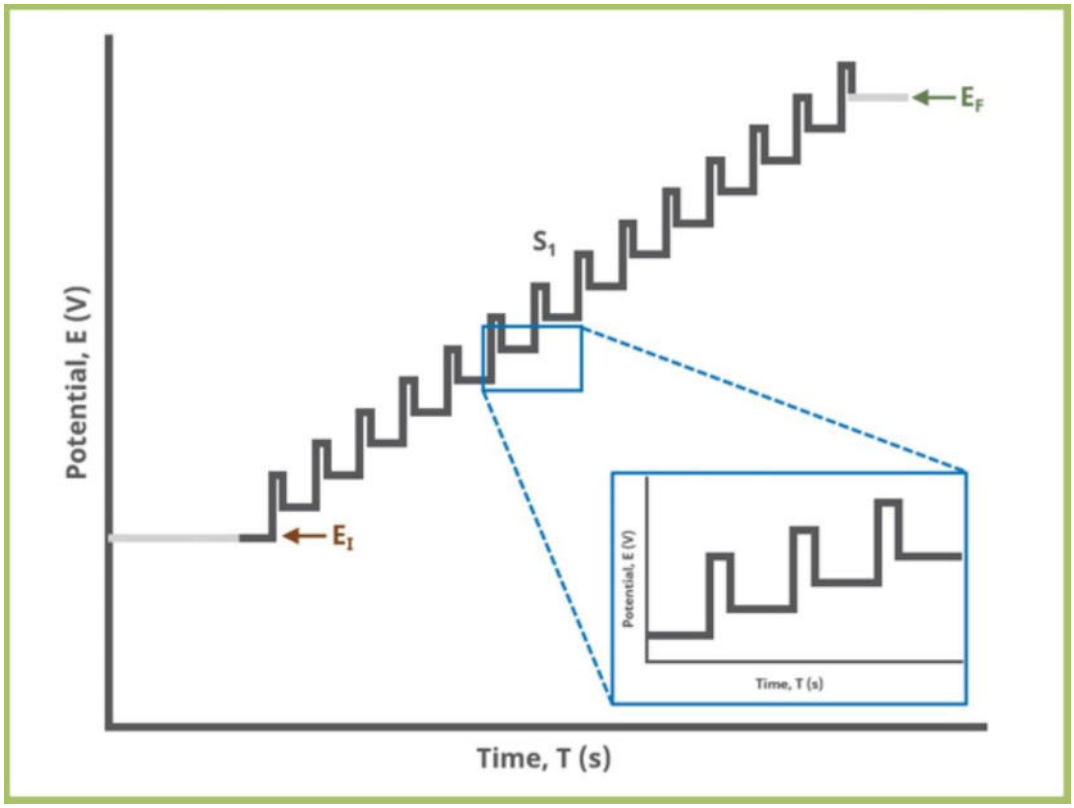

Figure 18 : Differential Pulse Voltammetry (DPV) One Segment Waveform

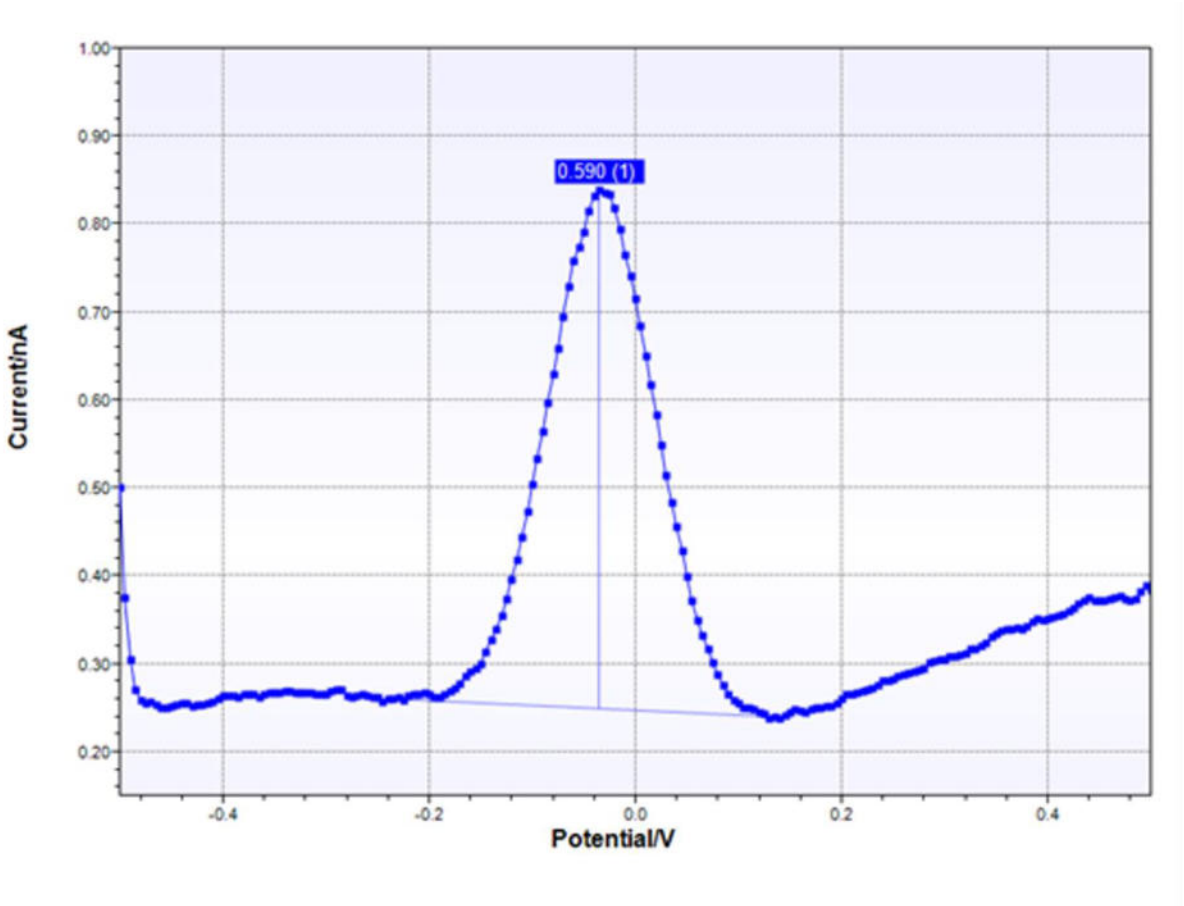

Figure 19: A differential pulse voltammogram's typical response[316]**.**

This potential corresponds to the point at which the wave height is halved. Likewise, within the context of differential pulse voltammetry (DPV), the maximum potential, E_p, can be approximated as being equivalent to $E_{1/2}$. As the irreversibility increases, the potential energy (E_p) deviates from the half-wave potential ($E_{1/2}$) due to the widening of the peak's base and the subsequent fall in its height. The DPV represents a graphical representation of the disparities between the measured currents and the applied potentials, as depicted in **Figure *19***. The user's text is not sufficient to rewrite in an academic manner. The utilisation of DPV has been found to yield superior outcomes in comparison to conventional pulse voltammetry, particularly when applied to solid electrodes, with a particular emphasis on investigations involving organic molecules. Given that they are typically absorbed by the electrode, it is plausible that a differential approach can effectively differentiate the effects that exhibit relatively consistent behaviour before and after the implementation of pulses. In general, voltametric pulse techniques, such as differential pulse voltammetry (DPV), exhibit higher sensitivity compared to linear sweep methods due to the reduction of capacitive current. Conversely, the utilisation

of CV is predominantly observed in the context of exploratory endeavours. So, it is standard procedure in sensor creation to use both pulse and cyclic voltammetry (CV) approaches. This is due to CV's essential insights into the reversibility of the process and the many redox processes involved in the analysis, including those involving the matrix, analyte, and electrode. Meanwhile, quantitative measurements are the main use of pulse methods.

2.4.3.3: Square Wave Voltammetry

SWV, also known as square wave voltammetry, is considered to be a highly efficient and exceptionally responsive method for conducting pulse voltammetry[317]. The detection limits of the method can be compared to those of spectroscopic and chromatographic techniques. Furthermore, the examination of the distinctive features of this methodology also facilitates the assessment of the mechanism and kinetics of the electrode process being investigated. Solid-State Voltammetry (SWV) uses potentials with a height of ΔE to calculate the form of the potential current curve (pulse amplitude). These potentials fluctuate depending on a millivolt-based potential step E_{step} and the time period τ(duration). The variable t represents the potential-time curve's pulse width (τ/2) whereas the variable f denotes the frequency of the pulse application and may be calculated as the reciprocal of t, or (1/t). Both the direct (I_1) and reverse (I_2) pulses' termination points are used to measure electric currents. The signal is obtained by measuring the strength of the differential current (ΔI).[318]. This particular method offers strong capacitive current rejection capacity and extraordinary sensitivity.

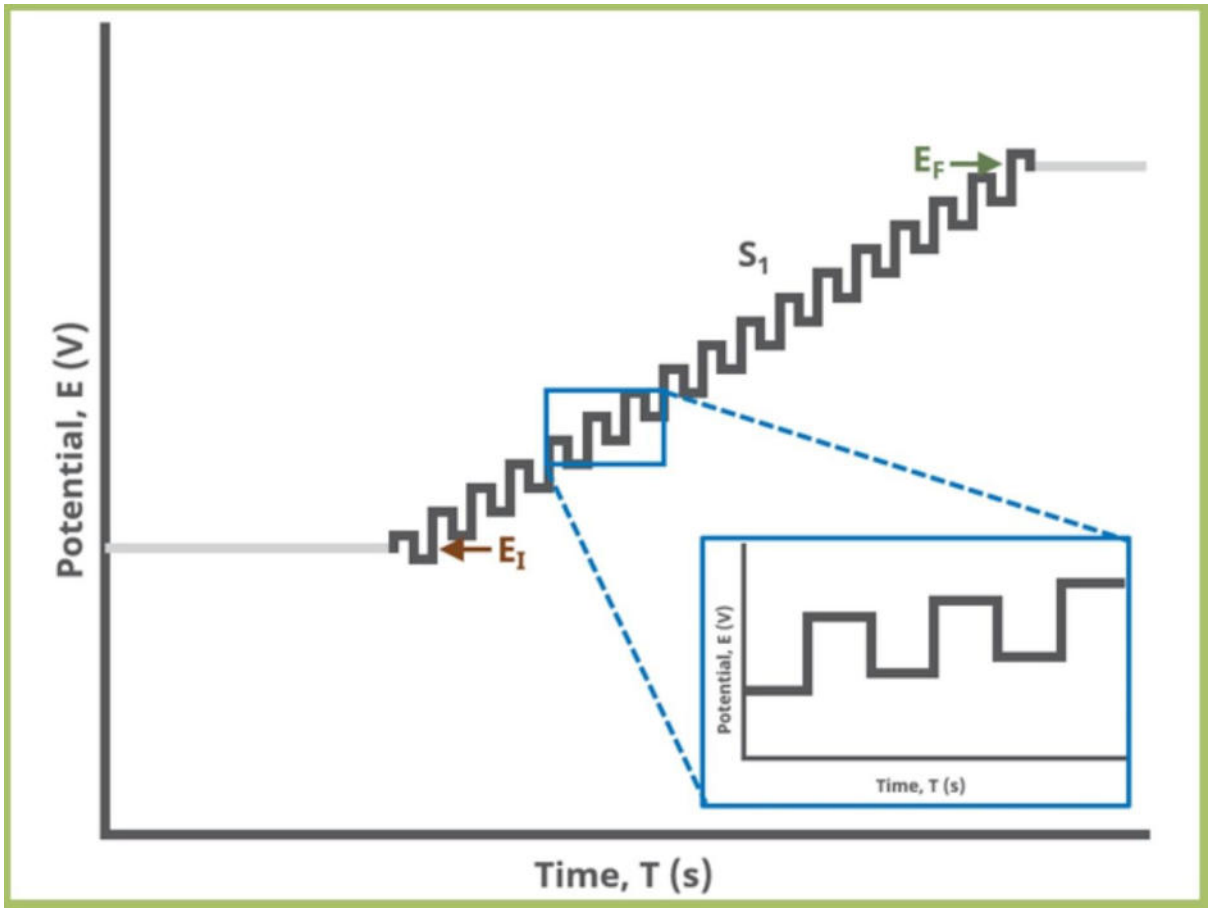

Figure 20: Square Wave Voltammetry

Prior to an initial period of time (t_i) in which the working electrode is polarized at a voltage that does not cause the redox reaction, the measurement is carried out. **Figure *20*** shows a representation of a hypothetical SWV (square wave voltammetry) application along with an explanation of the used parameters. **Figure *21*** depicts the theoretical voltammograms for (A) a reversible system and (B) an irreversible system. In contrast, For the direct, reverse, and resultant processes, these voltammograms show unique currents. Additionally, the results of square wave polarography are similar to both voltammetric profiles. The symmetry and distinctive features of the current-potential curves are usually visible. This phenomena results from the fact that all currents are only recorded at the end of each semi period, and that fluctuations in the size and duration of the potential pulse are always constant within a certain range of potential[73]. Voltammetric techniques, which establish a link between the electric potential and the current within the electrochemical cell, are used to synthesize and characterize materials using electrochemical techniques. Amperometric sensors operate by applying a consistent electric voltage to the electrochemical cell, resulting in the generation of a current

due to the redox processes taking place on the working electrode's surface. The present electrical flow has the potential to serve as a means of quantifying the reactions that are implicated.

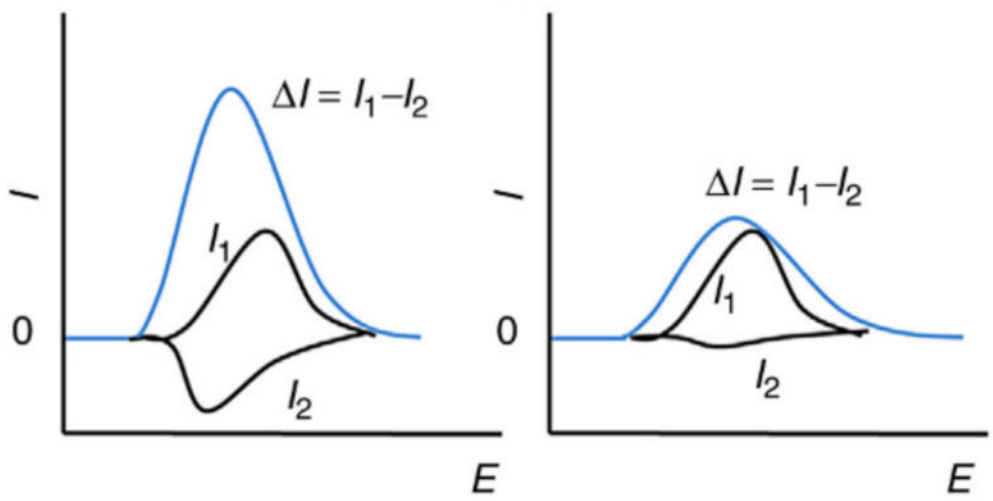

Figure 21: An irreversible system's redox process is shown by (B) in the schematic square wave voltammogram, while a reversible system's is represented by (A).

By using cyclic voltammetry (CV), a reliable method for the creation and characterization of diverse electroactive species, amperometric sensors can be used in an efficient manner. The current-potential characteristics connected to each of the oxidation or reduction reactions involved can be examined using this technique. For the goal of identifying species involved in redox reactions within electrochemical cells, voltammetric sensors are frequently used. The (Square Wave Voltammetry) SWV method has been used in the construction of biosensors and sensors due to its noteworthy qualities of increased sensitivity and selectivity. The use of biomarkers in disease detection and the identification of environmental pollutants, including heavy metals and chemical toxins, has generated a great deal of interest in the pharmaceutical industry. In contemporary society, these toxins represent a serious environmental risk.

2.4.3.4 Electrochemical Impedance Spectroscopy (EIS)

Electrochemical impedance spectroscopy (EIS) is a widely employed method for investigating and analysing the electrochemical phenomena taking place at the interface between an electrode and an electrolyte solution. The present approach entails the utilisation of a technique for the purpose of identification and estimation of parameters derived from a model that has been constructed on the basis of the frequency response exhibited by the electrochemical system being investigated. In these experiments, a frequency response analyzer is employed in conjunction with an electrochemical interface. With this configuration, it is possible to measure the system's current response as a function of the frequency of an input sinusoidal wave., denoted as $E = E_o \sin(\omega = 2\pi f)$, is varied. The input signal is applied to an unknown sample, and the resulting current, denoted as $I = I_o \sin(\omega t + \phi)$, is analysed by correlating it with the input signal. The phase angle displacement, represented by the symbol ϕ, is taken into consideration during the analysis[319], [320].

The vector sum impedance (Z) is given by:

$$Z = R - jX_c \quad \text{.....4}$$

Where, the variable "j" is defined as $\sqrt{1}$ *(Fourier). The symbol "R" represents resistance, while "*X_c*" denotes the capacitive reactance, which is equivalent to a1/ωC in units of ohms. Here, "w" represents the angular frequency, calculated as 2πf, where "f" represents the frequency. Lastly, "C" represents the capacitance of the electric double-layer. Hence, it is observed that R represents the real component (Z') and -j*X_c *represents the imaginary component (Z") of a1/ωC, which is measured in ohms. Here, w is equal to 2πf, where f denotes the frequency, and C represents the capacitance of the electric double-layer. Hence, it is observed that R represents the real component (Z') and -j*X_c *represents the imaginary component (Z") of the impedance.*

The displacement vector Z(ω) represents the complex impedance, which is derived by varying the alternating signal ω. By using these various parameters, the modulus $Z_o = E_o/I_o$ and the phase angle ϕ may be computed to ascertain the imaginary and real impedance values, as depicted in **Figure *22***.

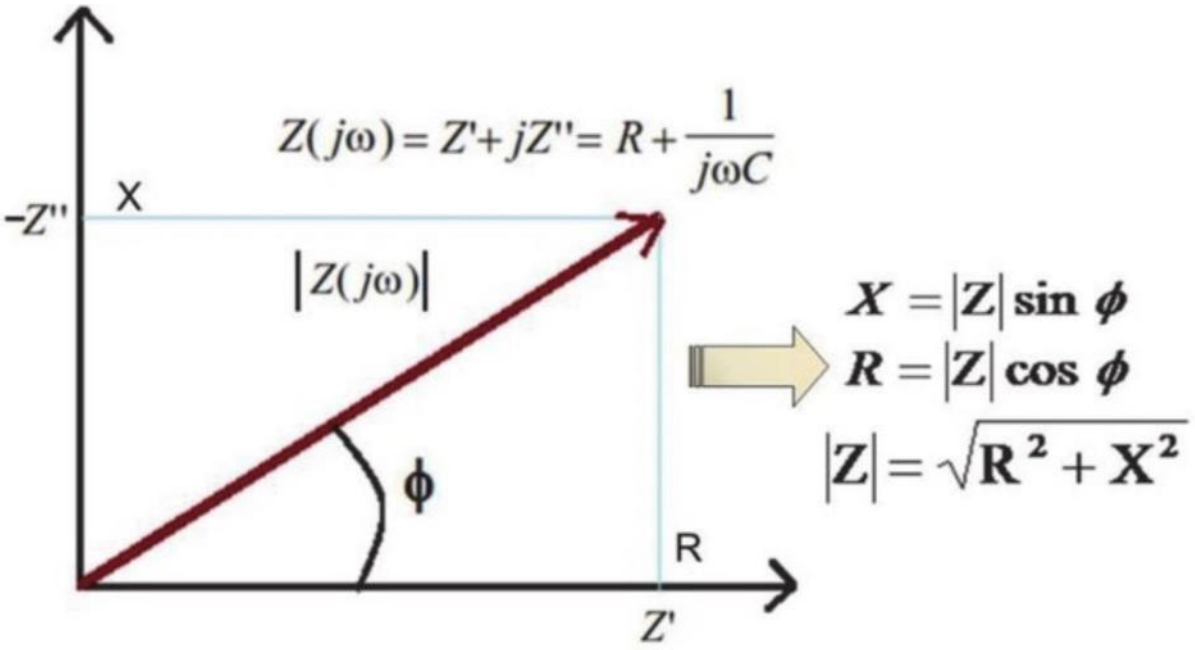

Figure 22:Vector Representation of EIS (Adapted from Electrochemical Impedance Spectroscopy Edited by Marwa El-Azazy, Mart Min and Paul Annus) [321]

A resistor (R_c) and capacitor are linked in parallel in **Figure *23*** simplified illustration of an electrochemical cell. Typically, the resulting spectrum has a semicircular form on the complex impedance plane. The imaginary component, denoted as Z'' or $-I_m$, is conventionally depicted on the y-axis as the opposite of the impedance multiplied by the sine of the angular frequency (ω). On the x-axis, the real components Z' (or R) and Z (or $Z_o \cos(\omega)$) are plotted.

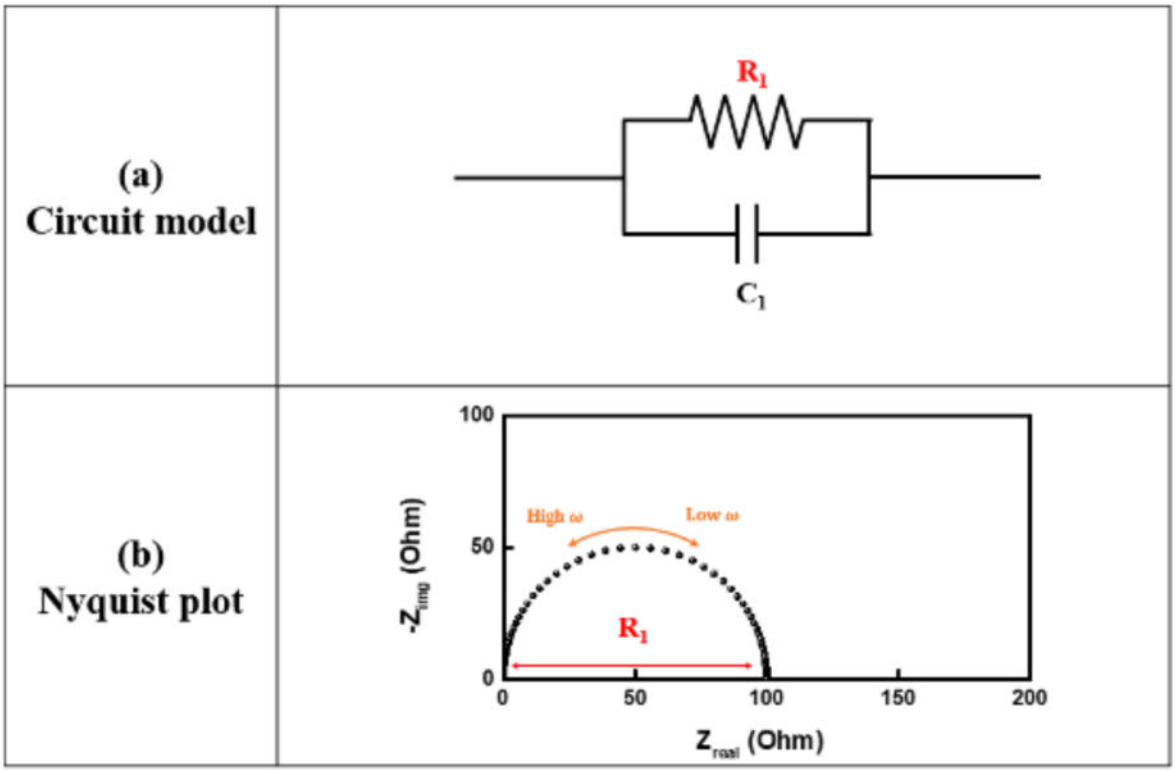

Figure 23:Schematic diagram of an EIS RC circuit[322]

According to the equation $2\pi f_o RC = 1$, the semicircle's top frequency reveals the resonance state of the circuit. Impedance spectroscopy is frequently employed as a method of investigation for films that are deposited on electrodes due to its ability to discern and differentiate the many conductivity mechanisms that manifest inside the material[322]. The results are commonly connected to an electrical circuit where it is possible to determine and compute variables like the capacitance of the electrical double layer, the conductivity of the ions, the resistance of electron transmission, and the resistance of the electrolyte.

CHAPTER 3: SYNTHESIS AND CHARACTERIZATIONS OF Nb_2CT_X MXENES FOR IMPROVED ELECTROCHEMICAL PERFORMANCE

This crucial chapter centres on the synthesis and characterization of materials, which play a vital role in improving electrochemical performance. This section provides a comprehensive exposition of the approaches employed for the synthesis of the MAX Phase Nb_2SnC and the etching methodology utilised for the production of Nb_2CT_x MXenes. The precise documentation of the electrode modification process utilising the synthesised MXenes is an essential component of the experimental procedure. The subsequent section of the chapter focuses on conducting a thorough investigation of the structural and morphological properties of the synthesised Nb_2SnC MAX phase and Nb_2CT_x MXenes. This analysis involves the utilisation of many techniques including Energy Dispersive Spectroscopy (EDS), X-ray Diffraction (XRD), Scanning Electron Microscopy (SEM), X-ray Photoelectron Spectroscopy (XPS), Transmission Electron Microscopy (TEM), and Fourier Transform Infrared (FTIR) analysis. These strategies serve as the foundational principles for comprehending the materials at a fundamental level. Subsequently, an investigation into the electrochemical properties of the synthesised Nb-based MXene is conducted, which is crucial for evaluating its potential in various electrochemical applications. The chapter concludes with a succinct overview, establishing the framework for following analyses and implementations of the amalgamated content.

3.1 Materials and Methods

The synthesis of MXenes represents a compelling integration of scientific investigation and technological advancement, with significant implications for many applications, particularly in the field of electrochemical sensing. As we commence our exploration into the realm of MXene synthesis, we find ourselves immersed in the complex domain of MAX phases. The MAX phases provide a notable combination of metallic and ceramic properties, serving as the foundational precursors for MXenes. Their gradual development paves the way for significant

advancements and transformative changes in the future. In the context of MXene synthesis, our exploration delves into the process of etching, which is considered a transformative technique. In this context, the once inert MAX phases undergo a transformation, transitioning from their bulky state to manifest as ultrathin nanosheets with exceptional characteristics. In this context, we are presented with two distinct avenues: the conventional acid etching methods, which have been extensively utilised and validated over a significant period, and the groundbreaking molten salt etching technique, a novel approach that has established its unique position by providing ease of use, accuracy, and ecological conscientiousness. Every individual etching technique possesses distinct qualities, and our investigation aims to reveal the complexities, benefits, and possible uses of each. This chapter functions as an essential basis for the wider scope of our research, whereby the synthesised MXenes will assume a crucial role as fundamental constituents in the advancement of electrochemical sensors with superior performance. This will lead to a redefinition of the boundaries within the field of analytical chemistry.

3.1.1 MAX Phase (Nb_2SnC)

The synthesis of the Nb_2SnC MAX phase was conducted with meticulousness, employing various unique procedures with the objective of attaining the desired material. Each of these procedures assumes a pivotal position in the comprehensive synthesis process, so making significant contributions to the formation of this exceptional substance.

- **Mechanical Blending and Milling**

The process of synthesising the Nb_2SnC MAX phase begins with the correct mixing of Nb powder (7.4 g), Sn powder (5.2 g), and graphite powder (0.48 g) in a carefully determined molar ratio of 2:1.1:1. The initial blending, performed through manual means using a mortar and pestle, guarantees the uniform dispersion of every individual component. Following this, the combination is subjected to a prolonged period of mechanical blending, lasting for a duration of 8 hours, with a planetary micro miller. The rigorous milling procedure conducted at the microstructural level improves the uniformity of the mixture, so preparing it for the succeeding synthesis steps.

- **Pellet Formation and Compression**

After undergoing mechanical blending, the resulting powder combination is transformed into uniformly shaped pellets, with each pellet weighing approximately 1g of the combined powder. The creation of pellets is accomplished by applying a uniaxial force of approximately 70 kg/cm^2 with the aid of a hydraulic press in a precise manner. The controlled compression process is an essential stage that bestows structural integrity upon the material and readies it for the subsequent phase of heat treatment.

- **Heat Treatment in Controlled Environment**

The crucial stage of the synthesis process takes place within a tube furnace that is managed to maintain specific air conditions. Within the confines of this regulated setting, the meticulously produced pellets are positioned inside aluminium crucible boats, a specific arrangement crucial for the effective implementation of the synthesis process. The tube furnace is precisely programmed to achieve and sustain a temperature of 1000°C for a duration of 8 hours. Simultaneously, a steady stream of nitrogen gas is introduced for the entirety of the procedure, thereby maintaining an inert environment within the furnace. The temperature changes within the tube furnace are performed with meticulous precision, whereby the heating and cooling rates are set at a constant rate of 10°C per minute. The utilisation of a regulated heat cycle plays a crucial role in facilitating the conversion of the pelletized mixture into the intended Nb_2SnC MAX phase.

- **Powderization and Storage**

After the heat treatment process is concluded, the resulting material is meticulously extracted from the furnace. At this particular stage, the material undergoes a transformation resulting in the manifestation of the unique attributes associated with the MAX phase. Subsequently, the altered material is subjected to hand grinding in order to generate finely powdered Nb_2SnC. Subsequently, the powdered substance is let to undergo a cooling process until it reaches the surrounding temperature, so guaranteeing its durability and coherence. The specimen is carefully preserved in a controlled and moisture-free setting, ensuring its preparedness for future scientific investigation and practical utilisation.

The effective synthesis of Nb_2SnC MAX phase, a versatile material with significant promise in diverse scientific and technological fields, is attributed to the precise execution of each of these processes.

3.1.2 Etching of Nb_2CTx MXene

When attempting to synthesise MXene, a group of two-dimensional materials known for their exceptional properties, it is commonly observed that conventional methodologies employed for other two-dimensional materials such as graphene and black phosphorus are not suitable. This is primarily due to the presence of strong metallic bonds within the $M_{n+1}AX_n$ Phase of MXene. Significantly, within this particular phase, it is noteworthy that the M-A bonds demonstrate a higher degree of chemical reactivity in comparison to the M-X bonds. As a result, the production of MXene primarily entails the targeted removal of the "A" element from the MAX phase through the use of strong acids, such as hydrofluoric acid (HF), lithium fluoride (LiF), or a combination of them. The application of etchants containing fluoride is a widely employed technique, with other approaches involving the use of heat. The objective of this study was to successfully synthesise MXene without the use of hydrofluoric acid (HF), a method that is recognised for its difficulties, lengthy process, and hazardous properties.

In order to navigate the intricacies associated with HF-based synthesis, we have opted for an alternate approach that exhibits considerable potential for the synthesis of Nb_2CT_x MXene. In this experimental procedure, a quantity of 500 mg of Nb_2SnC MAX phase powder was carefully mixed with 50 ml of phosphoric acid. The resulting mixture was subjected to magnetic stirring for a duration of 24 hours, maintaining a controlled temperature of 60°C. The intentional incubation process facilitated the gradual conversion of the MAX phase material into the targeted Nb_2CT_x MXene compound. Throughout this procedure, the pronounced affinity of phosphoric acid towards the "A" element played a crucial role in enabling the targeted extraction of the "A" element from the MAX phase structure. After this stage, the solution obtained was subjected to an extensive washing procedure in order to eliminate any remaining byproducts. The approach employed in this process adhered to the recognised protocols often utilised in the synthesis of MXene. Following that, the Nb_2CT_x MXene material was meticulously collected and subjected to a further 24-hour drying process, this time use an oven with a precisely regulated temperature of 70°C. The drying process was implemented to effectively eliminate any residual solvent, resulting in the formation of the Nb_2CT_x MXene material in its pristine state, characterised by its two-dimensional nanosheet morphology. The

utilisation of this innovative methodology, which circumvents the utilisation of hydrofluoric acid (HF), not only streamlines the process of synthesising Nb_2CT_x MXene but also mitigates the difficulties typically encountered, so establishing it as a more feasible and ecologically conscious pathway for the synthesis of Nb_2CT_x MXene (**Figure *24***).

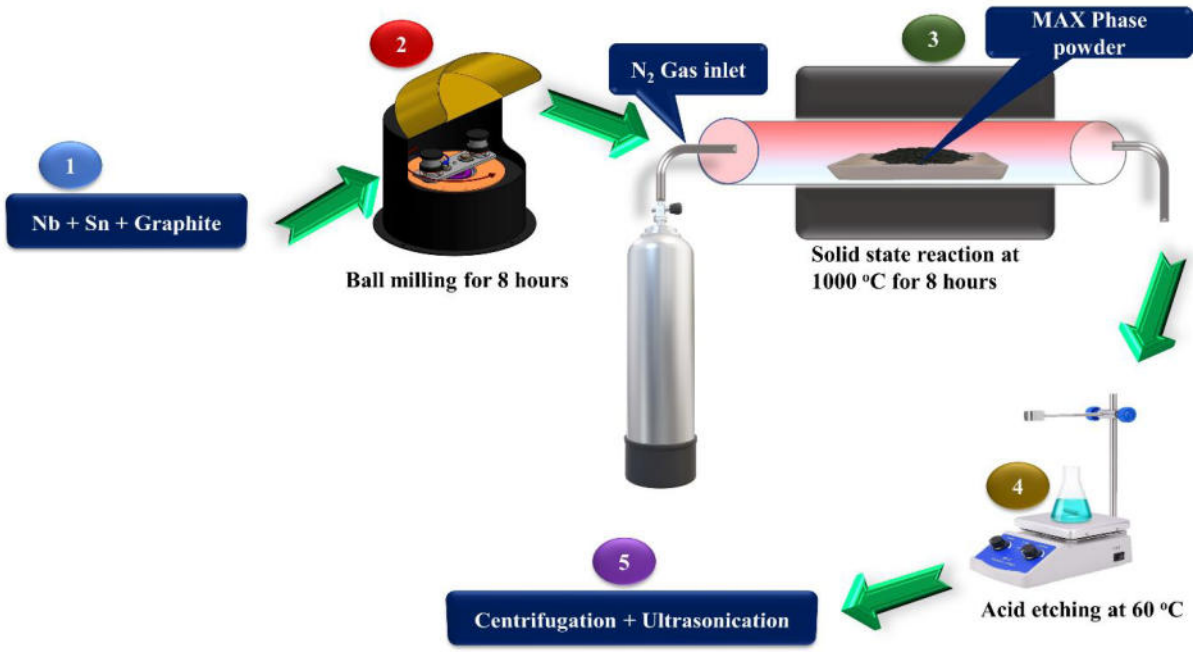

Figure 24: Schematic diagram for the synthesis of Nb_2SnC MAX Phase and Nb_2CT_x MXene

The precise execution of this alternative method for synthesising MXene materials has facilitated the attainment of MXene materials with unique characteristics, positioning them for potential utilisation in a wide range of scientific and technical fields.

3.1.3 Modification of electrodes with synthesized MXenes

- **Electrode Modification: The Drop-Cast Method**

To modify the working electrode in the three-electrode assembly, a careful approach was employed using the drop-cast method. The objective of this procedure was to achieve uniform

dispersion and consistent adhesion of etched Nb_2CT_x MXene onto the surface of the electrode, hence promoting effective electrochemical reactions. The expedition commenced with the formation of a uniform mixture. In a precise manner, a quantity of 5 mg of etched Nb_2CT_x MXene was carefully combined with 25 μL of Nafion and an equivalent volume of ethyl alcohol. The amalgamation was subjected to a thorough ultrasonication procedure lasting for a duration of three hours, which ensured the achievement of a uniform solution. After achieving solution harmonisation, the subsequent procedure was depositing the solution containing MXene onto a substrate made of nickel foam. It is imperative to acknowledge that prior to deposition, the nickel foam underwent thorough washing with a 2 M HCL solution. This meticulous process aimed to achieve surface cleanliness and enhance adhesion. The deposition process was performed in an iterative manner, ensuring the gradual formation of a uniform layer of MXene material that completely covered the nickel foam. This resulted in the successful creation of the modified electrode. In order to ensure the preservation of the modification's integrity, the nickel foam was thereafter treated to a drying regimen, involving an overnight stay in an oven maintained at a temperature of 70°C. The careful execution of this method not only guaranteed the complete elimination of any remaining solvents, but also strengthened the MXene layer, resulting in a durable and dependable modified electrode that is prepared to demonstrate its electrochemical capabilities.

The utilisation of the drop-cast method exemplifies our dedication to achieving accuracy and effectiveness in the modification of electrodes, hence laying the foundation for a thorough assessment of its electrochemical potential in later sections.

3.2: Structural and Morphological Characterizations of the synthesized Nb_2SnC MAX phase and Nb_2CT_xMXenes

3.2.1 EDS

The analysis of EDS is of utmost importance in the characterization of nanomaterials such as MXenes, as it provides essential information regarding their elemental composition and level of purity.–Having established the fundamental significance of EDS, we now proceed to explicate the distinct observations pertaining to Nb_2SnC MAX and Nb_2CT_x MXene. The

examination of EDS serves as a crucial method for determining the elemental composition of both the Nb_2SnC MAX phase and the resulting Nb_2CT_x MXene, as depicted in **Figure *25 (a).*** The EDS analysis demonstrates a significant alteration in elemental proportions, so presenting indisputable proof of the effective synthesis of Nb_2CT_x MXene[323]. In the context of Nb_2SnC MAX, the elemental composition notably exhibited a Sn content of 18.32%, suggesting the presence of Sn in the original MAX phase. Nevertheless, the Sn content experienced a significant reduction to a mere 0.02% in Nb_2CT_x MXene, highlighting the successful eradication of Sn into the MXene structure. Concurrently, there was a notable increase in the elemental composition of carbon (C), with a rise from 7.72% in Nb_2SnC to 54.37% in Nb_2CT_x MXene. The significant rise seen in this study provides strong evidence for the incorporation of carbon as a principal component inside the recently developed Nb_2CT_x MXene framework. Moreover, in comparison to its MAX predecessor, Nb_2C MXene exhibited an increased elemental content of niobium (Nb) and carbon (C). Overall we can conclude that eradication of Sn from the Nb_2SnC MAX phase leads to enlarge the relative atomic % of Nb and C. It is worth mentioning that the occurrence of oxygen in the energy-dispersive X-ray spectroscopy (EDS) spectra of Nb_2CT_x MXene can be ascribed to the existence of intercalated water molecules and surface termination OH ions, which are inherent to the structure of MXene. Significantly, the Energy Dispersive Spectroscopy (EDS) investigation reveals the absence of any impurities in the prepared sample, hence confirming the high level of purity and structural integrity of the synthesised Nb_2CT_x MXene material. The detailed analysis of energy-dispersive X-ray spectroscopy (EDS) plays a crucial role in characterising the Nb_2CT_x MXene. It provides essential insights into the elemental changes and purity of the material, which are necessary for further exploration of its electrochemical properties and potential applications.

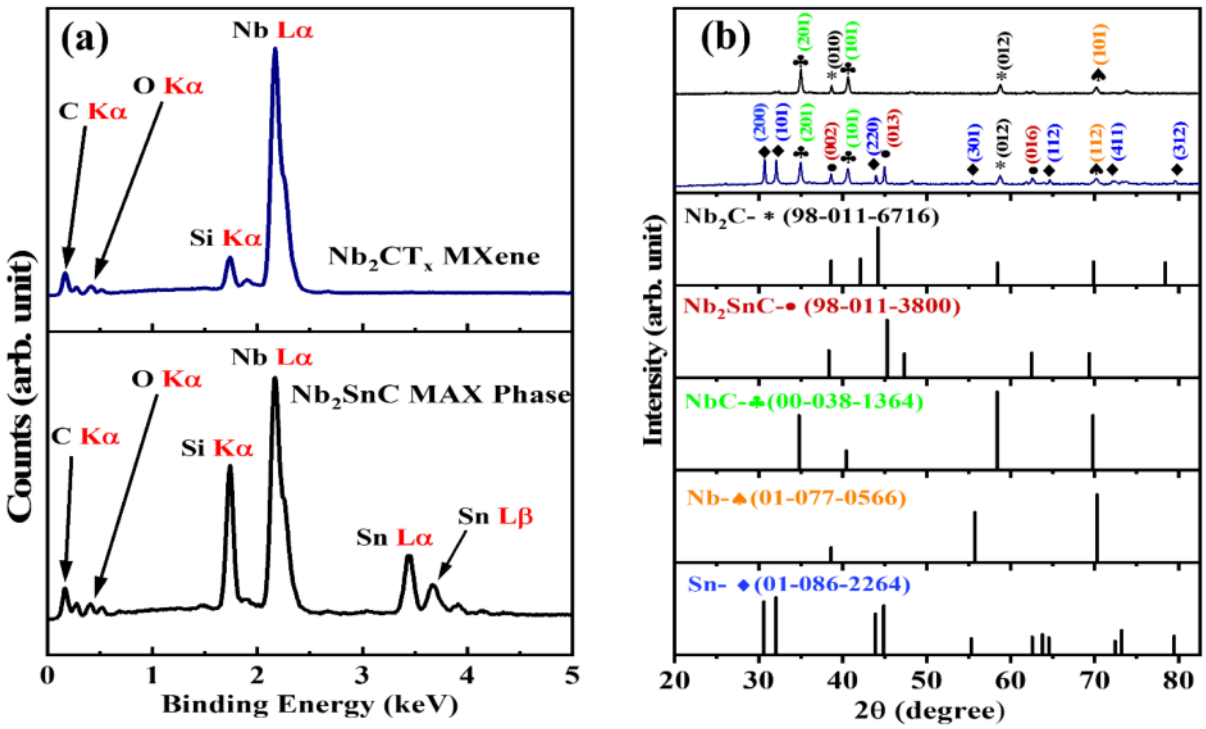

Figure 25: EDS and XRD analysis of Nb_2SnC MAX Phase and Nb_2CT_x MXene

3.2.2 XRD

X-ray Diffraction (XRD) analysis plays a crucial role in the domain of advanced materials, including MXenes. The study of the synthesized MAX Phase Nb_2SnC and Nb_2CT_x MXene materials, as demonstrated by the X-ray diffraction (XRD) investigation depicted in **Figure *25 (b)***, requires a comprehensive comprehension of crystallographic characteristics. The X-ray diffraction (XRD) results for the Nb_2SnC MAX phase are in excellent agreement with the crystal structure information provided in the International Crystal Structure Database (ICSD) file (98-011-3800 hexagonal 63/mmc) [324]. The observed peaks at 2θ = 38.76°, 45.01°, and 62.69° can be attributed to the crystallographic planes (002), (013), and (016), respectively[324]. Significantly, X-ray diffraction (XRD) analysis provides additional evidence supporting the existence of Sn, Nb, NbC, and Nb_2C phases, which is consistent with the information found in the ICSD files 01-086-2264, 01-077-0566, 00-038-1364, and 98-011-6716, respectively[325]–[327]. The conversion of Nb_2SnC MAX to Nb_2CT_x MXene, which is achieved through selective etching using H_3PO_4, is clearly observed in the X-ray diffraction (XRD) pattern. The observed transition is characterised by the absence of distinct peaks associated with Sn at specified angles of 2θ, namely 30.5°, 32.0°, 43.8°, 55.3°, 64.7°, and 72.25°. The X-ray diffraction (XRD) peaks of the Nb_2SnC MAX phase demonstrate a much

lower intensity in comparison to the same peaks observed in the Nb_2CT_x MXene. This observation highlights the structural evolution taking place between these two materials. The lattice parameter calculations provide additional clarification on this transformation. The hexagonal Nb_2SnC compound exhibits lattice parameters of a=b= 2.90 Å and c=12.9 Å, which differ from the typical values of a=b= 3.14 Å and c= 13.1 Å. In contrast, the cubic Nb_2CT_x has a lattice parameter of a= 3.99 Å, which deviates little from the conventional value of a= 4.2 Å. The X-ray diffraction (XRD) analysis presented in this study provides a comprehensive examination of the transition process from MAX phase to MXene. This research contributes to a deeper comprehension of the structural modifications, crystallographic characteristics, and phase transitions that are crucial for enhancing the properties of MXene in various applications.

3.2.3 SEM

This section examines the structural characteristics and changes of both Nb_2SnC MAX phase and Nb_2CT_x MXene by SEM characterizations.

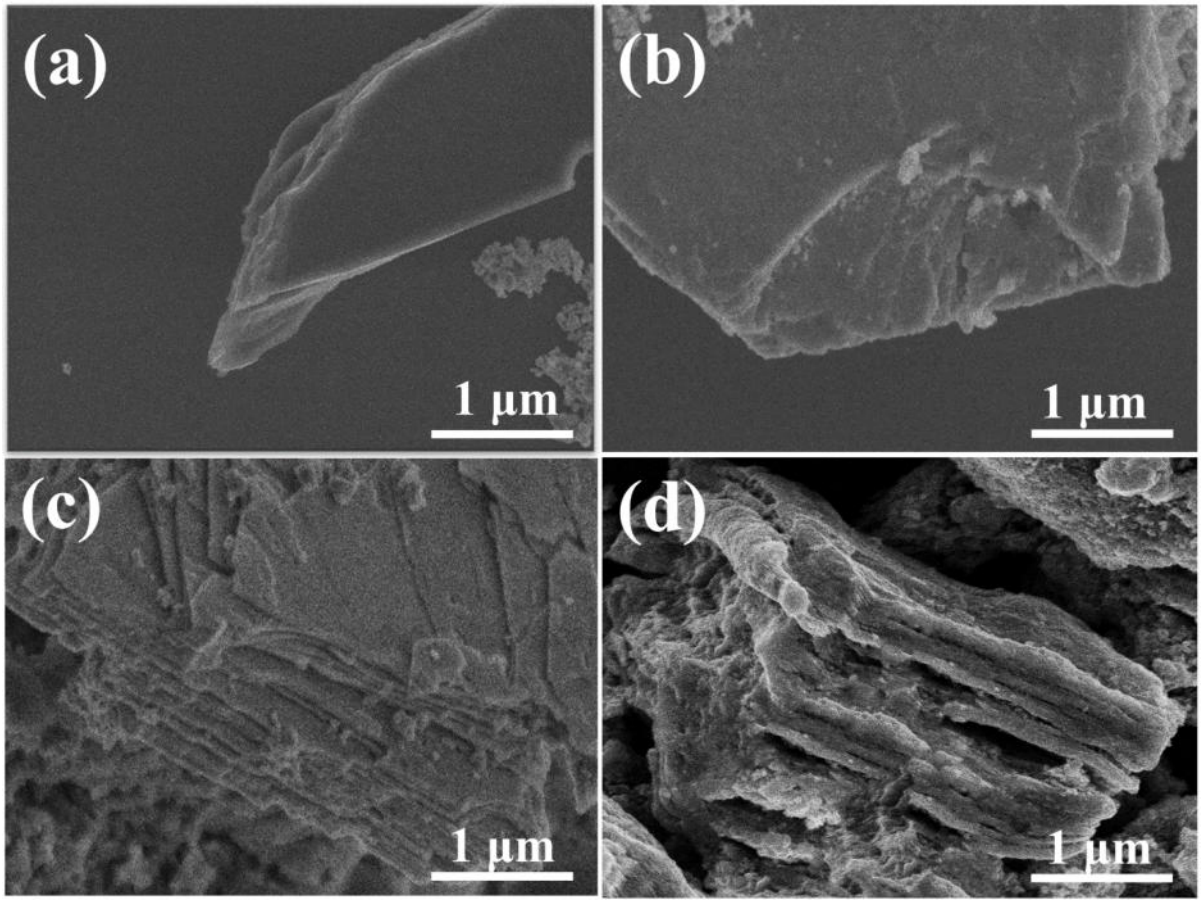

Figure 26: SEM analysis of Nb_2SnC MAX Phase and Nb_2CT_x MXene

In the particular setting of Nb_2SnC MAX Phase and Nb_2CT_x MXene, scanning electron microscopy (SEM) enables us to observe their transformations. The Nb_2SnC MAX Phase, as depicted in **Figure *26 (a) and (b)***, exhibits a pristine bulk structure that displays distinct characteristics. Nevertheless, after undergoing a process of post-etching using phosphoric acid (H_3PO_4), the material experiences a significant metamorphosis, resulting in the creation of sheet-like structures, as illustrated in **Figure *26 (c) and (d).*** The adjustment underscores the adaptability of MXenes, since they rapidly conform to structural alterations to suit diverse purposes. The Nb_2CT_x MXene exhibits two-dimensional sheets with diverse layer sizes, yet maintains a consistent organisation, as revealed by scanning electron microscopy (SEM). Significantly, the scanning electron microscope (SEM) allows for the observation of the increased distance between these layers. The increased interlayer spacing plays a crucial role in enabling efficient ion movement within the material, hence improving its electrochemical performance[328]. The findings of this discovery align with previous study results, which have shown that materials with greater surface areas, such as Nb_2CT_x MXene, exhibit remarkable electrochemical characteristics. Consequently, these materials are very suitable for various applications, including supercapacitors.

3.2.4 XPS

This section employs XPS analysis to unravel the surface chemistry and chemical states of Nb_2CT_x MXene and Nb_2SnC MAX phase, shedding light on their atomic-scale characteristics crucial for various applications, including electrochemical sensing and energy storage. X-ray Photoelectron Spectroscopy (XPS) is a significant technique in the field of material characterization, namely in the investigation of MXenes, where it provides valuable insights into their complicated properties.

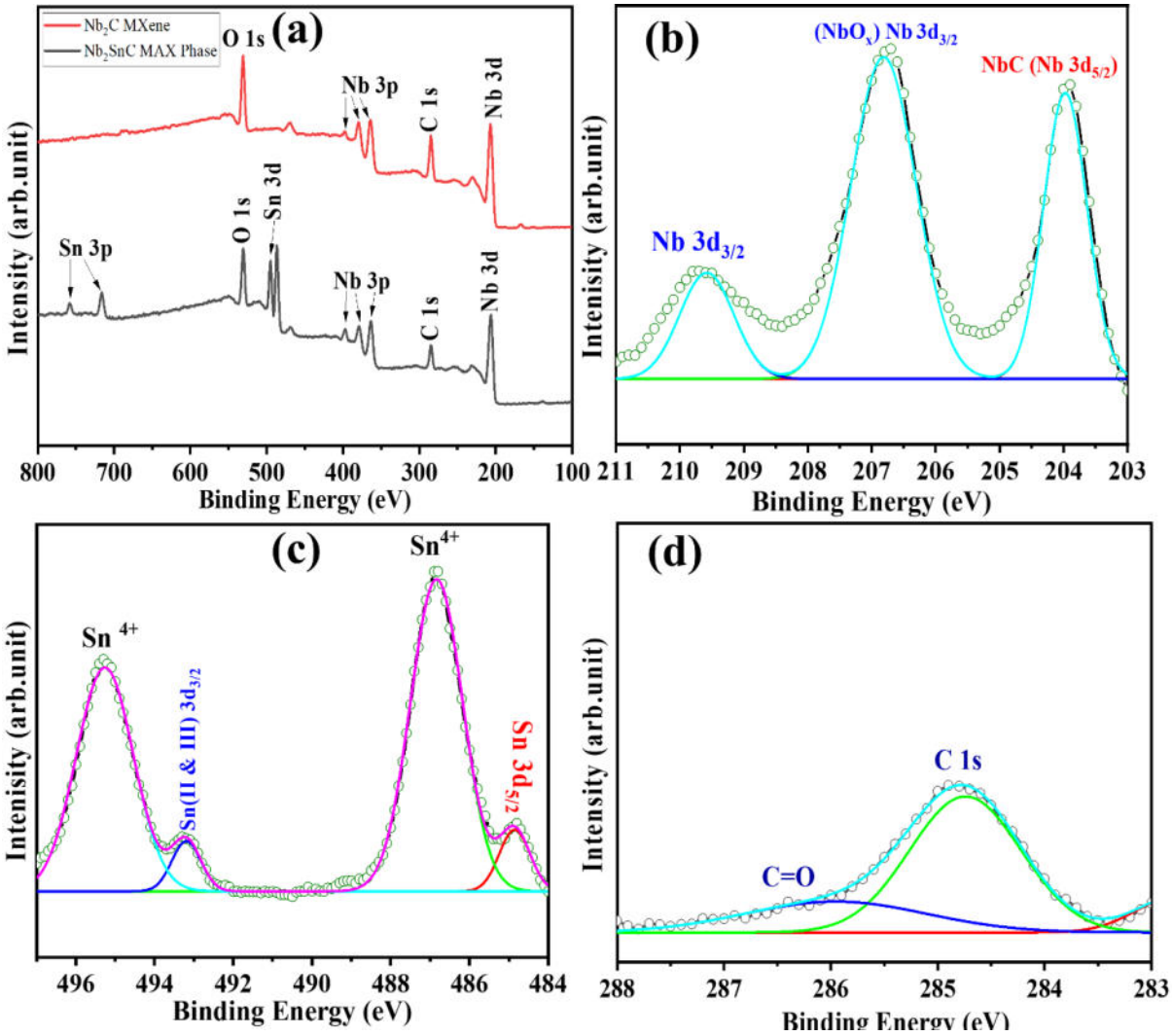

Figure 27: XPS High resolution analysis of (a) Nb_2SnC MAX Phase and Nb_2CT_x survey spectra, (b) Niobium (Nb), (c)Tin (Sn) & (d) Carbon(C).

To gain a more comprehensive comprehension of the synthesised materials, the utilisation of X-ray Photoelectron Spectroscopy (XPS) was employed to investigate their surface chemistry, revealing precise information regarding the elemental makeup and chemical states. **Figure *27 (a)*** effectively illustrates the X-ray photoelectron spectroscopy (XPS) survey spectra, providing an early insight into the chemical composition of both the Nb_2SnC MAX phase and Nb_2CT_x MXene. Upon closer examination, **Figure *27 (b)*** provides a detailed analysis of the high-resolution spectrum of the Nb 3d area in Nb_2CT_x MXene, uncovering captivating intricacies. The observed spectrum has a strong correlation with the distinctive attributes of Nb_2C MXene, as evidenced by the measured binding energies of Nb 3d at 204.8 eV and Nb $3d_{5/2}$ at 205.71 eV. Furthermore, the manifestation of oxidised niobium (Nb) can be observed at the energy

level of Nb $3d_{5/2}$, which is measured to be 209.72 electron volts (eV)[325], [327]. The observation highlights the many capabilities of MXenes, as they possess multiple chemical states of Nb that coexist and contribute to their varied features. **Figure *27 (c)*** highlights the Sn 3d area, where careful observation reveals peaks at 496.3 eV and 493.5 eV. These peaks can be attributed to the binding energies of Sn $3d_{3/2}$ oxide and metallic Sn, respectively, as stated in reference [329]. In the Sn $3d_{5/2}$ area, a parallel narrative emerges, characterised by the presence of peaks at 485.19 eV and 487.65 eV. These peaks correspond to the binding energies observed in $Sn3d_{5/2}$ oxide and metallic Sn, as documented in reference [327]. It is worth noting that the level of oxidation in tin (Sn) in its oxidised state is significantly higher than that in its metallic state, indicating the occurrence of surface oxidation [329]. The result carries significant consequences regarding the chemical reactivity of the materials and their prospective applications. Finally, **Figure *27 (d)*** focuses specifically on the C 1s region, elucidating the intricacies of carbon bonding. The observed peaks at 284.89 eV and 288.72 eV provide insight into the binding energies associated with C-C and C=O bonds, respectively. The discovery highlights the existence of many carbon species on the surface of the material, providing insights into potential functional groups and interactions.

3.2.5 TEM

Transmission Electron Microscopy (TEM) provides a significant opportunity to investigate the nanoscale realm, enabling scientists to examine materials at both atomic and nanoscale dimensions.

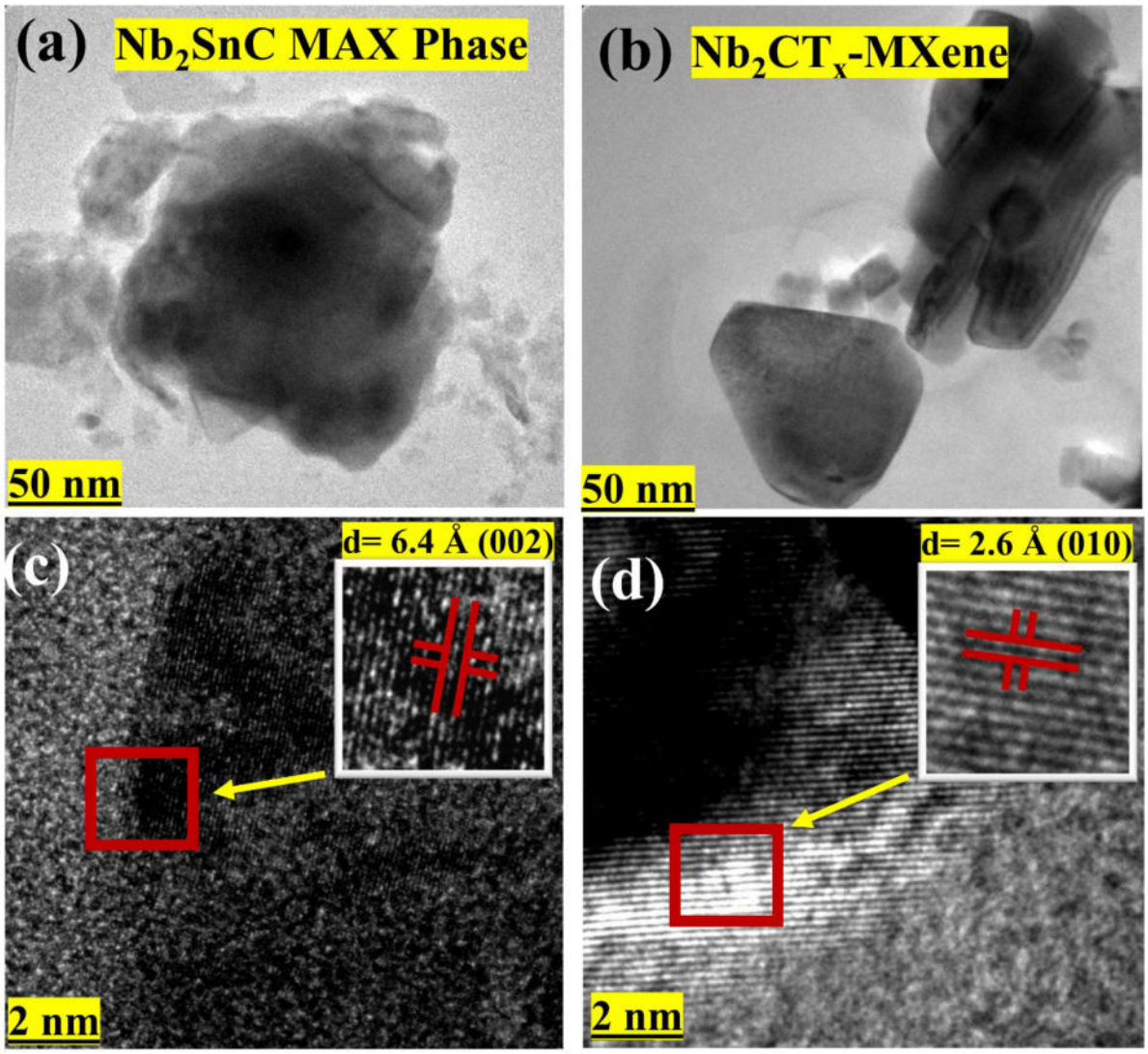

Figure 28: (a) & (b) TEM image of Nb_2SnC MAX Phase, (c) & (d) TEM image of Nb_2CT_x MXene

The transmission electron microscopy (TEM) study showcases **Figure *28 (a) and (b),*** which depict images of the Nb_2SnC MAX phase captured at different resolutions. The presented TEM analysis exhibit the distinct layer structure that is typically observed in Nb_2SnC MAX compounds. The precision of transmission electron microscopy (TEM) serves to support the observations made through scanning electron microscopy (SEM) imaging, providing further evidence for the layered pattern observed in the material. In addition, the determined d-spacing value of 6.4 Å, as depicted in **Figure *28 (b),*** corresponds to the (002) crystallographic plane, hence confirming the agreement between the X-ray diffraction (XRD) data and the Nb_2SnC MAX phase. In a similar vein, TEM pictures of Nb_2CT_x MXene at different resolutions are presented in **Figure *28 (c) and (d).*** The presented TEM analysis provides a visual

representation of the intrinsic two-dimensional layering found in Nb_2CT_x MXene. This can be observed in **Figure *28 (c)*** at a resolution of 50 nm. The structural attribute exhibits a flawless alignment with the observations obtained through scanning electron microscopy (SEM) imaging. It is worth mentioning that the determined d-spacing value of 2.6 Å, as illustrated in **Figure *28 (d),*** corresponds to the (010) crystallographic plane, which aligns with the X-ray diffraction (XRD) analysis conducted for Nb_2CT_x.

3.2.6 FTIR Analysis

The Fourier Transform Infrared (FTIR) spectra provide significant insights into the chemical composition of both the synthesised Nb_2CT_x MXene and the pristine Nb_2SnC MAX phase as shown in **Figure *29***. Numerous discernible absorption bands have been found within these spectra, providing valuable insights on the nature of these materials. The samples exhibit common absorption bands at wavenumbers of 2357 cm^{-1} and 2295 cm^{-1}[330]. The bands are representative of the diverse chemical bonds that exist within the materials. The spectra provide evidence of the existence of carbons with triple bonds, which are represented by the distinctive peaks of C≡C, as well as the presence of bonds between niobium and carbon, Nb-C [181]. Furthermore, it is observed in the MXene spectrum that there is a prominent peak at 1643 cm^{-1}, which is associated with unsaturation[181]. This can be mostly attributable to the existence of carbon-carbon double bonds within the structure of MXene. The identification of C-H bonds is discernible through the observation of bands at a wavenumber of 2947 cm^{-1}, while the existence of C=O bonds is indicated by peaks at a wavenumber of 1643 cm^{-1}. Significantly, the spectrum of MXene exhibits noteworthy characteristics, such as the presence of C-O and O-H bands, indicating surface functionalization and the incorporation of novel functional groups[330]. In contrast, the absence of these bonds is a notable characteristic observed in the MAX phase spectrum, hence emphasising the efficacy of the etching process and the resultant modification of the MXene's surface chemistry. The FTIR results presented in this study provide evidence supporting the alteration of surface functional groups and chemical bonds within the MXene structure. These findings have important implications for the prospective uses of MXene, specifically in the fields of electrochemical sensing and catalysis.

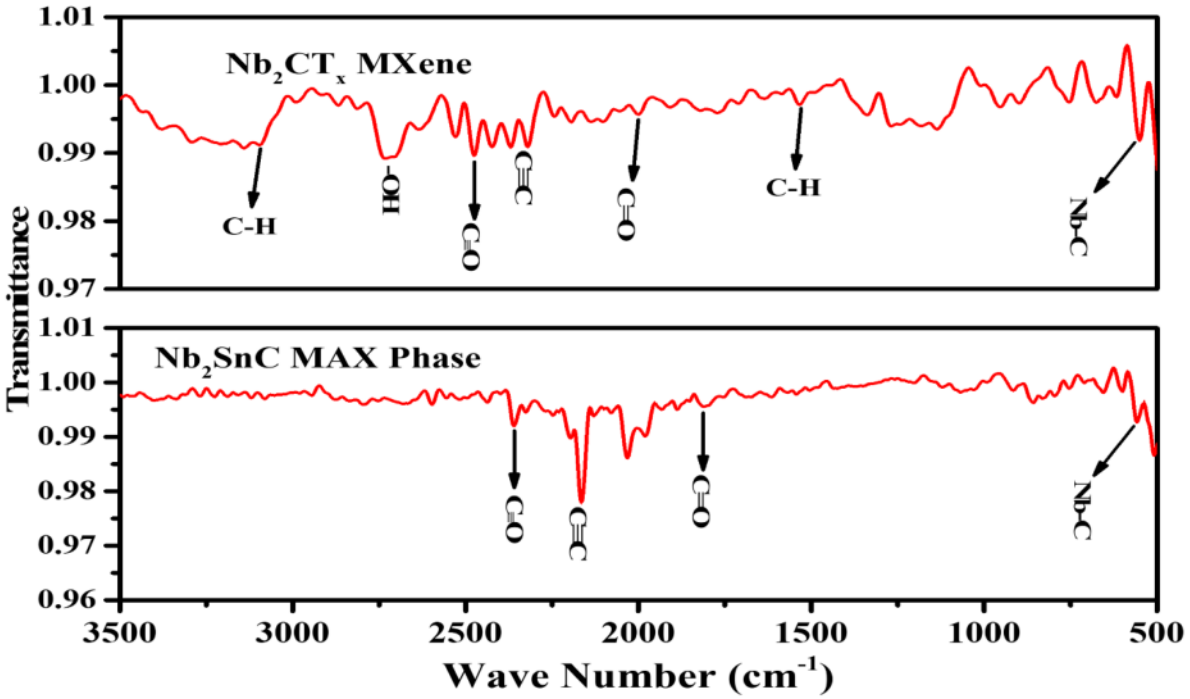

Figure 29: FTIR Spectra of Nb_2SnC MAX Phase and Nb_2CT_x MXene

3.3 Electrochemical Analysis of Synthesized Nb based MXene.

Electrochemical study serves as a primary methodology for assessing the supercapacitive characteristics of Nb_2CT_x MXene. The analysis was performed using a three-electrode configuration, in which the working electrode was nickel foam that had been modified by drop-casting the Nb_2CT_x MXene (**Figure *30***). In order to completely characterise the electrochemical performance, the following techniques were employed: cyclic voltammetry (CV), electrochemical impedance spectroscopy (EIS), and galvanostatic charge-discharge (GCD) tests were conducted within the established framework. Cyclic voltammetry (CV) is well recognised as a fundamental technique in the field of electrochemical investigation, namely in the study of the supercapacitive characteristics of materials such as MXenes[172], [220], [331], [332].-The importance of this technique encompasses the interpretation of several mechanisms including pseudocapacitance, ion diffusion, and charge transfer kinetics. These mechanisms play a crucial role in the development of high-performance supercapacitors and in comprehending the role of MXenes in enhancing energy storage[333]. In order to provide a more comprehensive understanding of the electrochemical performance, cyclic voltammetry (CV) tests were conducted throughout a spectrum of scan rates, spanning from 10 mVs^{-1} to 1000 mVs^{-1}. Significantly, the cyclic voltammetry (CV) curves exhibited a consistent

rectangular shape even under high scan rates, indicating exceptional capacitance and rapid ion response. The analysis of these curves yielded a particular capacitance value of 260.38 Fg^{-1} when the voltage scan rate was set at 10 mVs^{-1}. Significantly, the observed capacitance demonstrated strong retention, as the electrode maintained 45.53% of its original capacitance at a voltage scan rate of 1000 mVs^{-1}. The notable ability of this high rate can be ascribed to the remarkable ion conductivity of the electrolyte, making the Nb_2CT_x MXene appropriate for real-world implementations, exhibiting exceptional charge storage kinetics, little transfer resistance, and reduced diffusion lengths[220].

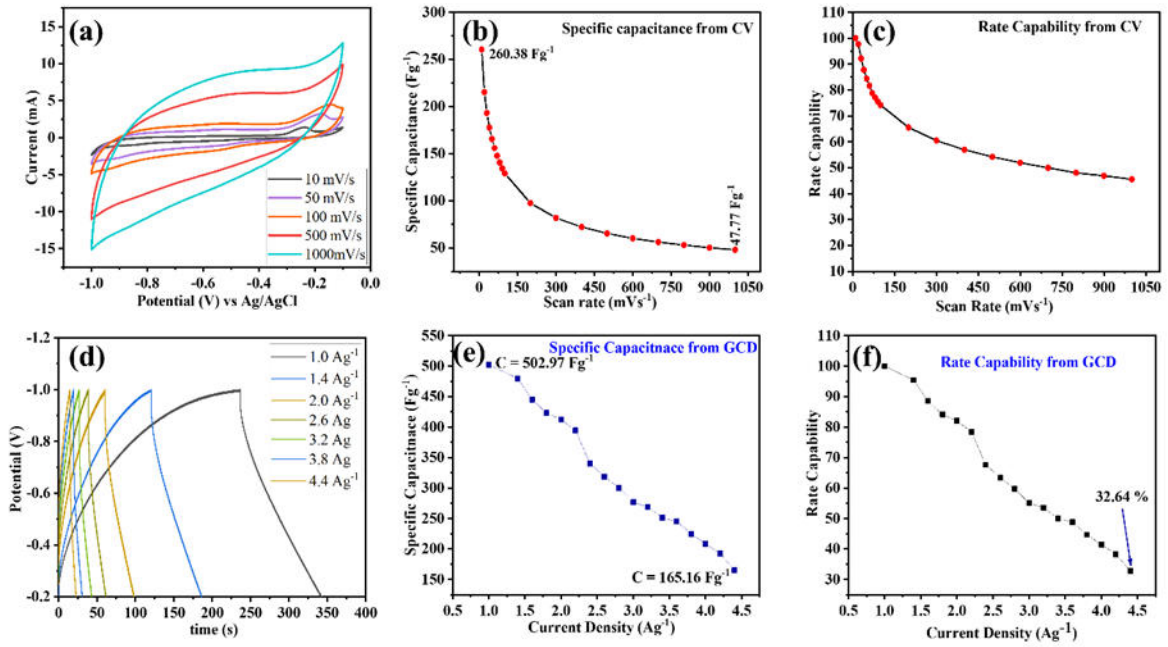

Figure 30:(a) CV for Nb_2CT_x at various scan rate, (b) Specific capacitance vs scan rate, (c) Rate capability calculated from CV, (d) GCD plot for Nb_2CT_x, (e) Specific capacitance vs current density and (f) Rate capability calculated from GCD.

The utilisation of the galvanostatic charge-discharge (GCD) technology played a crucial role in evaluating the cell's charging and discharging capacities. The Nb_2CT_x MXene exhibited a symmetrical triangular pattern in its galvanostatic charge-discharge (GCD) curves under different current densities, which is characteristic of the behaviour observed in electric double-layer capacitors (EDLCs). The determination of specific capacitance values using GCD curves resulted in a specific capacitance of 502.97 Fg^{-1} at a current density of 1.0 Ag^{-1}, which then fell to 165 Fg^{-1} at 4.4 Ag^{-1}. Significantly, the Nb_2CT_x nanocomposite exhibited a retention of

32.64% of its initial specific capacitance when subjected to an increase in current density from 1.0 Ag^{-1} to 4.4 Ag^{-1}, hence demonstrating a strong rate capacity[215], [333].

Electrochemical Impedance Spectroscopy (EIS) has gained prominence as a valuable diagnostic technique for comprehending the complexities associated with supercapacitors and evaluating the electrochemical efficacy of materials, including MXenes. The field of electrochemical impedance spectroscopy (EIS) provides a full understanding of the intricate interactions among different resistive and capacitive components present in electrochemical systems[223]. Electrochemical impedance spectroscopy (EIS) offers valuable insights into various aspects of supercapacitor behaviour, including charge transfer kinetics, ion diffusion, and the intrinsic resistance of electrodes. This is achieved by examining a broad variety of frequencies during the probing process. These parameters play a vital role in determining the overall performance of supercapacitors. Electrochemical Impedance Spectroscopy (EIS) is a valuable technique used in the study of MXene-based supercapacitors, as it provides insights into the fundamental electrochemical processes that contribute to the improved energy storage and rate capabilities of these devices. Electrochemical impedance spectroscopy (EIS) plays a crucial role in the customization of MXenes and electrode configurations to attain enhanced supercapacitive capabilities. Consequently, this facilitates the utilisation of MXenes in sophisticated energy storage devices[334].

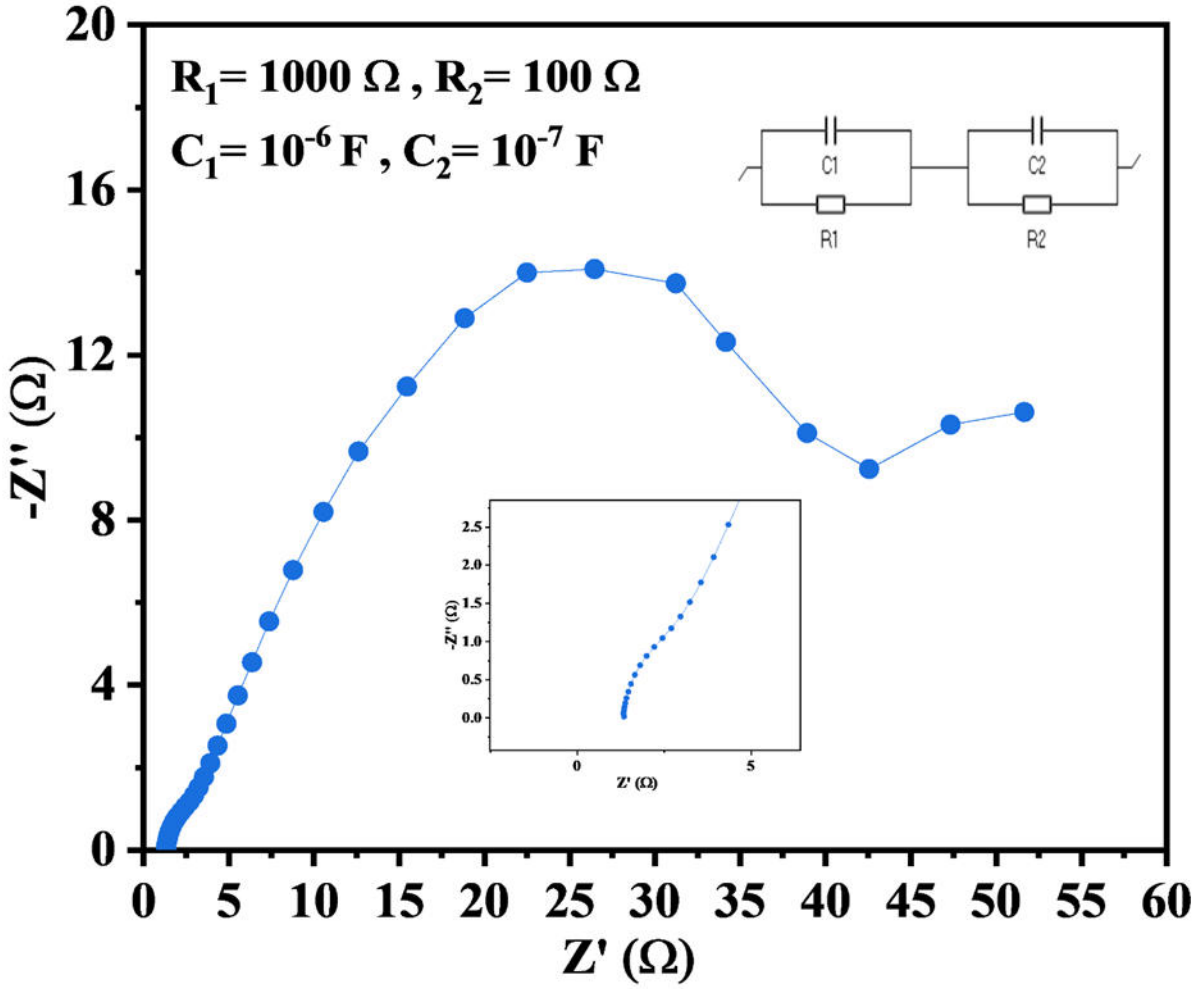

Figure 31: EIS Spectra of Nb_2CT_x MXene

The utilisation of electrochemical impedance spectroscopy (EIS) throughout a broad frequency range spanning from 100 millihertz to 100 kilohertz has revealed a notable reduction in electrode resistance. This finding provides more evidence supporting the enhanced electrochemical kinetics exhibited by Nb_2CT_x. The EIS spectra (**Figure *31***) were supported by the accompanying equivalent circuit, which demonstrated an equivalent series resistance of 1.37 Ω. In the medium-frequency region, the electrochemical impedance spectroscopy (EIS) demonstrated a linear response, which is indicative of both conventional capacitive behaviour and electric double-layer capacitor (EDLC) behaviour[223]. The enhanced electronic conductivity and charge-transfer kinetics of Nb_2CT_x resulted in a decrease in charge transfer resistance, hence accelerating electrochemical reactions[335].

In conclusion, the remarkable supercapacitive properties exhibited by 2D Nb_2CT_x MXene can be ascribed to multiple contributing reasons. The topology of the material has a sheet-like structure with several layers, as evidenced by scanning electron microscopy (SEM) pictures.

This unique structure offers a significant surface area and promotes efficient conductivity, hence enhancing the passage and absorption of ions onto the electrode surface. Furthermore, the electrocatalytic capabilities, ion transfer, and electrical conductivity are enhanced by the presence of surface functional groups, such as -O, as proven using EDS analysis after etching with phosphoric acid (H_3PO_4). This improvement in the electrochemical process is observed. The interlayer gap of Nb_2CT_x enables efficient ion diffusion, similar to the behaviour observed in electric double-layer capacitors (EDLCs), and also enhances the accessibility of active sites. The synthesised Nb_2CT_x MXene demonstrates its potential as a high-performance supercapacitor through a comparative examination with other MXenes commonly employed in supercapacitor applications.

3.4 Chapter Conclusion

In the present chapter, we have initiated an exploration into the domain of MXene synthesis, which signifies a crucial advancement in unlocking the revolutionary capabilities of these materials with two-dimensional structures. The technique of synthesising MXenes is a complex procedure that leverages the underlying principles of MAX phases, combining metallic and ceramic characteristics in novel manners. The scope of our investigation encompassed the transformative process of etching, with particular attention directed towards two important methodologies: standard acid etching and the pioneering technique of molten salt etching. Every technique possesses unique characteristics, and our study sought to reveal their intricacies, advantages, and possible uses. The synthesis of the Nb_2SnC MAX phase entails a series of precise steps, including mechanical blending and milling, pellet creation and compression, heat treatment under controlled conditions, and post-synthesis powderization and storage. The proficient implementation of these procedures is of utmost importance in attaining a versatile substance with substantial potential in diverse scientific and technical domains. The technique of etching MXene plays a crucial role in the synthesis of MXene. An alternate methodology has been investigated, which avoids the utilisation of hydrofluoric acid (HF), a technique that is associated with numerous difficulties and risks. In this study, a novel methodology was implemented, which entailed the utilisation of phosphoric acid. The approach enabled the progressive conversion of MAX phase material into the desired Nb_2CT_x MXene compound, representing a noteworthy advancement in the synthesis of MXene.

In addition, our investigation encompassed the use of the drop-cast technique to modify electrodes with synthesised MXenes. Our focus was on producing precise and effective outcomes, specifically in terms of attaining uniform dispersion and consistent adhesion of etched Nb_2CT_x MXene onto the surfaces of the electrodes. The thorough methodology described here serves as the fundamental basis for the further investigation of the electrochemical potential of MXenes in the forthcoming sections of our study. In the next sections, we conducted an in-depth analysis of the structural and morphological properties of the synthesised Nb_2SnC MAX phase and Nb_2CT_x MXenes. This analysis was carried out using several techniques including Energy Dispersive Spectroscopy (EDS), X-ray Diffraction (XRD), Scanning Electron Microscopy (SEM), X-ray Photoelectron Spectroscopy (XPS), and Transmission Electron Microscopy (TEM). The characterizations offered valuable insights into the composition, structure, and surface chemistry of these materials, establishing the groundwork for their future use in electrochemical sensing and energy storage. The electrochemical investigation of the synthesised Nb-based MXene, namely Nb_2CT_x MXene, demonstrated notable supercapacitive characteristics. The utilisation of cyclic voltammetry (CV) demonstrated remarkable capacitance and prompt ion response, even when subjected to elevated scan rates, hence emphasising its efficacy in charge storage. The rate capacity of the material was further validated using galvanostatic charge-discharge (GCD) testing, which exhibited a notable preservation of specific capacitance across different current densities. The application of electrochemical impedance spectroscopy (EIS) revealed a decrease in electrode resistance, which suggests an improvement in electrochemical kinetics, electronic conductivity, and charge-transfer abilities. In summary, the exceptional supercapacitive performance of 2D Nb_2CT_x MXene can be attributed to its distinctive structure, surface functional groups, and interlayer gap, which collectively enhance its charge storage and rate capabilities. As we draw this chapter to a close, we have established the fundamental basis for comprehending the electrochemical potential of Nb_2CT_x MXene across diverse applications, with a specific focus on electrochemical sensing and energy storage disciplines. The investigation into the synthesis of MXene has established a foundation for forthcoming studies and advancements in this dynamic and revolutionary domain.

CHAPTER 4 : MOLTEN SALT SYNTHESIZED AG NP/$Nb_4C_3T_X$ MXENES FOR ELECTROCHEMICAL SENSING APPLICATIONS

The present chapter explores the novel synthesis of Ag NP/$Nb_4C_3T_x$ MXenes, which plays a pivotal role in the advancement of electrochemical sensors. The present study provides a comprehensive elucidation of the synthesis process, specifically focusing on the technique of molten salt etching. This approach is examined in detail, with particular emphasis on its distinctive properties. Following the synthesis process, the structural and morphological features of the synthesised MXenes are examined by the utilisation of several techniques, including X-ray diffraction (XRD), scanning electron microscopy (SEM), and energy-dispersive X-ray spectroscopy (EDS). These characterizations offer significant insights into the properties of the materials. The subsequent emphasis is placed on electrochemical analyses, specifically discussing the production and modification of Screen-Printed Electrodes (SPE). This discussion underscores the significance of adequately preparing the electrode surface. The chapter thoroughly examines the process of optimising MXene dispersion for electrode modification, which is a crucial factor in guaranteeing the effectiveness of sensors. This study presents the utilisation of electrochemical techniques for the precise detection of hydrogen peroxide and riboflavin, highlighting the extensive range of applications these materials have in sensing. The chapter finishes by providing a concise overview that effectively summarises the accomplishments made thus far and establishes a foundation for future investigations into the field of electrochemical sensing.

4.1: Synthesis of Ag NP/$Nb_4C_3T_x$ MXenes

4.1.1 Molten Salt etching

Considerable progress has been made in the synthesis of MXene materials which belong to the category of two-dimensional transition metal carbides and nitrides, employing several techniques[268]. Among these methods, molten salt etching is a significant technology that provides a precise and controlled approach to fabricating MXene materials[171]. The significance of molten salt etching in the domain of MXene synthesis should not be underestimated, since it effectively addresses the difficulties associated with conventional etching techniques, such as the utilisation of potent acids, and offers a variety of notable benefits such as scalable production, selective etching, decreased environmental effect, high purity, increased crystallinity, faster processing, and tunable characteristics, while simultaneously minimising any potential damage to MXene sheets. The capacity for processing diversity and the capability to finely adjust MXene properties render molten salt etching a highly promising option for a wide range of applications, including energy storage, innovative materials, and sensors. The utilisation of molten salt etching presents a distinctive and advantageous methodology for the conversion of MAX phase precursors into MXene materials. In contrast to traditional acid-based etching procedures, this technology demonstrates a decrease in toxicity and a lower environmental footprint. The characteristic is in perfect harmony with current environmentally conscious research methodologies, so establishing molten salt etching as a favoured method for the synthesis of MXenes with negligible ecological consequences[263]. The conversion process from MAX phase precursors to MXene materials is a highly intricate and carefully planned process, consisting of multiple sequential stages, each of which plays a crucial role in the overall objective of obtaining pure MXene[263]. The procedure commences with a solid-state reaction, wherein Nb_4AlC_3 and AgCl are combined and subjected to grinding for a specific period. The importance of this initial step resides in its function as the fundamental basis, where the precursor elements are combined to guarantee uniformity and preparedness for the future phases. Subsequently, the synthesis progresses to the heat treatment stage. The mixture consisting of Nb_4AlC_3, AgCl, NaCl, and KCl was subjected to the molten salt etching method. This process was carried out using a Nabertherm B180 tube furnace, which was fitted with a gassing station to ensure an inert environment of nitrogen (N_2) was maintained throughout the procedure. The materials were put onto quartz carriers and positioned meticulously in the central region of the heating tube before the heating process commenced. The molten salt etching procedure was carried out at a temperature of 700 °C for a time duration of 18 hours, employing a regulated heating rate of 5 °C min^{-1}. In order to maintain stable circumstances, the heating tube's ends were actively cooled by circulating water to preserve ambient temperature. The unlocking of the essence of

the MAX phase occurs during the thermal transformation, leading to the occurrence of the MAX-to-MXene transition[144]. The utilisation of a controlled environment consisting of nitrogen gas serves to enhance the overall integrity of this particular procedure. The significance of this phenomenon resides in the process of metamorphosis, wherein the complex atomic arrangement of the MAX phase undergoes a transformation, resulting in the formation of two-dimensional nanosheets known as MXene[336]. The succeeding washing procedures play crucial roles in the transformation process from MAX phase to MXene. The solubility test serves as an early investigation into the interaction between the MAX phase and ammonia, providing a basis for future decision-making. The solubility of AgCl in a 4M NH_3 solution is demonstrated, highlighting its notable characteristics[337]. This discovery has implications for the selection of the future processing method. Upon introduction of a combination consisting of Nb_4AlC_3, AgCl, NaCl, and KCl in predetermined proportions into a 4M NH_3 solution, a series of transformative processes ensue. The application of magnetic stirring at room temperature for a duration of 2-3 hours facilitates the preferential separation of the "A" elements from the MAX phase structure. The adjustment of pH is a determining element in this stage, as it guarantees the preservation of a neutral setting, so preventing any inadvertent secondary reactions that could potentially undermine the desired conclusion of MXene. The filtration stage exemplifies the meticulousness and discernment inherent in the synthesis process. At this stage, the MXene material undergoes a process of separation from the residual components, which represents a remarkable point where careful attention to detail is necessary to assure the purity of the final product. The final stage of the process is the drying step, during which the purified MXene material is carefully desiccated in a vacuum oven at a temperature of 60°C for a duration of 48 hours. The thorough drying procedure not only finalises the synthesis but also imparts the MXene material with its intrinsic characteristics, making it suitable for utilisation in diverse scientific and technological contexts.

Reaction Mechanism:

$Nb_4AlC_3 + AgCl \rightarrow NbCl_3 + 4AlCl + 4C$ …… 1

$3Al + 3Cl_2 \rightarrow 2AlCl_3(\uparrow)$ …… 2

$4NbCl_3 + 3C \rightarrow Nb_4C_3T_x + 9Cl_2$ …… 3

Reaction 1 signifies a crucial step within the synthesis procedure, wherein the targeted removal of aluminium (Al) from the Nb_4AlC_4 MAX phase takes place using a process known as selective etching. During this particular stage, the solid Nb_4AlC_4 MAX phase undergoes a

reaction with aluminium chloride ($AlCl_3$), which is produced as a byproduct, resulting in the creation of niobium trichloride ($NbCl_3$), aluminium chloride (AlCl), and carbon (C)[338]. In essence, the MAX phase structure undergoes a process wherein aluminium is extracted and subsequently converted into aluminium chloride, while the niobium and carbon constituents stay intact. The compounds $NbCl_3$ and AlCl serve as crucial intermediates in the process, indicating the successful extraction of aluminium from the MAX phase. Reaction 2 elucidates the process by which aluminium (Al) undergoes a chemical transformation, resulting in the formation of aluminium chloride ($AlCl_3$). In this experimental setup, the element aluminium engages in a chemical reaction with chlorine gas (Cl_2) resulting in the formation of aluminium chloride. The process of converting aluminium from the MAX phase through selective etching relies on the crucial role of $AlCl_3$, which acts as a critical component in facilitating the extraction of aluminium while preserving the structural integrity of niobium carbide. Reaction 3 is indicative of the emergence of niobium carbide (Nb_4C_3) MAX phase as a result of the residual components generated during the etching procedure. During this particular stage, the compound niobium trichloride ($NbCl_3$) that is formed as a result of the etching process undergoes a reaction with carbon (C). This reaction leads to the production of niobium carbide as well as the release of chlorine gas (Cl_2). The reaction leads to the conversion of the extracted niobium (derived from the MAX phase) into niobium carbide, a distinct MAX phase material characterised by a dissimilar composition and crystal structure. The Nb_4AlC_3 MAX phase is frequently employed as a precursor in the synthesis of MXenes, such as $Nb_4C_3T_x$, whereby the variable T denotes surface functional groups or terminations. Fundamentally, every stage in this process of synthesis holds significant importance, as it contributes to the total achievement and accuracy of the molten salt etching approach within the domain of MXene synthesis. From the process of blending to the thermal transformation, and from conducting solubility tests to making pH adjustments, each action serves as evidence of the careful nature of materials science. These actions highlight the intricate equilibrium between precision and innovation that characterises this discipline.

4.2 Structural and morphological characterizations of Synthesized MXenes

4.2.1: XRD

The utilisation of X-ray diffraction (XRD) analysis was important in comprehending the structural changes that occurred during the synthesis process of $Nb_4C_3T_x$ MXene from the initial Nb_4AlC_3 material. **Figure *32*** depicts the X-ray diffraction (XRD) patterns of three distinct samples: the initial pristine Nb_4AlC_3, metallic Silver (Ag), and the resulting $Nb_4C_3T_x$ MXene after undergoing a washing process with 4M NH_3. The X-ray diffraction (XRD) pattern of the finished product demonstrates a notable alteration when compared to the unaltered Nb_4AlC_3. The observation of the significant reduction in the number of diffraction peaks formerly ascribed to Nb_4AlC_3 in the X-ray diffraction (XRD) pattern is a critical finding. The disappearance of these peaks serves as an indication of the significant structural modifications that have taken place during the synthesis procedure, leading to the effective transformation of Nb_4AlC_3 into $Nb_4C_3T_x$ MXene. Specifically, the observed disappearance of these peaks suggests the elimination of the aluminium (Al) layers inside the Nb_4AlC_3 compound. The interstitial spaces between the layers of niobium carbide (Nb_4C_3) are occupied by aluminium atoms in the Nb_4AlC_3 structure. During the synthesis procedure and subsequent treatment with a 4M NH_3 solution, the aluminium atoms undergo selective etching. The process of elimination results in the formation of vacancies within the structure, which correspond to the locations formerly occupied by aluminium atoms, so generating gaps. The presence of these gaps can be observed in the X-ray diffraction (XRD) pattern as peaks corresponding to the (00l) crystallographic planes. The presence of well-defined (00l) peaks observed in the X-ray diffraction (XRD) pattern serves as a definitive indication of the emergence of a novel crystalline structure in the $Nb_4C_3T_x$ MXene material. The observed (00l) peaks can be attributed to the systematic arrangement of the residual niobium carbide layers, which are interspersed with the regions previously occupied by aluminium. The presence of (00l) peaks in the data indicates the existence of an organised arrangement, which in turn suggests a consistent distance between the layers. The present study showcases the effective exfoliation process of Nb_4AlC_3, resulting in the synthesis of $Nb_4C_3T_x$ MXene. Consequently, a novel two-dimensional layered structure is generated, exhibiting unique structural and electrical characteristics in comparison to its predecessor material. The transition under consideration plays an important role in revealing the distinctive characteristics and potential uses linked to MXenes, so making this structural transformation a prominent subject of investigation in X-ray diffraction (XRD) study.[339]. The observed modifications in the diffraction pattern provide clear evidence of the effective conversion of Nb_4AlC_3 into the layered Nb_4C_3 (MXene)

structure[340]. A notable observation pertains to the displacement of the Nb_4C_3 (004) diffraction peaks, which transition from an angle of 7.41° to 6.23° in two theta degrees. The observed shift indicates a significant increase in the distance between layers, specifically from 8.8 Å to 10.9 Å, which corresponds to the typical interlayer spacing of MXenes. It is worth mentioning that the distinct and high-intensity peaks observed at around 2θ = 43.29°, 50.43°, and 74.13° can be reliably identified as metallic silver (Ag). The discovery provides support for the hypothesised etching method that involves a Lewis acid melt, as described in Equation 1.

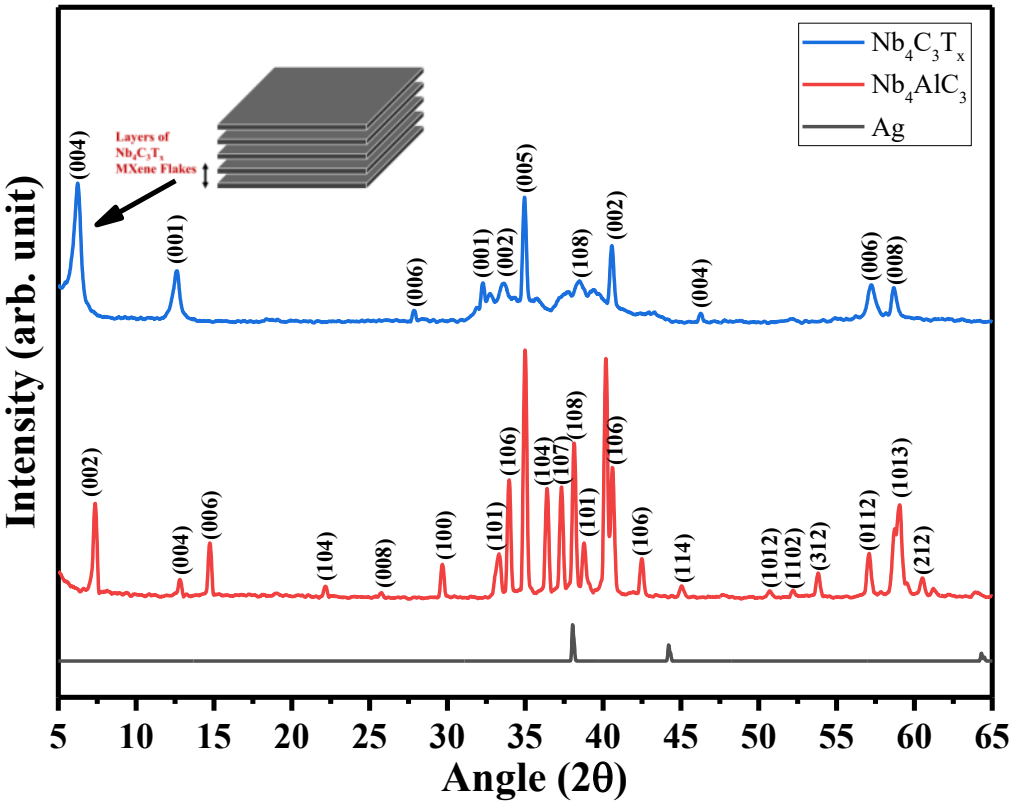

Figure 32: XRD analysis of Ag (metallic), Nb_4AlC_3 precursor and$Nb_4C_3T_x$ MXene

The XRD pattern of the finished product exhibits only the (00l) MXene peaks, which serves as definitive proof of the effective elimination of Ag during the synthesis procedure. The present study employs a detailed (XRD investigation to confirm the successful creation of $Nb_4C_3T_x$ MXene and elucidate the structural alterations that take place during the synthesis process.

4.2.2 SEM and EDS

The utilisation of SEM (Scanning Electron Microscopy) analysis is of utmost importance in comprehending the structural morphology that take place during the synthesis of Ag NP/$Nb_4C_3T_x$ MXene from the Nb_4AlC_3 MAX phase via the process of molten salt etching as shown in **Figure 33**. The utilisation of this analytical technique yields significant insights into the morphological attributes of materials at the micro and nanoscale. During the preliminary phase, we conducted an examination of the SEM images pertaining to the precursor of the Nb_4AlC_3 MAX phase. The laminated, hexagonal crystal structure is a well-documented characteristic of MAX phases[341]. SEM images provide evidence of the existence of many layers arranged in a stacked configuration within the MAX phase material, hence suggesting its voluminous characteristic. The MAX phase demonstrates a clearly defined three-dimensional structure characterised by discernible grain boundaries[341]. In contrast, a notable structural alteration becomes apparent when directing our attention onto the Ag NP/ $Nb_4C_3T_x$ MXene. The scanning electron microscopy (SEM) images of the MXene material exhibit a noticeable deviation from the macroscopic characteristics of the bulk MAX phase. In contrast, the structure is disclosed as a multi-layered, two-dimensional arrangement. The observed substantial alteration in morphology can be ascribed to the effective exfoliation and delamination of the MAX phase that occurs during the molten salt etching procedure. The observation of distinct layers inside the MXene structure serves as a definitive confirmation of the effective fabrication of two-dimensional MXene nanosheets[342]. The presence of distinct layers is a defining characteristic of MXenes, which are composed of transition metal carbides/nitrides that are intercalated with surface functional groups, including hydroxyl (-OH) and oxygen (-O) species[343]. In summary, the utilisation of SEM analysis proves to be a valuable instrument in comprehending the structural transformation from the bulk MAX phase to the two-dimensional Ag NP/ $Nb_4C_3T_x$ MXene nanosheets. The conversion highlights the importance of the molten salt etching technique in the fabrication of MXene materials possessing distinctive characteristics. The increased electrochemical performance of the manufactured sensor for the detection of hydrogen peroxide and riboflavin is based on the observation of the two-dimensional MXene structure using scanning electron microscopy (SEM)[344]. The two-dimensional (2D) structure of MXene materials, such as Ag NP/ $Nb_4C_3T_x$ MXene, is crucial for electrochemical sensing due to its high surface area, which provides an abundance of active sites for analyte interaction. This increases the probability of analyte molecules coming into contact with the sensor surface, enhancing sensitivity and

facilitating efficient electron transfer during electrochemical reactions[170]. MXene nanosheets typically have surface functional groups, such as hydroxyl (-OH) and oxygen (-O) species, which contribute to the surface's hydrophilicity and make it more amenable to chemical modifications[170]. Researchers can tailor the surface chemistry by introducing specific functional groups or molecules, further enhancing the selectivity of the sensor for a particular analyte[345]. The 2D structure allows for rapid mass transport of analyte molecules to the electrode surface, reducing diffusion limitations and ensuring quick response times in electrochemical measurements. This attribute is crucial for real-time monitoring and accurate detection[346]. The 2D geometry and excellent electronic conductivity of MXene materials promote efficient electron transfer kinetics at the electrode interface, resulting in sharper, well-defined electrochemical signals in techniques like cyclic voltammetry and differential pulse voltammetry[174]. MXenes are known for their chemical stability in various environments, including aqueous solutions with varying pH levels, making them suitable for long-term or continuous monitoring applications. Reduced fouling is another advantage of the 2D MXene structure, as the highly accessible and active surface area mitigates fouling effects, allowing for more reliable and accurate sensing[347].

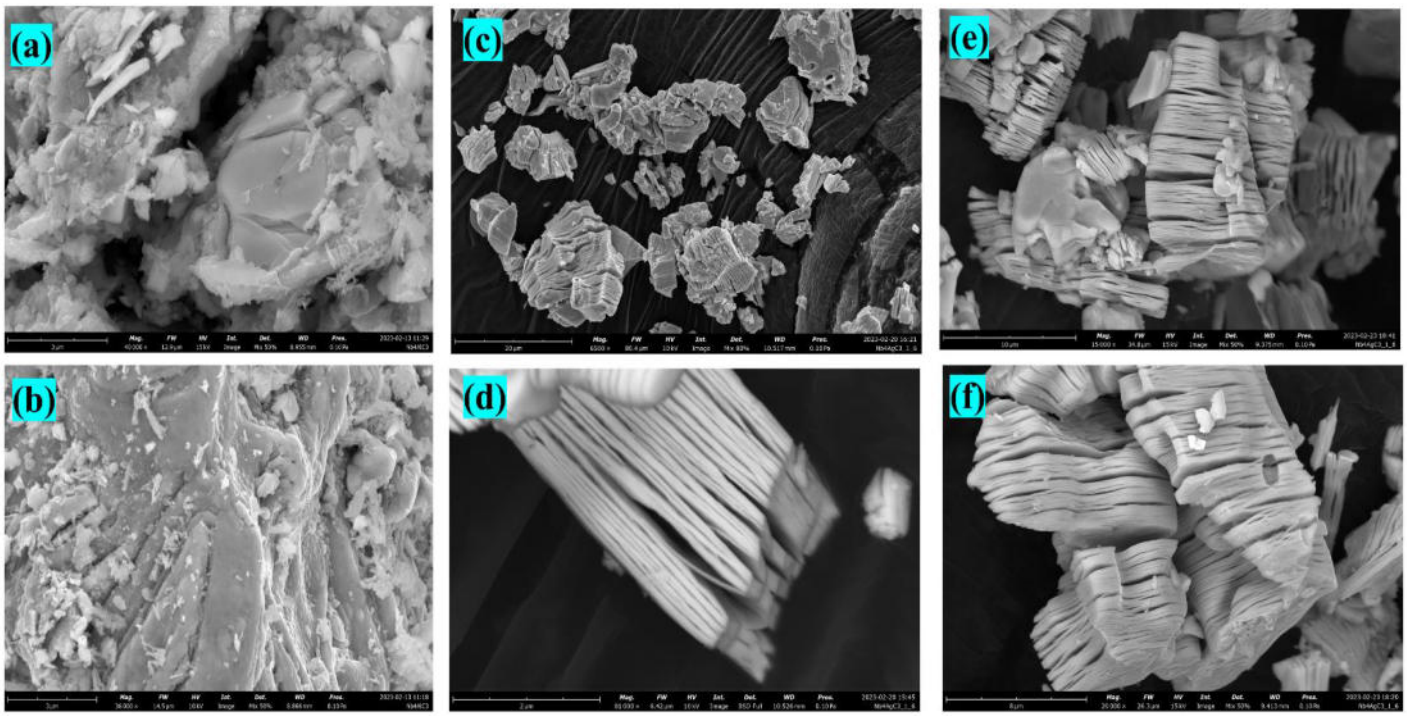

Figure 33: Fig: (a) & (b) SEM images of Nb_4AlC_3 MAX phase and (c), (d), (e) & (f) Ag NP/$Nb_4C_3T_x$ MXene

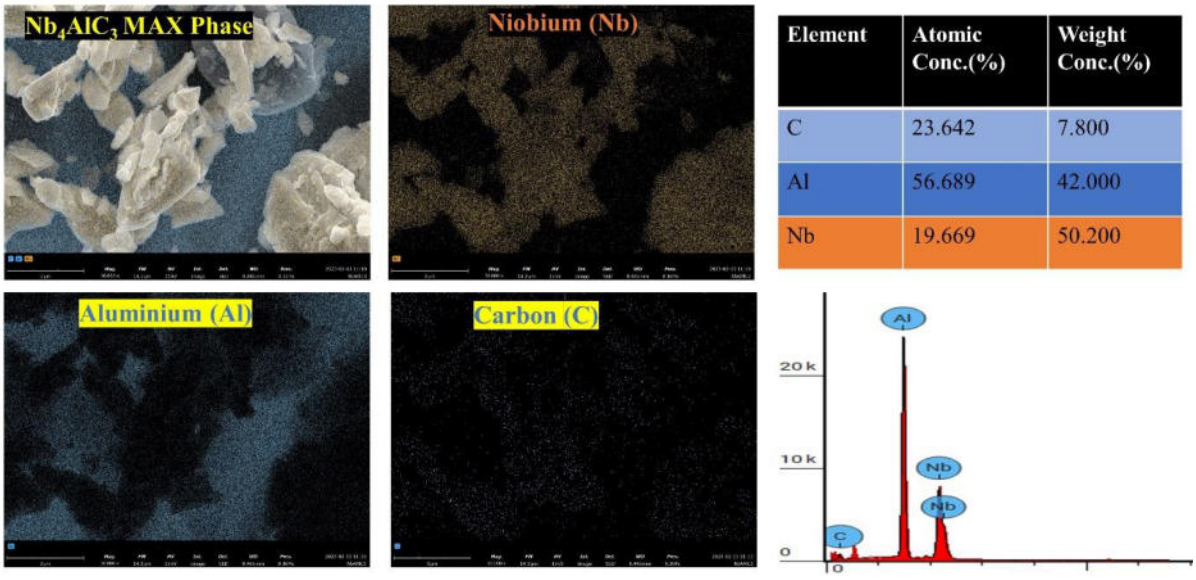

Element	Atomic Conc.(%)	Weight Conc.(%)
C	23.642	7.800
Al	56.689	42.000
Nb	19.669	50.200

Figure 34: EDS analysis of Nb_4AlC_3 MAX Phase Precursor

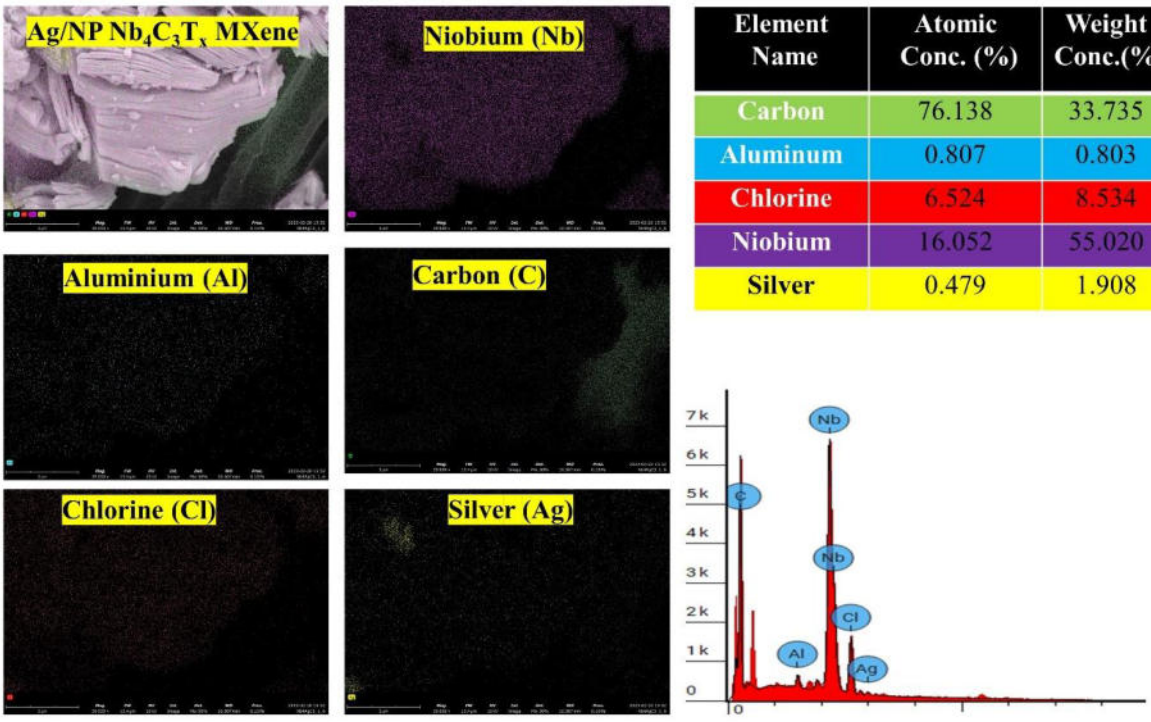

Element Name	Atomic Conc. (%)	Weight Conc.(%)
Carbon	76.138	33.735
Aluminum	0.807	0.803
Chlorine	6.524	8.534
Niobium	16.052	55.020
Silver	0.479	1.908

Figure 35: EDS analysis of Ag NP/$Nb_4C_3T_x$ MXene

The utilisation of Energy-Dispersive X-ray Spectroscopy (EDS) analysis was implemented in order to examine the elemental composition of both the Nb_4AlC_3 MAX phase precursor material and the Ag NP/$Nb_4C_3T_x$ MXene material that was generated from it which has been shown in **Figure *34* &** **Figure *35***. The primary emphasis of this investigation was the examination of alterations in the elemental composition that arise as a consequence of the etching procedure. Prior to the commencement of the etching technique, the Nb_4AlC_3 MAX phase displayed flakes of approximately 5 μm in size. The energy-dispersive X-ray spectroscopy (EDS) examination conducted on the bulk Nb_4AlC_3 material exhibited a notable reduction in the concentration of aluminium (Al) subsequent to the etching process. The concentrations of aluminium (Al) experienced a substantial reduction, declining from 56.68% to an almost negligible 0.40% in terms of atomic concentration, and from 42% to a paltry 0.6% in terms of weight concentration. In marked contrast, there was a significant change in the atomic and weight concentrations of niobium (Nb), with a decrease from 19.66% to 6.5% and 50.20% to 33.50%, respectively. Within the precursor of the MAX phase (Nb_4AlC_3), niobium (Nb) is enclosed within a layered configuration including niobium, aluminium, and carbon layers. In the synthesis of MXene, the procedure entails the targeted removal of the 'A' constituents, namely the aluminium and carbon layers, by a method known as selective etching. The etching technique effectively eliminates the aluminium (Al) and carbon (C) layers, while selectively preserving the niobium (Nb) layers, hence facilitating the creation of MXene. Consequently, the atomic and weight concentrations of niobium exhibit an augmented proportion relative to the residual substance. The observed decrease in atomic and weight percentages of Nb can be attributed to the removal of the original Al and C components. The Nb_4AlC_3 compound exhibits a disparity in the atomic masses of its constituent elements, with the aluminium and carbon layers being comparatively lighter than niobium. The elimination of these light elements leads to an augmentation in the weight percentage of niobium in the resultant MXene product. This phenomenon can be attributed to the observed reduction in the weight % of Nb in the MAX phase, and by a corresponding increase in the weight percentage

of Nb in the MXene. In brief, the observed reduction in atomic and weight concentrations of niobium in the MAX phase, as well as their corresponding increase in the MXene product, can be attributed to the preferential elimination of lighter aluminium and carbon layers during the synthesis of MXene. This process effectively enhances the niobium content in the resultant material. The significant rise in both the atomic and weight concentrations of carbon (C) was particularly intriguing. The atomic concentration of carbon (C) had a substantial increase, rising from 23.64% to a prevailing 78.214%. Similarly, the weight concentration also demonstrated a significant growth, escalating from 7.8% to a noteworthy 51.60%. The increase in carbon content can be ascribed to many processes, such as the elimination of aluminium (Al) and the consequent exposure of MXene layers that are rich in carbon during the etching process. Nevertheless, it is crucial to recognise that the residual aluminium signals observed in the EDS analysis can have several sources, which may include surface terminations, defects, or alterations in the structure of the MXene framework[229]. The observed deviation implies an abundance of carbon relative to the anticipated stoichiometric proportion of 3C:4Nb in $Nb_4C_3T_x$. The observed anomaly suggests the potential existence of surface terminations, flaws, or structural alterations inside the MXene framework. These factors significantly influence the composition and properties of $Nb_4C_3T_x$. The utilisation of Energy Dispersive Spectroscopy (EDS) analysis offers significant contributions in understanding the structural and compositional alterations that take place throughout the creation process of MXene materials[348].

4.2 Electrochemical Analysis with A NP/$Nb_4C_3T_x$ modified MXene SPE

4.2.1: Fabrication and Modification Screen-Printed Electrode: A Layer of MXene Brilliance

Screen-printing is a well-established technological process utilised for the production of many gadgets across diverse industries, including electronics, solar cells, and graphic arts. The screen-printing process has the capability to fabricate electrodes with thicknesses ranging from a few micrometres to 100 micrometres[349]. Consequently, the sensors produced using this method can be classified as thick-film electrodes. Different geometries can be readily achieved with straightforward modifications of the screen design. Additionally, supplementary printing stages can be employed to incorporate other elements, such as reference electrodes, counter electrodes, and dielectric layers. Carbon is an economically viable material that, when combined with screen-printing manufacturing techniques, can facilitate the cost-effective production of sensors in significant quantities. Consequently, these sensors can be seen as disposable, single-use devices. SPEs have electrochemical characteristics that are similar to those of costlier electrode materials, such as glassy carbon. However, SPEs possess the advantage of being disposable, eliminating the requirement for regeneration or pre-treatment prior to each measurement. Furthermore, this feature enables them utilisation by individuals with less training, since it does not require extensive knowledge of the intricate principles of electrochemistry and preparation. The process of screen printing technology involves the application of ink onto a substrate through a mesh, with certain areas being rendered impermeable to the ink by a stencil with a specific design. The process involves the utilisation of a squeegee to traverse the screen, effectively depositing ink into the exposed apertures of the webbing. Subsequently, a reverse stroke is executed, briefly bringing the screen into touch with the substrate. This phenomenon results in the transfer of ink onto the substrate, when the screen returns to its original position and the ink is drawn out of the mesh pores following the passage of the blade. **Figure *36*** presents a rudimentary representation of the screen-printing procedure. It showcases the motion of the squeegee, indicated in red, as it traverses the mesh region, distributing the paste, depicted in yellow, to produce the desired depiction in accordance with the predetermined pattern.

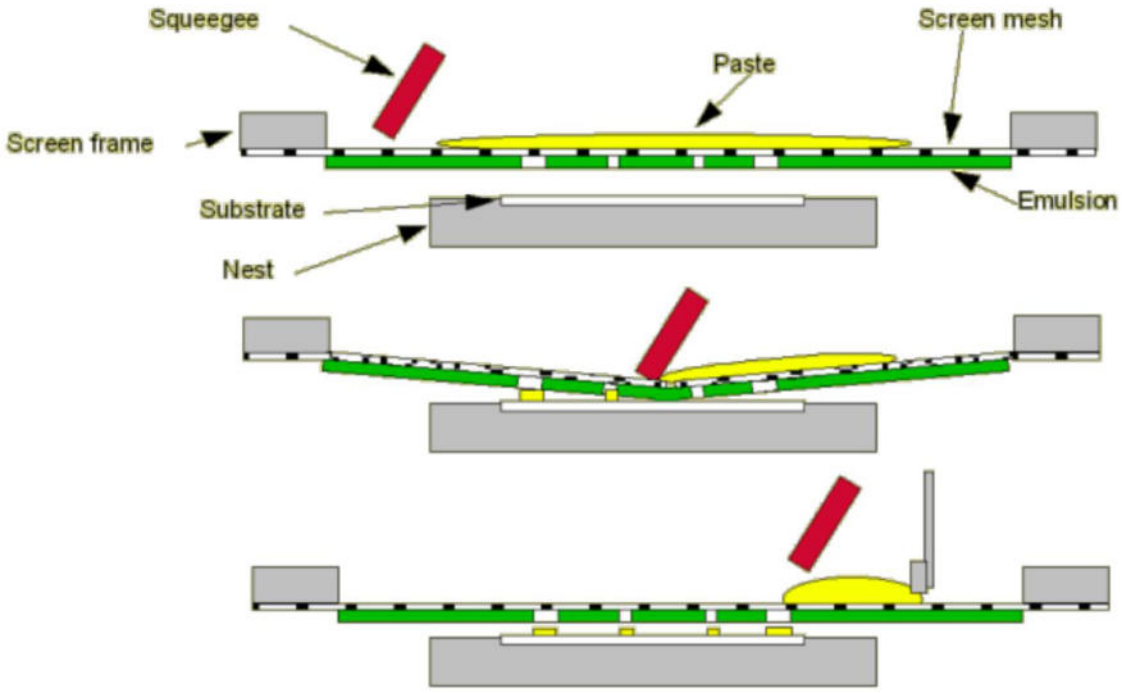

Figure 36: Basics of Screen Printing process

The fundamental rules governing all types of graphic reproduction remain consistent. In more straightforward language, graphic reproduction involves the application of ink or a similar viscous substance onto a film with a predetermined pattern and thickness. In the context of screen printing, this process involves exerting pressure to force ink to pass through a gauze or mesh onto a substrate positioned below. The necessary components for creating a screen print include: The screen consists of a frame that supports a stretched mesh. A photographic stencil depicting the designated design is affixed to the mesh. The squeegee consists of a holder that accommodates a flexible and robust blade. An ink or paste (hence referred to interchangeably as such) A stable foundation upon which the component to be printed can be securely placed. There exists an operator that can be utilised to amalgamate these five entities. Currently, there are three predominant materials that are commonly utilised: Nylon, Polyester, and Stainless Steel. A singular form of solution cannot adequately fulfil the requirements for all varieties of tasks and screen dimensions. The three different types of mesh are offered in a wide variety of weaves due to their versatility. Apart from their primary usage in printing, these meshes are also utilised for sieving, filtration, and strengthening purposes.

The screen template was created via the CorelDRAW Graphics Suite X8 design software, afterwards advancing its development on illustrative slides. In order to create the grids, the

polyester screen-printing mesh (SEFAR, 77/195-48) was first affixed to the aluminium screen printing frame (SEFAR) using the pneumatic tabletop stretching machine (G-STRETCH 202 A1, Grunig). The tension of the mesh was maintained at 28 N / cm, as measured by the fabric tension gauge TETKOMAT 7/50 (G-CHECK, Grunig). The crate was affixed with a two-component screen adhesive (KIWOBOND® & KIWODUR® 1100 Power Grip) to secure the mesh. Following the adhesive's drying process, the mesh underwent treatment with a degreasing liquid (KIWO® Mesh X-CEL). The water-based photosensitive emulsion, known as POLYCOR® S-HR, was manually applied onto the grid and afterwards placed in a drying chamber set at a temperature of 40 ºC using the COMBINETUVE ETABLI 608/1, TIFLEX apparatus. The grid was subsequently subjected to vacuum conditions and exposed to UV radiation using the COMBINETUVE ETABLI 608/1, TIFLEX equipment in the designated display room, utilising the corresponding design image transparency. Following exposure, the specimens underwent a thorough rinsing process using deionized water. This step aimed to eliminate any unpolymerized photosensitive material and facilitate the formation of the mould design. The specimens were considered ready for usage once they had been adequately dried. Appropriate grids were manufactured for the purpose of printing the active surface of the working electrode, encompassing the three aforementioned layers. The fabrication process involved the production of single layer graphite screen-printed electrodes (SPEs) with a working surface diameter of 3 mm. These electrodes were created by applying conductive carbon ink (LOCTITE, EDAG PF 407A) onto polyester sheets (Mac Dermid, Autostat CUS7) that were 175 μm thick. The screen-printing was carried out using a semi-automatic screen-printer (E2, EKRA) and a polyurethane squeegee with a durometer of 75. Following the printing process, the electrodes underwent a curing procedure in a standard oven at a temperature of 90 ◦C for a duration of 60 minutes. The screen that was artificially created for the purpose of this thesis is illustrated in **Figure *37* A**, while **Figure *37* B** provides a more detailed representation of the printing area. **Figure *37* C** displays the electrodes that were produced through the process of screen-printing.

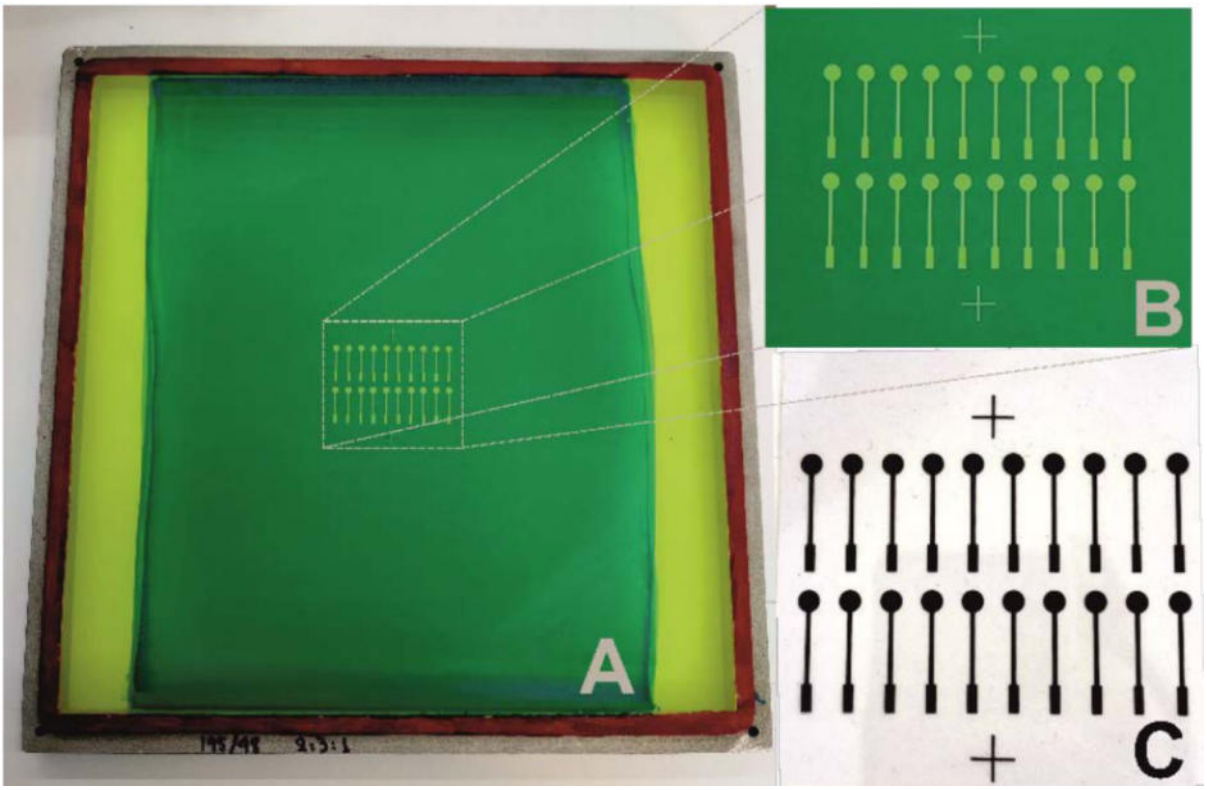

Figure 37: (A) Fabricated screen used in this work, (B) Close-up image of the electrode printing area, and (C) printed working electrodes used in this work.

In the field of electrode modification, specifically for screen printed carbon electrodes, an alternate method was utilised, thereby enhancing our repertoire of electrochemical techniques with comparable precision[350]. The integration of screen printing with $Nb_4C_3T_x$ MXene materials demonstrates a seamless combination of their versatile properties and electrochemical capabilities, hence offering the potential for outstanding performance. The commencement of the expedition involved the fabrication of functional electrodes through the utilisation of screen-printing technology. The electrode substrate was carefully coated with graphite ink, which served as the foundational material. The electrodes functioned as the medium on which our electrochemical masterpiece would be created. In order to include the electrochemical excellence of $Nb_4C_3T_x$ MXene into the working electrodes, a meticulously manufactured dispersion, which had been earlier fine-tuned to a concentration of 20 mg/ml in a mixture of deionized water and isopropanol, was utilised. The dispersion, which consists of $Nb_4C_3T_x$ MXene nanosheets, possesses the capability to enhance the performance of the electrode to unprecedented levels. The procedure of alteration was conducted with great attention to detail. The electrodes, which were prepared for potential modification, were covered with a substantial layer of the $Nb_4C_3T_x$ MXene dispersion. The constant and reliable electrochemical performance was contingent upon the uniform application of the dispersion.

After applying the coating, a controlled thermal treatment was conducted by exposing the modified electrodes to an oven maintained at a temperature of 60 degrees Celsius for a duration of one hour. The thermal treatment facilitated the adhesion of the $Nb_4C_3T_x$ MXene layer onto the electrode surface, resulting in its consolidation and improved electrochemical properties. The result of this rigorous procedure yielded a collection of carbon electrodes that were screen printed and embellished with a coating of $Nb_4C_3T_x$ MXene, showcasing its remarkable properties. The redesigned electrodes serve as a tangible representation of our unwavering dedication to accuracy and efficiency, positioned to revolutionise the limits of electrochemical sensing and analysis. In the subsequent chapters, we will explore a thorough assessment of the $Nb_4C_3T_x$ MXene-modified electrodes, revealing their noteworthy electrochemical prowess.

4.2.2 Optimization of Dispersion for electrode modification

The purity and stability of the MXene dispersion play a crucial role in determining the electrochemical performance of electrodes that have been treated with MXene. The art of optimising dispersion plays a crucial part in moulding the MXene's ability to lead charge transfer reactions effectively, akin to a master conductor in an electrochemical symphony[254]. The process of optimisation involves the careful consideration of solvent selection, concentration refinement, and polymer integration, all of which contribute significantly to the improvement of MXene's electrochemical performance. The process of optimising a solution begins with the careful selection of an appropriate solvent. A range of solvents, including Double Distilled Water (DDW) and Isopropanol, were examined, each possessing distinct characteristics. In order to identify the optimal solvent for achieving both uniform dispersion of MXene nanosheets and preservation of their stability during electrode modification, it is necessary to conduct a comprehensive investigation. Furthermore, the essential factor is in the concentration of MXene inside the dispersion. Concentrations ranging from 1 mg/ml to 80 mg/ml were systematically examined with great attention to detail, analogous to the process of tuning an orchestra to attain harmonious sound. Following a series of rigorous experiments, it was determined that a concentration of 20 mg/ml is the optimal point. This concentration achieves a harmonious combination of MXene loading and dispersion homogeneity, which in turn leads to enhanced electrochemical performance. The incorporation of polymers significantly enhances the amount of dispersion stability. Polyethyleneimine (PEI) and Nafion, well-known for their catalytic characteristics, were taken into consideration[351]. The

incorporation of 0.1% of each polymer into the DDW+Isopropanol dispersion yielded significant results. PEI demonstrated exceptional performance, resulting in improved dispersion stability and enhanced catalytic activity in electrochemical studies[352]. This passage confirms the significant contribution of PEI in improving the effectiveness of dispersion, and consequently, the electrochemical modification process. After careful evaluation of solvents, concentrations, and polymers, it was determined that the combination of DDW + Isopropanol, fortified with PEI, demonstrated unparalleled performance. The utilisation of optimised dispersion, in conjunction with MXene materials, functions as an exemplary conductor, facilitating improved sensitivity, selectivity, and stability in the realm of electrochemical sensing[353]. In essence, the road towards dispersion optimisation encapsulates the fundamental pursuit of precision within the field of materials research. MXene materials have the potential to significantly enhance electrochemical performance, hence revolutionising the fields of environmental monitoring, biomedical diagnostics, and other related areas[354]. This section serves as a demonstration of our dedication to achieving high standards, highlighting the exceptional performance of MXene-modified electrodes as pioneers in the field of electrochemical innovation.

4.3 Electrochemical techniques for Sensing of Hydrogen Peroxide

The identification and measurement of hydrogen peroxide (H_2O_2) holds significant significance within various scientific and industrial sectors. Hydrogen peroxide (H_2O_2), a relatively uncomplicated yet remarkably reactive compound, has extensive utility across a diverse range of applications owing to its formidable oxidative characteristics[355]. Hydrogen peroxide (H_2O_2) finds application in several industrial processes, including but not limited to paper and textile manufacture, electronics, and chemical synthesis. Its utility spans across functions such as bleaching, disinfection, and participation as a reactant in the synthesis of diverse chemicals[356]. In the field of healthcare, precise quantification of hydrogen peroxide (H_2O_2) plays a crucial role in the diagnosis of enzymatic problems, illnesses associated with oxidative stress, and many diseases[357]. For example, increased concentrations of hydrogen peroxide (H_2O_2) may serve as a potential indicator of underlying medical conditions such as infections, cancer, and neurological illnesses. The assessment of the oxidative condition of ecosystems and the detection of environmental toxins in environmental monitoring are

dependent on the detection of H_2O_2[358]. Furthermore, within burgeoning sectors such as clean energy, hydrogen peroxide (H_2O_2) is seen as a promising environmentally friendly fuel source and plays a crucial role in fuel cell utilisation. The use of hydrogen peroxide (H_2O_2) necessitates the implementation of accurate and dependable detection techniques in order to effectively exploit its advantages while maintaining safety and efficiency. Given the wide range of potential uses, there has been a significant focus on the study and development of sophisticated and highly responsive sensors for the detection of hydrogen peroxide (H_2O_2). This chapter delves into the development and comprehensive characterisation of an electrochemical sensor that utilises silver nanoparticle modified $Nb_4C_3T_x$ (MXene) for the purpose of detecting hydrogen peroxide with a high level of sensitivity and selectivity. The sensor showcased in this study not only showcases its potential for a wide range of practical applications, but also makes a noteworthy addition to the field of analytical chemistry and sensing technology.

- **Comparison of CV among plain SPE (Screen Printed Electrode) and Ag NP/$Nb_4C_3T_x$ Modified SPE**

Cyclic Voltammetry (CV) was utilised to evaluate the electrochemical behaviour of two different electrodes: a Screen-Printed Electrode (SPE) and a $Nb_4C_3T_x$ (MXene) electrode modified with Silver Nanoparticles (Ag NPs). The CV measurements were performed within a potential range of -1V to 0.3 V, covering both cathodic and anodic regions. Prior to reaching the current CV range, a series of preliminary experiments were conducted to investigate different potential ranges. These studies aimed to identify the optimal circumstances for the electrochemical study. The -1V to 0.3 V range was chosen among the examined ranges because to its ability to provide the most comprehensive understanding of the electrode's behaviour. The specified range effectively encompasses the redox reactions taking place at the electrode interface, enabling a thorough evaluation of electrochemical behaviour. The cyclic voltammetry (CV) curve derived from the unmodified Screen-Printed Electrode (SPE) exhibits a predominantly horizontal shape over the specified potential range, indicating limited electrochemical reactivity at the unadorned electrode interface[359]. Essentially, the unmodified SPE does not demonstrate any notable intrinsic redox activity within the designated voltage range, hence affirming the need for electrode modification in order to improve its electrochemical performance. The CV curve obtained (as shown in **Figure *38***) from the Ag

NP/ $Nb_4C_3T_x$ modified MXene electrode exhibits a notable and instructive electrochemical behaviour, which stands in sharp contrast to other observed phenomena. Significantly, the modified electrode has discernible redox peaks at around 0.16 V and -0.06 V. The observed peaks in the electrochemical processes on the electrode's surface can be attributed to the oxidation and reduction reactions involving the silver nanoparticles (Ag NPs) present in the modified electrode. The presence of an oxidation peak at approximately 0.16 V indicates the occurrence of the anodic process, which involves the conversion of Ag NPs into Ag^+ ions through oxidation. On the other hand, the observed reduction peak occurring at around -0.06 V indicates the occurrence of the cathodic process, in which Ag^+ ions undergo reduction to become metallic silver (Ag)[360].

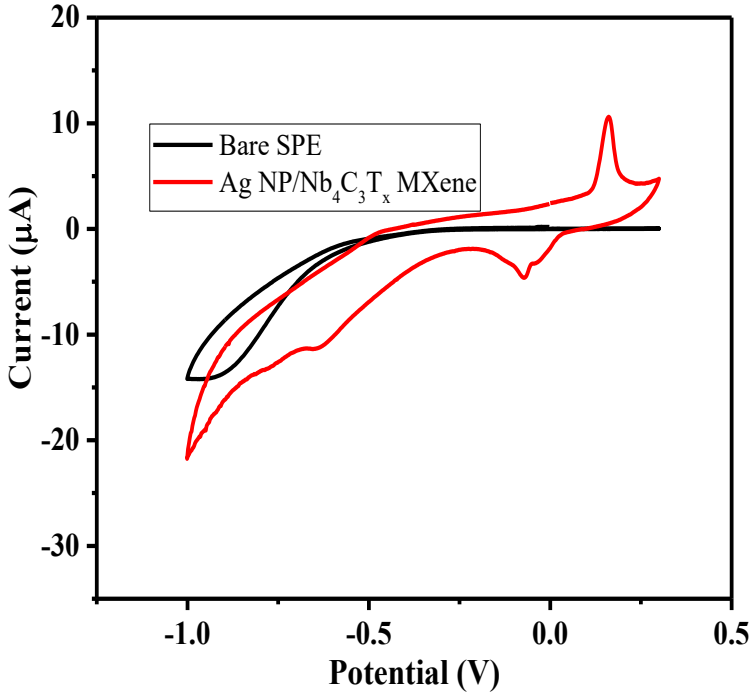

Figure 38: Cyclic Voltammetry of Plane SPE and Ag NP/$Nb_4C_3T_x$ MXene modified SPE

The observed electrochemical behaviour provides evidence for the reactivity of the silver nanoparticles and highlights the effective alteration of the electrode. Cyclic Voltammetry is a crucial analytical technique utilised extensively in the production of electrochemical sensors[361]. This approach facilitates the methodical investigation of several parameter ranges in order to determine the optimal circumstances for a given electrochemical application. The chosen potential range in this instance revealed the unique electrochemical behaviour of

the Ag NP/ $Nb_4C_3T_x$ modified MXene electrode. Through the process of revealing the redox behaviour of the electrode, cyclic voltammetry (CV) offers valuable insights into the functioning of the sensor. This analytical technique plays a crucial role in optimising the sensor's performance, particularly in the realm of selectively detecting hydrogen peroxide and other analytes that are of interest.

- **Electrochemical Detection of Hydrogen Peroxide Using Ag NP/$Nb_4C_3T_x$ Modified MXene: CV Analysis**

Cyclic Voltammetry (CV) is a crucial electrochemical technique utilised in our investigation to detect hydrogen peroxide (H_2O_2) by employing Ag NP/ $Nb_4C_3T_x$ modified MXene electrodes as shown in **Figure *39***. In this study, two consecutive cross-validation analyses were performed. In the first step, cyclic voltammetry (CV) was conducted on the Ag NP/ $Nb_4C_3T_x$ modified MXene electrode without the presence of hydrogen peroxide (H_2O_2). The CV experiment was conducted across a voltage range spanning from -1 V to 0.3 V. The cyclic voltammetry (CV) analysis revealed the presence of two distinct peaks at around 0.16 V and -0.06 V, which were notably conspicuous. The observed peaks are indicative of discrete oxidation and reduction reactions taking place at the electrode interface. The oxidation of silver nanoparticles (Ag NPs) is shown by the peak observed at 0.16 V, whereas the reduction of Ag NPs is represented by the peak observed at -0.06 V. Following this, in order to examine the electrochemical reaction to H_2O_2, a solution containing a concentration of 5 mM of H_2O_2 was injected into the electrolyte, and cyclic voltammetry (CV) was performed again. In the second CV, a notable characteristic was observed in the form of a decrease peak occurring at around 0.72 V, which suggests the occurrence of H_2O_2 reduction. The observed decrease peak at a potential of 0.72 V provides a distinct indication of the successful detection of hydrogen peroxide when using Ag NP/ $Nb_4C_3T_x$ modified MXene electrodes.

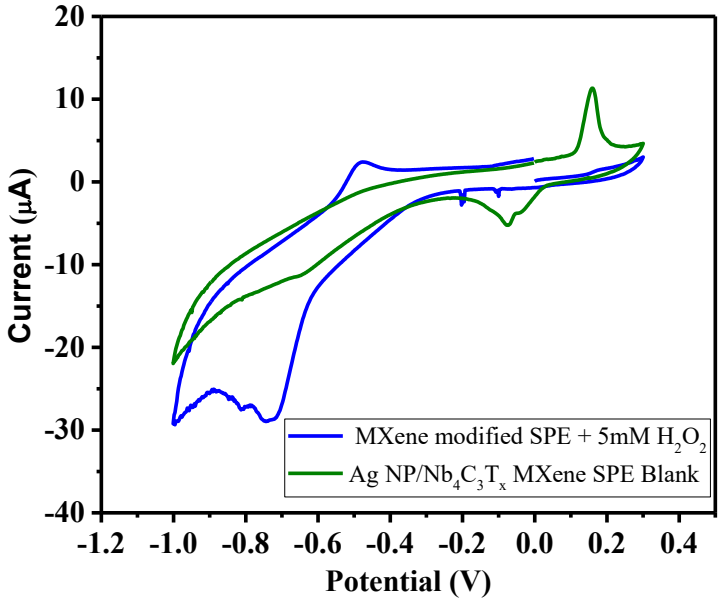

Figure 39: Cyclic Voltammetry (CV) Analysis of Ag NP/$Nb_4C_3T_x$ Modified MXene Electrode in the Presence of 5mM Hydrogen Peroxide(H_2O_2). The CV curve shows the reduction peak around 0.72 V attributed to the electrochemical detection of hydrogen peroxide.

It is important to acknowledge that the selection of this particular CV range was considered to be the most appropriate among several alternative ranges that were examined during the course of our study. Cyclic Voltammetry is a crucial technique employed during the early phases of electrochemical sensor fabrication. The analysis of cyclic voltammetry (CV) provides significant insights into the electrochemical behaviour of the changed electrode surface and offers crucial information regarding the redox processes that are involved in the operation of the sensor. The preliminary CV analysis plays a pivotal role in the advancement of a hydrogen peroxide sensor, as it aids in establishing the fundamental electrochemical reaction and acts as a basis for subsequent sensor enhancement.

The provided **Figure *40*** exhibits a set of four cyclic voltammetry (CV) curves, each demonstrating discernible electrochemical behaviours across the potential range spanning from -0.8V to 0 V. The chosen range is specifically intended to mitigate any potential interference caused by redox peaks related to silver nanoparticles (Ag NP). The CV presented in blue represents a basic screen-printed electrode (SPE). The presented curve has a continuous and

uniform shape devoid of discernible peaks, indicating the absence of inherent electrochemical reactivity or external disturbances. In the following curriculum vitae (CV), depicted in the colour red, the electrode has been subjected to modification using Ag NP/$Nb_4C_3T_x$. The modified Screen-Printed Electrode (SPE) method has a noteworthy characteristic of a consistently smooth and peak-free cyclic voltammogram (CV), which highlights the absence of undesirable interference from silver nanoparticles. This finding provides more evidence to support the durability and reliability of the electrode.

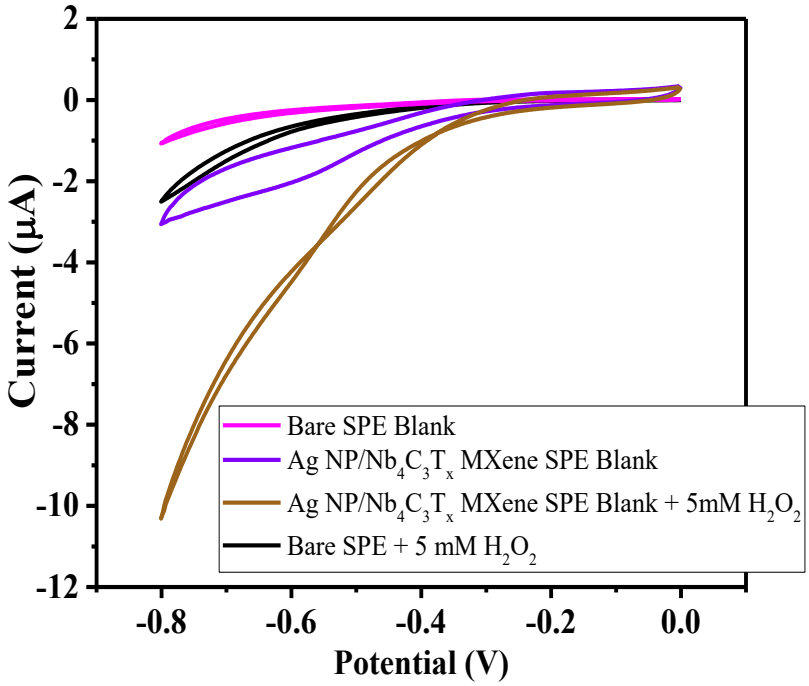

Figure 40: Comparative cyclic voltammetry (CV) analysis in the range of -0.8V to 0V, featuring a plain screen-printed electrode (SPE), an Ag NP/$Nb_4C_3T_x$-modified SPE, and their respective responses to 5mM hydrogen peroxide (H_2O_2).

The complexity of the narrative intensifies with the addition of a 5mM concentration of hydrogen peroxide (H_2O_2) into the electrochemical cell. The third cyclic voltammogram (CV), illustrated in black, portrays the unadorned Screen-Printed Electrode (SPE) electrochemical reaction when exposed to a concentration of 5 millimolar (mM) hydrogen peroxide (H_2O_2). In this context, a slight decrease in electrical current is observed, with a measurement of about 1.5 µA. The observed decrease in the measured quantity can be ascribed to the interaction between the electrode and H_2O_2, hence suggesting a restricted level of sensitivity. In contrast, the fourth cyclic voltammetry (CV), corresponds to the Ag NP/ $Nb_4C_3T_x$ -modified Screen-

Printed Electrode (SPE) technique under identical conditions characterised by an abundance of H_2O_2. The electrode that has been altered exhibits a notable improvement in electrochemical performance, as evidenced by a significant change in current of roughly 7 μA compared to the control cyclic voltammetry. The significant disparity observed between the modified electrode and the unmodified screen-printed electrode (SPE) upon exposure to hydrogen peroxide (H_2O_2) emphasises the remarkable sensitivity and selectivity exhibited by the silver nanoparticle (Ag NP)/niobium carbide ($Nb_4C_3T_x$) MXene-modified electrode. This characteristic positions it as a highly suitable option for accurate determination of hydrogen peroxide levels in electrochemical systems.

- **Enhancing Hydrogen Peroxide Detection Using Ag NP/$Nb_4C_3T_x$ MXene Modified Electrochemical Sensors through Chronoamperometry**

Chronoamperometry is a fundamental technique within the field of electrochemical sensors, serving as a critical component in their operational framework. The method entails the continuous observation of electric current at a consistent applied voltage across a duration of time[362]. Although it may appear straightforward initially, this methodology carries significant consequences for the development of sensors. The sensor offers a live view of the constantly changing electrochemical reactions taking place on its surface. Chronoamperometry is a valuable technique for the determination of concentrations of many substances, including biomolecules, contaminants, and reactive species such as hydrogen peroxide[363]. It provides significant insights into the quantitative analysis of these substances. Electrochemical sensors can attain exceptional sensitivity and precision by assessing the rate and extent of redox reactions occurring at the electrode contact[364]. The aforementioned technique serves as a fundamental basis for a diverse array of applications, spanning from the monitoring of environmental conditions to the diagnosis of medical ailments. This exemplifies its essential function within the realm of contemporary analytical chemistry[365].

In this particular electrochemical analysis, the technique of chronoamperometry is utilised to examine and explore the redox behaviour of hydrogen peroxide (H_2O_2). Chronoamperometry is a technique that primarily focuses on the measurement of current at a constant potential (-0.4 V in this particular instance) as a function of time. The efficacy of this technique is dependent on the electrochemical reduction of H_2O_2, a fundamental process that forms the basis of its detection. When a consistent voltage is provided to the electrode, the H_2O_2 molecules

present in the solution make contact with the surface of the electrode. At this particular contact, an intriguing electrochemical phenomenon occurs. The reduction of H_2O_2 occurs by the transfer of electrons (e^-) from the electrode to the H_2O_2 molecules. The aforementioned electron transfer mechanism facilitates the transformation of hydrogen peroxide (H_2O_2) into innocuous water (H_2O) and oxygen (O_2), as represented by the following chemical equation: The chemical equation provided represents the reduction of hydrogen peroxide (H_2O_2) in an acidic solution[366]. In this reaction, two hydrogen ions (H^+) and two electrons (e^-) are consumed, resulting in the formation of two water molecules (H_2O).

$$H_2O_2 + 2H^+ + 2e^- \rightarrow 2H_2O$$

In the above equation, the compound H_2O_2 undergoes a reduction process by accepting two electrons ($2e^-$) from the electrode, resulting in its conversion into water. Significantly, this reduction reaction can be employed for the precise detection of H_2O_2 concentrations because to the direct correlation between the rate of this electrochemical process and the concentration of H_2O_2 present in the solution.

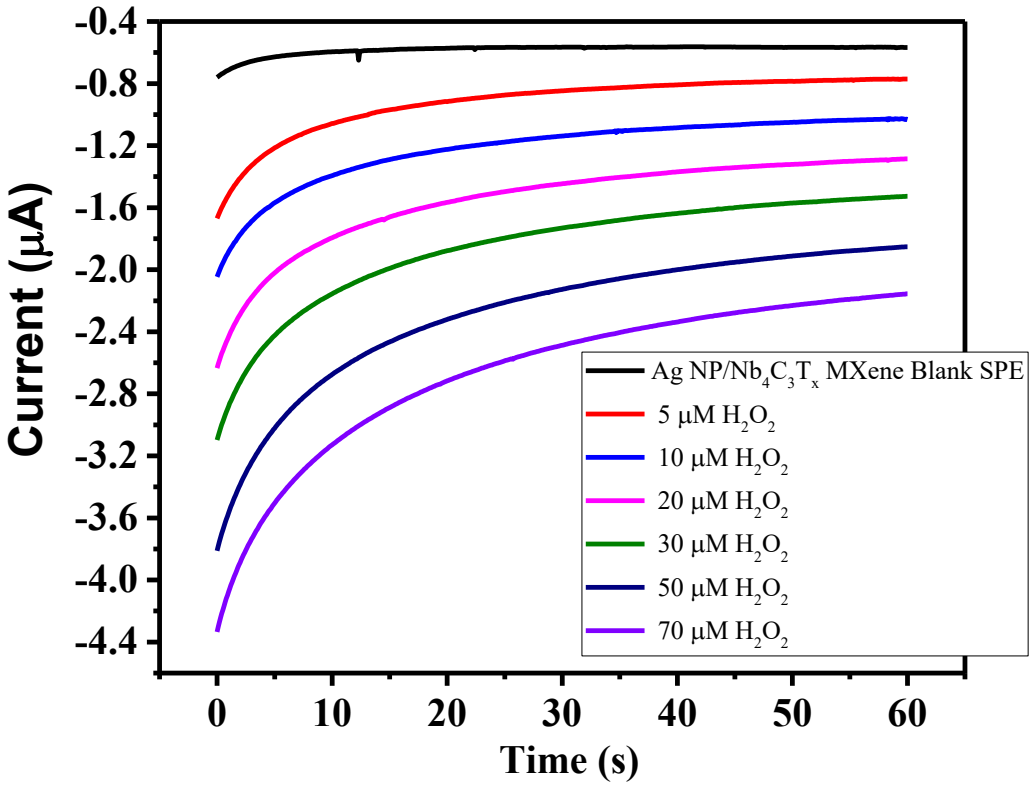

Figure 41:Chronoamperometric measurements for hydrogen peroxide detection using Ag NP/$Nb_4C_3T_x$ MXene modified screen-printed electrode (SPE) in phosphate buffer saline (PBS) pH 7.

Now, let us proceed to analyse the observations made during the chronoamperometric experiments as shown in **Figure *41***. The electrode is maintained at a constant voltage of -0.4 V, and the resultant current is continually monitored. The rate of decrease at the electrode surface fluctuates in accordance with the incremental concentrations (5 μM, 10 μM, 20 μM, 30 μM, 50 μM, and 70 μM) at which H_2O_2 is injected into the solution. At lower concentrations of hydrogen peroxide (H_2O_2), the reduction reaction exhibits a decreased rate, leading to a diminished current response. In contrast, elevated concentrations of H_2O_2 result in an accelerated rate of decrease, hence leading to increased current levels. The observed fluctuations in the electrical current response exhibit a clear correlation with the quantity of hydrogen peroxide (H_2O_2) present in the solution, hence enabling accurate and very sensitive quantification. The chronoamperometric graphs obtained in the course of these experiments offer a visual depiction of the electrochemical phenomena under investigation. Through the examination of the correlation between the concentration of current and H_2O_2, it is possible to

create a calibration curve that facilitates precise measurement of H_2O_2 levels in samples obtained from real-world scenarios. This methodology, based on the fundamental principles of electrochemistry, underscores the significant importance of chronoamperometry in the development of electrochemical sensors for a wide range of applications, spanning from environmental surveillance to clinical diagnostics[311]. The calibration plot and analytical parameters are essential components in scientific research and analysis. The calibration plot is a graphical representation that allows for the assessment and validation of the accuracy and precision of a measurement method or instrument. It involves plotting the observed values against the reference. The calibration plot (as shown in **Figure *42***) was carefully generated by graphing the measured current against a series of known concentrations of hydrogen peroxide (H_2O_2) in order to determine its concentration. The strong connection between the concentration of H_2O_2 and the current was emphasised by a high coefficient of determination (R^2) of 0.99938, providing clear evidence of a significant relationship between these important variables.

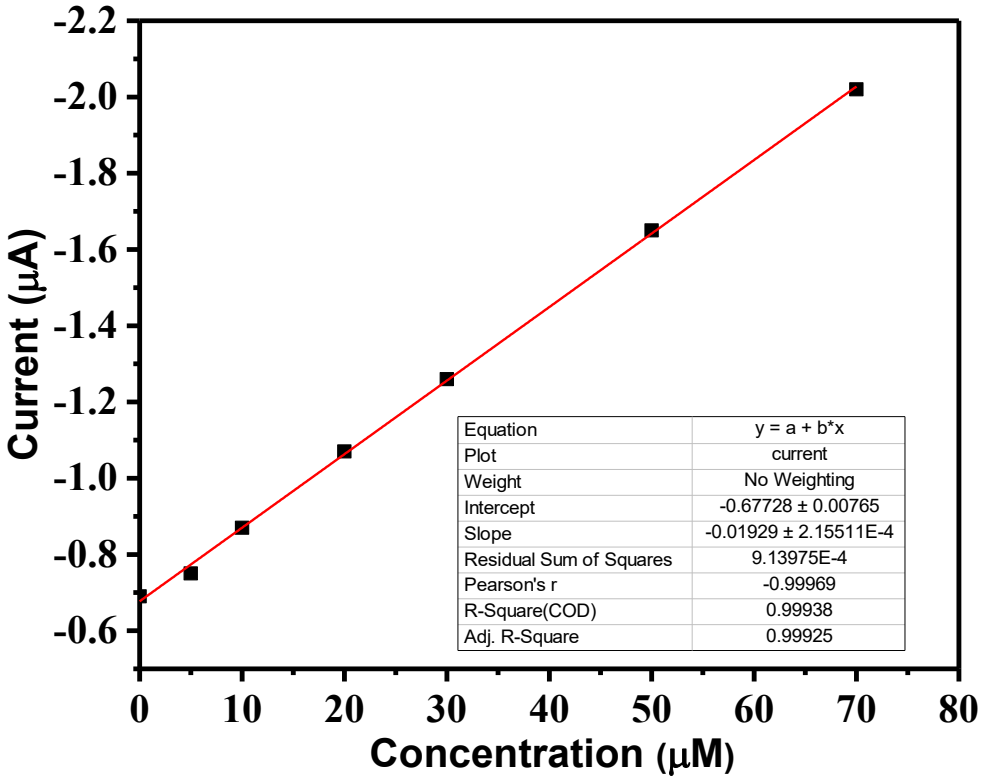

Figure 42: Calibration Plot from chronoamperometry

The linear equation derived from the calibration plot was concisely expressed as follows: The equation for the current (µA) can be expressed as -0.01929 multiplied by the concentration of H_2O_2 (µM) -0.67. The linear equation presented in this study is a highly effective and dependable method for accurately measuring the concentration of H_2O_2 in an electrochemical system. In addition, we have derived a number of essential analytical characteristics in order to thoroughly assess the functioning of the sensor. The Limit of Detection (LOD) was carefully determined to represent the minimum concentration of H_2O_2 that may be detected with a high degree of reliability, but it may not be accurately quantified. By utilising the formula Limit of Detection (LOD) = 3.3 * (Standard Deviation of the Blank) / Slope, it has been determined that the LOD for this particular sensor is measured at 58.78 µM, thereby highlighting its noteworthy level of sensitivity. Sensitivity: The sensitivity of the sensor is shown by the slope of the calibration curve (-0.01929 µA/µM), which indicates its ability to detect small changes in H_2O_2 concentration. The sensitivity value highlights the sensor's capacity to accurately perceive and measure alterations in H_2O_2 concentration. The Limit of Quantification (LOQ) refers to the

minimum concentration of H_2O_2 that can be accurately and precisely measured. This finding reaffirms the sensor's ability to accurately measure and quantify substances with a high level of precision. The outstanding reliability and sensitivity of the Ag NP/ $Nb_4C_3T_x$ MXene-modified sensor are highlighted by the analytical characteristics. This sensor demonstrates accurate measurement of H_2O_2 concentrations, especially within the limits of the calculated LOD and LOQ. The exceptional performance features of the sensor make it a very promising candidate for a wide range of applications that require accurate and reliable detection of H_2O_2.

In summary, the electrochemical investigation performed on the sensor modified with Ag NP/$Nb_4C_3T_x$ has demonstrated its significant capability for accurately detecting hydrogen peroxide (H_2O_2). The modified sensor was subjected to cyclic voltammetry (CV) analysis, revealing the emergence of discernible redox peaks at 0.16 V and -0.06 V. These peaks can be ascribed to the oxidation and reduction processes of silver nanoparticles (Ag NP) that are present on the surface of the electrode. The modification of the CV response in the presence of hydrogen peroxide (H_2O_2) highlights the increased sensitivity of the sensor towards this particular analyte. The heightened sensitivity seen can be attributed to the surface chemistry and composition of the improved electrode. The surface modified with Ag NP/ $Nb_4C_3T_x$ provides a substrate that is electrochemically active, enabling the efficient and quick electroreduction of H_2O_2. The inclusion of silver nanoparticles not only plays a role in the observed redox behaviour in the cyclic voltammetry (CV) analysis, but also acts as catalytic sites for the electrochemical reduction of hydrogen peroxide (H_2O_2), hence improving the analytical performance of the sensor. In addition, the sensor's capacity to detect H_2O_2 at different micromolar concentrations was confirmed using chronoamperometric tests, which demonstrated a significant decrease in current following the introduction of H_2O_2. The real-time monitoring highlights the sensor's ability to respond promptly to H_2O_2, which is a crucial attribute for precise and swift measurement. The calibration plot that was obtained demonstrated a strong analytical capability in properly estimating H_2O_2 concentrations, as indicated by the high coefficient of determination ($R^2 = 0.99938$). The determined Limit of Detection (LOD) and Limit of Quantification (LOQ) highlight the sensor's dependability and accuracy in the process of quantification. The sensor exhibits a determined limit of detection (LOD) of 58.78 μM. These performance characteristics enable the sensor to effectively detect and quantify H_2O_2 at low concentrations, rendering it well-suited for applications that need high sensitivity and precision. The Ag NP/$Nb_4C_3T_x$-modified sensor exhibits significant potential for detecting H_2O_2 in a wide range of applications, including environmental

monitoring and clinical diagnostics. The exceptional performance features of this tool, which are based on its surface chemistry and electrocatalytic qualities, establish it as a very effective instrument for accurately measuring levels of H_2O_2.

4.4 Electrochemical Analysis for the detection of Riboflavin

Riboflavin, alternatively referred to as Vitamin B2, is a hydrophilic essential component that assumes a central part in several physiological mechanisms occurring in living organisms[367]. Riboflavin, an essential member of the flavin family, plays a crucial role in several biochemical events, specifically in energy metabolism, cellular growth, and the preservation of general well-being[368]. The diverse nature of its functions highlights the utmost need of employing precise and responsive techniques for its identification. The determination of Riboflavin holds great importance in various domains, encompassing food analysis, medicines, and clinical diagnostics[369]. Within the domain of food analysis, Riboflavin functions as a pivotal determinant of nutritional excellence. The evaluation of the freshness and stability of diverse food goods, such as dairy, meat, and cereal items, is of paramount importance. The correlation between the presence of Riboflavin and the quality and shelf-life of a product is a significant factor, necessitating the accurate measurement of Riboflavin as a crucial component in ensuring food safety and maintaining quality control[370]. Riboflavin occupies a significant role within the pharmaceutical sector, serving as an essential constituent of numerous drugs and dietary supplements. Precise quantification of the Riboflavin content is crucial in order to verify compliance with regulatory requirements and ascertain the desired therapeutic effects of pharmaceutical formulations. In addition, the detection of Riboflavin plays a crucial role in the field of clinical diagnostics. A lack of this crucial mineral can result in many health complications, such as dermatitis, anaemia, and visual impairments. Hence, the precise measurement of Riboflavin in clinical samples is crucial for timely detection and efficient treatment of health disorders associated with Riboflavin[369]. In order to cater to the wide range of requirements for accurate quantification of Riboflavin in different applications, scholars have investigated a variety of analytical methods[371]. This chapter provides a comprehensive examination of the currently available techniques for the determination of Riboflavin. This study centres on the field of electrochemical sensing, with a specific emphasis on the utilisation of electrodes modified with Ag NP/ $Nb_4C_3T_x$ for various applications. Electrochemical sensors demonstrate considerable potential in augmenting the precision,

sensitivity, and expeditiousness of Riboflavin detection, rendering them valuable instruments in several analytical and clinical contexts[372].

- **Cyclic Voltammetry (CV) for Riboflavin Detection: Surface Chemistry and Electrochemical Insights**

Cyclic Voltammetry (CV) is a crucial electrochemical technique utilised to assess the electrocatalytic efficacy of electrodes modified with Ag NP/$Nb_4C_3T_x$ in the detection of Riboflavin. This section provides a comprehensive examination of the CV curves acquired under different conditions, offering significant insights into the surface chemistry and electrochemical phenomena occurring on these modified electrodes. During the preliminary phase of our investigation, we performed blank cyclic voltammetry (CV) measurements to evaluate the electrochemical characteristics of three types of electrodes: bare Screen-Printed Electrodes (SPE), the precursor Nb_4AlC_3 MAX phase (from which the MXene is synthesised), and Ag NP/ $Nb_4C_3T_x$ MXene-modified electrodes as shown in **Figure *43***. These measurements were conducted in an acetate buffer solution with a pH value of 4.5. Significantly, the cyclic voltammetry (CV) curve obtained for the unaltered solid Screen-Printed Electrode (SPE) had a comparatively low current response, suggesting a limited level of electrochemical reactivity on the surface that had not undergone any modifications.

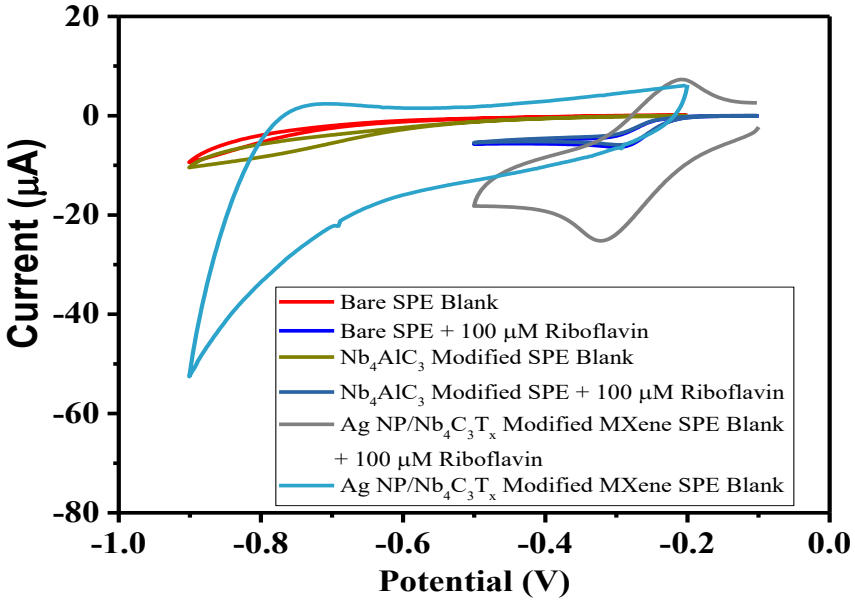

Figure 43: Cyclic Voltammetry (CV) curves of the bare Screen-Printed Electrode (SPE), precursor Nb_4AlC_3 MAX phase, and Ag NP/$Nb_4C_3T_x$ MXene-modified electrode in an acetate buffer solution at pH 4.5, along with the modified electrode's CV response after adding 100 µM Riboflavin, highlighting distinctive redox peaks.

In contrast, the cyclic voltammetry (CV) curve obtained for the precursor Nb_4AlC_3 MAX phase had a similar behaviour to that of the unmodified Screen-Printed Electrode (SPE), indicating that the MAX phase in isolation did not make a substantial contribution to the electrocatalytic activity. Nevertheless, a significant breakthrough took place with the introduction of Ag NP/ $Nb_4C_3T_x$ MXene as a modification layer on the surface of the electrode. The current response of the modified MXene demonstrated a significant improvement, suggesting its exceptional electrocatalytic performance. The inclusion of 100 µM Riboflavin in the electrochemical cell resulted in the generation of CV curves that yielded more comprehensive understanding of the underlying electrochemical mechanisms. It is noteworthy that both the bare SPE (Screen Printed Electrode) and the precursor MAX ($M_{n+1}AX_n$) phase exhibited cyclic voltammetry (CV) curves featuring peak pairs at around -0.23 V and -0.28 V. The observed peaks, albeit detectable, did not exhibit significant prominence, suggesting limited interaction between Riboflavin and the unaltered surfaces. In stark contrast, the cyclic voltammetry (CV) curve of the electrode treated with Ag NP/ $Nb_4C_3T_x$ MXene displayed significant peaks at -0.20 V and -0.32 V with the addition of Riboflavin. The observed redox peaks exhibited distinct characteristics that can be attributed to the oxidation and reduction reactions of Riboflavin. This indicates that Riboflavin was effectively detected on the surface of the modified electrode.

The unique electrochemical response observed highlights the remarkable capacity of MXene to enhance the transport of electrons between Riboflavin and the surface of the electrode. The heightened prominence of the redox peaks serves as an indication of the MXene material's ability to effectively adsorb and catalyse Riboflavin molecules, hence augmenting their electrochemical reactivity[373]. The remarkable electrocatalytic activity seen in this study can be ascribed to the combined influence of the highly conductive silver nanoparticles and the distinctive MXene structure. The higher electrochemical response exhibited in the cyclic voltammetry (CV) curve can be attributed to several factors, namely the increased surface area, facilitated electron transfer, and the MXene's capacity to adsorb Riboflavin molecules[374]. In summary, the cyclic voltammetry (CV) findings provide a comprehensive understanding of the complex relationship between surface chemistry and electrochemistry on the surface of the Ag NP/ $Nb_4C_3T_x$ MXene-modified electrode. The modified electrode demonstrates heightened electrocatalytic activity, particularly when Riboflavin is present, highlighting its potential as a discerning and exclusive platform for detecting Riboflavin in diverse applications, such as food quality control and clinical diagnostics. The demonstrated electrochemical performance exhibits potential for further investigation of Riboflavin sensing by the utilisation of Ag NP/ $Nb_4C_3T_x$ MXene-modified electrodes.

- **Enhanced Electrochemical Performance of Ag NP/$Nb_4C_3T_x$ Modified SPE Compared to Precursor MAX Phase**

The analysis of differential pulse voltammetry (DPV) measurements conducted on three distinct electrodes, specifically the unmodified Screen-Printed Electrode (SPE), the Nb_4AlC_3 Modified SPE, and the Ag NP/ $Nb_4C_3T_x$ Modified SPE, yields significant findings on their individual electrochemical characteristics. The experiment began by conducting blank differential pulse voltammetry (DPV) observations until a consistent signal was obtained. Subsequently, a concentration of 50 nM Riboflavin was added to the electrochemical cell. The preconcentration period lasted for 90 seconds, and the electrolyte used was an acetate buffer with a pH of 4.5. The empirical findings suggest a significant disparity in the electrochemical characteristics shown by these electrodes (**Figure *44***). Both the bare Screen-Printed Electrode (SPE) and the Nb_4AlC_3 Modified SPE had comparable Differential Pulse Voltammetry (DPV) responses, which were characterised by the absence of notable peaks. The observed similarity in behaviour can be ascribed to the difficulties encountered in achieving sufficient dispersion and modification of the surface of the Screen-Printed Electrode (SPE) with the precursor material known as MAX phase Nb_4AlC_3. On the other hand, the dispersion of Ag NP/ $Nb_4C_3T_x$

exhibited significant alteration of the Screen Printed Electrode (SPE), resulting in improved electrochemical performance for the detection of Riboflavin.

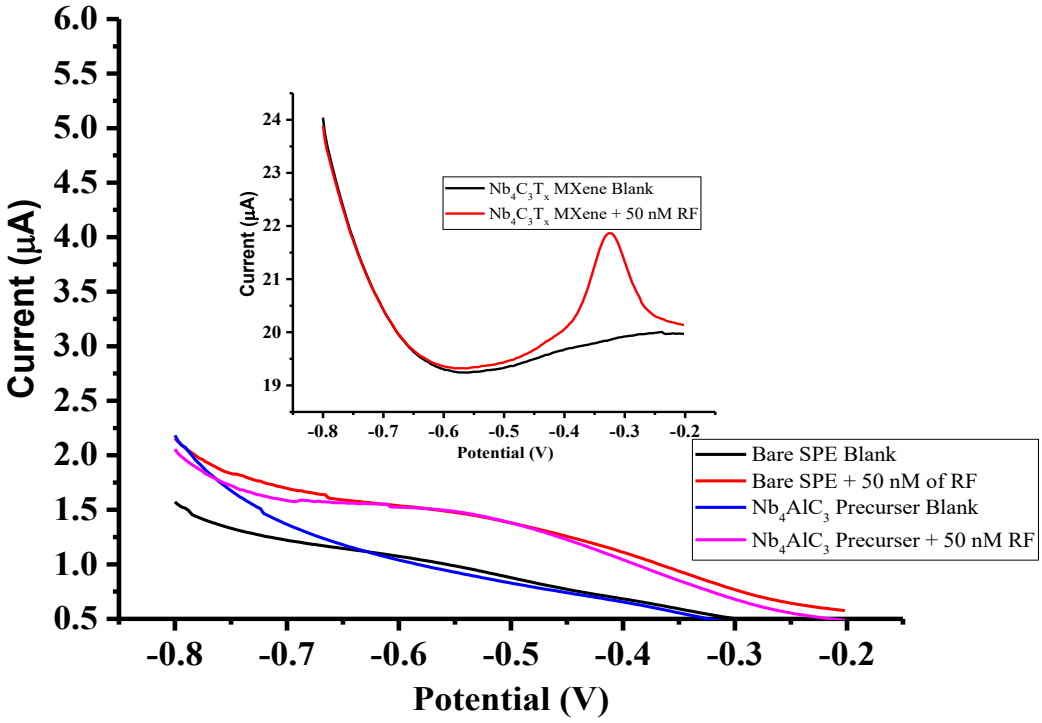

Figure 44: Comparison of DPV Measurements Among Bare SPE, Nb_4AlC_3 Modified SPE, and Ag NP/$Nb_4C_3T_x$ Modified SPE for 50 nM Riboflavin Detection

The enhanced efficiency exhibited by the Ag NP/ $Nb_4C_3T_x$ Modified Screen Printed Electrode (SPE) can be due to multiple contributing variables. To begin with, the incorporation of Ag nanoparticles (Ag NPs) enhances the dispersion characteristics of $Nb_4C_3T_x$ MXene on the electrode surface, resulting in the formation of an interface that exhibits exceptional conductivity and catalytic activity. The improved dispersion and intrinsic electrocatalytic characteristics of MXenes work together to provide effective electron transfer and enable the detection of riboflavin[375]. Moreover, the distinctive stratified arrangement and ample surface terminations of MXenes offer a multitude of active sites for the adsorption of analytes and electrochemical processes, hence augmenting the sensitivity and selectivity of the sensor. In brief, the Ag NP/$Nb_4C_3T_x$ Modified Screen Printed Electrode (SPE) exhibits superior performance compared to the precursor MAX phase Nb_4AlC_3 and the unmodified SPE. This can be attributed to the greater dispersion, higher conductivity, and the electrocatalytic

characteristics of MXenes[376]. The aforementioned comparison underscores the notable electrochemical benefits provided by electrodes treated with MXene, hence rendering them exceedingly attractive for a diverse array of electrochemical sensing applications[346].

- **Differential Pulse Voltammetry (DPV) Analysis for Riboflavin Detection**

During the initial series of differential pulse voltammetry (DPV) experiments performed in an acetate buffer solution with a pH of 4.5, two distinct DPV curves were seen as displayed in **Figure *45***. The DPV curve of the Ag NP/$Nb_4C_3T_x$ -modified electrode initially displayed a featureless profile with no observable peaks. This observation implies that the electrode surface, after modification, exhibited minimal reactivity in the absence of any analyte. Furthermore, no substantial electrochemical activity was seen within the examined potential range. Following the introduction of 10 μM of Riboflavin into the electrochemical cell and a preconcentration period of 60 seconds before to recording the differential pulse voltammetry (DPV) measurements, a significant alteration in the DPV curve was noted. A distinct decrease peak was observed at a potential of roughly -0.4 V. The observed decrease in peak intensity can be ascribed to the electrochemical reduction of Riboflavin occurring on the surface of the modified electrode. The identification of a prominent peak in the data suggests that Riboflavin detection was effectively achieved. This peak also serves to emphasise the electrocatalytic characteristics of the Ag NP/$Nb_4C_3T_x$ -modified electrode, which enhances the ability to reduce Riboflavin molecules.

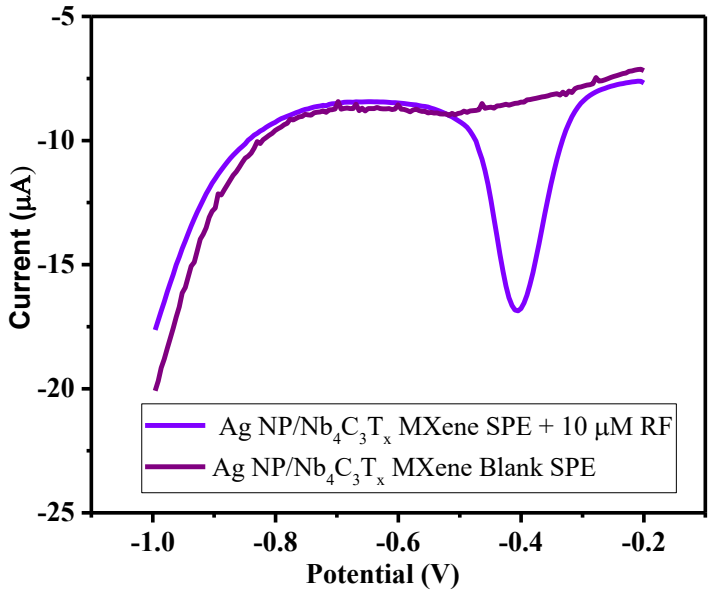

Figure 45: DPV analysis of Riboflavin on Ag NP/$Nb_4C_3T_x$-modified SPE, showing a distinct reduction peak at -0.4 V upon adding 10 uM Riboflavin.

The aforementioned discovery highlights the heightened responsiveness and specificity of the altered electrode in detecting Riboflavin, as the decrease peak is discernible just when Riboflavin is present. The preconcentration procedure serves to augment the buildup of Riboflavin at the electrode surface, hence enhancing the signal response and facilitating the accurate quantification of Riboflavin concentrations[377]. The findings presented in this study illustrate the capability of the Ag NP/ $Nb_4C_3T_x$ -modified electrode as a promising and efficient platform for the electrochemical detection of Riboflavin in aqueous solutions.

- **Effect of Preconcentration time with Ag NP/$Nb_4C_3T_x$ Modified SPE for the detection of Riboflavin.**

In this set of experiments utilising differential pulse voltammetry (DPV) for the purpose of detecting riboflavin, the investigation went beyond examining changes in concentration and instead examined the influence of preconcentration time on the sensitivity of detection as shown in **Figure *46***. A DPV curve was initially constructed at a riboflavin concentration of 10 µM. Following this, a methodical examination was conducted, which covered various lower quantities of riboflavin, namely 1 µM, 2 µM, and 5 µM. This enabled us to assess the sensor's performance over a wider range of analyte concentrations. In addition, in order to enhance the efficiency of the detection process, the durations of preconcentration were thoroughly investigated, namely 10 seconds, 30 seconds, and 60 seconds.

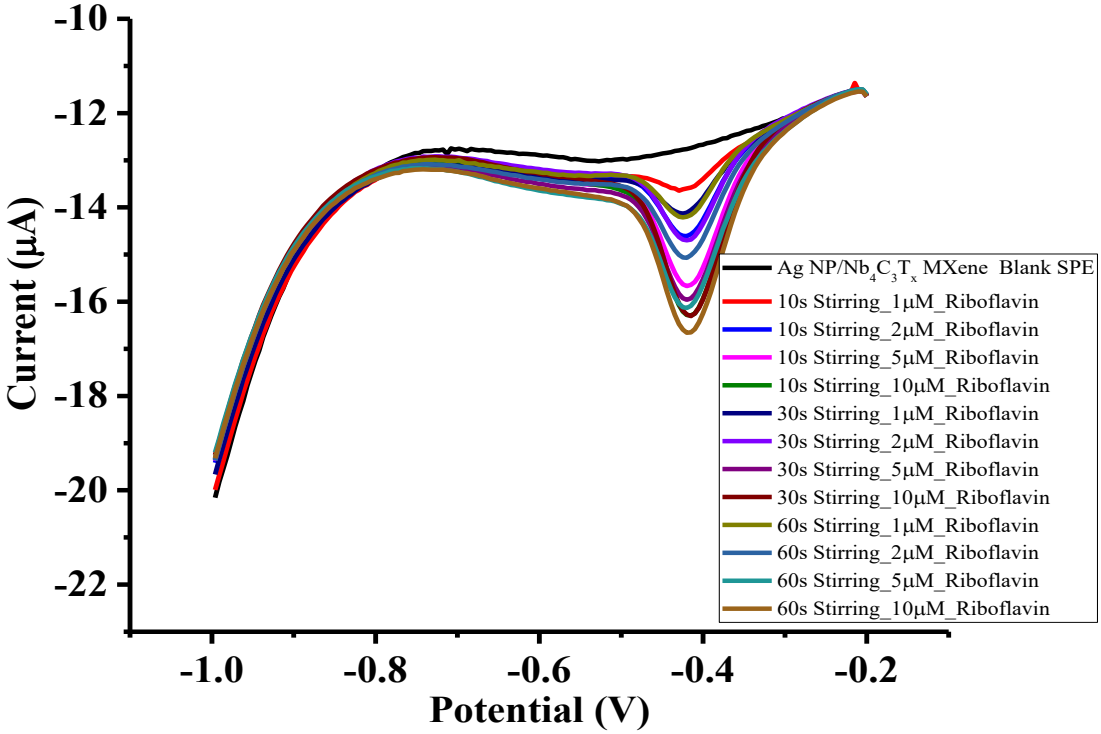

Figure 46: DPV measurements for riboflavin detection with Ag NP/$Nb_4C_3T_x$ MXene modified SPE at varying concentrations (1 µM to 10 µM) and preconcentration times (10s, 30s, 60s) in pH 4.5 acetate buffer. Longer preconcentration times improve riboflavin detection sensitivity.

The significance of preconcentration time is crucial in augmenting the results obtained using differential pulse voltammetry (DPV). As the duration of preconcentration is extended, the electrochemical sensor allows for a greater period of time during which riboflavin molecules can selectively accumulate on the surface of the modified electrode. The extended duration of interaction between the analyte and the electrode leads to a greater buildup of riboflavin species at the electrode interface, hence enhancing the likelihood of successful detection[378]. As a result, the differential pulse voltammetry (DPV) curves generated by increasing the preconcentration durations demonstrate more prominent and distinguishable peaks associated with the reduction of riboflavin. The observed improvement in detection sensitivity highlights the significant impact of preconcentration time on the optimisation of electrochemical detection of riboflavin, utilising the Ag NP/$Nb_4C_3T_x$ MXene-modified electrode. The ramifications of these discoveries are of great importance for applications that necessitate accurate and dependable quantification of riboflavin.

- **How Electrolyte pH Impacts Riboflavin Detection: Optimizing Electrochemical Performance**

The impact of pH on the electrochemical detection of riboflavin is a critical aspect to take into account when aiming to enhance the analytical performance of the sensor. The redox behaviour of analytes and the overall sensitivity of the sensor can be considerably influenced by pH in electrochemical processes[379]. The present work as shown in **Figure *47*** investigated the effects of four distinct pH conditions on the experimental system, namely severely acidic (pH 3), moderately acidic (pH 4.5), slightly acidic (pH 6), and alkaline (pH 9) environments. The selection of electrolyte pH significantly influences the surface charge and reactivity of the modified electrode. Under conditions of high acidity (pH 3), it was observed that the sensor demonstrated reduced sensitivity towards riboflavin, particularly at elevated doses. The reduced effectiveness of the sensor in detecting the analyte can be ascribed to the suboptimal pH conditions for the riboflavin redox reaction, which therefore impacts its electrochemical properties. The significant decrease in electrical current seen at lower concentrations of riboflavin indicates a potential limitation or inhibition of the electrochemical response inside this acidic milieu. In contrast, at conditions of mild acidity (pH 4.5, utilising an acetate buffer), the sensor exhibited exceptional performance. The significant decrease in the measured electrical current following the introduction of riboflavin suggests a pronounced electrochemical reaction. The detection sensitivity of riboflavin is likely enhanced by the favourable redox reactions facilitated by the appropriate pH range on the modified electrode surface. Moderate results were obtained while using a phosphate buffer with a pH of 6 and under alkaline circumstances with a pH of 9 in phosphate-buffered saline (PBS). Although the inhibitory effects on riboflavin detection were not as pronounced as those observed in very acidic settings, the performance of the samples did not reach the level achieved in the moderately acidic pH 4.5 environment. This finding indicates that a pH level of 4.5 offers an ideal equilibrium between the redox activity of riboflavin and the electrochemical response of the sensor. Several variables can be attributed to the selection of acetate buffer at pH 4.5 as the most effective electrolyte for riboflavin detection. The acetate buffer's mildly acidic pH settings create an ideal environment for facilitating riboflavin's redox action. The redox reactions of riboflavin are recognised to be influenced by changes in pH. It is hypothesised that these

reactions are most advantageous for facilitating electron transport on the surface of the modified electrode when the pH is 4.5. As a result, there is an enhanced and heightened electrochemical reaction. Additionally, the electrochemical behaviour might be influenced by the composition of the buffer. The acetate buffer solution is composed of acetic acid and acetate ions, which serve to stabilise reaction intermediates and maintain the proper pH level, hence enabling the facilitation of redox processes[204]. This factor enhances the overall efficacy of riboflavin detection. Additionally, the surface characteristics of the modified electrode in an acetate buffer at pH 4.5 may be highly suitable for the adsorption of riboflavin and facilitation of electron transfer. The electrode treated with MXene offers a sufficient number of active sites for the adsorption of riboflavin and facilitates effective electron transfer, hence augmenting the efficacy of the sensor. It is imperative to highlight that the pH of the electrolyte solution plays a pivotal role in determining the electrochemical response of the sensor. The performance of the sensor for riboflavin detection can be hindered by both acidic settings (pH 3) and extremely alkaline conditions (PBS, pH 9). However, a moderately acidic environment (acetate buffer, pH 4.5) provides the most favourable equilibrium between riboflavin's redox activity and the electrochemical response of the sensor. The aforementioned discovery emphasises the importance of pH optimisation in electrochemical sensing approaches, specifically emphasising the preference for acetate buffer pH 4.5 for detecting riboflavin on the Ag NP/ $Nb_4C_3T_x$ MXene-modified sensor, as it offers both sensitivity and reliability. In summary, the pH of a solution significantly influences the electrochemical detection of riboflavin. The experimental findings indicate that the optimal conditions for accurate and precise detection of riboflavin on the Ag NP/$Nb_4C_3T_x$ MXene-modified sensor are in a mildly acidic environment with a pH of 4.5. The significance of pH control in electrochemical sensing applications is emphasised by this discovery, as it enables the precise identification of analytes such as riboflavin in samples obtained from real-world scenarios[369].

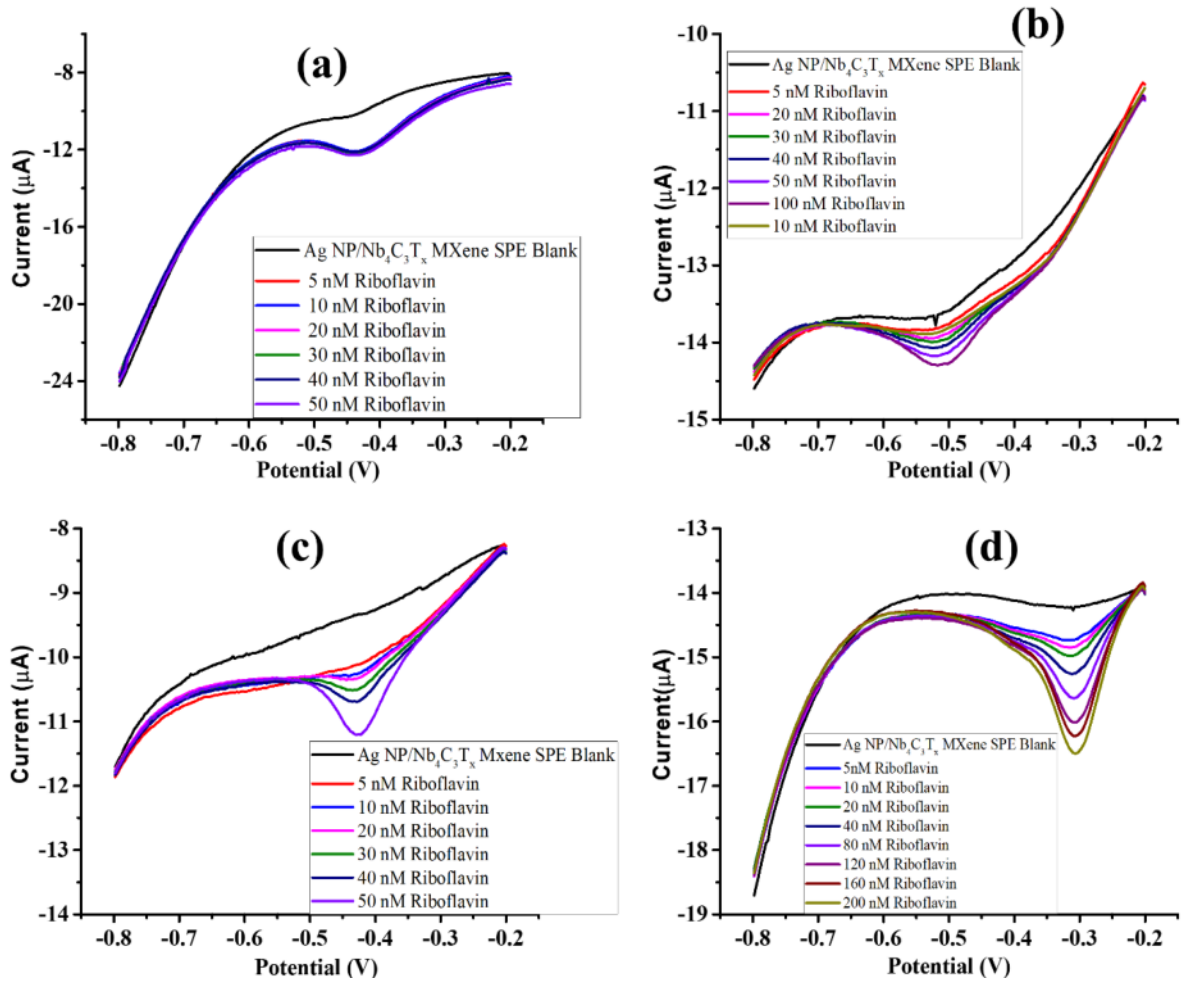

Figure 47: Differential Pulse Voltammetry (DPV) measurements for the detection of riboflavin at various electrolyte pH conditions. (a) Acetate buffer pH 3, (b) PBS pH 9, (c) Phosphate pH 6, and (d) Acetate buffer pH 4.5. The DPV curves reveal the impact of pH on the sensor's performance, with acetate buffer at pH 4.5 demonstrating superior riboflavin detection capabilities.

- **Optimization of Preconcentration Time for Ag NP/$Nb_4C_3T_x$-Modified SPE in Riboflavin Detection**

In the following section, we conducted an optimisation of the preconcentration time for our silver nanoparticle/niobium carbide-modified Screen-Printed Electrode (SPE) method in the electrochemical detection of Riboflavin. In the course of these tests, a constant concentration of 80 nM of Riboflavin was utilised, as it was chosen as a suitable concentration for our comprehensive examination of the impact of preconcentration time on the differential pulse voltammetry (DPV) response. The main objective of this section was to enhance the preconcentration time for the Ag NP/ $Nb_4C_3T_x$ -modified Screen-Printed Electrode (SPE),

which exhibited potential in earlier experimental studies. The electrolyte that was chosen as the most suitable, based on the results of the pH optimisation studies, was an acetate buffer solution with a pH value of 4.5. In this conducive electrochemical setting (**Figure *48***), a comprehensive examination was conducted on six distinct preconcentration durations: 30 seconds, 60 seconds, 90 seconds, 120 seconds, 150 seconds, and 180 seconds. At first, it was noted that there was a positive correlation between the preconcentration time and the strength of the differential pulse voltammetry (DPV) peak. This relationship suggests that there was an enhancement in the electrochemical response of the silver nanoparticle/niobium carbide-modified screen-printed electrode (SPE) as the preconcentration time rose. The tendency has brought attention to the significant importance of preconcentration time in the attainment of effective analyte accumulation and electrochemical detection. Nevertheless, a captivating finding was made when the duration of preconcentration beyond 90 seconds. At preconcentration durations of 120 seconds, 150 seconds, and 180 seconds, the electrochemical response demonstrated either a plateau or a reduction in intensity as compared to the preconcentration duration of 90 seconds.

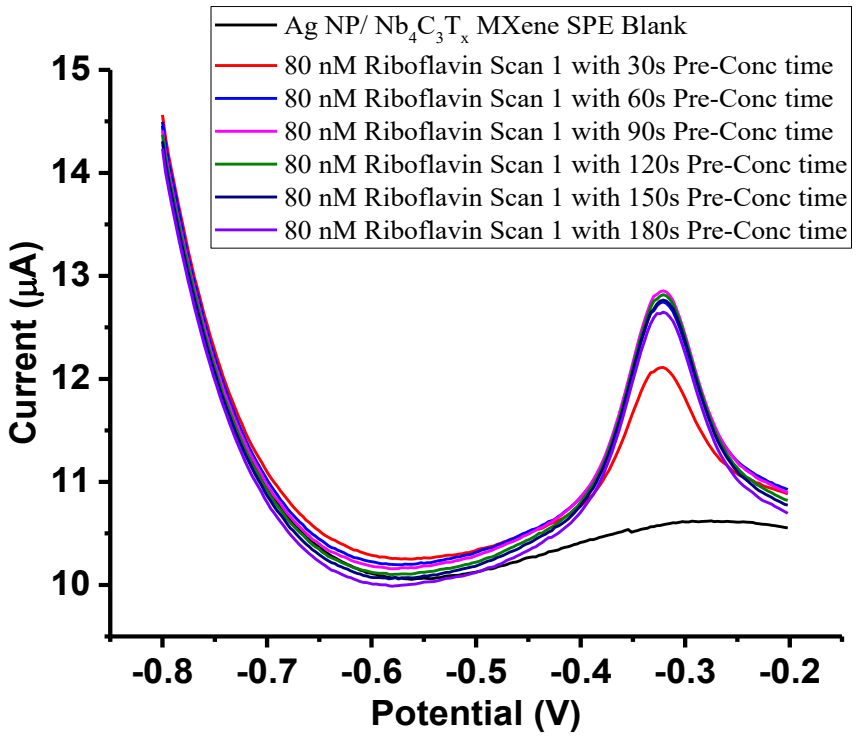

Figure 48: Effect of Preconcentration Time on Riboflavin Detection: DPV measurements with varying preconcentration times (30s, 60s, 90s, 120s, 150s, and 180s) at a fixed

concentration of 80 nM Riboflavin in acetate buffer (pH 4.5). The results reveal the influence of preconcentration time on the electrochemical response of our Ag NP/$Nb_4C_3T_x$-modified SPE.

The elucidation of this phenomena can be achieved by taking into account the saturation kinetics of the active sites on the electrode. Following an ideal preconcentration duration of 90 seconds, the surface of the silver nanoparticle/niobium carbide-modified Screen-Printed Electrode (SPE) becomes fully saturated with Riboflavin molecules. Subsequent extensions of the preconcentration period do not result in any further accumulation. On the contrary, extended preconcentration durations may facilitate the process of desorption or lead to inadequate binding of the analyte molecules, hence causing a decrease in the electrochemical response. In summary, the DPV studies highlight the significant importance of preconcentration time in the process of optimising the electrochemical detection of Riboflavin on the Ag NP/$Nb_4C_3T_x$ -modified SPE. The researchers determined that a preconcentration time of 90 seconds was the most effective duration, as it achieved a suitable level of analyte accumulation while minimising the declining returns that can occur with longer preconcentration times. The optimisation procedure was conducted under the advantageous circumstances of utilising an acetate buffer with a pH value of 4.5, as ascertained in previous experimental investigations. The Ag NP/$Nb_4C_3T_x$ -modified Screen-Printed Electrode (SPE), when subjected to an optimised preconcentration period, exhibits a resilient and highly sensitive electrochemical reaction, hence establishing its potential as a favourable option for a wide range of analytical purposes.

- **Assessment of Repeatability: Ensuring Consistency in Ag NP/$Nb_4C_3T_x$ Modified SPE Sensor**

The assessment of repeatability is a fundamental element within the field of electrochemical sensors, and it has substantial importance for the Ag NP/$Nb_4C_3T_x$ modified SPE sensor. Achieving precise and reliable analytical measurements necessitates the establishment of a sensor that is capable of constantly replicating outcomes. In order to assess this, we conducted a comprehensive evaluation of the modified electrode's efficacy by submitting it to eight consecutive scans while detecting 80 nM riboflavin, a chemical of significant significance in diverse domains (**Figure *49***). The noteworthy observation that demonstrated the sensor's

durability was the consistent and highly similar DPV responses observed throughout all eight scans. The result highlights the sensor's capacity to produce results that are consistently reliable and can be replicated with a high degree of accuracy when subjected to constant experimental parameters. This quality is crucial in practical situations where accurate and dependable data is not just desirable but necessary. The modified Screen-Printed Electrode (SPE) sensor, incorporating silver nanoparticles (Ag NP) and niobium carbide ($Nb_4C_3T_x$), exhibits a high level of reliability and reproducibility. This sensor is highly adaptable and plays a crucial role in various analytical situations, particularly where accurate evaluations of riboflavin or other analytes are essential. Therefore, it is evident that electrochemical sensing holds significant value in scientific research and practical applications, establishing itself as a reliable option in this field[207].

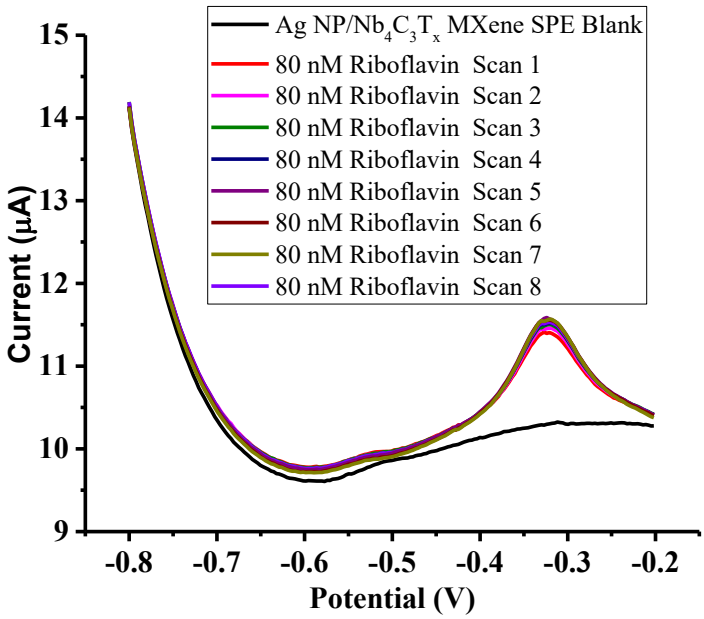

Figure 49: DPV measurements depicting the repeatability of the Ag NP/$Nb_4C_3T_x$-modified SPE sensor for the detection of 80 nM Riboflavin. Eight successive scans exhibit consistent peak responses, demonstrating the reliability and repeatability of the sensor.

The Relative Standard Deviation (RSD), often used as a measure of precision in analytical chemistry, was calculated to assess the consistency of the obtained data. For this calculation, five different measurements of the current peak obtained from the Ag NP/ $Nb_4C_3T_x$ MXene-modified SPE were considered: 1.309 µA, 1.289 µA, 1.300 µA, 1.238 µA, and 1.235 µA. The average current peak was determined to be 1.3376 µA, with a corresponding standard deviation

of 0.041. Utilizing these values, the RSD was computed using the formula: RSD (%) = (Standard Deviation (SD) / Average) * 100, resulting in an RSD of 3.067%. This low RSD percentage indicates a high level of precision and consistency in the electrochemical measurements, underlining the reliability of the Ag NP/$Nb_4C_3T_x$ MXene-modified sensor in detecting Riboflavin concentrations.

- **Reproducibility Assessment of Ag NP/$Nb_4C_3T_x$ Modified SPE for Riboflavin Detection**

The measurement of a sensor's repeatability is a crucial component in evaluating its performance, especially in the case of the Ag NP/$Nb_4C_3T_x$ modified SPE developed for detecting Riboflavin. The objective of this investigation was to determine the level of consistency and reliability exhibited by our sensor's performance when several electrodes are manufactured simultaneously. In order to examine the reproducibility of the experiment, a total of seven distinct electrodes were separately subjected to modification using Ag NP/$Nb_4C_3T_x$ as shown in **Figure *50***. Before commencing any measurements, blank runs were executed to verify the stability of the signals obtained from the electrodes. The initial step holds significant importance as it guarantees the inclusion of any signal variations arising from electrode preparation prior to the injection of the analyte. Following this, a concentration of 50 nanomolar (nM) Riboflavin, which served as a representative analyte, was delivered into every electrochemical cell. A preconcentration period of 90 seconds was employed, enabling the Riboflavin molecules to collect at the surface of the electrode. The selection of a 90-second duration was optimised in a preceding section to achieve enhanced sensitivity. To evaluate the reproducibility of the Ag NP/ $Nb_4C_3T_x$ MXene-modified SPE, the Relative Standard Deviation (RSD) was calculated based on current peak measurements from five different electrodes:

Current Peak SPE 1 = 0.967 µA

Current Peak SPE 2 = 0.949 µA

Current Peak SPE 3 = 0.8501 µA

Current Peak SPE 4 = 1.23 µA

Current Peak SPE 5 = 1.246 µA

The average current peak among these measurements was determined to be 1.082 µA, with a corresponding standard deviation of 0.1599. Utilizing these values, the RSD was computed as follows: RSD (%) = (Standard Deviation (SD) / Average) * 100, resulting in an RSD of 15.27%. Additionally, the RSD for specific electrodes was calculated:

RSD for SPE 1, SPE 2, and SPE 3 = 6.826%

This assessment demonstrates the reproducibility of the Ag NP/ $Nb_4C_3T_x$ MXene-modified SPE for the detection of Riboflavin and underscores its capability for consistent performance among multiple electrodes, as evidenced by the RSD values.

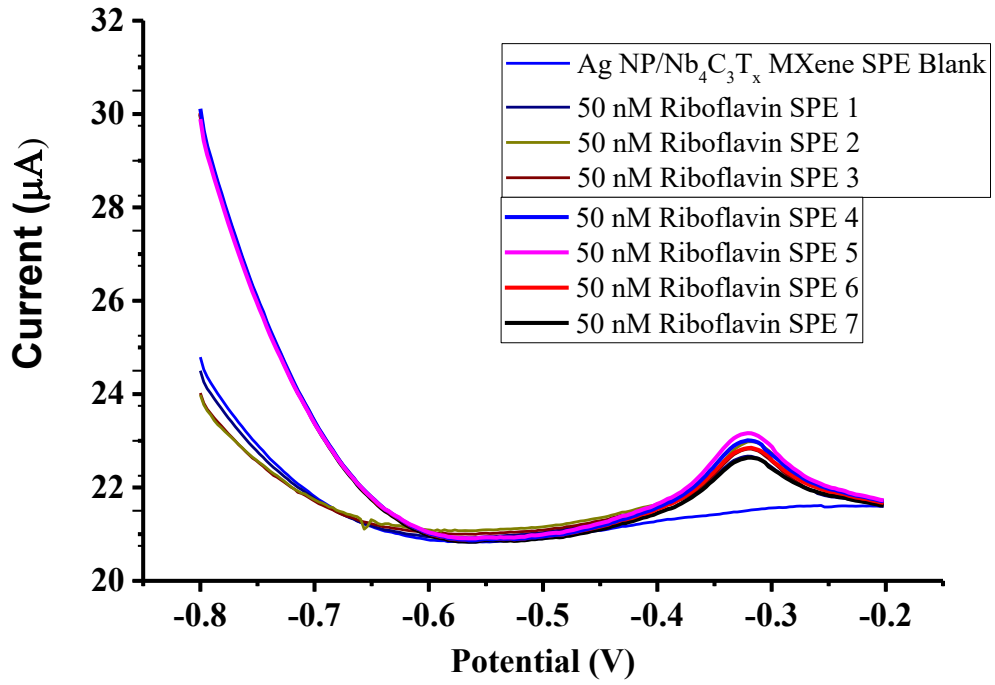

Figure 50: Reproducibility of Riboflavin Detection: DPV Measurements on Seven Ag NP/$Nb_4C_3T_x$ Modified SPEs with 50 nM Riboflavin.

Significantly, while doing DPV measurements on a per-electrode basis, a significant degree of consistency and comparability was detected in the responses obtained. The consistent outcomes observed among various electrodes highlight the strong reliability of our silver nanoparticle/niobium carbide modified screen-printed electrode-based sensor. The significance of repeatability holds great weight in the field of analytical chemistry[380]. The primary objective of this measure is to guarantee the reliable production of the sensor and its consistent delivery of precise outcomes, irrespective of minor discrepancies in the manufacturing procedure. In analytical contexts that prioritise precision and reliability, the sensor's proven

reproducibility strengthens its credibility as a valuable tool in diverse applications, ranging from quality control in the food and pharmaceutical sectors to environmental monitoring and clinical diagnostics[381].

- **Interference Testing and Selectivity of the Ag NP/$Nb_4C_3T_x$ MXene-Modified Sensor for Riboflavin Detection**

The conducted interference test on the Ag NP/$Nb_4C_3T_x$ MXene-modified screen-printed electrode (SPE) yields significant insights on the robustness and selectivity of the sensor, particularly when applied to complicated real-world samples such as energy drinks. Within these beverages, a multitude of components are present alongside Riboflavin, encompassing Glucose, Ascorbic acid, Sucrose, Dopamine, Vitamin B12, and caffeine. Detailed research was conducted to assess the performance of the sensor in the presence of probable interferents as shown in **Figure *51***. The experiment commenced by conducting blank differential pulse voltammetry (DPV) observations in order to establish a stable electrochemical signal. Following this, a concentration of 100 nM Riboflavin was injected into the electrochemical cell, and further measurements using differential pulse voltammetry (DPV) were recorded. In order to replicate real-life situations, subsequent to this, each disruptive factor was delivered separately at three distinct concentrations: 100 nM, 500 nM, and 1 μM. Distinct sets of electrodes and electrochemical cells were allocated to each interferent, hence assuring stringent testing conditions. The key finding of this study was that none of the interfering substances tested had any impact on the differential pulse voltammetry (DPV) peak of 100 nM Riboflavin within the designated potential range utilised for Riboflavin analysis. The aforementioned outcome underscores the remarkable selectivity of the sensor, as each interfering molecule exhibits a unique range of oxidation potential that does not intersect with that of Riboflavin. Furthermore, the introduction of interfering chemicals did not result in any noteworthy modifications in the DPV peak of Riboflavin. The statement underscores the dependability of the Ag NP/$Nb_4C_3T_x$ MXene-modified Screen-Printed Electrode (SPE) technique, even when subjected to a combination of probable interfering substances typically found in energy beverages.

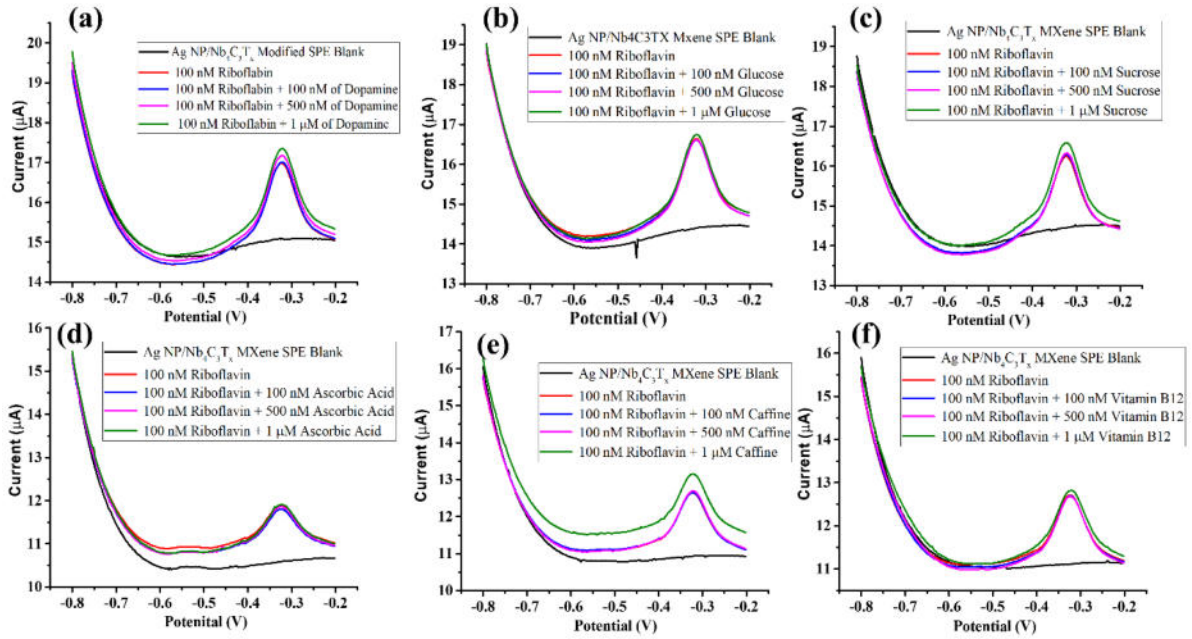

Figure 51: Effect of Interfering Agents on Riboflavin Detection: DPV Responses for (a) Dopamine, (b) Glucose, (c) Sucrose, (d) Ascorbic Acid, (e) Caffeine, and (f) Vitamin B12 at 100 nM, 500 nM, and 1 µM Concentrations.

The experimental conditions employed in this investigation were carefully regulated, involving the utilisation of an acetate buffer solution with a pH value of 4.5 and a preconcentration duration of 90 seconds. The results of this study highlight the capabilities of the electrochemical sensor in accurately and selectively detecting Riboflavin in complex sample matrices, including energy drinks. This suggests that the sensor holds promise for practical applications in the analysis of food and beverages. The bar graph (shown in **Figure *52***) depicting the interference measurements provides a comprehensive view of the fabricated electrochemical sensor's selectivity and robustness in the presence of potential interferents commonly found in energy drink samples. Each interfering agent, including ascorbic acid (100 nM: 99.23%, 500 nM: 104.58%, 1 µM: 106.58%), vitamin B12 (100 nM: 101.95%, 500 nM: 103.77%, 1 µM: 103.31%), caffeine (100 nM: 101.90%, 500 nM: 103.59%, 1 µM: 104.38%), dopamine (100 nM: 101.14%, 500 nM: 104.03%, 1 µM: 105.87%), glucose (100 nM: 103.04%, 500 nM: 104.12%, 1 µM: 106.52%), and sucrose (100 nM: 101.78%, 500 nM: 105%, 1 µM: 107.38%), was individually introduced at three different concentrations (100 nM, 500 nM, and 1 µM) in the electrochemical cell under the same experimental conditions. The reference point for comparison was the detection of 100 nM riboflavin, considered as 100%.

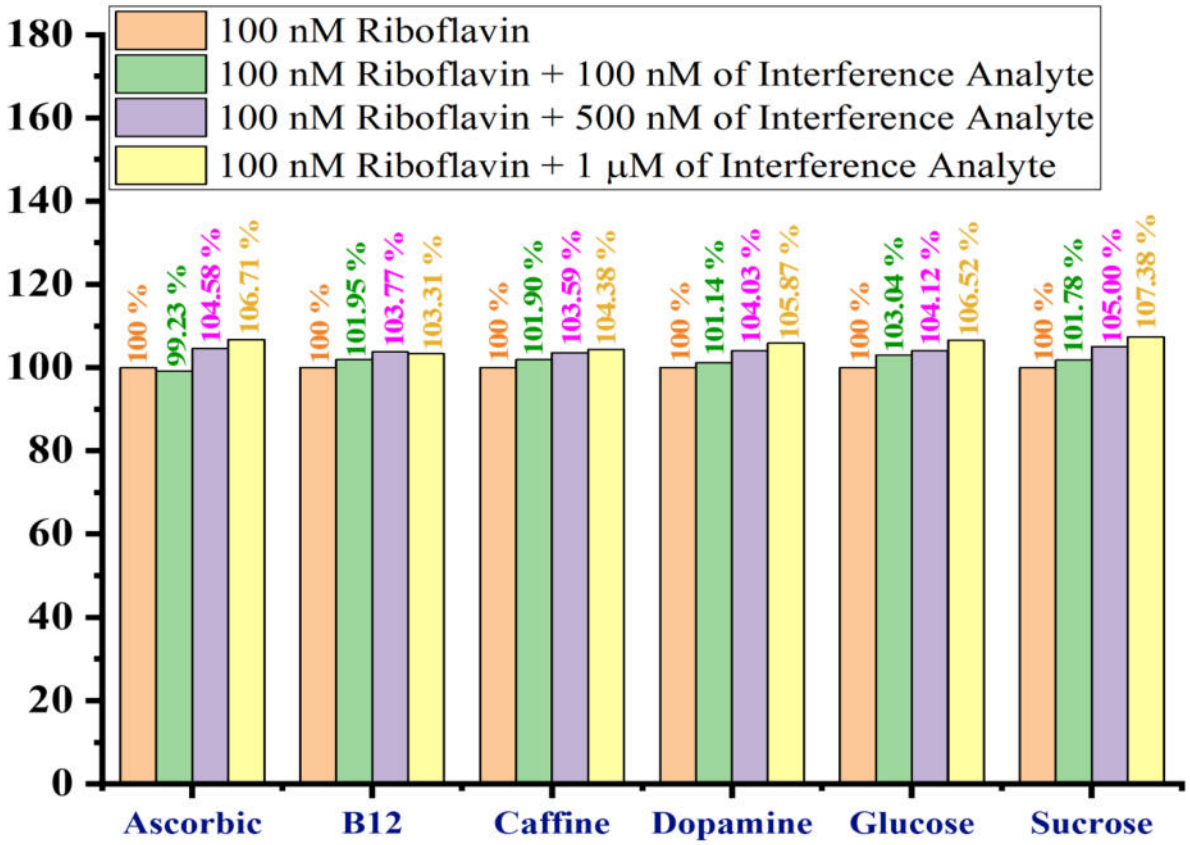

Figure 52 :Percentage interference levels of various analytes compared to 100 nM Riboflavin, demonstrating the selectivity of the Ag NP/$Nb_4C_3T_x$ MXene-modified sensor.

These results of the interference tests reveal the sensor's exceptional specificity for riboflavin even in the presence of these potential interferents. Notably, for all interfering agents and concentrations tested, the DPV peak corresponding to 100 nM riboflavin exhibited negligible variation. This implies that the electrochemical sensor's response to riboflavin remained essentially unaltered despite the presence of interfering substances. The slight fluctuations observed in some cases, typically within a range of 1-7%, were well within acceptable limits, demonstrating the sensor's robustness and selectivity for riboflavin detection. These findings underscore the reliability and practical utility of the Ag NP/$Nb_4C_3T_x$ MXene-modified SPE for accurate and interference-resistant determination of riboflavin in complex samples, such as energy drinks. The ability to discern riboflavin from potential interferents is vital in ensuring the accuracy of analytical results when assessing the riboflavin content in real-world samples, making this sensor a valuable tool in various applications, including quality control and nutritional analysis[380].

- **Performance Evaluation of Ag NP/$Nb_4C_3T_x$ MXene-Modified SPE for Riboflavin Detection**

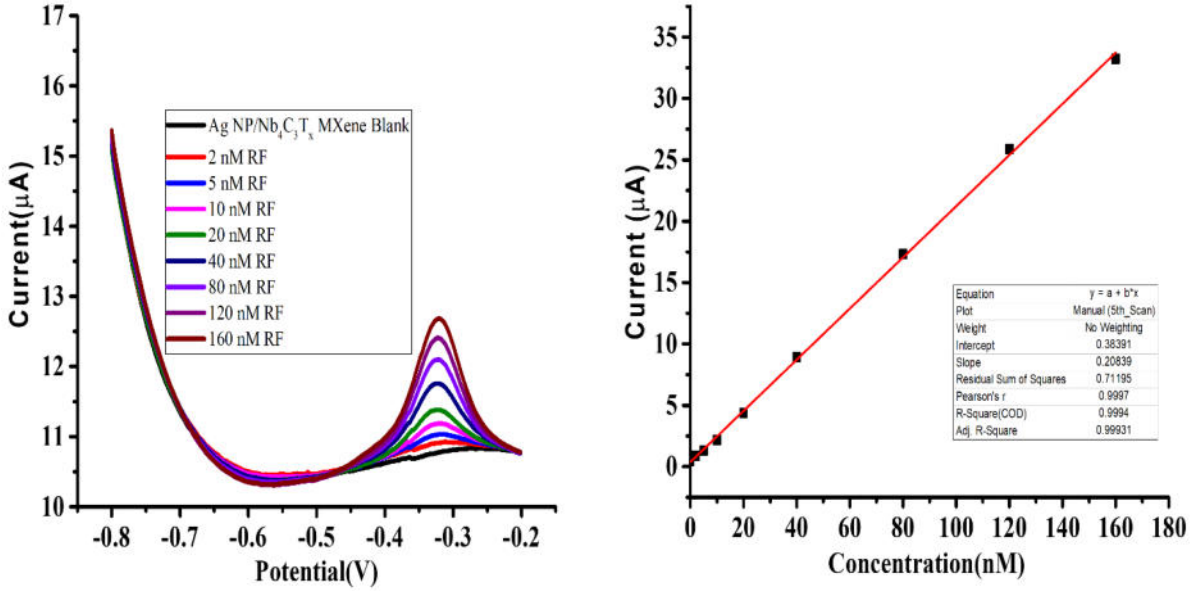

Figure 53: DPV and Calibration plot illustrating the electrochemical response of the Ag NP/$Nb_4C_3T_x$ MXene-modified SPE to various Riboflavin concentrations, demonstrating exceptional sensitivity, a low limit of quantification (LOQ), and a high degree of linearity.

The utilisation of the calibration plot is of utmost importance in the assessment of the Ag NP/ $Nb_4C_3T_x$ MXene-modified Screen-Printed Electrode (SPE) technique for Riboflavin detection. This plot (Shown in **Figure *53***) enables the evaluation of many key parameters that are vital for determining the analytical capabilities of the technique. The present investigation involved the thorough execution of Differential Pulse Voltammetry (DPV) measurements, which yielded a calibration plot that offered useful insights into the performance of the sensor. The essential parameter of the sensor is its sensitivity, which has been calculated to be -0.0094 μA/nM. Sensitivity refers to the capacity of the sensor to perceive even subtle variations in Riboflavin concentrations. A greater sensitivity value highlights the sensor's capacity to promptly and accurately measure Riboflavin concentrations over a broad range of values. This characteristic is especially advantageous in contexts where precise quantification of analyte concentrations, such as Riboflavin, is of utmost importance[374]. The significance of the defined limit of quantification (LOQ) at 5 nM cannot be overstated. The limit of quantification (LOQ) denotes the minimum concentration of Riboflavin that can be accurately measured, hence indicating the sensor's capacity to detect and quantify Riboflavin at low concentrations with precision. The aforementioned characteristic holds significant value in situations involving samples that include minute quantities of the analyte[371].

In addition, the crucial parameter of interest is the limit of detection (LOD), which has been determined to be 1.66 nM by calculations. The limit of detection (LOD) refers to the minimum concentration of Riboflavin that can be detected by the sensor, however its quantifiability may not be accurate. The significance of this parameter becomes especially critical when analysing samples that require the confirmation of Riboflavin existence, even at exceedingly low levels. The calibration plot exhibits linearity, as evidenced by the high coefficient of determination (R^2) of 0.99838, indicating a strong correlation between the sensor's response and the quantity of Riboflavin. The property of linearity is crucial in ensuring that the output of the sensor is directly proportional to the concentration of the analyte. This characteristic simplifies the process of quantification and improves the dependability of the sensor. In the course of these studies, a uniform preconcentration duration of 90 seconds and an electrolyte solution with a pH value of 4.5 were utilised. The findings presented collectively underscore the dependability and effectiveness of the Ag NP/$Nb_4C_3T_x$ MXene-modified Screen-Printed Electrode (SPE) technique in accurately quantifying Riboflavin levels. The sensor demonstrates remarkable sensitivity, a low limit of quantification, and a high level of linearity, rendering it a potential option for a range of applications that necessitate precise detection of Riboflavin, especially in situations where analysis at trace levels is of utmost importance.

- **Real Sample Analysis: Validating the Utility of the Ag NP/$Nb_4C_3T_x$ MXene-Modified SPE for Riboflavin Detection**

The practicality and accuracy of the Ag NP/$Nb_4C_3T_x$ MXene-modified Screen Printed Electrode (SPE) for detecting Riboflavin were further confirmed by analysing real samples. In this study, a commercially available energy drink was used as a test matrix. Two separate spike concentrations of Riboflavin were utilised, facilitating an assessment of the sensor's efficacy in analysing intricate samples from the real world. In the initial experimental setup, a solution containing Riboflavin at a concentration of 10 nM was added to the energy drink. Subsequently, a sequence of differential pulse voltammetry (DPV) measurements was conducted at predetermined concentrations of 10 nM, 20 nM, and 30 nM. A DPV measurement was conducted for each concentration addition, and the obtained data was utilised to create a calibration plot that is specific to the DPV scan. The Riboflavin concentration at a spike concentration of 10 nM was determined to be around 16.49 nM based on the calibration plot

(**Figure *54***). Likewise, in the case of the 20 nM spike concentration (**Figure *55***), the resultant concentration was determined to be around 48.02 nM after to the addition. The concentrations obtained following the addition of a known amount of substance and subsequent analysis were approximately 6.614 nM and 24.58 nM, respectively. This resulted in recovery percentages of 99.25% and 107.7%. The results indicate the effectiveness of the Ag NP/ $Nb_4C_3T_x$ MXene-modified Screen-Printed Electrode (SPE) in accurately detecting Riboflavin in authentic samples. These findings underscore the prospective usefulness of this modified SPE in real-world analytical scenarios.

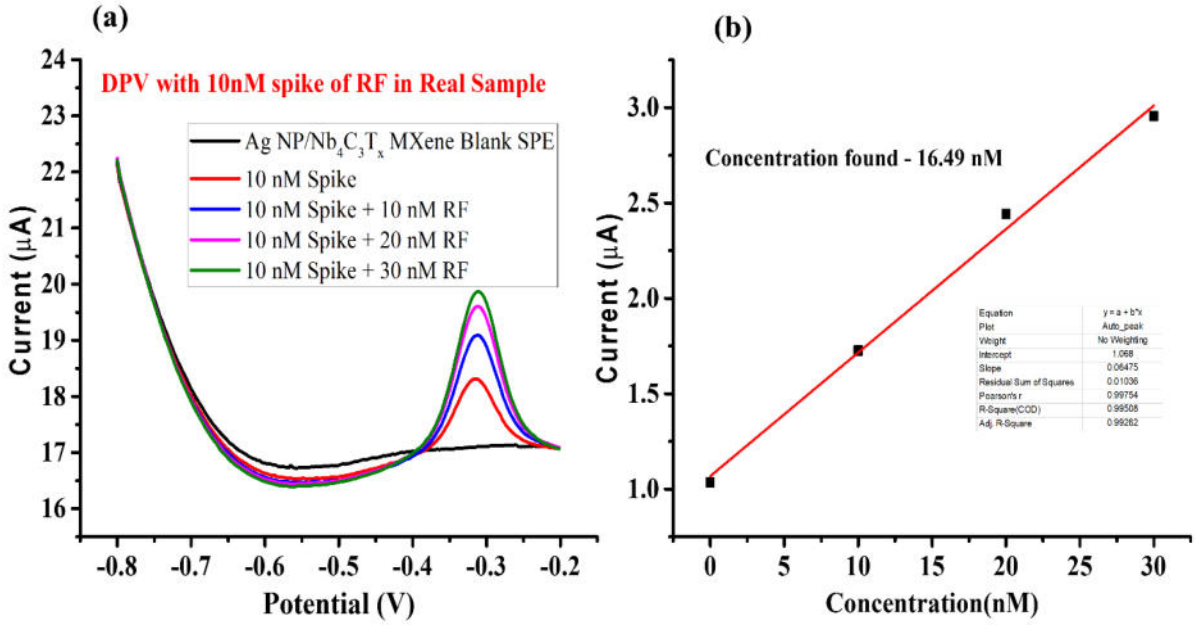

Figure 54: Differential Pulse Voltammetry (DPV) measurements and corresponding calibration plot for riboflavin detection in a real energy drink sample with a 10 nM riboflavin spike.

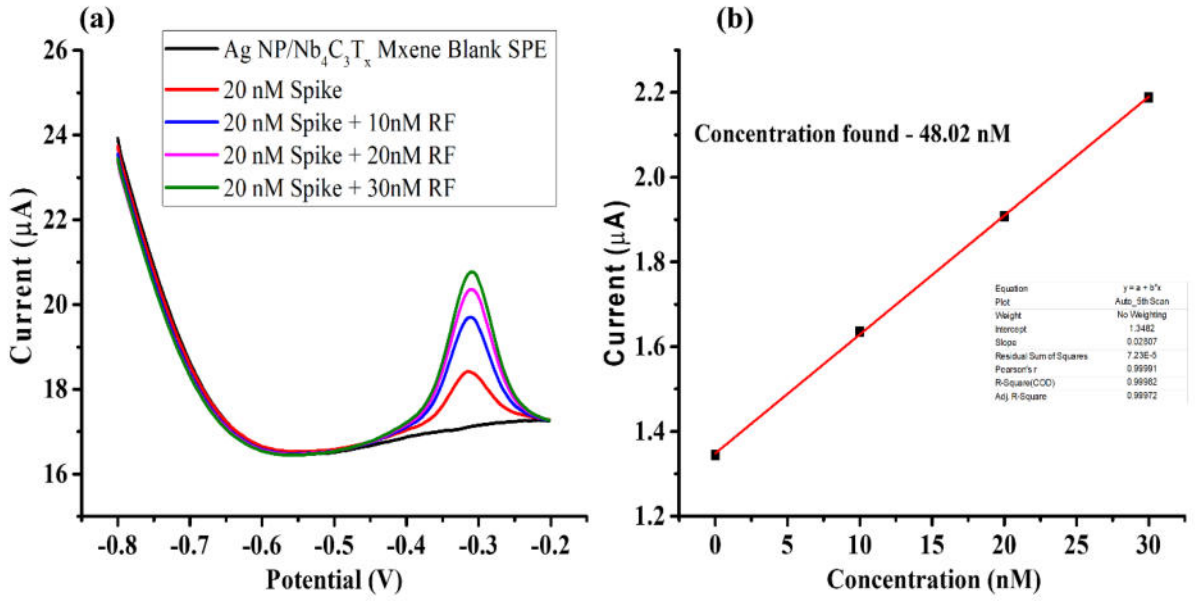

Figure 55: Differential Pulse Voltammetry (DPV) measurements and corresponding calibration plot for riboflavin detection in a real energy drink sample with a 20 nM riboflavin spike.

The examination of actual samples plays a vital role in verifying the practical effectiveness and dependability of any analytical sensor or methodology. Conducting real sample analysis in the context of the Ag NP/$Nb_4C_3T_x$ MXene-modified Screen-Printed Electrode (SPE) for Riboflavin detection serves multiple crucial objectives. To begin with, it is important to note that real samples, such as the energy drink utilised in this investigation, typically encompass an intricate matrix comprising diverse chemicals and constituents. The act of subjecting the sensor to these samples serves to replicate real-world situations and offers valuable observations regarding the sensor's efficacy when confronted with potential sources of interference. The experiment showcases the sensor's selectivity, specificity, and capacity to differentiate the analyte of interest (Riboflavin) from other constituents often present in energy drinks. Furthermore, the practical applicability of the sensor is strongly influenced by the precision of its measurements in real samples. Individuals use energy drinks with the intention of obtaining the promoted nutritional advantages, such as the presence of Riboflavin. Accurate determination of the concentration of Riboflavin in these products is of utmost importance for purposes of quality control and providing consumers with relevant information. Furthermore, empirical sample analysis demonstrates the sensor's sensitivity and capacity for capturing a wide range of values. In order to assess the sensor's efficacy throughout a range of concentrations, it is necessary to introduce predetermined quantities of Riboflavin into the energy drink. This is particularly important for scenarios where the analyte's concentration

exhibits significant variability. The inclusion of actual samples also functions as a means of validating the calibration curve of the sensor, so ensuring the durability and applicability of the correlation established between the sensor's response and the concentration of Riboflavin in real-life situations.

Table 4: Recovery % of fabricated electrochemical sensor with real sample analysis in commercially purchased energy drink.

Real Sample	Found Concentration	Spiked Concentration	Concentration after addition	Recovery (%)
Energy Drink 1	6.614 nM	10 nM	16.49 nM	99.25 %
Energy Drink 2	24.58 nM	20 nM	48.02 nM	107.7 %

The successful detection of Riboflavin in real samples, as exemplified by the implementation of the Ag NP/$Nb_4C_3T_x$ MXene-modified Screen-Printed Electrode (SPE) technique, highlights its considerable potential for many practical applications. The sensor's capacity to precisely and consistently identify Riboflavin in intricate, real-life samples, whether in the food sector for quality control, in healthcare for nutritional assessment, or in research for environmental monitoring, serves as evidence of its analytical proficiency and significance[382]. This exemplar analysis not only demonstrates the capabilities of the sensor but also lays the foundation for its incorporation into other domains where the determination of Riboflavin is crucial, emphasising its importance as a versatile and reliable analytical instrument[374].

4.5 Concluding Remarks and Summary

The achievement of synthesising Ag NP/$Nb_4C_3T_x$ MXene materials by the unique technique of molten salt etching represents a significant milestone in the field of materials science. The employed methodology not only obviates the requirement for strong acids but also presents a sustainable approach with a multitude of benefits, such as scalability, ecological compatibility, exceptional purity, and adjustable characteristics. The maintenance of MXene sheet integrity during this process guarantees its suitability in several domains, ranging from energy storage to state-of-the-art sensors. The synthesis process described below is a multifaceted procedure that encompasses various technical steps. It commences with a solid-state reaction and culminates in a controlled nitrogen environment heat treatment. This heat treatment facilitates the change from MAX to MXene. The subsequent washing procedures, which include

solubility tests, magnetic stirring, pH adjustment, filtration, and drying, result in the production of a refined MXene product. Every individual stage in this process is crucial in guaranteeing the ultimate quality and appropriateness of the final material for diverse applications. Analytical methodologies, such as X-ray diffraction (XRD), are employed to elucidate the structural modifications that transpire during the process of synthesis. The X-ray diffraction (XRD) patterns of the Nb_4AlC_3 precursor exhibit a notable transition, wherein the majority of the Nb_4AlC_3 peaks disappear and are replaced by separate peaks corresponding to the (00l) crystallographic planes. The observed shifts in the sample indicate the effective transformation into $Nb_4C_3T_x$ MXene. This transformation is further emphasised by the noticeable increase in the gap between layers, a characteristic feature of two-dimensional MXene structures. The observation of distinct metallic silver peaks in the X-ray diffraction (XRD) patterns provides compelling evidence on the effectiveness of the etching procedure. Additional insights on the transition from MAX phase to MXene can be obtained through the utilisation of Scanning Electron Microscopy (SEM) studies. The MAX phase is characterised by a three-dimensional structure that displays distinct grain boundaries. In contrast, the Ag NP/$Nb_4C_3T_x$ MXene has a two-dimensional arrangement with several layers, indicating successful exfoliation. Energy-Dispersive X-ray Spectroscopy (EDS) plays a crucial role in verifying alterations in composition. The Nb_4AlC_3 MAX phase exhibits a decrease in aluminium concentration while experiencing a rise in niobium concentration. This observation strongly suggests the selective elimination of the lighter aluminium and carbon layers. A notable change is noticed in the carbon content, increasing from 23.64% to 78.214%. The substantial rise in this phenomenon can be ascribed to the removal of aluminium, so exposing layers of MXene that are rich in carbon. The observed deviations in the carbon-to-niobium (C:Nb) ratio suggest the presence of surface terminations, flaws, or structural modifications in the $Nb_4C_3T_x$ MXene material. The study of EDS enables a thorough comprehension of the various changes in structure and composition that occur during the synthesis of MXene. In brief, the utilisation of molten salt etching demonstrates a potentially advantageous pathway for the production of MXenes while minimising adverse environmental effects. The rigorous and thorough analytical methods employed in this procedure shed light on the successful transformation of Nb_4AlC_3 into a two-dimensional $Nb_4C_3T_x$ MXene, with features that are highly suitable for many applications. The exploration of materials science in this context presents opportunities for the development of sustainable and precise materials, with a concurrent focus on minimising the environmental impact. The statement serves as evidence of the ever-changing nature of scientific advancement.

Transitioning the discussion, attention is redirected towards the design and characterisation of an electrochemical sensor specifically designed for the purpose of detecting H_2O_2. This unpretentious molecule is intricately integrated into numerous sectors, encompassing paper and textile production, electronics, and chemical synthesis. Within the field of healthcare, the accurate quantification of H_2O_2 plays a pivotal role in the identification and diagnosis of enzymatic abnormalities and many illnesses that arise as a result of oxidative stress. Moreover, the level of H_2O_2 concentration might serve as an indicative indicator of latent medical diseases such as infections, cancer, and neurological illnesses. In addition to the field of healthcare, the process of environmental monitoring heavily relies on the precise detection of H_2O_2 in order to assess the oxidative condition of ecosystems and to identify potential environmental pollutants. In the context of the rapidly expanding clean energy sector, H_2O_2 is gaining prominence as an environmentally friendly fuel option that plays a crucial role in fuel cell technology. In response to the diverse range of applications for H_2O_2, an electrochemical sensor has emerged as a prominent solution. The sensor exploits the distinctive characteristics of silver nanoparticles (Ag NP) deposited on a surface of niobium carbide ($Nb_4C_3T_x$) MXene. The present tale initiates an academic exploration, opening with a comprehensive comparative examination of Cyclic Voltammetry (CV) methodology between a conventional Screen-Printed Electrode (SPE) and the modified Ag NP/$Nb_4C_3T_x$ SPE. The range of potential from -1V to 0.3V is utilised as a means to examine and analyse the electrochemical characteristics of these electrodes. The unaltered SPE narrative portrays a restricted level of electrochemical reactivity, as seen by the nearly flat cyclic voltammetry (CV) curve. The initial restrained reaction establishes the basis for further improvements via electrode adjustment. In sharp contrast, the Ag NP/$Nb_4C_3T_x$-modified MXene electrode exhibits distinct redox peaks around 0.16V and -0.06V, indicating its enhanced electrochemical activity. The observed peaks serve as significant markers of oxidation and reduction reactions involving silver nanoparticles (Ag NPs), and they represent the electrochemical reactivity of the electrode. At this particular point, the electrode's aptness for detecting H_2O_2 becomes evident. The written discourse effortlessly shifts into the domain of electrochemical H_2O_2 detection utilising the Ag NP/$Nb_4C_3T_x$-modified MXene, beginning on a series of cyclic voltammetry (CV) studies. Two significant experiments are conducted, with the first experiment serving as the basis for comprehending the behaviour of the electrode, in which H_2O_2 is not present. The redesigned electrode surface demonstrates the fascinating interplay of oxidation and reduction processes of Ag NPs, as seen by the redox

peaks observed at 0.16V and -0.06V. The current scenario is now prepared for the injection of the 5mM H_2O_2 solution. The narrative presents a visually descriptive account of the emergence of a reduction peak at around 0.72V, which serves as a conclusive indication of successful H_2O_2 detection. The chosen potential range is identified as the optimal point, precisely calibrated for this specific objective. The subsequent portion of the narrative explores the domain of chronoamperometry, which is a basic technique in the field of electrochemistry. The procedure entails the ongoing observation of electric current at a consistent potential, namely at -0.4V, as a function of time. The process under consideration involves the intricate movement of electrons, which plays a crucial role in the identification of H_2O_2, ultimately leading to its transformation into water and oxygen. The chronoamperometric data reveal a distinct pattern, characterised by fluctuations in current that correspond to the changing concentrations of H_2O_2 added to the solution. The aforementioned performance highlights the sensor's aptitude to adjust and react to the constantly fluctuating levels of H_2O_2. In order to enhance comprehension, the utilisation of a calibration plot is observed. Based on the analysis of current measurements and H_2O_2 concentrations, the plot presented in this study serves as a reliable tool for precise quantification, as it demonstrates a strong correlation ($R^2 = 0.99938$) that supports the underlying mechanism. Ultimately, the electrochemical sensor that has been upgraded with Ag NP/$Nb_4C_3T_x$ demonstrates its robustness as a vigilant guardian, protecting the thresholds of H_2O_2 detection with exceptional sensitivity and selectivity. The cyclic voltammetry (CV) analysis demonstrates the dynamic redox behaviour of silver nanoparticles (Ag NPs) on the surface of the electrode, revealing the improved performance resulting from the alteration. The sensitivity of the sensor to hydrogen peroxide (H_2O_2) is revealed by the use of chronoamperometric analysis, which highlights a strong linear correlation between the current and the concentration of H_2O_2. The sensor exhibits exceptional sensitivity, characterised by a remarkably low Limit of Detection (LOD) of 58.78 µM. The key principle emphasised in this context is accuracy. The calibration plot, accompanied with analytical data, serves as evidence of its exceptional performance, establishing it as a versatile instrument suitable for a wide range of applications, including environmental monitoring and clinical diagnostics.

Now, directing our focus towards riboflavin (Vitamin B2), we commence an exploration that unveils the complex interconnections of this indispensable component inside several realms of existence. Riboflavin assumes a crucial function in energy metabolism and cellular growth, as well as in the maintenance of overall well-being, so establishing itself as an essential and inconspicuous participant. The narrative is set in the field of food analysis, with a focus on the

role of riboflavin in evaluating the nutritional content, freshness, and stability of various food items. It plays a crucial role in the operational framework of ensuring food safety and maintaining quality control. Riboflavin is extensively utilised in many pharmaceutical medications and dietary supplements within the pharmaceutical industry. In this context, the prioritisation lies in the accurate measurement and quantification, which serves the purpose of meeting regulatory requirements and achieving desired treatment outcomes. Nevertheless, the function of riboflavin extends beyond its application in laboratory settings and extends into the domain of clinical diagnostics. The timely detection and treatment of riboflavin-related health issues are contingent upon this crucial factor. This chapter delves extensively into analytical techniques that have been specifically developed to elucidate the intricate properties and characteristics of riboflavin. The focus of attention lies on the utilisation of niobium carbide ($Nb_4C_3T_x$) platforms, which are decorated with silver nanoparticles (Ag NP), in the context of electrode applications. This essay highlights the significance of electrochemical sensors as highly efficient tools that enhance accuracy, sensitivity, and efficiency in the detection of riboflavin. This study primarily examines the application of Cyclic Voltammetry (CV) analysis in investigating the electrocatalytic properties of Ag NP/$Nb_4C_3T_x$-modified electrodes for the purpose of riboflavin detection. The alteration revitalises the electrodes, imbuing them with enhanced electrochemical reactivity. It's in the presence of riboflavin that the modified electrode truly shines, with CV curves that tell an appealing story. The electrode in question assumes an active role in the process of riboflavin detection, exerting a significant influence on the outcome. This holds true whether the detection is carried out within the realm of food quality control or in the field of clinical diagnostics. The exploration doesn't stop here. Differential Pulse Voltammetry (DPV) has gained significant attention due to its ability to highlight the enhanced performance of Ag NP/$Nb_4C_3T_x$-modified electrodes compared to their ancestors. The key to achieving this level of perfection can be attributed to the improved dispersion, increased conductivity, and enhanced electrocatalytic characteristics. These attributes imbue vitality into a proficient framework for the detection of riboflavin. The expedition temporarily halts to engage in introspection, focusing on the period of preconcentration as a pivotal factor in the pursuit of increased sensitivity. The narrative suggests the existence of an ideal preconcentration time, with 90 seconds being identified as the golden figure. This duration achieves an optimal equilibrium between the accumulation of analytes and the efficiency of the sensor.

The examination of pH's influence on riboflavin detection is subject to careful analysis. The research uncovers a fascinating discovery. Under mildly acidic conditions with a pH of 4.5, particularly in the presence of an acetate buffer, the riboflavin's redox reactions on the Ag NP/$Nb_4C_3T_x$-modified sensor are highly favourable. It is important to consider the fundamental aspects of reproducibility and repeatability. The primary importance lies in guaranteeing the consistency and reliability of the sensor modified with Ag NP/$Nb_4C_3T_x$. The aforementioned attributes render it a reliable instrument in several contexts, ranging from the assessment of food quality to the field of clinical diagnostics. The selectivity of the sensor is a characteristic that withstands rigorous scrutiny without being compromised. The sensor demonstrates a high level of resilience, since it effectively withstands interference caused by a range of compounds usually present in energy drinks. The demonstrated durability of the sensor highlights its ability to accurately detect riboflavin even in the presence of intricate sample matrices. The narrative reaches its climax upon the revelation of the calibration scheme. In this context, the sensor's ability to reliably measure riboflavin concentrations throughout a wide range is effectively demonstrated through the integration of sensitivity, the limit of quantification (LOQ), and linearity. The attribute of sensitivity, which is commonly associated with accuracy, exhibits an impressive value of -0.0094 μA/nM. The sensor's impressive capabilities are highlighted by its limit of quantification (LOQ) of 5 nM and limit of detection (LOD) of 1.66 nM, which enable it to accurately detect and measure low amounts of riboflavin. The sensor's efficacy is brought to the forefront, thus completing the story and providing real-world validation. The sensor demonstrates its effectiveness in the examination of a genuine energy drink sample. The results oftheis study present a strong case for the potential of the Ag NP/$Nb_4C_3T_x$-modified sensor in various situations, confirming its significance and practical usefulness in a wide range of applications, including food quality control and clinical diagnostics. To summarise, the utilisation of molten salt etching in the synthesis of MXene materials demonstrates the potential of sustainable materials design. The electrochemical sensor utilised in the detection of H_2O_2 demonstrates enhanced precision and sensitivity, hence providing a versatile instrument suitable for a wide range of applications. The examination of riboflavin delves into the realm of essential chemical identification, highlighting a sensor that has the capacity to revolutionise various domains such as food quality assurance and clinical diagnostics. These articles do not merely function as independent sections; rather, they embody a more comprehensive narrative of creativity, advancement, and flexibility when confronted with intricate obstacles.

CHAPTER 5: CONCLUSION AND PERSPECTIVE

This thesis explores the diverse applications of MXene materials in the fields of science and technology, delving into their potential and significance. The investigation commenced with a thorough analysis of MXene production, a complex procedure that exploits the distinct characteristics of MAX phases, effectively combining metallic and ceramic properties in novel manners. Our study delved into the process of etching, with a specific emphasis on two significant techniques: the conventional acid etching method and the innovative molten salt etching approach. These methodologies exhibit unique traits, benefits, and great prospects for the future. The synthesis of the Nb_2SnC MAX phase was thoroughly described, including detailed procedures such as mechanical blending, milling, pellet creation, controlled heat treatment, and post-synthesis powderization. The accuracy in carrying out these operations is of utmost importance in producing a versatile material with significant potential in various scientific and technical fields. A crucial element of our study involved the formulation of an alternate approach that circumvents the use of hydrofluoric acid (HF), a substance associated with a multitude of difficulties and hazards. Our research team successfully developed a pioneering method that utilises phosphoric acid to facilitate the progressive conversion of MAX phase material into the highly desirable Nb_2CTx MXene compound. This development represents a notable advancement in the field of MXene synthesis, providing a safer and more regulated alternative. Moreover, we explored the realm of electrode alteration by the utilisation of the drop-cast approach. The aim of our study was to achieve a high level of accuracy and efficiency by emphasising the even distribution and reliable adherence of etched Nb_2CTx MXene onto electrode surfaces. The careful execution of this systematic process established the fundamental basis for our subsequent investigation into the electrochemical potential of MXenes. The scope of our scientific investigation involved a comprehensive examination of the structural and morphological characteristics of the synthesised Nb_2SnC MAX phase and Nb_2CTx MXenes. By utilising a range of methodologies, such as Energy Dispersive Spectroscopy (EDS), X-ray Diffraction (XRD), Scanning Electron Microscopy (SEM), X-ray Photoelectron Spectroscopy (XPS), and Transmission Electron Microscopy (TEM), we have acquired significant knowledge regarding the composition, structure, and surface chemistry of these materials. The acquisition of this fundamental information establishes the framework for subsequent utilisation in the fields of electrochemical sensing and energy storage. The

exploration of electrochemical examination in our study was similarly captivating, with a specific emphasis on the potential of Nb_2CT_x, a synthesised MXene compound based on niobium. The MXene material exhibited exceptional supercapacitive characteristics. The effectiveness of charge storage was underscored by the remarkable capacitance and quick ion response observed in the Cyclic Voltammetry (CV) tests, even at elevated scan rates. The results obtained from galvanostatic charge-discharge (GCD) tests provide evidence of a significant preservation of specific capacitance values at different current densities. The utilisation of electrochemical impedance spectroscopy (EIS) unveiled a decrease in electrode resistance, indicating enhanced electrochemical kinetics, electronic conductivity, and charge-transfer abilities. In brief, the remarkable supercapacitive performance of 2D Nb_2CT_x MXene can be ascribed to its distinctive structure, surface functional groups, and interlayer gap, which combined augment charge storage and rate capacities. In conclusion, this chapter has provided the necessary knowledge base to explore the electrochemical potential of Nb_2CT_x MXene in many applications, focusing specifically on electrochemical sensing and energy storage fields. This exploration serves as a foundational platform for future studies and developments in this dynamic and transformative topic. When considering the future, the possibilities are boundless. MXenes have the potential to significantly transform various industries, including energy storage and electrochemical sensing. With every new finding, we make progress towards unravelling the complete capabilities of these extraordinary substances, thereby facilitating advancements that will profoundly influence the trajectory of scientific and technological development. The future trajectory is imbued with a sense of anticipation, and it is incumbent upon us to persist in the pursuit of exploration, innovation, and the expansion of the limits of MXenes' potential. This thesis encompasses a range of advanced advancements in materials science and analytical chemistry, alongside our investigation of MXene materials. Our research encompassed the synthesis of MXene materials, the design and fabrication of an electrochemical sensor for the detection of hydrogen peroxide (H_2O_2), and a comprehensive investigation into the diverse implications of riboflavin (Vitamin B2) analysis. In conclusion, this study synthesises the many perspectives obtained from these inquiries and elucidates their ramifications and potential future developments.

The Utilisation of MXene Materials: A Promising Avenue towards Sustainability and Innovation

The process of synthesising MXene materials, specifically Ag NP/$Nb_4C_3T_x$, from the Nb_4AlC_3 MAX phase using molten salt etching, represents a significant advancement in the field of materials science. This method holds immense importance. This methodology not only provides a sustainable alternative to conventional acid-based methods but also enables the precise manipulation of materials, hence opening up a wide range of potential applications. Molten salt etching offers several notable advantages in the field of materials engineering. These advantages encompass scalability, selectivity, reduced environmental impact, high purity, increased crystallinity, faster processing, and customizable characteristics. Consequently, molten salt etching establishes novel benchmarks within the discipline. This method is not solely focused on the creation of materials; rather, it serves as evidence of our dedication to sustainable practises, in line with the worldwide push for environmentally friendly and ethically responsible scientific endeavours. The effectiveness of molten salt etching is highlighted by the structural changes identified via X-ray diffraction (XRD) analysis and the morphological transitions revealed through Scanning Electron Microscopy (SEM). The utilisation of these analytical approaches is of utmost importance in the characterization of the transition from the voluminous MAX phase, characterised by its three-dimensional structures, to the two-dimensional MXene, as exemplified by the Ag NP/$Nb_4C_3T_x$ material. Energy-Dispersive X-ray Spectroscopy (EDS) enhances our comprehension by elucidating alterations in composition, highlighting the selective elimination of lighter components like aluminium and carbon, and the increase in carbon concentration, which is crucial for the formation of carbon-rich MXene layers. The extensive knowledge and understanding provided by these comprehensive insights lay the foundation for a transformative period in the field of materials engineering. The field of electrochemical sensing provides a valuable avenue for achieving accurate and precise detection capabilities. The interdisciplinary nature of scientific research is exemplified by the creation of an electrochemical sensor, where silver nanoparticles (Ag NP) are immobilised on a surface composed of niobium carbide ($Nb_4C_3T_x$) MXene. The development of this sensor, which has been meticulously designed for the purpose of detecting hydrogen peroxide (H_2O_2), highlights the significant significance of precise and reliable analytical methodologies. Hydrogen peroxide (H_2O_2) plays a significant and influential role in various industries, ranging from healthcare to clean energy. The sensor being described has outstanding levels of sensitivity and selectivity. The present study highlights the importance of innovation through a comparative investigation of cyclic voltammetry (CV) between a conventional Screen-Printed Electrode (SPE) and a modified SPE with Ag NP/$Nb_4C_3T_x$. Although the unmodified SPE faces challenges in demonstrating significant electrochemical

reactivity, the modified electrode surpasses these limitations by exhibiting clear redox peaks. Consequently, the modified electrode establishes itself as a superior platform for the detection of hydrogen peroxide (H_2O_2). The sensor's capabilities are further highlighted by subsequent electrochemical measurement of H_2O_2 using cyclic voltammetry (CV) and chronoamperometry techniques. This electrochemical breakthrough is dedicated to the accurate and responsive detection of H_2O_2, which plays a critical role in a wide range of applications, including healthcare and environmental monitoring. The sensor's potential as a flexible tool in our analytical arsenal is reaffirmed by its great accuracy, as demonstrated by the calibration curve, and its low Limit of Detection (LOD) of 58.78 μM.

Analysis of Riboflavin: From Nutritional Evaluation to Therapeutic Applications

The investigation into the analysis of riboflavin (Vitamin B2) presents a wide range of potential applications, encompassing areas such as food analysis, medicines, and clinical diagnostics. The significance of riboflavin in evaluating the nutritional adequacy and safety of food products cannot be overemphasised. In the field of pharmaceuticals, accurately quantifying a substance is not only necessary to meet regulatory requirements, but also essential for ensuring therapeutic effectiveness. Furthermore, the detection of riboflavin is essential for promptly identifying and treating health issues associated with its insufficiency. The sensor modified with Ag NP/$Nb_4C_3T_x$, which is a result of advanced electrochemical research, demonstrates its efficacy in the analysis of riboflavin. The sensor demonstrates notable sensitivity, as evidenced by the calibration plot, and its strong performance is emphasised by its low Limit of Quantification (LOQ) of 5 nM and Limit of Detection (LOD) of 1.66 nM. The ability of the sensor to exhibit selectivity towards common interferents, including those commonly present in energy drinks, is a significant achievement within the field of analytical chemistry. Cultivating the Foundations of Innovation In today's rapidly evolving world, fostering an environment that nurtures innovation has become a critical aspect of organisational success. This perspective explores the significance of cultivating the seeds of innovation and highlights the key factors that contribute to its growth and development. By understanding Upon contemplation of our trajectory, it becomes apparent that these advancements are not solely scientific achievements; rather, they serve as the catalysts for innovative progress. They have the capacity to generate innovative applications and have an influence on several fields, ranging

from the development of environmentally friendly energy resources to the creation of extremely accurate diagnostic equipment. The utilisation of interdisciplinary methodologies in research is a testament to the efficacy of joint efforts, and it is expected that there will be further exchange and integration of ideas within the scientific community. It is anticipated that there will be further advancements in utilising MXenes for various applications beyond the scope of those already mentioned, hence leading to significant transformations in domains such as energy storage and the facilitation of new sensing technologies. The electrochemical sensor designed for the detection of hydrogen peroxide (H_2O_2) exhibits notable sensitivity and versatility, rendering it suitable for various applications in healthcare, such as facilitating early disease diagnosis, as well as in environmental monitoring for rapid detection of toxins. The riboflavin analysis approach, characterised by its notable sensitivity and selectivity, holds great potential for advancements in the domains of food safety, medicine research, and the detection of health issues. As our comprehension of the involvement of riboflavin in diverse biological processes becomes more profound, novel potential applications may arise.

In summary, this thesis presents the potential for a future in which sustainability and precision converge, leading to innovative applications in several domains. The responsibility of further scientific investigation is now transferred, and we anticipate with enthusiasm the emergence of innovative intellects who will propel it farther. The future harbours intriguing prospects, driven by the principles of inquisitiveness, ingenuity, and conscientious scientific practises. The culmination of a particular voyage signifies the commencement of a subsequent one.

REFERENCES

[1] M. F. Ashby, P. J. Ferreira, and D. L. Schodek, *Nanomaterials, nanotechnologies and design: An introduction for engineers and architects*. 2009.

[2] K. Gajanan and S. N. Tijare, "Applications of nanomaterials," *Mater. Today Proc.*, vol. 5, no. 1, pp. 1093–1096, 2018, doi: 10.1016/j.matpr.2017.11.187.

[3] J. R. Siqueira and O. N. Oliveira, "Carbon-based nanomaterials," *Nanostructures*, pp. 233–249, 2017, doi: 10.1016/B978-0-323-49782-4.00009-7.

[4] K. Scida, P. W. Stege, G. Haby, G. A. Messina, and C. D. García, "Recent applications of carbon-based nanomaterials in analytical chemistry: Critical review," *Anal. Chim. Acta*, vol. 691, no. 1–2, pp. 6–17, 2011, doi: 10.1016/j.aca.2011.02.025.

[5] H. Aydın, F. Yakuphanoglu, and C. Aydın, "Al-doped ZnO as a multifunctional nanomaterial: Structural, morphological, optical and low-temperature gas sensing properties," *J. Alloys Compd.*, vol. 773, pp. 802–811, 2019, doi: 10.1016/j.jallcom.2018.09.327.

[6] A. T. Babu and R. Antony, "Green synthesis of silver doped nano metal oxides of zinc & copper for antibacterial properties, adsorption, catalytic hydrogenation & photodegradation of aromatics," *J. Environ. Chem. Eng.*, vol. 7, no. 1, 2019, doi: 10.1016/j.jece.2018.102840.

[7] M. Bangal *et al.*, "Semiconductor nanoparticles," *Hyperfine Interact.*, vol. 160, no. 1–4, pp. 81–94, 2005, doi: 10.1007/s10751-005-9151-y.

[8] N. Sharma, V. Sharma, S. K. Sharma, and K. Sachdev, "Gas sensing behaviour of green synthesized reduced graphene oxide (rGO) for H2 and NO," *Mater. Lett.*, vol. 236, pp. 444–447, 2019, doi: 10.1016/j.matlet.2018.10.145.

[9] R. Barstugan, M. Barstugan, and I. Ozaytekin, "PBO/graphene added β-PVDF piezoelectric composite nanofiber production," *Compos. Part B Eng.*, vol. 158, pp. 141–148, 2019, doi: 10.1016/j.compositesb.2018.09.059.

[10] R. Ghosh Chaudhuri and S. Paria, "Core/shell nanoparticles: Classes, properties, synthesis mechanisms, characterization, and applications," *Chem. Rev.*, vol. 112, no. 4, pp. 2373–2433, 2012, doi: 10.1021/cr100449n.

[11] A. Ghorban Shiravizadeh, S. M. Elahi, S. A. Sebt, and R. Yousefi, "High performance of visible-NIR broad spectral photocurrent application of monodisperse PbSe nanocubes decorated on rGO sheets," *J. Appl. Phys.*, vol. 123, no. 8, 2018, doi: 10.1063/1.5017226.

[12] M. S. A. Bhuyan, M. N. Uddin, M. M. Islam, F. A. Bipasha, and S. S. Hossain, "Synthesis of graphene," *Int. Nano Lett.*, vol. 6, no. 2, pp. 65–83, 2016, doi: 10.1007/s40089-015-0176-1.

[13] D. D. L. Chung, "Exfoliation of graphite," *J. Mater. Sci.*, vol. 22, no. 12, pp. 4190–4198, 1987, doi: 10.1007/BF01132008.

[14] X. Zhou, J. Zheng, H. Wu, H. Yang, J. Zhang, and S. Guo, "Reducing graphene oxide via hydroxylamine: A simple and efficient route to graphene," *J. Phys. Chem. C*, vol. 115, no. 24, pp. 11957–11961, 2011, doi: 10.1021/jp202575j.

[15] Y. Zhu, S. Murali, M. D. Stoller, A. Velamakanni, R. D. Piner, and R. S. Ruoff, "Microwave assisted exfoliation and reduction of graphite oxide for ultracapacitors," *Carbon N. Y.*, vol. 48, no. 7, pp. 2118–2122, 2010, doi: 10.1016/j.carbon.2010.02.001.

[16] H. Chen, M. B. Müller, K. J. Gilmore, G. G. Wallace, and D. Li, “Mechanically strong, electrically conductive, and biocompatible graphene paper,” *Adv. Mater.*, vol. 20, no. 18, pp. 3557–3561, 2008, doi: 10.1002/adma.200800757.

[17] E. Ferdosi, H. Bahiraei, and D. Ghanbari, “Investigation the photocatalytic activity of CoFe2O4/ZnO and CoFe2O4/ZnO/Ag nanocomposites for purification of dye pollutants,” *Sep. Purif. Technol.*, vol. 211, pp. 35–39, 2019, doi: 10.1016/j.seppur.2018.09.054.

[18] S. I. Siddiqui, O. Manzoor, M. Mohsin, and S. A. Chaudhry, “Nigella sativa seed based nanocomposite-MnO2/BC: An antibacterial material for photocatalytic degradation, and adsorptive removal of Methylene blue from water,” *Environ. Res.*, vol. 171, pp. 328–340, 2019, doi: 10.1016/j.envres.2018.11.044.

[19] H. Tedla, I. Díaz, T. Kebede, and A. M. Taddesse, “Synthesis, characterization and photocatalytic activity of zeolite supported ZnO/Fe2O3/MnO2 nanocomposites,” *J. Environ. Chem. Eng.*, vol. 3, no. 3, pp. 1586–1591, 2015, doi: 10.1016/j.jece.2015.05.012.

[20] A. Enotiadis, N. J. Fernandes, N. A. Becerra, M. Zammarano, and E. P. Giannelis, “Nanocomposite electrolytes for lithium batteries with reduced flammability,” *Electrochim. Acta*, vol. 269, pp. 76–82, 2018, doi: 10.1016/j.electacta.2018.02.079.

[21] S. A. Gaware, K. A. Rokade, and S. N. Kale, “Silica-chitosan nanocomposite mediated pH-sensitive drug delivery,” *J. Drug Deliv. Sci. Technol.*, vol. 49, pp. 345–351, 2019, doi: 10.1016/j.jddst.2018.11.022.

[22] W. Chen, F. Deng, M. Xu, J. Wang, Z. Wei, and Y. Wang, “GO/Cu2O nanocomposite based QCM gas sensor for trimethylamine detection under low concentrations,” *Sensors Actuators, B Chem.*, vol. 273, pp. 498–504, 2018, doi: 10.1016/j.snb.2018.06.062.

[23] P. Thakur and A. Thakur, “Introduction to Nanotechnology,” *Synth. Appl. Nanoparticles*, vol. 30, no. May, pp. 1–17, 2022, doi: 10.1007/978-981-16-6819-7_1.

[24] B. Sarkar, A. Mahanty, S. K. Gupta, A. R. Choudhury, A. Daware, and S. Bhattacharjee, “Nanotechnology: A next-generation tool for sustainable aquaculture,” *Aquaculture*, vol. 546, no. December 2020, p. 737330, 2022, doi: 10.1016/j.aquaculture.2021.737330.

[25] D. A. Bazylinski and D. Trubitsyn, “Magnetotactic bacteria and magnetosomes,” *Magn. Nanoparticles Biosensing Med.*, pp. 251–284, 2019, doi: 10.1017/9781139381222.009.

[26] S. He, Z. Guo, Y. Zhang, S. Zhang, J. Wang, and N. Gu, “Biosynthesis of gold nanoparticles using the bacteria Rhodopseudomonas capsulata,” *Mater. Lett.*, vol. 61, no. 18, pp. 3984–3987, 2007, doi: 10.1016/j.matlet.2007.01.018.

[27] G. Singaravelu, J. S. Arockiamary, V. G. Kumar, and K. Govindaraju, “A novel extracellular synthesis of monodisperse gold nanoparticles using marine alga, Sargassum wightii Greville,” *Colloids Surfaces B Biointerfaces*, vol. 57, no. 1, pp. 97–101, 2007, doi: 10.1016/j.colsurfb.2007.01.010.

[28] A. Ahmad *et al.*, “Extracellular biosynthesis of silver nanoparticles using the fungus Fusarium oxysporum,” *Colloids Surfaces B Biointerfaces*, vol. 28, no. 4, pp. 313–318, 2003, doi: 10.1016/S0927-7765(02)00174-1.

[29] N. M. Y. Zhang *et al.*, “One-step synthesis of cyclodextrin-capped gold nanoparticles for ultra-sensitive and highly-integrated plasmonic biosensors,” *Sensors Actuators, B Chem.*, vol. 286, pp. 429–436, 2019, doi: 10.1016/j.snb.2019.01.166.

[30] T. Zhang, J. Liu, C. Wang, X. Leng, Y. Xiao, and L. Fu, “Synthesis of graphene and related two-

dimensional materials for bioelectronics devices," *Biosens. Bioelectron.*, vol. 89, pp. 28–42, 2017, doi: 10.1016/j.bios.2016.06.072.

[31] R. Fan, S. W. Chew, V. V. Cheong, and B. P. Orner, "Fabrication of gold nanoparticles inside unmodified horse spleen apoferritin," *Small*, vol. 6, no. 14, pp. 1483–1487, 2010, doi: 10.1002/smll.201000457.

[32] H. Wu, J. Wang, Z. Wang, D. R. Fisher, and Y. Lin, "Apoferritin-templated yttrium phosphate nanoparticle conjugates for radioimmunotherapy of cancers," *J. Nanosci. Nanotechnol.*, vol. 8, no. 5, pp. 2316–2322, 2008, doi: 10.1166/jnn.2008.177.

[33] S. S. Shankar, A. Rai, A. Ahmad, and M. Sastry, "Rapid synthesis of Au, Ag, and bimetallic Au core-Ag shell nanoparticles using Neem (Azadirachta indica) leaf broth," *J. Colloid Interface Sci.*, vol. 275, no. 2, pp. 496–502, 2004, doi: 10.1016/j.jcis.2004.03.003.

[34] G. S. Shekhawat and V. Arya, "Biological synthesis of Ag nanoparticles through in vitro cultures of Brassica juncea C. zern," *Adv. Mater. Res.*, vol. 67, pp. 295–299, 2009, doi: 10.4028/www.scientific.net/AMR.67.295.

[35] M. Banerjee, B. Dey, J. Talukdar, and M. Chandra Kalita, "Production of biodiesel from sunflower oil using highly catalytic bimetallic gold-silver core-shell nanoparticle," *Energy*, vol. 69, pp. 695–699, 2014, doi: 10.1016/j.energy.2014.03.065.

[36] S. Dutz *et al.*, "Hysteresis losses of magnetic nanoparticle powders in the single domain size range," *J. Magn. Magn. Mater.*, vol. 308, no. 2, pp. 305–312, 2007, doi: 10.1016/j.jmmm.2006.06.005.

[37] A. Erlebach, H. D. Kurland, J. Grabow, F. A. Müller, and M. Sierka, "Structure evolution of nanoparticulate Fe2O3," *Nanoscale*, vol. 7, no. 7, pp. 2960–2969, 2015, doi: 10.1039/c4nr06989g.

[38] T. Hyeon, Su Seong Lee, J. Park, Y. Chung, and Hyon Bin Na, "Synthesis of highly crystalline and monodisperse maghemite nanocrystallites without a size-selection process," *J. Am. Chem. Soc.*, vol. 123, no. 51, pp. 12798–12801, 2001, doi: 10.1021/ja016812s.

[39] L. Bu *et al.*, "Assessment and comparison of magnetic nanoparticles as MRI contrast agents in a rodent model of human hepatocellular carcinoma," *Contrast Media Mol. Imaging*, vol. 7, no. 4, pp. 363–372, 2012, doi: 10.1002/cmmi.494.

[40] A. K. Haghi and G. E. Zaikov, *Handbook of research on nanomaterials, nanochemistry and smart materials*. 2012.

[41] A. Maleki, R. Rahimi, S. Maleki, and N. Hamidi, "Synthesis and characterization of magnetic bromochromate hybrid nanomaterials with triphenylphosphine surface-modified iron oxide nanoparticles and their catalytic application in multicomponent reactions," *RSC Adv.*, vol. 4, no. 56, pp. 29765–29771, 2014, doi: 10.1039/c4ra04654d.

[42] H. Dong *et al.*, "Lanthanide Nanoparticles: From Design toward Bioimaging and Therapy," *Chem. Rev.*, vol. 115, no. 19, pp. 10725–10815, 2015, doi: 10.1021/acs.chemrev.5b00091.

[43] S. Zhao, J. Guo, W. Li, H. Guo, and B. You, "Fabrication of cobalt aluminate nanopigments by coprecipitation method in threonine waterborne solution," *Dye. Pigment.*, vol. 151, pp. 130–139, 2018, doi: 10.1016/j.dyepig.2017.12.062.

[44] T. Hu, X. Mei, Y. Wang, X. Weng, R. Liang, and M. Wei, "Two-dimensional nanomaterials: fascinating materials in biomedical field," *Sci. Bull.*, vol. 64, no. 22, pp. 1707–1727, 2019, doi: 10.1016/j.scib.2019.09.021.

[45] W. Qiu, X. Feng, H. Zhang, and H. Huang, “Synthesis and luminescence properties of CaB 4 O 7 :Eu 3+ via two-step hydrothermal method,” *Optik (Stuttg).*, vol. 182, pp. 1039–1045, 2019, doi: 10.1016/j.ijleo.2019.01.109.

[46] U. Wongpratat, S. Maensiri, and E. Swatsitang, “EXAFS study of cations distribution dependence of magnetic properties in Co1-xZnxFe2O4 nanoparticles prepared by hydrothermal method,” *Microelectron. Eng.*, vol. 146, pp. 68–75, 2015, doi: 10.1016/j.mee.2015.03.059.

[47] J. Zhang, J. M. Song, H. L. Niu, C. J. Mao, S. Y. Zhang, and Y. H. Shen, “ZnFe2O4 nanoparticles: Synthesis, characterization, and enhanced gas sensing property for acetone,” *Sensors Actuators, B Chem.*, vol. 221, pp. 55–62, 2015, doi: 10.1016/j.snb.2015.06.040.

[48] M. Ahamed, M. J. Akhtar, H. A. Alhadlaq, and A. Alshamsan, “Copper ferrite nanoparticle-induced cytotoxicity and oxidative stress in human breast cancer MCF-7 cells,” *Colloids Surfaces B Biointerfaces*, vol. 142, pp. 46–54, 2016, doi: 10.1016/j.colsurfb.2016.02.043.

[49] P. G. Jamkhande, N. W. Ghule, A. H. Bamer, and M. G. Kalaskar, “Metal nanoparticles synthesis: An overview on methods of preparation, advantages and disadvantages, and applications,” *J. Drug Deliv. Sci. Technol.*, vol. 53, p. 101174, 2019, doi: 10.1016/j.jddst.2019.101174.

[50] A. Hassanjani-Roshan, M. R. Vaezi, A. Shokuhfar, and Z. Rajabali, “Synthesis of iron oxide nanoparticles via sonochemical method and their characterization,” *Particuology*, vol. 9, no. 1, pp. 95–99, 2011, doi: 10.1016/j.partic.2010.05.013.

[51] J. Seidlerová, O. Životský, K. Drobíková, and K. Mamulová Kutláková, “Modification of microwave assisted preparation of FexOy nanoparticles,” *Mater. Today Proc.*, vol. 5, pp. S52–S60, 2018, doi: 10.1016/j.matpr.2018.05.057.

[52] S. De and R. Madhuri, *Functionalized nanomaterials for electronics and electrical and energy industries*. INC, 2020.

[53] D. Perera, “PHOTOCATALYTIC PROPERTIES OF ZINC SELENIDE / CADMIUM SULFIDE CORE-SHELL NANOPARTICLES Jayalath Pathirannehelage Dimuthu Nuwan Perera A Thesis Submitted to the Graduate College of Bowling Green State University in partial fulfillment of the requirements f,” no. August, 2013.

[54] J. Wu *et al.*, “Three-dimensional gold nanoparticles-modified graphene hydrogel for high-sensitive NO2 and NH3 detection with enhanced resistance to humidity,” *Sensors Actuators, B Chem.*, vol. 344, no. June, p. 130259, 2021, doi: 10.1016/j.snb.2021.130259.

[55] S. Kantipudi *et al.*, “Diospyros assimilis root extract assisted biosynthesised silver nanoparticles and their evaluation of antimicrobial activity,” *IET Nanobiotechnology*, vol. 12, no. 2, pp. 133–137, 2018, doi: 10.1049/iet-nbt.2017.0042.

[56] C. Vanlalveni, S. Lallianrawna, A. Biswas, M. Selvaraj, B. Changmai, and S. L. Rokhum, “Green synthesis of silver nanoparticles using plant extracts and their antimicrobial activities: a review of recent literature,” *RSC Adv.*, vol. 11, no. 5, pp. 2804–2837, 2021, doi: 10.1039/d0ra09941d.

[57] K. V. V. Satyanarayana, M. Ravi Chandra, P. Atchuta Ramaiah, Y. L. N. Murty, E. N. Pandit, and S. V. N. Pammi, “A novel reusable and efficient nano-ZnS catalyst for green synthesis of xanthenes and its derivatives under solvent free conditions,” *Inorg. Chem. Front.*, vol. 1, no. 4, pp. 306–310, 2014, doi: 10.1039/c3qi00016h.

[58] N. D. Jaji, H. L. Lee, M. H. Hussin, H. M. Akil, M. R. Zakaria, and M. B. H. Othman, “Advanced

nickel nanoparticles technology: From synthesis to applications," *Nanotechnol. Rev.*, vol. 9, no. 1, pp. 1456–1480, 2020, doi: 10.1515/ntrev-2020-0109.

[59] H. Sharma, P. K. Mishra, S. Talegaonkar, and B. Vaidya, "Metal nanoparticles: A theranostic nanotool against cancer," *Drug Discov. Today*, vol. 20, no. 9, pp. 1143–1151, 2015, doi: 10.1016/j.drudis.2015.05.009.

[60] M. A. Ghaz-Jahanian, F. Abbaspour-Aghdam, N. Anarjan, A. Berenjian, and H. Jafarizadeh-Malmiri, "Application of Chitosan-Based Nanocarriers in Tumor-Targeted Drug Delivery," *Mol. Biotechnol.*, vol. 57, no. 3, pp. 201–218, 2015, doi: 10.1007/s12033-014-9816-3.

[61] J. Liu *et al.*, "PH-Sensitive nano-systems for drug delivery in cancer therapy," *Biotechnol. Adv.*, vol. 32, no. 4, pp. 693–710, 2014, doi: 10.1016/j.biotechadv.2013.11.009.

[62] C. L. Hastings, E. T. Roche, E. Ruiz-Hernandez, K. Schenke-Layland, C. J. Walsh, and G. P. Duffy, "Drug and cell delivery for cardiac regeneration," *Adv. Drug Deliv. Rev.*, vol. 84, pp. 85–106, 2015, doi: 10.1016/j.addr.2014.08.006.

[63] C. Chellaram *et al.*, "Significance of Nanotechnology in Food Industry," *APCBEE Procedia*, vol. 8, no. Caas 2013, pp. 109–113, 2014, doi: 10.1016/j.apcbee.2014.03.010.

[64] S. Siddiqui and S. A. Alrumman, "Influence of nanoparticles on food: An analytical assessment," *J. King Saud Univ. - Sci.*, vol. 33, no. 6, p. 101530, 2021, doi: 10.1016/j.jksus.2021.101530.

[65] B. Naseer, G. Srivastava, O. S. Qadri, S. A. Faridi, R. U. Islam, and K. Younis, "Importance and health hazards of nanoparticles used in the food industry," *Nanotechnol. Rev.*, vol. 7, no. 6, pp. 623–641, 2018, doi: 10.1515/ntrev-2018-0076.

[66] S. T. Hussain, K. V. S. Gopala, and K. Sastry, "Silica Fume (SF), Compressive strength (CS)," *IJRET Int. J. Res. Eng. Technol.*, pp. 2321–7308, 2014, [Online]. Available: http://www.ijret.org.

[67] U. Anik, "Electrochemical medical biosensors for POC applications," in *Medical Biosensors for Point of Care (POC) Applications*, Elsevier Inc., 2017, pp. 275–292.

[68] B. Ruot, A. Plassais, F. Olive, L. Guillot, and L. Bonafous, "TiO2-containing cement pastes and mortars: Measurements of the photocatalytic efficiency using a rhodamine B-based colourimetric test," *Sol. Energy*, vol. 83, no. 10, pp. 1794–1801, 2009, doi: 10.1016/j.solener.2009.05.017.

[69] M. M. Khin, A. S. Nair, V. J. Babu, R. Murugan, and S. Ramakrishna, "A review on nanomaterials for environmental remediation," *Energy Environ. Sci.*, vol. 5, no. 8, pp. 8075–8109, 2012, doi: 10.1039/c2ee21818f.

[70] Y. Wu *et al.*, "Environmental remediation of heavy metal ions by novel-nanomaterials: A review," *Environ. Pollut.*, vol. 246, pp. 608–620, 2019, doi: 10.1016/j.envpol.2018.12.076.

[71] F. D. Guerra, M. F. Attia, D. C. Whitehead, and F. Alexis, "Nanotechnology for environmental remediation: Materials and applications," *Molecules*, vol. 23, no. 7, pp. 1–23, 2018, doi: 10.3390/molecules23071760.

[72] A. . Power, B. Gorey, and J. C. S. Chandra, "Carbon nanomaterials and their application to electrochemical sensors," 2011.

[73] A. Chen and B. Shah, "Electrochemical sensing and biosensing based on square wave voltammetry," *Anal. Methods*, vol. 5, no. 9, pp. 2158–2173, 2013, doi: 10.1039/c3ay40155c.

[74] H. C. Ananda Murthy, K. Gebremedhn Kelele, C. R. Ravikumar, H. P. Nagaswarupa, A. Tadesse,

and T. Desalegn, “Graphene-supported nanomaterials as electrochemical sensors: A mini review,” *Results Chem.*, vol. 3, p. 100131, 2021, doi: 10.1016/j.rechem.2021.100131.

[75] X. T. Ran, Z. Wang, and L. Yang, “Fabrication of a carbon nanotube gas sensor microelectrodes and its application for ammonia detection,” *Appl. Mech. Mater.*, vol. 431, pp. 306–311, 2013, doi: 10.4028/www.scientific.net/AMM.431.306.

[76] R. Petrucci, M. Bortolami, P. Di Matteo, and A. Curulli, “Gold Nanomaterials-Based Electrochemical Sensors and Biosensors for Phenolic Antioxidants Detection: Recent Advances,” *Nanomaterials*, vol. 12, no. 6, 2022, doi: 10.3390/nano12060959.

[77] N. S. Alsaiari, K. M. M. Katubi, F. M. Alzahrani, S. M. Siddeeg, and M. A. Tahoon, “The application of nanomaterials for the electrochemical detection of antibiotics: A review,” *Micromachines*, vol. 12, no. 3, 2021, doi: 10.3390/mi12030308.

[78] L. K. Sannegowda, “Metal nanoparticles for electrochemical sensing applications,” *Handb. Nanomater. Sens. Appl.*, pp. 589–629, 2021, doi: 10.1016/B978-0-12-820783-3.00001-4.

[79] X. Luo, A. Morrin, A. J. Killard, and M. R. Smyth, “Application of nanoparticles in electrochemical sensors and biosensors,” *Electroanalysis*, vol. 18, no. 4, pp. 319–326, 2006, doi: 10.1002/elan.200503415.

[80] D. W. Kimmel, G. Leblanc, M. E. Meschievitz, and D. E. Cliffel, “Electrochemical sensors and biosensors,” *Anal. Chem.*, vol. 84, no. 2, pp. 685–707, 2012, doi: 10.1021/ac202878q.

[81] F. Yang, P. Song, M. Ruan, and W. Xu, “Recent progress in two-dimensional nanomaterials: Synthesis, engineering, and applications,” *FlatChem*, vol. 18, no. August, p. 100133, 2019, doi: 10.1016/j.flatc.2019.100133.

[82] M. Taghioskoui, “Trends in graphene research,” *Mater. Today*, vol. 12, no. 10, pp. 34–37, 2009, doi: 10.1016/S1369-7021(09)70274-3.

[83] H. Zhang, H. M. Cheng, and P. Ye, “2D nanomaterials: Beyond graphene and transition metal dichalcogenides,” *Chem. Soc. Rev.*, vol. 47, no. 16, pp. 6009–6012, 2018, doi: 10.1039/c8cs90084a.

[84] T. Giousis *et al.*, “Synthesis of 2D Germanane (GeH): a New, Fast, and Facile Approach,” *Angew. Chemie - Int. Ed.*, vol. 60, no. 1, pp. 360–365, 2021, doi: 10.1002/anie.202010404.

[85] E. Salomon, T. Angot, L. Lew Yan Voon, and G. Le Lay, *Silicene*. 2022.

[86] K. Kalantar-zadeh, J. Z. Ou, T. Daeneke, A. Mitchell, T. Sasaki, and M. S. Fuhrer, “Two dimensional and layered transition metal oxides,” *Appl. Mater. Today*, vol. 5, pp. 73–89, 2016, doi: 10.1016/j.apmt.2016.09.012.

[87] L. Zhao *et al.*, “MOF-Based Supramolecule Helical Nanomaterials: Toward Highly Enantioselective Electrochemical Recognition of Penicillamine,” *ACS Appl. Mater. Interfaces*, vol. 12, no. 1, pp. 1533–1538, 2020, doi: 10.1021/acsami.9b18183.

[88] H. Li, J. Wu, Z. Yin, and H. Zhang, “Preparation and applications of mechanically exfoliated single-layer and multilayer MoS2 and WSe2 nanosheets,” *Acc. Chem. Res.*, vol. 47, no. 4, pp. 1067–1075, 2014, doi: 10.1021/ar4002312.

[89] J. Yu, J. Li, W. Zhang, and H. Chang, “Synthesis of high quality two-dimensional materials via chemical vapor deposition,” *Chem. Sci.*, vol. 6, no. 12, pp. 6705–6716, 2015, doi: 10.1039/c5sc01941a.

[90] A. Rabenau, “The Role of Hydrothermal Synthesis in Preparative Chemistry,” *Angew. Chemie*

Int. Ed. English, vol. 24, no. 12, pp. 1026–1040, 1985, doi: 10.1002/anie.198510261.

[91] U. Alam, M. Fleisch, I. Kretschmer, D. Bahnemann, and M. Muneer, "One-step hydrothermal synthesis of Bi-TiO2 nanotube/graphene composites: An efficient photocatalyst for spectacular degradation of organic pollutants under visible light irradiation," *Appl. Catal. B Environ.*, vol. 218, pp. 758–769, 2017, doi: 10.1016/j.apcatb.2017.06.016.

[92] Y. Shi *et al.*, "Synthesis of few-layer hexagonal boron nitride thin film by chemical vapor deposition," *Nano Lett.*, vol. 10, no. 10, pp. 4134–4139, 2010, doi: 10.1021/nl1023707.

[93] R. Ma and T. Sasaki, "Two-Dimensional Oxide and Hydroxide Nanosheets : Controllable High-Quality Exfoliation , Molecular Assembly , and Exploration of Functionality Published as part of the Accounts of Chemical Research special issue ' 2D Nanomaterials beyond Graphene ' .," *Acc. Chem. Res.*, vol. 48, no. 1, pp. 136–143, 2015.

[94] M. Zhao, Q. Lu, Q. Ma, and H. Zhang, "Two-Dimensional Metal–Organic Framework Nanosheets," *Small Methods*, vol. 1, no. 1–2, pp. 1–8, 2017, doi: 10.1002/smtd.201600030.

[95] V. Nicolosi, M. Chhowalla, M. G. Kanatzidis, M. S. Strano, and J. N. Coleman, "Liquid exfoliation of layered materials," *Science (80-.).*, vol. 340, no. 6139, 2013, doi: 10.1126/science.1226419.

[96] T. X. Phuoc, B. H. Howard, D. V. Martello, Y. Soong, and M. K. Chyu, "Synthesis of Mg(OH)2, MgO, and Mg nanoparticles using laser ablation of magnesium in water and solvents," *Opt. Lasers Eng.*, vol. 46, no. 11, pp. 829–834, 2008, doi: 10.1016/j.optlaseng.2008.05.018.

[97] K. S. Novoselov *et al.*, "Electric field in atomically thin carbon films," *Science (80-.).*, vol. 306, no. 5696, pp. 666–669, 2004, doi: 10.1126/science.1102896.

[98] A. R. Urade, I. Lahiri, and K. S. Suresh, "Graphene Properties, Synthesis and Applications: A Review," *Jom*, vol. 75, no. 3, pp. 614–630, 2023, doi: 10.1007/s11837-022-05505-8.

[99] Y. F. Guan and A. J. Pedraza, "Synthesis and alignment of Zn and ZnO nanoparticles by laser-assisted chemical vapor deposition," *Nanotechnology*, vol. 19, no. 4, 2008, doi: 10.1088/0957-4484/19/04/045609.

[100] Q. Lu, Y. Yu, Q. Ma, B. Chen, and H. Zhang, "2D Transition-Metal-Dichalcogenide-Nanosheet-Based Composites for Photocatalytic and Electrocatalytic Hydrogen Evolution Reactions," *Adv. Mater.*, vol. 28, no. 10, pp. 1917–1933, 2016, doi: 10.1002/adma.201503270.

[101] W. Choi, N. Choudhary, G. H. Han, J. Park, D. Akinwande, and Y. H. Lee, "Recent development of two-dimensional transition metal dichalcogenides and their applications," *Mater. Today*, vol. 20, no. 3, pp. 116–130, 2017, doi: 10.1016/j.mattod.2016.10.002.

[102] H. Lin, X. Chen, H. Li, M. Yang, and Y. Qi, "Hydrothermal synthesis and characterization of MoS2 nanorods," *Mater. Lett.*, vol. 64, no. 15, pp. 1748–1750, 2010, doi: 10.1016/j.matlet.2010.04.032.

[103] Z. Feng, P. Yang, G. Wen, H. Li, Y. Liu, and X. Zhao, "One-step synthesis of MoS2 nanoparticles with different morphologies for electromagnetic wave absorption," *Appl. Surf. Sci.*, vol. 502, p. 144129, 2020, doi: 10.1016/j.apsusc.2019.144129.

[104] Y. Guo and J. Li, "MoS2 quantum dots: synthesis, properties and biological applications," *Mater. Sci. Eng. C*, vol. 109, p. 110511, 2020, doi: 10.1016/j.msec.2019.110511.

[105] W. Chen, W. Wu, Z. Pan, X. Wu, and H. Zhang, "PEG400-assisted synthesis of oxygen-incorporated MoS2 ultrathin nanosheets supported on reduced graphene oxide for sodium ion batteries," *J. Alloys Compd.*, vol. 763, pp. 257–266, 2018, doi:

10.1016/j.jallcom.2018.05.301.

[106] J. Li *et al.*, "Ionic liquid assisted hydrothermal synthesis of hollow core/shell MoS2 microspheres," *Mater. Lett.*, vol. 160, pp. 550–554, 2015, doi: 10.1016/j.matlet.2015.08.049.

[107] H. Li *et al.*, "Activating and optimizing MoS2 basal planes for hydrogen evolution through the formation of strained sulphur vacancies," *Nat. Mater.*, vol. 15, no. 1, pp. 48–53, 2016, doi: 10.1038/nmat4465.

[108] K. Zhang, Y. Feng, F. Wang, Z. Yang, and J. Wang, "Two dimensional hexagonal boron nitride (2D-hBN): Synthesis, properties and applications," *J. Mater. Chem. C*, vol. 5, no. 46, pp. 11992–12022, 2017, doi: 10.1039/c7tc04300g.

[109] Q. Weng, X. Wang, X. Wang, Y. Bando, and D. Golberg, "Functionalized hexagonal boron nitride nanomaterials: Emerging properties and applications," *Chem. Soc. Rev.*, vol. 45, no. 14, pp. 3989–4012, 2016, doi: 10.1039/c5cs00869g.

[110] F. Paquin, J. Rivnay, A. Salleo, N. Stingelin, and C. Silva, "Multi-phase semicrystalline microstructures drive exciton dissociation in neat plastic semiconductors," *J. Mater. Chem. C*, vol. 3, pp. 10715–10722, 2015, doi: 10.1039/b000000x.

[111] N. Rono, J. K. Kibet, B. S. Martincigh, and V. O. Nyamori, "A review of the current status of graphitic carbon nitride," *Crit. Rev. Solid State Mater. Sci.*, vol. 46, no. 3, pp. 189–217, 2021, doi: 10.1080/10408436.2019.1709414.

[112] L. Deng *et al.*, "Functionalization of small black phosphorus nanoparticles for targeted imaging and photothermal therapy of cancer," *Sci. Bull.*, vol. 63, no. 14, pp. 917–924, 2018, doi: 10.1016/j.scib.2018.05.022.

[113] M. Akhtar *et al.*, "Recent advances in synthesis, properties, and applications of phosphorene," *npj 2D Mater. Appl.*, vol. 1, no. 1, pp. 1–12, 2017, doi: 10.1038/s41699-017-0007-5.

[114] H. Liu, Y. Du, Y. Deng, and P. D. Ye, "Semiconducting black phosphorus: Synthesis, transport properties and electronic applications," *Chem. Soc. Rev.*, vol. 44, no. 9, pp. 2732–2743, 2015, doi: 10.1039/c4cs00257a.

[115] L. Kou, C. Chen, and S. C. Smith, "Phosphorene: Fabrication, properties, and applications," *J. Phys. Chem. Lett.*, vol. 6, no. 14, pp. 2794–2805, 2015, doi: 10.1021/acs.jpclett.5b01094.

[116] Y. Chen *et al.*, "Two-Dimensional Metal Nanomaterials: Synthesis, Properties, and Applications," *Chemical Reviews*, vol. 118, no. 13. American Chemical Society, pp. 6409–6455, Jul. 11, 2018, doi: 10.1021/acs.chemrev.7b00727.

[117] M. S. Lal, T. Lavanya, and S. Ramaprabhu, "An efficient electrode material for high performance solid-state hybrid supercapacitors based on a Cu/CuO/porous carbon nanofiber/TiO2 hybrid composite," *Beilstein J. Nanotechnol.*, vol. 10, pp. 781–793, 2019, doi: 10.3762/BJNANO.10.78.

[118] P. Xiong, R. Ma, N. Sakai, L. Nurdiwijayanto, and T. Sasaki, "Unilamellar Metallic MoS2/Graphene Superlattice for Efficient Sodium Storage and Hydrogen Evolution," *ACS Energy Lett.*, vol. 3, no. 4, pp. 997–1005, 2018, doi: 10.1021/acsenergylett.8b00110.

[119] H. Hu *et al.*, "Graphene-assisted construction of electrocatalysts for carbon dioxide reduction," *Chem. Eng. J.*, vol. 425, no. February, p. 130587, 2021, doi: 10.1016/j.cej.2021.130587.

[120] K. S. Kumar, N. Choudhary, Y. Jung, and J. Thomas, "Recent Advances in Two-Dimensional

Nanomaterials for Supercapacitor Electrode Applications," *ACS Energy Lett.*, vol. 3, no. 2, pp. 482–495, 2018, doi: 10.1021/acsenergylett.7b01169.

[121] Y. Chen *et al.*, "Two-Dimensional Metal Nanomaterials: Synthesis, Properties, and Applications," *Chem. Rev.*, vol. 118, no. 13, pp. 6409–6455, 2018, doi: 10.1021/acs.chemrev.7b00727.

[122] Q. Ke and J. Wang, "Graphene-based materials for supercapacitor electrodes – A review," *J. Mater.*, vol. 2, no. 1, pp. 37–54, 2016, doi: 10.1016/j.jmat.2016.01.001.

[123] P. Forouzandeh, V. Kumaravel, and S. C. Pillai, "Electrode materials for supercapacitors: A review of recent advances," *Catalysts*, vol. 10, no. 9, pp. 1–73, 2020, doi: 10.3390/catal10090969.

[124] L. Liu *et al.*, "Tuning the Surface Chemistry of MXene to Improve Energy Storage: Example of Nitrification by Salt Melt," *Adv. Energy Mater.*, vol. 13, no. 2, 2023, doi: 10.1002/aenm.202202709.

[125] M. Luo, T. Fan, Y. Zhou, H. Zhang, and L. Mei, "2D Black Phosphorus–Based Biomedical Applications," *Adv. Funct. Mater.*, vol. 29, no. 13, pp. 1–19, 2019, doi: 10.1002/adfm.201808306.

[126] H. Xu, M. K. Akbari, and S. Zhuiykov, "2D Semiconductor Nanomaterials and Heterostructures: Controlled Synthesis and Functional Applications," *Nanoscale Res. Lett.*, vol. 16, no. 1, 2021, doi: 10.1186/s11671-021-03551-w.

[127] J. Fang, Z. Zhou, M. Xiao, Z. Lou, Z. Wei, and G. Shen, "Recent advances in low-dimensional semiconductor nanomaterials and their applications in high-performance photodetectors," *InfoMat*, vol. 2, no. 2, pp. 291–317, 2020, doi: 10.1002/inf2.12067.

[128] S. Su *et al.*, "Two-dimensional nanomaterials for biosensing applications," *TrAC - Trends Anal. Chem.*, vol. 119, 2019, doi: 10.1016/j.trac.2019.07.021.

[129] E. Kim *et al.*, "Microsupercapacitor with a 500 nm gap between MXene/CNT electrodes," *Nano Energy*, vol. 81, no. July 2020, p. 105616, 2021, doi: 10.1016/j.nanoen.2020.105616.

[130] X. M. Yi, F. L. Wang, W. J. Qin, X. J. Yang, and J. L. Yuan, "Near-infrared fluorescent probes in cancer imaging and therapy: An emerging field," *Int. J. Nanomedicine*, vol. 9, no. 1, pp. 1347–1365, 2014, doi: 10.2147/IJN.S60206.

[131] X. Yan *et al.*, "Highly green fluorescent Nb2C MXene quantum dots for Cu2+ ion sensing and cell imaging," *Chinese Chem. Lett.*, vol. 31, no. 12, pp. 3173–3177, 2020, doi: 10.1016/j.cclet.2020.05.020.

[132] X. Chen *et al.*, "CVD-grown monolayer MoS2 in bioabsorbable electronics and biosensors," *Nat. Commun.*, vol. 9, no. 1, pp. 1–12, 2018, doi: 10.1038/s41467-018-03956-9.

[133] A. T. Lawal, "Graphene-based nano composites and their applications. A review," *Biosens. Bioelectron.*, vol. 141, no. March, p. 111384, 2019, doi: 10.1016/j.bios.2019.111384.

[134] A. K. Geim, "Graphene: Status and prospects," *Science (80-.).*, vol. 324, no. 5934, pp. 1530–1534, 2009, doi: 10.1126/science.1158877.

[135] S. Manzeli, D. Ovchinnikov, D. Pasquier, O. V. Yazyev, and A. Kis, "2D transition metal dichalcogenides," *Nat. Rev. Mater.*, vol. 2, 2017, doi: 10.1038/natrevmats.2017.33.

[136] E. Benavente, M. A. Santa Ana, F. Mendizábal, and G. González, "Intercalation chemistry of molybdenum disulfide," *Coord. Chem. Rev.*, vol. 224, no. 1–2, pp. 87–109, 2002, doi:

10.1016/S0010-8545(01)00392-7.

[137] H. W. Lee, D. H. Kang, J. H. Cho, S. Lee, D. H. Jun, and J. H. Park, “Highly Sensitive and Reusable Membraneless Field-Effect Transistor (FET)-Type Tungsten Diselenide (WSe2) Biosensors,” *ACS Appl. Mater. Interfaces*, vol. 10, no. 21, pp. 17639–17645, 2018, doi: 10.1021/acsami.8b03432.

[138] M. Naguib *et al.*, “Two-dimensional nanocrystals produced by exfoliation of Ti 3AlC 2,” *Adv. Mater.*, vol. 23, no. 37, pp. 4248–4253, 2011, doi: 10.1002/adma.201102306.

[139] M. Naguib *et al.*, “Two-dimensional transition metal carbides,” *ACS Nano*, vol. 6, no. 2, pp. 1322–1331, 2012, doi: 10.1021/nn204153h.

[140] B. Anasori *et al.*, “Two-Dimensional, Ordered, Double Transition Metals Carbides (MXenes),” *ACS Nano*, vol. 9, no. 10, pp. 9507–9516, 2015, doi: 10.1021/acsnano.5b03591.

[141] B. Anasori, M. R. Lukatskaya, and Y. Gogotsi, “2D metal carbides and nitrides (MXenes) for energy storage,” *Nat. Rev. Mater.*, vol. 2, no. 2, 2017, doi: 10.1038/natrevmats.2016.98.

[142] B. Anasori and Y. Gogotsi, “2D Metal Carbides and Nitrides (MXenes).”

[143] H. Chen *et al.*, “A Series of MAX Phases with MA-Triangular-Prism Bilayers and Elastic Properties,” *Angew. Chemie*, vol. 131, no. 14, pp. 4624–4628, 2019, doi: 10.1002/ange.201814128.

[144] M. Sokol, V. Natu, S. Kota, and M. W. Barsoum, “On the Chemical Diversity of the MAX Phases,” *Trends Chem.*, vol. 1, no. 2, pp. 210–223, 2019, doi: 10.1016/j.trechm.2019.02.016.

[145] Y. Zhou, H. Xiang, and C. Hu, “Extension of MAX phases from ternary carbides and nitrides (X = C and N) to ternary borides (X = B, C, and N): A general guideline,” *Int. J. Appl. Ceram. Technol.*, vol. 20, no. 2, pp. 803–822, 2023, doi: 10.1111/ijac.14223.

[146] J. Gonzalez-Julian, “Processing of MAX phases: From synthesis to applications,” *J. Am. Ceram. Soc.*, vol. 104, no. 2, pp. 659–690, 2021, doi: 10.1111/jace.17544.

[147] C. E. Shuck *et al.*, “Effect of Ti3AlC2 MAX Phase on Structure and Properties of Resultant Ti3C2Tx MXene,” *ACS Appl. Nano Mater.*, vol. 2, no. 6, pp. 3368–3376, 2019, doi: 10.1021/acsanm.9b00286.

[148] P. A. Miloserdov, V. A. Gorshkov, I. D. Kovalev, and D. Y. Kovalev, “High-temperature synthesis of cast materials based on Nb2AlC MAX phase,” *Ceram. Int.*, vol. 45, no. 2, pp. 2689–2691, 2019, doi: 10.1016/j.ceramint.2018.10.198.

[149] P. Sharma, K. Singh, and O. P. Pandey, “Investigation on oxidation stability of V2AlC MAX phase,” *Thermochim. Acta*, vol. 704, no. April, 2021, doi: 10.1016/j.tca.2021.179010.

[150] M. A. Hadi, “New ternary nanolaminated carbide Mo2Ga2C: A first-principles comparison with the MAX phase counterpart Mo2GaC,” *Comput. Mater. Sci.*, vol. 117, pp. 422–427, 2016, doi: 10.1016/j.commatsci.2016.02.018.

[151] S. N. Perevislov, T. V. Sokolova, and V. L. Stolyarova, “The Ti3SiC2 max phases as promising materials for high temperature applications: Formation under various synthesis conditions,” *Mater. Chem. Phys.*, vol. 267, no. April, p. 124625, 2021, doi: 10.1016/j.matchemphys.2021.124625.

[152] M. Hossein-Zadeh, O. Mirzaee, H. Mohammadian-Semnani, and M. Razavi, “Microstructure investigation of V2AlC MAX phase synthesized through spark plasma sintering using two various sources V and V2O5 as the starting materials,” *Ceram. Int.*, vol. 45, no. 18, pp. 23902–

23916, 2019, doi: 10.1016/j.ceramint.2019.07.236.

[153] C. Li, S. Kota, C. Hu, and M. W. Barsoum, “On the synthesis of low-cost, titanium-based mxenes,” *J. Ceram. Sci. Technol.*, vol. 7, no. 3, pp. 301–306, 2016, doi: 10.4416/JCST2016-00042.

[154] B. Anasori, M. R. Lukatskaya, and Y. Gogotsi, “2D metal carbides and nitrides (MXenes) for energy storage,” *Nature Reviews Materials*, vol. 2, no. 2. Nature Publishing Group, Jan. 17, 2017, doi: 10.1038/natrevmats.2016.98.

[155] G. Lv, J. Wang, Z. Shi, and L. Fan, “Intercalation and delamination of two-dimensional MXene (Ti3C2Tx) and application in sodium-ion batteries,” *Mater. Lett.*, vol. 219, pp. 45–50, 2018, doi: 10.1016/j.matlet.2018.02.016.

[156] M. A. Hope *et al.*, “NMR reveals the surface functionalisation of Ti3C2 MXene,” *Phys. Chem. Chem. Phys.*, vol. 18, no. 7, pp. 5099–5102, 2016, doi: 10.1039/c6cp00330c.

[157] J. Halim *et al.*, “X-ray Photoelectron Spectroscopy of Select Multi-layered Transition Metal Carbides (MXenes),” pp. 1–36.

[158] M. Khazaei *et al.*, “Novel electronic and magnetic properties of two-dimensional transition metal carbides and nitrides,” *Adv. Funct. Mater.*, vol. 23, no. 17, pp. 2185–2192, 2013, doi: 10.1002/adfm.201202502.

[159] M. Khazaei, A. Ranjbar, M. Arai, T. Sasaki, and S. Yunoki, “Electronic properties and applications of MXenes: a theoretical review,” *J. Mater. Chem. C*, vol. 5, no. 10, pp. 2488–2503, 2017, doi: 10.1039/c7tc00140a.

[160] Y. Xie and P. R. C. Kent, “Hybrid density functional study of structural and electronic properties of functionalized Tin+1Xn (X=C, N) monolayers,” *Phys. Rev. B - Condens. Matter Mater. Phys.*, vol. 87, no. 23, pp. 1–10, 2013, doi: 10.1103/PhysRevB.87.235441.

[161] Y. Xie *et al.*, “Role of surface structure on li-ion energy storage capacity of two-dimensional transition-metal carbides,” *J. Am. Chem. Soc.*, vol. 136, no. 17, pp. 6385–6394, 2014, doi: 10.1021/ja501520b.

[162] M. Naguib *et al.*, “New two-dimensional niobium and vanadium carbides as promising materials for li-ion batteries,” *J. Am. Chem. Soc.*, vol. 135, no. 43, pp. 15966–15969, 2013, doi: 10.1021/ja405735d.

[163] M. Ghidiu *et al.*, “Synthesis and characterization of two-dimensional Nb4C3 (MXene),” *Chem. Commun.*, vol. 50, no. 67, pp. 9517–9520, 2014, doi: 10.1039/c4cc03366c.

[164] J. Yin *et al.*, “Nb2C MXene-Functionalized Scaffolds Enables Osteosarcoma Phototherapy and Angiogenesis/Osteogenesis of Bone Defects,” *Nano-Micro Lett.*, vol. 13, no. 1, 2021, doi: 10.1007/s40820-020-00547-6.

[165] X. Han *et al.*, “Therapeutic mesopore construction on 2D Nb2C MXenes for targeted and enhanced chemo-photothermal cancer therapy in NIR-II biowindow,” *Theranostics*, vol. 8, no. 16, pp. 4491–4508, 2018, doi: 10.7150/thno.26291.

[166] S. Zhao *et al.*, “Flexible Nb4C3Tx Film with Large Interlayer Spacing for High-Performance Supercapacitors,” *Adv. Funct. Mater.*, vol. 30, no. 47, pp. 1–8, 2020, doi: 10.1002/adfm.202000815.

[167] L. Gao *et al.*, “Ultrafast Relaxation Dynamics and Nonlinear Response of Few-Layer Niobium Carbide MXene,” *Small Methods*, vol. 4, no. 8, pp. 1–11, 2020, doi: 10.1002/smtd.202000250.

[168] C. (John) Zhang *et al.*, “Layered Orthorhombic Nb2O5@Nb4C3Tx and TiO2@Ti3C2Tx Hierarchical Composites for High Performance Li-ion Batteries,” *Adv. Funct. Mater.*, vol. 26, no. 23, pp. 4143–4151, 2016, doi: 10.1002/adfm.201600682.

[169] P. A. Rasheed, R. P. Pandey, F. Banat, and S. W. Hasan, “Recent advances in niobium MXenes: Synthesis, properties, and emerging applications,” *Matter*, vol. 5, no. 2, pp. 546–572, 2022, doi: 10.1016/j.matt.2021.12.021.

[170] A. Sinha *et al.*, “MXene: An emerging material for sensing and biosensing,” *TrAC - Trends Anal. Chem.*, vol. 105, pp. 424–435, 2018, doi: 10.1016/j.trac.2018.05.021.

[171] J. Hu *et al.*, “Lewis acidic molten salts etching route driven construction of double-layered MXene-Fe/carbon nanotube/silicone rubber composites for high-performance microwave absorption,” *Carbon N. Y.*, vol. 204, no. December 2022, pp. 136–146, 2023, doi: 10.1016/j.carbon.2022.12.050.

[172] J. Zhao *et al.*, “One-step synthesis of few-layer niobium carbide MXene as a promising anode material for high-rate lithium ion batteries,” *Dalt. Trans.*, vol. 48, no. 38, pp. 14433–14439, 2019, doi: 10.1039/c9dt03260f.

[173] J. Halim *et al.*, “Synthesis of two-dimensional nb1.33c (mxene) with randomly distributed vacancies by etching of the quaternary solid solution (nb2/3sc1/3)2alc max phase,” *ACS Appl. Nano Mater.*, vol. 1, no. 6, pp. 2455–2460, 2018, doi: 10.1021/acsanm.8b00332.

[174] P. Abdul Rasheed *et al.*, “Nb-based MXenes for efficient electrochemical sensing of small biomolecules in the anodic potential,” *Electrochem. commun.*, vol. 119, no. July, p. 106811, 2020, doi: 10.1016/j.elecom.2020.106811.

[175] M. Song, S. Y. Pang, F. Guo, M. C. Wong, and J. Hao, “Fluoride-Free 2D Niobium Carbide MXenes as Stable andBiocompatible Nanoplatforms for Electrochemical Biosensors with Ultrahigh Sensitivity,” *Adv. Sci.*, vol. 7, no. 24, Dec. 2020, doi: 10.1002/advs.202001546.

[176] L. Verger, V. Natu, M. Carey, and M. W. Barsoum, “MXenes: An Introduction of Their Synthesis, Select Properties, and Applications,” *Trends Chem.*, vol. 1, no. 7, pp. 656–669, 2019, doi: 10.1016/j.trechm.2019.04.006.

[177] T. Yu and C. B. Breslin, “Review—Two-Dimensional Titanium Carbide MXenes and Their Emerging Applications as Electrochemical Sensors,” *J. Electrochem. Soc.*, vol. 167, no. 3, p. 037514, 2020, doi: 10.1149/2.0142003jes.

[178] M. Wu, Y. He, L. Wang, Q. Xia, and A. Zhou, “Synthesis and electrochemical properties of V2C MXene by etching in opened/closed environments,” *J. Adv. Ceram.*, vol. 9, no. 6, pp. 749–758, 2020, doi: 10.1007/s40145-020-0411-8.

[179] A. Lipatov *et al.*, “High Breakdown Current Density in,” 2021, doi: 10.1021/acsmaterialslett.1c00324.

[180] Y. Wei, P. Zhang, R. A. Soomro, Q. Zhu, and B. Xu, “Advances in the Synthesis of 2D MXenes,” *Adv. Mater.*, vol. 33, no. 39, pp. 1–30, 2021, doi: 10.1002/adma.202103148.

[181] Z. U. Din Babar *et al.*, “Magnetic phase transition from paramagnetic in Nb2AlC-MAX to superconductivity-like diamagnetic in Nb2C-MXene: An experimental and computational analysis,” *RSC Adv.*, vol. 10, no. 43, pp. 25669–25678, 2020, doi: 10.1039/d0ra04568c.

[182] F. R. Simões and M. G. Xavier, *Electrochemical Sensors*. Elsevier Inc., 2017.

[183] J. Brugger, “Editorial: Nanotechnology impact on sensors,” *Nanotechnology*, vol. 20, no. 43, pp. 19–21, 2009, doi: 10.1088/0957-4484/20/43/430206.

[184] “Pandora’s hope: essays on the reality of science studies,” *Choice Reviews Online*, vol. 37, no. 03. pp. 37-1511-37–1511, 1999, doi: 10.5860/choice.37-1511.

[185] Eni, *済無No Title No Title No Title*, no. Mi. 1967.

[186] L. Nei, “Some Milestones in the 50-year History of Electrochemical Oxygen Sensor Development,” *ECS Trans.*, vol. 2, no. 25, pp. 33–38, 2007, doi: 10.1149/1.2409016.

[187] K. Sakai, “Atomic Force Microscope (AFM),” *Meas. Tech. Pract. Colloid Interface Phenom.*, vol. 56, no. 9, pp. 51–57, 2019, doi: 10.1007/978-981-13-5931-6_8.

[188] A. C. Anderson *et al.*, “Granato, in Internal I"reaction and Ultrasonic Attenuation in Crystalline Solids,” *Phys. Rev*, vol. 49, no. 1, p. 6196, 1975.

[189] M. Alhabeb *et al.*, “Guidelines for Synthesis and Processing of Two-Dimensional Titanium Carbide (Ti3C2Tx MXene),” *Chem. Mater.*, vol. 29, no. 18, pp. 7633–7644, 2017, doi: 10.1021/acs.chemmater.7b02847.

[190] J. Zhu *et al.*, “Recent advance in MXenes: A promising 2D material for catalysis, sensor and chemical adsorption,” *Coord. Chem. Rev.*, vol. 352, pp. 306–327, 2017, doi: 10.1016/j.ccr.2017.09.012.

[191] E. Satheeshkumar, T. Makaryan, A. Melikyan, H. Minassian, Y. Gogotsi, and M. Yoshimura, “One-step Solution Processing of Ag, Au and Pd@MXene Hybrids for SERS,” *Sci. Rep.*, vol. 6, no. August, pp. 1–9, 2016, doi: 10.1038/srep32049.

[192] L. Lorencova *et al.*, “Highly stable Ti3C2Tx (MXene)/Pt nanoparticles-modified glassy carbon electrode for H2O2 and small molecules sensing applications,” *Sensors Actuators, B Chem.*, vol. 263, pp. 360–368, 2018, doi: 10.1016/j.snb.2018.02.124.

[193] Q. Xu *et al.*, “High photoluminescence quantum yield of 18.7% by using nitrogen-doped Ti3C2 MXene quantum dots,” *J. Mater. Chem. C*, vol. 6, no. 24, pp. 6360–6369, 2018, doi: 10.1039/c8tc02156b.

[194] R. B. Rakhi, P. Nayuk, C. Xia, and H. N. Alshareef, “Novel amperometric glucose biosensor based on MXene nanocomposite,” *Sci. Rep.*, vol. 6, Nov. 2016, doi: 10.1038/srep36422.

[195] S. Kumar, Y. Lei, N. H. Alshareef, M. A. Quevedo-Lopez, and K. N. Salama, “Biofunctionalized two-dimensional Ti3C2 MXenes for ultrasensitive detection of cancer biomarker,” *Biosens. Bioelectron.*, vol. 121, no. August, pp. 243–249, 2018, doi: 10.1016/j.bios.2018.08.076.

[196] J. Liu *et al.*, “MXene-Enabled Electrochemical Microfluidic Biosensor: Applications toward Multicomponent Continuous Monitoring in Whole Blood,” *Adv. Funct. Mater.*, vol. 29, no. 6, pp. 1–9, 2019, doi: 10.1002/adfm.201807326.

[197] J. Zheng *et al.*, “ An Inkjet Printed Ti 3 C 2 -GO Electrode for the Electrochemical Sensing of Hydrogen Peroxide ,” *J. Electrochem. Soc.*, vol. 165, no. 5, pp. B227–B231, 2018, doi: 10.1149/2.0051807jes.

[198] F. Wang, C. H. Yang, M. Duan, Y. Tang, and J. F. Zhu, “TiO2 nanoparticle modified organ-like Ti3C2 MXene nanocomposite encapsulating hemoglobin for a mediator-free biosensor with excellent performances,” *Biosens. Bioelectron.*, vol. 74, pp. 1022–1028, 2015, doi: 10.1016/j.bios.2015.08.004.

[199] J. Zheng, B. Wang, A. Ding, B. Weng, and J. Chen, “Synthesis of MXene/DNA/Pd/Pt nanocomposite for sensitive detection of dopamine,” *J. Electroanal. Chem.*, vol. 816, no. March, pp. 189–194, 2018, doi: 10.1016/j.jelechem.2018.03.056.

[200] Y. Lei *et al.*, “Facile preparation of sulfonic groups functionalized Mxenes for efficient removal of methylene blue,” *Ceram. Int.*, vol. 45, no. 14, pp. 17653–17661, 2019, doi: 10.1016/j.ceramint.2019.05.331.

[201] W. Sun, Z. Q. Zhai, D. D. Wang, S. F. Liu, and K. Jiao, “Electrochemistry of hemoglobin entrapped in a Nafion/nano-ZnO film on carbon ionic liquid electrode,” *Bioelectrochemistry*, vol. 74, no. 2, pp. 295–300, 2009, doi: 10.1016/j.bioelechem.2008.11.001.

[202] F. Wang, C. Yang, C. Duan, D. Xiao, Y. Tang, and J. Zhu, “An Organ-Like Titanium Carbide Material (MXene) with Multilayer Structure Encapsulating Hemoglobin for a Mediator-Free Biosensor,” vol. 162, no. 1, pp. 16–21, 2015, doi: 10.1149/2.0371501jes.

[203] P. Zhang, F. Jiang, and H. Chen, “Enhanced catalytic hydrogenation of aqueous bromate over Pd/mesoporous carbon nitride,” *Chem. Eng. J.*, vol. 234, pp. 195–202, 2013, doi: 10.1016/j.cej.2013.08.111.

[204] P. A. Rasheed, R. P. Pandey, K. Rasool, and K. A. Mahmoud, “Ultra-sensitive electrocatalytic detection of bromate in drinking water based on Nafion/Ti3C2Tx (MXene) modified glassy carbon electrode,” *Sensors Actuators, B Chem.*, vol. 265, pp. 652–659, 2018, doi: 10.1016/j.snb.2018.03.103.

[205] X. Cetó, C. P. Saint, C. W. K. Chow, N. H. Voelcker, and B. Prieto-Simón, “Electrochemical detection of N-nitrosodimethylamine using a molecular imprinted polymer,” *Sensors Actuators, B Chem.*, vol. 237, pp. 613–620, 2016, doi: 10.1016/j.snb.2016.06.136.

[206] L. Goldkind and L. Laine, “A systematic review of NSAIDs withdrawn from the market due to hepatotoxicity: Lessons learned from the bromfenac experience,” *Pharmacoepidemiol. Drug Saf.*, vol. 15, no. 4, pp. 213–220, 2006, doi: 10.1002/pds.1207.

[207] Y. Zhang, X. Jiang, J. Zhang, H. Zhang, and Y. Li, “Simultaneous voltammetric determination of acetaminophen and isoniazid using MXene modified screen-printed electrode,” *Biosens. Bioelectron.*, vol. 130, pp. 315–321, 2019, doi: 10.1016/j.bios.2019.01.043.

[208] X. Peng, Y. Zhang, D. Lu, Y. Guo, and S. Guo, “Ultrathin Ti3C2 nanosheets based ‘off-on’ fluorescent nanoprobe for rapid and sensitive detection of HPV infection,” *Sensors Actuators, B Chem.*, vol. 286, pp. 222–229, 2019, doi: 10.1016/j.snb.2019.01.158.

[209] H. Huang *et al.*, “Recent development and prospects of surface modification and biomedical applications of MXenes,” *Nanoscale*, vol. 12, no. 3, pp. 1325–1338, 2020, doi: 10.1039/c9nr07616f.

[210] H. Yu, Y. Wang, Y. Jing, J. Ma, C. F. Du, and Q. Yan, “Surface Modified MXene-Based Nanocomposites for Electrochemical Energy Conversion and Storage,” *Small*, vol. 15, no. 25, pp. 1–20, 2019, doi: 10.1002/smll.201901503.

[211] R. B. Rakhi, P. Nayak, C. Xia, and H. N. Alshareef, “Erratum: Novel amperometric glucose biosensor based on MXene nanocomposite (Scientific Reports (2016) 6(36422) DOI: 10.1038/srep36422),” *Sci. Rep.*, vol. 6, p. 38465, 2016, doi: 10.1038/srep38465.

[212] W. Yuan, K. Yang, H. Peng, F. Li, and F. Yin, “A flexible VOCs sensor based on a 3D Mxene framework with a high sensing performance,” *J. Mater. Chem. A*, vol. 6, no. 37, pp. 18116–18124, 2018, doi: 10.1039/c8ta06928j.

[213] Y. Cai *et al.*, “Stretchable Ti3C2Tx MXene/Carbon Nanotube Composite Based Strain Sensor with Ultrahigh Sensitivity and Tunable Sensing Range,” *ACS Nano*, vol. 12, no. 1, pp. 56–62, 2018, doi: 10.1021/acsnano.7b06251.

[214] M. Hu, H. Zhang, T. Hu, B. Fan, X. Wang, and Z. Li, “Emerging 2D MXenes for supercapacitors: Status, challenges and prospects,” *Chem. Soc. Rev.*, vol. 49, no. 18, pp. 6666–6693, 2020, doi: 10.1039/d0cs00175a.

[215] S. Wang *et al.*, “PANI nanofibers-supported Nb2CTx nanosheets-enabled selective NH3 detection driven by TENG at room temperature,” *Sensors Actuators, B Chem.*, vol. 327, Jan. 2021, doi: 10.1016/j.snb.2020.128923.

[216] R. Zeng *et al.*, “CRISPR-Cas12a-driven MXene-PEDOT:PSS piezoresistive wireless biosensor,” *Nano Energy*, vol. 82, p. 105711, 2021, doi: 10.1016/j.nanoen.2020.105711.

[217] A. S. Etman, J. Halim, and J. Rosen, “Mo1.33CTz–Ti3C2Tz mixed MXene freestanding films for zinc-ion hybrid supercapacitors,” *Mater. Today Energy*, vol. 22, p. 100878, 2021, doi: 10.1016/j.mtener.2021.100878.

[218] B. N. Rashmi *et al.*, “MoO3nanoparticles based electrodes as novel electrochemical sensors for the detection of H2O2,” *Mater. Today Proc.*, vol. 46, no. xxxx, pp. 5931–5935, 2020, doi: 10.1016/j.matpr.2020.09.161.

[219] A. K. Mohiuddin and S. Jeon, “Highly efficient Ag doped δ-MnO2 decorated graphene: Comparison and application in electrochemical detection of H2O2,” *Appl. Surf. Sci.*, vol. 592, no. January, p. 153162, 2022, doi: 10.1016/j.apsusc.2022.153162.

[220] J. Li *et al.*, “Achieving High Pseudocapacitance of 2D Titanium Carbide (MXene) by Cation Intercalation and Surface Modification,” *Adv. Energy Mater.*, vol. 7, no. 15, 2017, doi: 10.1002/aenm.201602725.

[221] Y. Dall’Agnese, P. Rozier, P. L. Taberna, Y. Gogotsi, and P. Simon, “Capacitance of two-dimensional titanium carbide (MXene) and MXene/carbon nanotube composites in organic electrolytes,” *J. Power Sources*, vol. 306, pp. 510–515, 2016, doi: 10.1016/j.jpowsour.2015.12.036.

[222] M. Tang *et al.*, “Organics-MXene Composites as Electrode Materials for Energy Storage,” *Batter. Supercaps*, vol. 6, no. 1, 2023, doi: 10.1002/batt.202200402.

[223] A. C. Lazanas and M. I. Prodromidis, “Electrochemical Impedance Spectroscopy–A Tutorial,” *ACS Meas. Sci. Au*, 2022, doi: 10.1021/acsmeasuresciau.2c00070.

[224] T. Kshetri *et al.*, “Recent advances in MXene-based nanocomposites for electrochemical energy storage applications,” *Prog. Mater. Sci.*, vol. 117, no. May 2019, p. 100733, 2021, doi: 10.1016/j.pmatsci.2020.100733.

[225] X. Li *et al.*, “Enhanced Redox Kinetics and Duration of Aqueous I2/I− Conversion Chemistry by MXene Confinement,” *Adv. Mater.*, vol. 33, no. 8, 2021, doi: 10.1002/adma.202006897.

[226] M. Saraf *et al.*, “Vanadium and Niobium MXenes—Bilayered V2O5 Asymmetric Supercapacitors,” *Small Methods*, vol. 2201551, pp. 1–8, 2023, doi: 10.1002/smtd.202201551.

[227] X. Tang, X. Guo, W. Wu, and G. Wang, “2D Metal Carbides and Nitrides (MXenes) as High-Performance Electrode Materials for Lithium-Based Batteries,” *Adv. Energy Mater.*, vol. 8, no. 33, pp. 1–21, 2018, doi: 10.1002/aenm.201801897.

[228] J. Mei, G. A. Ayoko, C. Hu, J. M. Bell, and Z. Sun, “Two-dimensional fluorine-free mesoporous Mo2C MXene via UV-induced selective etching of Mo2Ga2C for energy storage,” *Sustain. Mater. Technol.*, vol. 25, p. e00156, 2020, doi: 10.1016/j.susmat.2020.e00156.

[229] B. Soundiraraju and B. K. George, “Two-Dimensional Titanium Nitride (Ti2N) MXene:

Synthesis, Characterization, and Potential Application as Surface-Enhanced Raman Scattering Substrate," *ACS Nano*, vol. 11, no. 9, pp. 8892–8900, 2017, doi: 10.1021/acsnano.7b03129.

[230] M. Alhabeb *et al.*, "Guidelines for Synthesis and Processing of Two-Dimensional Titanium Carbide (Ti3C2Tx MXene)," *Chem. Mater.*, vol. 29, no. 18, pp. 7633–7644, Sep. 2017, doi: 10.1021/acs.chemmater.7b02847.

[231] M. Naguib, V. N. Mochalin, M. W. Barsoum, and Y. Gogotsi, "25th anniversary article: MXenes: A new family of two-dimensional materials," *Adv. Mater.*, vol. 26, no. 7, pp. 992–1005, 2014, doi: 10.1002/adma.201304138.

[232] S. Kajiyama *et al.*, "Enhanced Li-Ion Accessibility in MXene Titanium Carbide by Steric Chloride Termination," *Adv. Energy Mater.*, vol. 7, no. 9, pp. 1–8, 2017, doi: 10.1002/aenm.201601873.

[233] X. Wang *et al.*, "A new etching environment (FeF3/HCl) for the synthesis of two-dimensional titanium carbide MXenes: A route towards selective reactivity: Vs. water," *J. Mater. Chem. A*, vol. 5, no. 41, pp. 22012–22023, 2017, doi: 10.1039/c7ta01082f.

[234] F. Liu *et al.*, "Preparation of Ti 3 C 2 and Ti 2 C MXenes by fluoride salts etching and methane adsorptive properties," *Appl. Surf. Sci.*, vol. 416, pp. 781–789, 2017, doi: 10.1016/j.apsusc.2017.04.239.

[235] O. Mashtalir *et al.*, "Intercalation and delamination of layered carbides and carbonitrides," *Nat. Commun.*, vol. 4, 2013, doi: 10.1038/ncomms2664.

[236] M. Ghidiu, M. R. Lukatskaya, M. Q. Zhao, Y. Gogotsi, and M. W. Barsoum, "Conductive two-dimensional titanium carbide 'clay' with high volumetric capacitance," *Nature*, vol. 516, no. 7529, pp. 78–81, 2015, doi: 10.1038/nature13970.

[237] X. Sang *et al.*, "Atomic defects in monolayer titanium carbide (Ti3C2Tx) MXene," *ACS Nano*, vol. 10, no. 10, pp. 9193–9200, 2016, doi: 10.1021/acsnano.6b05240.

[238] M. Ghidiu, J. Halim, S. Kota, D. Bish, Y. Gogotsi, and M. W. Barsoum, "Ion-Exchange and Cation Solvation Reactions in Ti3C2 MXene," *Chem. Mater.*, vol. 28, no. 10, pp. 3507–3514, 2016, doi: 10.1021/acs.chemmater.6b01275.

[239] S. Yang *et al.*, "Fluoride-Free Synthesis of Two-Dimensional Titanium Carbide (MXene) Using A Binary Aqueous System," *Angew. Chemie*, vol. 130, no. 47, pp. 15717–15721, 2018, doi: 10.1002/ange.201809662.

[240] J. Zhou *et al.*, "A Two-Dimensional Zirconium Carbide by Selective Etching of Al3C3 from Nanolaminated Zr3Al3C5," *Angew. Chemie - Int. Ed.*, vol. 55, no. 16, pp. 5008–5013, 2016, doi: 10.1002/anie.201510432.

[241] F. Shahzad *et al.*, "Electromagnetic interference shielding with 2D transition metal carbides," *MXenes From Discov. to Appl. Two-Dimensional Met. Carbides Nitrides*, pp. 933–947, 2023, doi: 10.1201/9781003306511-47.

[242] J. Zhou *et al.*, "Synthesis and Electrochemical Properties of Two-Dimensional Hafnium Carbide," *ACS Nano*, vol. 11, no. 4, pp. 3841–3850, 2017, doi: 10.1021/acsnano.7b00030.

[243] P. Urbankowski *et al.*, "Synthesis of two-dimensional titanium nitride Ti4N3 (MXene)," *Nanoscale*, vol. 8, no. 22, pp. 11385–11391, 2016, doi: 10.1039/c6nr02253g.

[244] M. Naguib and Y. Gogotsi, "Synthesis of two-dimensional materials by selective extraction," *Acc. Chem. Res.*, vol. 48, no. 1, pp. 128–135, 2015, doi: 10.1021/ar500346b.

[245] Q. Tao *et al.*, “Two-dimensional Mo1.33C MXene with divacancy ordering prepared from parent 3D laminate with in-plane chemical ordering,” *Nat. Commun.*, vol. 8, pp. 1–7, 2017, doi: 10.1038/ncomms14949.

[246] M. Khazaei, A. Ranjbar, K. Esfarjani, D. Bogdanovski, R. Dronskowski, and S. Yunoki, “Insights into exfoliation possibility of MAX phases to MXenes,” *Phys. Chem. Chem. Phys.*, vol. 20, no. 13, pp. 8579–8592, 2018, doi: 10.1039/c7cp08645h.

[247] H. W. Wang, M. Naguib, K. Page, D. J. Wesolowski, and Y. Gogotsi, “Resolving the Structure of Ti3C2Tx MXenes through Multilevel Structural Modeling of the Atomic Pair Distribution Function,” *Chem. Mater.*, vol. 28, no. 1, pp. 349–359, 2016, doi: 10.1021/acs.chemmater.5b04250.

[248] B. Anasori *et al.*, “Experimental and theoretical characterization of ordered MAX phases Mo2TiAlC2 and Mo2Ti2AlC3,” *J. Appl. Phys.*, vol. 118, no. 9, 2015, doi: 10.1063/1.4929640.

[249] C. J. Rawn, M. W. Barsoum, T. El-Raghy, A. Procipio, C. M. Hoffmann, and C. R. Hubbard, “Structure of Ti4AlN3 - a layered Mn+1AXn nitride,” *Mater. Res. Bull.*, vol. 35, no. 11, pp. 1785–1796, 2000, doi: 10.1016/S0025-5408(00)00383-4.

[250] P. Urbankowski *et al.*, “Synthesis of two-dimensional titanium nitride Ti4N3 (MXene),” *Nanoscale*, vol. 8, no. 22, pp. 11385–11391, Jun. 2016, doi: 10.1039/c6nr02253g.

[251] J. Xuan *et al.*, “Organic-Base-Driven Intercalation and Delamination for the Production of Functionalized Titanium Carbide Nanosheets with Superior Photothermal Therapeutic Performance,” *Angew. Chemie - Int. Ed.*, vol. 55, no. 47, pp. 14569–14574, 2016, doi: 10.1002/anie.201606643.

[252] X. Xie *et al.*, “Surface Al leached Ti3AlC2as a substitute for carbon for use as a catalyst support in a harsh corrosive electrochemical system,” *Nanoscale*, vol. 6, no. 19, pp. 11035–11040, 2014, doi: 10.1039/c4nr02080d.

[253] M. R. Lukatskaya *et al.*, “Cation intercalation and high volumetric capacitance of two-dimensional titanium carbide,” *Science (80-.).*, vol. 341, no. 6153, pp. 1502–1505, 2013, doi: 10.1126/science.1241488.

[254] K. Maleski, V. N. Mochalin, and Y. Gogotsi, “Dispersions of Two-Dimensional Titanium Carbide MXene in Organic Solvents,” *Chem. Mater.*, vol. 29, no. 4, pp. 1632–1640, 2017, doi: 10.1021/acs.chemmater.6b04830.

[255] M. Naguib, R. R. Unocic, B. L. Armstrong, and J. Nanda, “Large-scale delamination of multi-layers transition metal carbides and carbonitrides ‘MXenes,’” pp. 9353–9358, 2015, doi: 10.1039/c5dt01247c.

[256] Y. Ying *et al.*, “Two-dimensional titanium carbide for efficiently reductive removal of highly toxic chromium(VI) from water,” *ACS Appl. Mater. Interfaces*, vol. 7, no. 3, pp. 1795–1803, 2015, doi: 10.1021/am5074722.

[257] O. Mashtalir, K. M. Cook, V. N. Mochalin, M. Crowe, M. W. Barsoum, and Y. Gogotsi, “Dye adsorption and decomposition on two-dimensional titanium carbide in aqueous media,” *J. Mater. Chem. A*, vol. 2, no. 35, pp. 14334–14338, 2014, doi: 10.1039/c4ta02638a.

[258] M. Choucair, P. Thordarson, and J. A. Stride, “Gram-scale production of graphene based on solvothermal synthesis and sonication,” *Nat. Nanotechnol.*, vol. 4, no. 1, pp. 30–33, 2009, doi: 10.1038/nnano.2008.365.

[259] Y. Hernandez *et al.*, “High-yield production of graphene by liquid-phase exfoliation of

graphite," *Nat. Nanotechnol.*, vol. 3, no. 9, pp. 563–568, 2008, doi: 10.1038/nnano.2008.215.

[260] D. Li, M. B. Müller, S. Gilje, R. B. Kaner, and G. G. Wallace, "Processable aqueous dispersions of graphene nanosheets," *Nat. Nanotechnol.*, vol. 3, no. 2, pp. 101–105, 2008, doi: 10.1038/nnano.2007.451.

[261] S. Bae *et al.*, "Roll-to-roll production of 30-inch graphene films for transparent electrodes," *Nat. Nanotechnol.*, vol. 5, no. 8, pp. 574–578, 2010, doi: 10.1038/nnano.2010.132.

[262] J. Yang *et al.*, "Two-Dimensional Nb-Based M4C3 Solid Solutions (MXenes)," *J. Am. Ceram. Soc.*, vol. 99, no. 2, pp. 660–666, 2016, doi: 10.1111/jace.13922.

[263] M. Li *et al.*, "Element Replacement Approach by Reaction with Lewis Acidic Molten Salts to Synthesize Nanolaminated MAX Phases and MXenes," *J. Am. Chem. Soc.*, vol. 141, no. 11, pp. 4730–4737, 2019, doi: 10.1021/jacs.9b00574.

[264] Y. Li *et al.*, "A general Lewis acidic etching route for preparing MXenes with enhanced electrochemical performance in non-aqueous electrolyte," *Nat. Mater.*, vol. 19, no. 8, pp. 894–899, 2020, doi: 10.1038/s41563-020-0657-0.

[265] K. R. G. Lim, M. Shekhirev, B. C. Wyatt, B. Anasori, Y. Gogotsi, and Z. W. Seh, "Fundamentals of MXene synthesis," *Nat. Synth.*, vol. 1, no. 8, pp. 601–614, 2022, doi: 10.1038/s44160-022-00104-6.

[266] C. E. Shuck, K. Ventura-Martinez, A. Goad, S. Uzun, M. Shekhirev, and Y. Gogotsi, "Safe Synthesis of MAX and MXene: Guidelines to Reduce Risk During Synthesis," *ACS Chem. Heal. Saf.*, Aug. 2021, doi: 10.1021/acs.chas.1c00051.

[267] X. Li *et al.*, "In Situ Electrochemical Synthesis of MXenes without Acid/Alkali Usage in/for an Aqueous Zinc Ion Battery," *Adv. Energy Mater.*, vol. 10, no. 36, pp. 1–8, 2020, doi: 10.1002/aenm.202001791.

[268] K. Deshmukh, T. Kovářík, and S. K. Khadheer Pasha, "State of the art recent progress in two dimensional MXenes based gas sensors and biosensors: A comprehensive review," *Coord. Chem. Rev.*, vol. 424, 2020, doi: 10.1016/j.ccr.2020.213514.

[269] O. D. Renedo, M. A. Alonso-Lomillo, and M. J. A. Martínez, "Recent developments in the field of screen-printed electrodes and their related applications," *Talanta*, vol. 73, no. 2, pp. 202–219, 2007, doi: 10.1016/j.talanta.2007.03.050.

[270] J. P. Hart and S. A. Wring, "Recent developments in the design and application of screen-printed electrochemical sensors for biomedical, environmental and industrial analyses," *TrAC - Trends Anal. Chem.*, vol. 16, no. 2, pp. 89–103, 1997, doi: 10.1016/S0165-9936(96)00097-0.

[271] C. Tortolini, P. Bollella, M. L. Antonelli, R. Antiochia, F. Mazzei, and G. Favero, "DNA-based biosensors for Hg2+ determination by polythymine-methylene blue modified electrodes," *Biosens. Bioelectron.*, vol. 67, pp. 524–531, 2015, doi: 10.1016/j.bios.2014.09.031.

[272] F. Arduini *et al.*, "Electrochemical biosensors based on nanomodified screen-printed electrodes: Recent applications in clinical analysis," *TrAC - Trends Anal. Chem.*, vol. 79, pp. 114–126, 2016, doi: 10.1016/j.trac.2016.01.032.

[273] C. J. Mei, N. A. Yusof, S. Ainliah, and A. Ahmad, "Electrochemical determination of lead & copper ions using carbon electrode," *Chemosensors*, vol. 9, no. 7, p. 157, 2021.

[274] S. Balu, S. Palanisamy, V. Velusamy, and T. C. K. Yang, "Sonochemical synthesis of gum guar biopolymer stabilized copper oxide on exfoliated graphite: Application for enhanced electrochemical detection of H2O2 in milk and pharmaceutical samples," *Ultrason.*

Sonochem., vol. 56, no. April, pp. 254–263, 2019, doi: 10.1016/j.ultsonch.2019.04.023.

[275] G. S. Ustabasi, M. Ozcan, and I. Yilmaz, "Review—Voltammetric Determination of Heavy Metals with Carbon-Based Electrodes," *J. Electrochem. Soc.*, vol. 168, no. 9, p. 097508, 2021, doi: 10.1149/1945-7111/ac253e.

[276] M. Awan, M. Nasir, S. Iqbal, K. Manshad, A. Hayat, and H. Ajab, "Fabrication of novel electroactive nickel sulfide@graphene oxide nanocomposite integrated transduction platform for non-enzymatic electrochemical sensing of Hydrogen Peroxide in environmental and biological samples," *Synth. Met.*, vol. 292, no. September 2022, p. 117240, 2023, doi: 10.1016/j.synthmet.2022.117240.

[277] K. Nemčeková and J. Labuda, "Advanced materials-integrated electrochemical sensors as promising medical diagnostics tools: A review," *Mater. Sci. Eng. C*, vol. 120, p. 111751, 2021, doi: 10.1016/j.msec.2020.111751.

[278] R. Cartwright, "Book Reviews: Book Reviews," *Perspect. Public Health*, vol. 130, no. 5, pp. 239–239, 2010, doi: 10.1177/1757913910379198.

[279] A. Chauhan, "Powder XRD Technique and its Applications in Science and Technology," *J. Anal. Bioanal. Tech.*, vol. 5, no. 6, 2014, doi: 10.4172/2155-9872.1000212.

[280] H. Khan, A. S. Yerramilli, A. D'Oliveira, T. L. Alford, D. C. Boffito, and G. S. Patience, "Experimental methods in chemical engineering: X-ray diffraction spectroscopy—XRD," *Can. J. Chem. Eng.*, vol. 98, no. 6, pp. 1255–1266, 2020, doi: 10.1002/cjce.23747.

[281] J. Epp, *X-Ray Diffraction (XRD) Techniques for Materials Characterization*. Elsevier Ltd, 2016.

[282] H. H. W. Stanjek, "3-Basics of X-Ray Diffraction," pp. 107–119, 2004, [Online]. Available: https://doi.org/10.1023/B:HYPE.0000032028.60546.38.

[283] J. Zhang, K. A. S. Usman, M. A. N. Judicpa, D. Hegh, P. A. Lynch, and J. M. Razal, "Applications of X-Ray-Based Characterization in MXene," vol. 2201527, pp. 1–16, 2023, doi: 10.1002/smtd.202201527.

[284] P. S. Prevéy, "Current applications of XRD diffraction residual stress measurement," *Dev. Mater. Charact. Technol. ASM Int.*, no. 513, pp. 103–110, 1996.

[285] P. D. Ngo, "Energy Dispersive Spectroscopy," *Fail. Anal. Integr. Circuits*, pp. 205–215, 1999, doi: 10.1007/978-1-4615-4919-2_12.

[286] V. D. Hodoroaba, *Energy-dispersive X-ray spectroscopy (EDS)*, no. X. Elsevier Inc., 2019.

[287] J. Long, A. Nand, and S. Ray, "Application of spectroscopy in additive manufacturing," *Materials (Basel).*, vol. 14, no. 1, pp. 1–29, 2021, doi: 10.3390/MA14010203.

[288] S. Pascarelli, O. Mathon, M. Munõz, T. Mairs, and J. Susini, "Energy-dispersive absorption spectroscopy for hard-X-ray micro-XAS applications," *J. Synchrotron Radiat.*, vol. 13, no. 5, pp. 351–358, 2006, doi: 10.1107/S0909049506026938.

[289] M. Scimeca, S. Bischetti, H. K. Lamsira, R. Bonfiglio, and E. Bonanno, "Energy dispersive X-ray (EDX) microanalysis: A powerful tool in biomedical research and diagnosis," *Eur. J. Histochem.*, vol. 62, no. 1, pp. 89–99, 2018, doi: 10.4081/ejh.2018.2841.

[290] D. Zhang, L. Yu, D. Wang, Y. Yang, Q. Mi, and J. Zhang, "Multifunctional latex/ polytetrafluoroethylene-based triboelectric nanogenerator for self-powered organ-like mxene/metal-organic framework-derived cuo nanohybrid ammonia sensor," *ACS Nano*, vol. 15, no. 2, pp. 2911–2919, 2021, doi: 10.1021/acsnano.0c09015.

[291] W. Zhou, R. Apkarian, Z. L. Wang, and D. Joy, “Fundamentals of scanning electron microscopy (SEM),” *Scanning Microsc. Nanotechnol. Tech. Appl.*, pp. 1–40, 2007, doi: 10.1007/978-0-387-39620-0_1.

[292] K. Iwata and K. Ueda, “Edge Formation Based on Direct Scanning Electron,” *Wear*, vol. 60, pp. 329–331, 1980.

[293] T. Radetic, “Fundamentals of scanning electron microscopy and energy dispersive X-ray analysis in SEM and TEM,” *NFMC Spring Sch. Electron Microsc.*, no. April, pp. 1–52, 2011, [Online]. Available: file:///C:/Users/win10/Downloads/zbook_tamara-20radetic_642206 (1).pdf.

[294] H. Kriaa, A. Guitton, and N. Maloufi, “Fundamental and experimental aspects of diffraction for characterizing dislocations by electron channeling contrast imaging in scanning electron microscope,” *Sci. Rep.*, vol. 7, no. 1, pp. 1–8, 2017, doi: 10.1038/s41598-017-09756-3.

[295] E. R. Fischer, B. T. Hansen, V. Nair, F. H. Hoyt, and D. W. Dorward, *Scanning electron microscopy*, no. SUPPL.25. 2012.

[296] H. Alnoor *et al.*, “Exploring MXenes and their MAX phase precursors by electron microscopy,” *Mater. Today Adv.*, vol. 9, 2021, doi: 10.1016/j.mtadv.2020.100123.

[297] K. Maleski, C. E. Ren, M. Q. Zhao, B. Anasori, and Y. Gogotsi, “Size-Dependent Physical and Electrochemical Properties of Two-Dimensional MXene Flakes,” *ACS Appl. Mater. Interfaces*, vol. 10, no. 29, pp. 24491–24498, 2018, doi: 10.1021/acsami.8b04662.

[298] M. P. Seah, “The quantitative analysis of surfaces by XPS: A review,” *Surf. Interface Anal.*, vol. 2, no. 6, pp. 222–239, 1980, doi: 10.1002/sia.740020607.

[299] T. Yamashita and P. Hayes, “Analysis of XPS spectra of Fe 2+ and Fe 3+ ions in oxide materials,” *Appl. Surf. Sci.*, vol. 254, no. 8, pp. 2441–2449, 2008, doi: 10.1016/j.apsusc.2007.09.063.

[300] X. Chen, X. Wang, and D. Fang, “A review on C1s XPS-spectra for some kinds of carbon materials,” *Fullerenes Nanotub. Carbon Nanostructures*, vol. 0, no. 0, pp. 1048–1058, 2020, doi: 10.1080/1536383X.2020.1794851.

[301] D. R. Baer *et al.*, “Practical guides for x-ray photoelectron spectroscopy: First steps in planning, conducting, and reporting XPS measurements,” *J. Vac. Sci. Technol. A*, vol. 37, no. 3, p. 031401, 2019, doi: 10.1116/1.5065501.

[302] V. Natu, M. Benchakar, C. Canaff, A. Habrioux, S. Célérier, and M. W. Barsoum, “A critical analysis of the X-ray photoelectron spectra of Ti3C2Tz MXenes,” *Matter*, vol. 4, no. 4, pp. 1224–1251, 2021, doi: 10.1016/j.matt.2021.01.015.

[303] J. Zhang, K. A. S. Usman, M. A. N. Judicpa, D. Hegh, P. A. Lynch, and J. M. Razal, “Applications of X-Ray-Based Characterization in MXene Research,” *Small Methods*, vol. 2201527, pp. 1–16, 2023, doi: 10.1002/smtd.202201527.

[304] Z. Fan *et al.*, “In Situ Transmission Electron Microscopy for Energy Materials and Devices,” *Adv. Mater.*, vol. 31, no. 33, pp. 1–22, 2019, doi: 10.1002/adma.201900608.

[305] C. F. Escalante, C. Fabian, and E. Sierra, “Fundamentals of transmission electron microscopy, the technique with the best resolution in the world Transmission electron microscopy View project Fundamentals of transmission electron microscopy, the technique with the best resolution in the world,” *Screen*, vol. 9, no. February, p. 10, 2019, [Online]. Available: https://www.researchgate.net/profile/Cristian-

Escalante/publication/330999184_Fundamentals_of_transmission_electron_microscopy_the_technique_with_the_best_resolution_in_the_world/links/5c60490ea6fdccb608b758a5/Fundamentals-of-transmission-electron-microsc.

[306] Q. Type, P. Sample, S. Mean, D. Discrm, and E. Frequency, "2: Transmission electron microscopy (hide)(regrade)," pp. 3–8.

[307] M. Winey, J. B. Meehl, E. T. O'Toole, and T. H. Giddings, "Conventional transmission electron microscopy," *Mol. Biol. Cell*, vol. 25, no. 3, pp. 319–323, 2014, doi: 10.1091/mbc.E12-12-0863.

[308] K. Rasool, M. Helal, A. Ali, C. E. Ren, Y. Gogotsi, and K. A. Mahmoud, "Antibacterial Activity of Ti3C2Tx MXene," *ACS Nano*, vol. 10, no. 3, pp. 3674–3684, 2016, doi: 10.1021/acsnano.6b00181.

[309] W. H. Melhuish, *Molecular Luminescence Spectroscopy - Vi.*, vol. 56, no. 2. 1984.

[310] C. Del Gratta and G. L. Romani, "MEG: Principles, methods, and applications," *Biomed. Tech.*, vol. 44, no. s2, pp. 11–23, 1999, doi: 10.1515/bmte.1999.44.s2.11.

[311] P. Brunswick, H. Mayaudon, V. Albin, V. Lair, A. Ringuede, and M. Cassir, "Use of Ni electrodes chronoamperometry for improved diagnostics of diabetes and cardiac diseases," *Annu. Int. Conf. IEEE Eng. Med. Biol. - Proc.*, vol. 33, no. 1, pp. 4544–4547, 2007, doi: 10.1109/IEMBS.2007.4353350.

[312] F. Manea, A. Remes, C. Radovan, R. Pode, S. Picken, and J. Schoonman, "Simultaneous electrochemical determination of nitrate and nitrite in aqueous solution using Ag-doped zeolite-expanded graphite-epoxy electrode," *Talanta*, vol. 83, no. 1, pp. 66–71, 2010, doi: 10.1016/j.talanta.2010.08.042.

[313] G. J. Hills, D. J. Schiffrin, and J. Thompson, "Electrochemical nucleation from molten salts-I. Diffusion controlled electrodeposition of silver from alkali molten nitrates," *Electrochim. Acta*, vol. 19, no. 11, pp. 657–670, 1974, doi: 10.1016/0013-4686(74)80008-3.

[314] S. Girousi, S. Karastogianni, and C. Serpi, *Electrochemical Techniques as Promising Analytical Tools in the DNA Electrochemistry (A Review)*, vol. 7, no. Cv. 2012.

[315] J. O. Bockris, A. K. N. Reddy, and M. Gamboa-Aldeco, *MODERN ELECTROCHEMISTRY SECOND EDITION Ionics*. 2002.

[316] D. Harley, "Chapter 11 Electrochemical Methods Section 11A Overview of Electrochemistry Section 11B Potentiometric Methods Section 11C Coulometric Methods Section 11D Voltammetric and Amperometric Methods Section 11E Key Terms Section 11F Chapter Summary Section 11G ," *Anal. Chem.*, pp. 1–115, 2018, [Online]. Available: http://www.asdlib.org/onlineArticles/ecourseware/Analytical Chemistry 2.0/Text_Files.html.

[317] V. Mirceski, S. Skrzypek, and L. Stojanov, "Square-wave voltammetry," *ChemTexts*, vol. 4, no. 4, pp. 1–14, 2018, doi: 10.1007/s40828-018-0073-0.

[318] D. De Souza, S. A. S. Machado, and L. A. Avaca, "Square wave voltammetry. Part I: Theoretical aspects," *Quim. Nova*, vol. 26, no. 1, pp. 81–89, 2003, doi: 10.1590/s0100-40422003000100015.

[319] P. Agarwal, M. E. Orazem, and L. H. Garcia-Rubio, "Application of Measurement Models to Impedance Spectroscopy: III . Evaluation of Consistency with the Kramers-Kronig Relations," *J. Electrochem. Soc.*, vol. 142, no. 12, pp. 4159–4168, 1995, doi: 10.1149/1.2048479.

[320] D. D. Macdonald, E. Sikora, and G. Engelhardt, "Characterizing electrochemical systems in the

frequency domain," *Electrochim. Acta*, vol. 43, no. 1–2, pp. 87–107, 1998, doi: 10.1016/S0013-4686(97)00238-7.

[321] H. Herrera Hernández *et al.*, "Electrochemical Impedance Spectroscopy (EIS): A Review Study of Basic Aspects of the Corrosion Mechanism Applied to Steels," *Electrochem. Impedance Spectrosc.*, pp. 1–35, 2020, doi: 10.5772/intechopen.94470.

[322] W. Choi, H. C. Shin, J. M. Kim, J. Y. Choi, and W. S. Yoon, "Modeling and applications of electrochemical impedance spectroscopy (Eis) for lithium-ion batteries," *J. Electrochem. Sci. Technol.*, vol. 11, no. 1, pp. 1–13, 2020, doi: 10.33961/jecst.2019.00528.

[323] K. Arole *et al.*, "Exfoliation, delamination, and oxidation stability of molten salt etched Nb2CTz MXene nanosheets," *Chem. Commun.*, vol. 58, no. 73, pp. 10202–10205, 2022, doi: 10.1039/d2cc02237k.

[324] A. D. Bortolozo, O. H. S. Anna, M. S. Luz, and C. A. M, "Superconductivity in the Nb 2 SnC compound."

[325] S. Zhao, Y. Dall'Agnese, X. Chu, X. Zhao, Y. Gogotsi, and Y. Gao, "Electrochemical Interaction of Sn-Containing MAX Phase (Nb2SnC) with Li-Ions," *ACS Energy Lett.*, vol. 4, pp. 2452–2457, 2019, doi: 10.1021/acsenergylett.9b01580.

[326] M. Romero, L. Huerta, T. Akachi, J. L. S. Llamazares, and R. Escamilla, "X-ray photoelectron spectroscopy studies of the electronic structure of superconducting Nb2SnC and Nb2SC," *J. Alloys Compd.*, vol. 579, pp. 516–520, 2013, doi: 10.1016/j.jallcom.2013.05.214.

[327] T. El-Raghy, S. Chakraborty, and M. W. Barsoum, "Synthesis and characterization of Hf2PbC, Zr2PbC and M2SnC (M = Ti, Hf, Nb or Zr)," *J. Eur. Ceram. Soc.*, vol. 20, no. 14–15, pp. 2619–2625, 2000, doi: 10.1016/S0955-2219(00)00127-8.

[328] Y. Wang, Y. Song, and Y. Xia, "Electrochemical capacitors: Mechanism, materials, systems, characterization and applications," *Chem. Soc. Rev.*, vol. 45, no. 21, pp. 5925–5950, 2016, doi: 10.1039/c5cs00580a.

[329] T. Li *et al.*, "Fluorine-Free Synthesis of High-Purity Ti3C2Tx (T=OH, O) via Alkali Treatment," *Angew. Chemie - Int. Ed.*, vol. 57, no. 21, pp. 6115–6119, 2018, doi: 10.1002/anie.201800887.

[330] M. O. Guerrero-Pérez and G. S. Patience, "Experimental methods in chemical engineering: Fourier transform infrared spectroscopy—FTIR," *Can. J. Chem. Eng.*, vol. 98, no. 1, pp. 25–33, 2020, doi: 10.1002/cjce.23664.

[331] S. Yang *et al.*, "Fluoride-Free Synthesis of Two-Dimensional Titanium Carbide (MXene) Using A Binary Aqueous System," *Angew. Chemie - Int. Ed.*, vol. 57, no. 47, pp. 15491–15495, 2018, doi: 10.1002/anie.201809662.

[332] H. Lin, S. Gao, C. Dai, Y. Chen, and J. Shi, "A Two-Dimensional Biodegradable Niobium Carbide (MXene) for Photothermal Tumor Eradication in NIR-I and NIR-II Biowindows," *J. Am. Chem. Soc.*, vol. 139, no. 45, pp. 16235–16247, 2017, doi: 10.1021/jacs.7b07818.

[333] Y. Gogotsi and R. M. Penner, "Energy Storage in Nanomaterials - Capacitive, Pseudocapacitive, or Battery-like?," *ACS Nano*, vol. 12, no. 3, pp. 2081–2083, 2018, doi: 10.1021/acsnano.8b01914.

[334] J. Aguedo, L. Lorencova, M. Barath, P. Farkas, and J. Tkac, "Electrochemical impedance spectroscopy on 2d nanomaterial mxene modified interfaces: Application as a characterization and transducing tool," *Chemosensors*, vol. 8, no. 4, pp. 1–21, 2020, doi: 10.3390/chemosensors8040127.

[335] Y. Ouyang *et al.*, “Hierarchical Structure Electrodes of NiO Ultrathin Nanosheets Anchored to NiCo 2 O 4 on Carbon Cloth with Excellent Cycle Stability for Asymmetric Supercapacitors,” *Chem. Eng. J.*, 2018, doi: 10.1016/j.cej.2018.08.142.

[336] L. Verger, C. Xu, V. Natu, H. M. Cheng, W. Ren, and M. W. Barsoum, “Overview of the synthesis of MXenes and other ultrathin 2D transition metal carbides and nitrides,” *Curr. Opin. Solid State Mater. Sci.*, vol. 23, no. 3, pp. 149–163, 2019, doi: 10.1016/j.cossms.2019.02.001.

[337] J. F. Liebman, “Paradigms and paradoxes: The solubility of AgCl in water: Some thermochemical issues of aqueous Ag+ ion,” *Struct. Chem.*, vol. 15, no. 2, pp. 165–168, 2004, doi: 10.1023/B:STUC.0000011251.85406.ed.

[338] S. Siddique *et al.*, “Fluorine-free MXenes via molten salt Lewis acidic etching: Applications, challenges, and future outlook,” *Prog. Mater. Sci.*, vol. 139, no. January, p. 101183, 2023, doi: 10.1016/j.pmatsci.2023.101183.

[339] C. E. Shuck *et al.*, “Scalable Synthesis of Ti3C2Tx MXene,” *Adv. Eng. Mater.*, vol. 22, no. 3, pp. 1–8, 2020, doi: 10.1002/adem.201901241.

[340] M. Naguib *et al.*, “New two-dimensional niobium and vanadium carbides as promising materials for li-ion batteries,” *J. Am. Chem. Soc.*, vol. 135, no. 43, pp. 15966–15969, Oct. 2013, doi: 10.1021/ja405735d.

[341] M. Griseri *et al.*, “Synthesis, properties and thermal decomposition of the Ta 4 AlC 3 MAX phase,” *J. Eur. Ceram. Soc.*, vol. 39, no. 10, pp. 2973–2981, 2019, doi: 10.1016/j.jeurceramsoc.2019.04.021.

[342] Y. Bai *et al.*, “MXene-Copper/Cobalt Hybrids via Lewis Acidic Molten Salts Etching for High Performance Symmetric Supercapacitors,” *Angew. Chemie*, vol. 133, no. 48, pp. 25522–25526, 2021, doi: 10.1002/ange.202112381.

[343] W. Cui, Z. Y. Hu, R. R. Unocic, G. Van Tendeloo, and X. Sang, “Atomic defects, functional groups and properties in MXenes,” *Chinese Chem. Lett.*, vol. 32, no. 1, pp. 339–344, 2021, doi: 10.1016/j.cclet.2020.04.024.

[344] T. Ramachandran and A. I. Mourad, “Nb 2 CT x -Based MXenes Most Recent Developments : From Principles to New Applications,” 2023.

[345] P. O. Å. Persson and J. Rosen, “Current state of the art on tailoring the MXene composition, structure, and surface chemistry,” *Curr. Opin. Solid State Mater. Sci.*, vol. 23, no. 6, p. 100774, 2019, doi: 10.1016/j.cossms.2019.100774.

[346] C. Verma and K. K. Thakur, “Recent advances in MXene-based electrochemical sensors,” *Eur. J. Mol. Clin. Med.*, vol. 7, no. 7, pp. 4429–4450, 2020.

[347] X. Wu, P. Ma, Y. Sun, F. Du, D. Song, and G. Xu, “Application of MXene in Electrochemical Sensors: A Review,” *Electroanalysis*, vol. 33, no. 8. John Wiley and Sons Inc, pp. 1827–1851, Aug. 01, 2021, doi: 10.1002/elan.202100192.

[348] N. Murugan, R. Jerome, M. Preethika, A. Sundaramurthy, and A. K. Sundramoorthy, “2D-titanium carbide (MXene) based selective electrochemical sensor for simultaneous detection of ascorbic acid, dopamine and uric acid,” *J. Mater. Sci. Technol.*, vol. 72, pp. 122–131, 2021, doi: 10.1016/j.jmst.2020.07.037.

[349] A. Hayat and J. L. Marty, “Disposable screen printed electrochemical sensors: Tools for environmental monitoring,” *Sensors (Switzerland)*, vol. 14, no. 6, pp. 10432–10453, 2014, doi:

10.3390/s140610432.

[350] A. García-Miranda Ferrari, S. J. Rowley-Neale, and C. E. Banks, “Screen-printed electrodes: Transitioning the laboratory in-to-the field,” *Talanta Open*, vol. 3, no. December 2020, 2021, doi: 10.1016/j.talo.2021.100032.

[351] M. D. Rubianes and G. A. Rivas, “Dispersion of multi-wall carbon nanotubes in polyethylenimine: A new alternative for preparing electrochemical sensors,” *Electrochem. commun.*, vol. 9, no. 3, pp. 480–484, 2007, doi: 10.1016/j.elecom.2006.08.057.

[352] S. H. Park, H. N. Yang, D. C. Lee, K. W. Park, and W. J. Kim, “Electrochemical properties of polyethyleneimine-functionalized Pt-PEI/carbon black as a catalyst for polymer electrolyte membrane fuel cell,” *Electrochim. Acta*, vol. 125, pp. 141–148, 2014, doi: 10.1016/j.electacta.2014.01.095.

[353] M. Malaki, A. Maleki, and R. S. Varma, “MXenes and ultrasonication,” *J. Mater. Chem. A*, vol. 7, no. 18, pp. 10843–10857, 2019, doi: 10.1039/c9ta01850f.

[354] A. Sohan, P. Banoth, M. Aleksandrova, A. Nirmala Grace, and P. Kollu, “Review on MXene synthesis, properties, and recent research exploring electrode architecture for supercapacitor applications,” *Int. J. Energy Res.*, vol. 45, no. 14, pp. 19746–19771, 2021, doi: 10.1002/er.7068.

[355] J. E. Giaretta, H. Duan, F. Oveissi, S. Farajikhah, F. Dehghani, and S. Naficy, “Flexible Sensors for Hydrogen Peroxide Detection: A Critical Review,” *ACS Appl. Mater. Interfaces*, vol. 14, no. 18, pp. 20491–20505, 2022, doi: 10.1021/acsami.1c24727.

[356] G. Goor, “Hydrogen Peroxide: Manufacture and Industrial Use for Production of Organic Chemicals,” pp. 13–43, 1992, doi: 10.1007/978-94-017-0984-2_2.

[357] G. Zhu, Q. Wang, S. Lu, and Y. Niu, “Hydrogen Peroxide: A Potential Wound Therapeutic Target?,” *Med. Princ. Pract.*, vol. 26, no. 4, pp. 301–308, 2017, doi: 10.1159/000475501.

[358] C. S. Christensen, S. Brodsgaard, P. Mortensen, K. Egmose, and S. A. Linde, “Determination of hydrogen peroxide in workplace air: Interferences and method validation,” *J. Environ. Monit.*, vol. 2, no. 4, pp. 339–343, 2000, doi: 10.1039/b001799j.

[359] S. Kubendhiran *et al.*, “Electrochemically activated screen printed carbon electrode decorated with nickel nano particles for the detection of glucose in human serum and human urine sample,” *Int. J. Electrochem. Sci.*, vol. 11, no. 9, pp. 7934–7946, 2016, doi: 10.20964/2016.09.11.

[360] D. Combs *et al.*, “Reduction of silver ions in molybdates: elucidation of framework acidity as the factor controlling charge balance mechanisms in aqueous zinc-ion electrolyte,” *RSC Adv.*, vol. 11, no. 62, pp. 39523–39533, 2021, doi: 10.1039/d1ra07765a.

[361] N. Elgrishi, K. J. Rountree, B. D. McCarthy, E. S. Rountree, T. T. Eisenhart, and J. L. Dempsey, “A Practical Beginner’s Guide to Cyclic Voltammetry,” *J. Chem. Educ.*, vol. 95, no. 2, pp. 197–206, 2018, doi: 10.1021/acs.jchemed.7b00361.

[362] B. Schumm, *Encyclopedia of Applied Electrochemistry*. 2014.

[363] B. Patella, R. Inguanta, S. Piazza, and C. Sunseri, “A nanostructured sensor of hydrogen peroxide,” *Sensors Actuators, B Chem.*, vol. 245, pp. 44–54, 2017, doi: 10.1016/j.snb.2017.01.106.

[364] D. Tyagi *et al.*, “Recent advances in two-dimensional-material-based sensing technology toward health and environmental monitoring applications,” *Nanoscale*, vol. 12, no. 6, pp.

3535–3559, 2020, doi: 10.1039/c9nr10178k.

[365] M. H. Hassan, R. Khan, and S. Andreescu, “Advances in electrochemical detection methods for measuring contaminants of emerging concerns,” *Electrochem. Sci. Adv.*, no. October, pp. 1–27, 2021, doi: 10.1002/elsa.202100184.

[366] H. Dai, Y. Chen, X. Niu, C. Pan, H. L. Chen, and X. Chen, “High-performance electrochemical biosensor for nonenzymatic H 2 O 2 sensing based on Au@C-Co 3 O 4 heterostructures,” *Biosens. Bioelectron.*, vol. 118, pp. 36–43, 2018, doi: 10.1016/j.bios.2018.07.022.

[367] V. Massey, “The Chemical and Biological Versatility of Riboflavin,” *Biochem. Soc. Trans.*, vol. 28, no. 4, p. 283, 2000, doi: 10.1042/0300-5127:0280283.

[368] K. Thakur, S. K. Tomar, A. K. Singh, S. Mandal, and S. Arora, “Riboflavin and health: A review of recent human research,” *Crit. Rev. Food Sci. Nutr.*, vol. 57, no. 17, pp. 3650–3660, 2017, doi: 10.1080/10408398.2016.1145104.

[369] T. Zhou, H. Li, M. Shang, D. Sun, C. Liu, and G. Che, “Recent analytical methodologies and analytical trends for riboflavin (vitamin B2) analysis in food, biological and pharmaceutical samples,” *TrAC - Trends Anal. Chem.*, vol. 143, p. 116412, 2021, doi: 10.1016/j.trac.2021.116412.

[370] J. L. Golbach, S. C. Ricke, C. A. O’Bryan, and P. G. Crandall, “Riboflavin in Nutrition, Food Processing, and Analysis - A Review,” *J. Food Res.*, vol. 3, no. 6, p. 23, 2014, doi: 10.5539/jfr.v3n6p23.

[371] D. M. Stanković, D. Kuzmanović, E. Mehmeti, and K. Kalcher, “Sensitive and selective determination of riboflavin (Vitamin B2) based on boron-doped diamond electrode,” *Monatshefte fur Chemie*, vol. 147, no. 6, pp. 995–1000, 2016, doi: 10.1007/s00706-016-1665-2.

[372] I. H. Cho, D. H. Kim, and S. Park, “Electrochemical biosensors: Perspective on functional nanomaterials for on-site analysis,” *Biomater. Res.*, vol. 24, no. 1, pp. 1–12, 2020, doi: 10.1186/s40824-019-0181-y.

[373] R. Sangavi, M. Keerthana, and T. Pushpa, “Design of an Electrochemical Sensor for the Determination of Riboflavin using Cobalt Doped Dysprosium Oxide Nanocubes Modified Glassy Carbon Electrode,” vol. 202201661, 2022, doi: 10.1002/slct.202201661.

[374] E. Priyadarshini and K. Rawat, “Multimode sensing of riboflavin via Ag @ carbon dot conjugates,” *Appl. Nanosci.*, no. 0123456789, 2019, doi: 10.1007/s13204-019-01090-6.

[375] D. H. Ho, Y. Y. Choi, S. B. Jo, J. M. Myoung, and J. H. Cho, “Sensing with MXenes: Progress and Prospects,” *Advanced Materials*. John Wiley and Sons Inc, 2021, doi: 10.1002/adma.202005846.

[376] R. Khan, A. Radoi, S. Rashid, A. Hayat, A. Vasilescu, and S. Andreescu, “Two-dimensional nanostructures for electrochemical biosensor,” *Sensors*, vol. 21, no. 10. MDPI AG, May 02, 2021, doi: 10.3390/s21103369.

[377] G. Tigari, J. G. Manjunatha, C. Raril, and N. Hareesha, “Determination of Riboflavin at Carbon Nanotube Paste Electrodes Modified with an Anionic Surfactant,” *ChemistrySelect*, vol. 4, no. 7, pp. 2168–2173, 2019, doi: 10.1002/slct.201803191.

[378] W. Yantasee, Y. Lin, X. Li, G. E. Fryxell, T. S. Zemanian, and V. V. Viswanathan, “Nanoengineered electrochemical sensor based on mesoporous silica thin-film functionalized with thiol-terminated monolayer,” *Analyst*, vol. 128, no. 7, pp. 899–904, 2003, doi:

10.1039/b303973k.

[379] F. Wang, J. Yang, and K. Wu, “Mesoporous silica-based electrochemical sensor for sensitive determination of environmental hormone bisphenol A,” *Anal. Chim. Acta*, vol. 638, no. 1, pp. 23–28, 2009, doi: 10.1016/j.aca.2009.02.013.

[380] E. Desimoni and B. Brunetti, “Presenting Analytical Performances of Electrochemical Sensors. Some Suggestions,” *Electroanalysis*, vol. 25, no. 7, pp. 1645–1651, 2013, doi: 10.1002/elan.201300150.

[381] K. Y. Hwa and B. Subramani, “Synthesis of zinc oxide nanoparticles on graphene-carbon nanotube hybrid for glucose biosensor applications,” *Biosens. Bioelectron.*, vol. 62, pp. 127–133, 2014, doi: 10.1016/j.bios.2014.06.023.

[382] G. Tigari and J. G. Manjunatha, “A surfactant enhanced novel pencil graphite and carbon nanotube composite paste material as an effective electrochemical sensor for determination of riboflavin,” *J. Sci. Adv. Mater. Devices*, vol. 5, no. 1, pp. 56–64, 2020, doi: 10.1016/j.jsamd.2019.11.001.